Exon, N.F., Kennett, J.P., Malone, M.J., et al., 2001
Proceedings of the Ocean Drilling Program, Initial Reports Volume 189

5. Site 1170[1]

Shipboard Scientific Party[2]

PRINCIPAL RESULTS

Site 1170 is located in deep water (2704 m) on the flat western part of the South Tasman Rise (STR), 400 km south of Tasmania and 40 km east of Site 1169. It is 10 km west of a fault scarp, ~500 m high and trending north-south, that separates the lower western and higher central blocks of the STR. The site lies within present-day northern subantarctic surface waters, ~150 km south of the Subtropical Front and well north of the Subantarctic Front. The primary objectives of Site 1170 were to core and log (1) an Eocene detrital section deposited during early rifting between the STR and Antarctica to ascertain marine paleoenvironmental conditions before and leading into the initial marine connection that developed between the southern Indian and Pacific Oceans as the Tasmanian gateway opened during the mid-Paleogene, (2) an Oligocene to Holocene pelagic carbonate sequence to document the paleoceanographic and paleoclimatic responses to the opening of the Tasmanian gateway and subsequent expansion of the Southern Ocean, and (3) an upper Neogene sequence to construct a high-resolution subantarctic biostratigraphy and a high-resolution record of paleoclimatic change.

Plate tectonic reconstructions show the site as being in the broad northwest-southeast Tasmanian-Antarctic Shear Zone during the Cretaceous and moving south with Antarctica until the latest Cretaceous, when it became welded to the remainder of the STR as part of the Australian plate. From the earliest Paleogene, the site was close to the active rift. A shallow sea associated with Paleogene rifting and east-west spreading between Australia and Antarctica placed the site in the far southeastern corner of the restricted Australo-Antarctic Gulf, on the Indian Ocean side of the Tasmanian land bridge. The ridge of the Tasman Fracture Zone (TFZ), 80 km west of the site, formed soon after fast spreading began in the middle Eocene and must have provided east-flowing debris. Marine magnetic lineations show that in the late Oli-

[1]Examples of how to reference the whole or part of this volume.
[2]Shipboard Scientific Party addresses.

Ms 189IR-105

gocene (26–27 Ma) the east-west spreading axis was just west of the TFZ at Chron 8. The passing of the axis probably caused nearby uplift followed by subsidence.

Seismic profiles and regional correlations suggest that the site was subject to steady deposition of prograded siliciclastic deltaic sediments from the Cretaceous into the Eocene, and hemipelagic sedimentation grading to pelagic sedimentation thereafter (Fig. **F1**). Much of the Cenozoic siliciclastic detritus must have come from the higher central block 10 km to the east, believed to consist largely of continental basement and Cretaceous to Eocene sedimentary rocks. Parts of the central block, which was initially the Tasmanian land bridge, may have remained subaerial and, hence, a source of siliciclastic sediments well into the Oligocene. Seismic profiles suggest that there was a period of current erosion against the fault scarp of the central block, probably during the Miocene. A wedge of sediments was deposited in the depression.

At Site 1170 we cored one advanced hydraulic piston corer/extended core barrel (APC/XCB) hole, two more with the APC, and a rotary-cored hole (Table **T2,** p. 94, in the "Leg 189 Summary" chapter). Because suboptimal weather conditions affected the APC coring, construction of a composite section of the triple-cored portion of the sedimentary sequence was possible only to 70 m below seafloor (mbsf) (early late Pliocene). Beyond that, there are limited gaps, but overall core recovery averaged 90.4%. Hole 1170A reached 464.3 mbsf with 81.8% recovery. Hole 1170B was APC cored to 175.8 mbsf with 102.2% recovery, and Hole 1170C reached 180.1 mbsf with 99.7% recovery. Hole 1170D was rotary cored from 425 to 779.8 mbsf with 81.1% recovery. Wireline logging was conducted over ~540–770 mbsf in Hole 1170D with the triple-combination (triple combo) tool string, the geological high-sensitivity magnetic (GHMT)-sonic tool string, and the Formation MicroScanner (FMS)-sonic tool. Logging was terminated when the drill pipe became stuck in the hole, and the bottom-hole assembly (BHA) had to be severed with explosives.

Site 1170, with a total sediment thickness of 780 m, ranges in age from the middle Eocene (43 Ma) to the Quaternary. The older sequence consists broadly of ~282 m of rapidly deposited shallow-water silty claystones of middle and late Eocene age (lithostratigraphic Unit V, see below), overlain by 25 m of shallow-water glauconite-rich clayey siltstone deposited slowly during the latest Eocene to earliest Oligocene (Unit IV). Unit IV is overlain by 472 m of slowly deposited deep-water pelagic nannofossil chalk and ooze of early Oligocene through Quaternary age (Units III–I); limestone and siliceous limestone beds are low in the Oligocene section. There is a hiatus of ~4 m.y. in the mid-Oligocene between Units IV and III. The Neogene is almost completely continuous except for a hiatus of ~4 m.y. in the upper Miocene.

The lithostratigraphic sequence has been divided into five units and a number of subunits.

Lithostratigraphic Unit I (0–93 mbsf), of early Pliocene to Pleistocene age, is a nannofossil ooze with abundant siliceous microfossils. It is generally white with some darker laminations and bioturbation. Carbonate content averages 80 wt%, and organic carbon content is <1 wt%. Average sedimentation rates are low. Deposition was in an open, well-oxygenated ocean in lower bathyal water depths. The considerable kaolinite in the clay fraction may be ancient material derived by increased wind erosion from a more arid Australia.

Lithostratigraphic Unit II (93–373 mbsf) of early Miocene to early Pliocene age has three subunits: Subunit IIA to 181 mbsf, Subunit IIB to

F1. Postdrilling interpretation for local seismic profile AGSO 125-14 across Site 1170, p. 60.

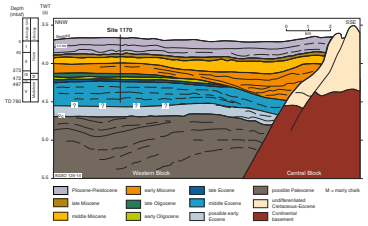

290 mbsf, and Subunit IIC to 373 mbsf. The unit generally consists of white nannofossil ooze or chalk, with more calcium carbonate (average 95 wt%) than Unit I. Organic carbon content is generally very low (<0.5 wt%) between 220 and 270 mbsf. Average sedimentation rates are low. Deposition was in lower bathyal water depths in open-ocean conditions.

Subunit IIA is late early Pliocene to late middle Miocene in age. It is uniform white nannofossil ooze with laminations that are light bluish to greenish gray. Subunit IIB is an upper to lower middle Miocene white nannofossil ooze that lacks laminations. Subunit IIC is white nannofossil ooze to chalk, with some laminations that are light bluish to greenish gray. The presence of quartz grains in the lower middle Miocene supports the evidence from the seismic profiles of a period of increased current activity and scouring (removing all the Oligocene) against the scarp 10 km to the east.

Lithostratigraphic Unit III (373–472 mbsf) is a light greenish gray nannofossil chalk of early Miocene to earliest Oligocene age. The lower part of the unit (below 446.6 mbsf), which is more clay rich, also contains pale gray clay-bearing limestone with evidence of pressure solution and thin, hard siliceous limestone layers. Calcium carbonate percentages are lower (78 to 93 wt%) than in Unit II. Both calcareous (foraminifers and nannofossils) and siliceous (diatoms and radiolarians) microfossils are abundant throughout the unit. Organic carbon content is very low, except in the lower part where it reaches ~0.5 wt%. Sedimentation rates are moderate. Paleoenvironmental indicators suggest increasing water depths and more oxygenation from outermost shelf or upper bathyal depths in the lower part of the unit to perhaps lower bathyal depths in the upper part. Although the contact between the limestone and underlying siltstone is very sharp, the sediment character in the lowermost part of the limestone suggests a continued shallow-water influence.

Lithostratigraphic Unit IV (472–497 mbsf) is a dark greenish gray, glauconitic-rich, sandy to clayey siltstone of earliest Oligocene to latest Eocene age. Crystalline quartz, diatoms, and glauconite are very abundant in the upper part of the unit but decrease downward as it becomes more clayey. About 1.5 m below the top of the unit, there is a break between sandier and harder sediments above and muddier sediments below. Calcium carbonate content is very low (5 wt% average, but as much as 10 wt%) and calcareous fossils are rare, whereas organic carbon content increases to <1 wt%. Carbonaceous fragments and bioturbation are ubiquitous. Sedimentation rates are low. Abundant palynomorphs (dinocysts, spores, and pollen) suggest a cool climate, and temperate forest was on the adjacent land. The clay minerals (illite/smectite) tend to support the evidence of a cool climate. The lithologic transition to the underlying sequence is gradational.

Lithostratigraphic Unit V (497–779.8 mbsf) is a bioturbated, dark gray, glauconite-bearing silty claystone to clayey siltstone of late to middle Eocene age that has two subdivisions: Subunit VA to 534.9 mbsf and Subunit VB to 780 mbsf (total depth). Calcium carbonate content is low (<5 wt% on average) and calcareous microfossils are rare. Organic carbon exhibits a steady downward increase from ~0.5 wt% in the upper part of Unit V to <3.5 wt% toward the base. Sedimentation rates are high. Palynolomorphs and clay minerals (mainly smectite) both suggest that conditions were warm, and rainforests cloaked the nearby land. Dinocysts are present in massive concentrations.

Subunit VA is late Eocene in age. It consists of clayey quartzose siltstone with glauconite-rich intervals and some carbonate. Subunit VB is an upper middle Eocene silty claystone. Some horizons contain abun-

dant small (1 mm diameter) white siliceous tubes. There are occasional occurrences of volcanic glass, solitary corals, bivalves, and pyrite nodules. There are also some decimeter-thick beds of grayish or brownish limestone in the lower part.

From a generalized biostratigraphic perspective, calcareous nannofossils at Site 1170 are abundant except in the lowermost Oligocene and the Eocene. Planktonic foraminifers and diatoms are abundant down to the middle Miocene but generally decline in older sediments. Benthic foraminifers are present, except in the upper Eocene, and suggest that water depths were 50–100 m during the middle and late Eocene and deepened rapidly during the early Oligocene. Dinoflagellate cysts are common down to the upper Pliocene, are abundant in the lowermost Oligocene and upper Eocene strata, and reach massive concentrations in the Eocene. In the middle Eocene, dinoflagellate cysts, diatoms, and nannoplankton show intriguing cycles thought to be related to variations in nutrient levels (degree of eutrophication), perhaps related to fluctuations in sea level and/or ventilation. Calcareous nannofossils suggest the possibility of two long hiatuses, one in Unit IV (Eocene/Oligocene boundary) and the other in Subunit VB (middle/late Eocene boundary). However, the existence of such hiatuses is refuted by sedimentologic and paleontologic (palynomorphs + diatoms) information.

Sedimentation rates determined from the fossil record were rapid (10 cm/k.y.) during the early rifting phase of the middle Eocene, followed by slow sedimentation and condensed sequences during the late Eocene, slow sedimentation during the early Oligocene (1 cm/k.y.), moderate sedimentation for a brief period during the late early Oligocene (5 cm/k.y.), slow sedimentation from the mid-Oligocene to the early middle Miocene (1 cm/k.y.), rapid sedimentation during the late middle Miocene (4 cm/k.y.), and slow sedimentation to the present day (2 cm/k.y.). Intervals of minimal sedimentation or erosion mark the late Oligocene and late Miocene sequences.

The geochemistry data show a very sharp change at the base of the carbonates at the Eocene/Oligocene boundary. This sharp change is associated with a diffusion barrier for pore waters and dissolved gases (e.g., methane is abundant below the barrier but absent above). Organic carbon below the barrier averages 0.5 wt% and is dominantly marine in origin. However organic carbon peaks up to 2 wt% in the lower part of the Eocene and appears to have been caused by increased nonmarine input. A variety of evidence suggests that, despite an only slightly higher than normal present-day thermal gradient, the organic matter is nearing thermal maturity. Gases deep in the hole may have been produced thermogenically, and bitumen traces appear to be present. As at Site 1168, pore waters become fresher with depth. Determination of the source of the fresher (low Cl^-) waters awaits further work.

The wireline logs covered only Subunit VB in the bottom of Hole 1170D because of hole stability problems. However, they show a very clear cyclicity of 4.1 m in the Th log, which awaits more paleontologic control before it can be converted into a time series. Magnetostratigraphy provided better results than at Site 1168, but these were convincing only in the Pliocene–Pleistocene, the middle and upper lower Miocene, and the uppermost Oligocene intervals.

The sedimentary succession of Site 1170 records three major phases of paleoenvironmental development:

1. Middle to early late Eocene rapid deposition of shallow-water siliciclastic sediments during rifting between Antarctica and the

STR, a time of minimal or no connection between the southern Indian and Pacific Oceans.
2. A transitional interval of slow sedimentation, with shallow-water upper Eocene glauconitic siliciclastic sediments giving way suddenly to lowermost Oligocene clayey biogenic carbonates, representing the activation of bottom currents as the Tasmanian Gateway opened and deepened during early drifting.
3. Oligocene through Quaternary deposition of biogenic carbonate sediments in increasingly deep waters and in increasingly open-ocean conditions, as the Southern Ocean developed and expanded with the northward flight of the STR and the Australian continent. The sedimentary sequence, in conjunction with information from earlier Ocean Drilling Program (ODP) results, seems to record an integrated history of interplay between decreasing continental influence, rifting and subsidence of the rise, antarctic cooling, Antarctic Circumpolar Current development, and other related factors.

A question being addressed by this and the other nearby sites is why there was such a sharp change from siliciclastic to carbonate sedimentation at the Eocene/Oligocene boundary. A very broad, shallow Australian-Antarctic shelf had been supplied with siliciclastic sediment for tens of millions of years, and, even though rifting, subsidence, and compaction had begun early in the Cretaceous, sedimentation kept up, and shallow-marine sediments were deposited. In the Tasmanian–STR area there was also subsidence related to the Late Cretaceous opening of the Tasman Sea. Rifting between Australia and Antarctica gave way to almost complete separation of the continents and fast spreading during the middle Eocene (43 Ma). This separation could be expected to increase the rate of subsidence, after a time lag, as the thermal anomaly under the margin dissipated. At Site 1170, siliciclastic sedimentation kept up until the Eocene/Oligocene boundary (33 Ma), some 10 m.y. after the onset of fast spreading, even though the local sedimentation rate had declined in the late Eocene. A variety of information suggests that the ridge of the TFZ formed during the middle Eocene fast spreading and was probably a major source of clayey detritus until the late Eocene. Then, the climate changed quickly, the supply of siliciclastics dropped off, slow deposition of pelagic carbonate was established, and the sea deepened rapidly. The most likely explanation is that climatic cooling led to greatly reduced rainfall, weathering, and erosion, and hence to greatly reduced siliciclastic supply. Such changes, from siliciclastic to biogenic sedimentation, appear to be apparent and synchronous wherever ODP drilling has taken place on the Antarctic margin.

In summary, the Eocene siliciclastic sedimentary interval contains a remarkable sequence of abundant organic dinocysts, pollen, and spores in addition to sufficiently persistent calcareous microfossils to assist with age control. The microfossils will provide an integrated record of terrestrial and shallow-marine paleoclimatic history of the antarctic continental margin in the middle Eocene through early Oligocene. The Oligocene pelagic biogenic sediments provide a sequence of calcareous and siliceous microfossils for integrated studies of the early development of the Southern Ocean, as the STR both subsided and migrated toward the north. The younger Neogene succession generally contains a sequence of calcareous and siliceous microfossils that are abundant and well preserved throughout and will provide excellent paleoceanographic records.

BACKGROUND AND OBJECTIVES

Site 1170 is located on the western part of the STR 400 km south of Tasmania and 40 km east of Site 1169, in relatively shallow water (~2705 m) (Fig. F3, p. 68, in the "Leg 189 Summary" chapter). The site lies within northern subantarctic surface waters, ~150 km south of the Subtropical Front and well north of the Subantarctic Front. Primary objectives of Site 1170 were to (1) core and log an Eocene detrital section deposited during rifting of the STR from East Antarctica for its paleoceanographic and paleoclimatic history; (2) core and log an Oligocene to Holocene pelagic carbonate section to determine, at moderately high resolution, history of the development of the Tasmanian gateway, subsequent expansion of the Southern Ocean, and paleoceanographic and paleoclimatic effects; and (3) core a Cenozoic sequence to construct subantarctic biostratigraphies in the Australian region and to obtain high-resolution records of paleoclimatic change.

Site 1170 is on thinned continental crust on the eastern side of the western block of the STR, which moved with Antarctica until the middle Eocene (43 Ma) and then became welded to the eastern block of the STR (Royer and Rollet, 1997). The block is elongated north-south and is 500 km long by 150 km wide (Exon et al., 1997). Cretaceous and Cenozoic sediments of the Ninene Basin cover most of the block. The block was cut into a number of complex transtensional sub-basins during the Late Cretaceous to Eocene by strike-slip faults that developed as Australia slid northward past Antarctica. The faults, some of which have throws of several thousand meters, trend northwest-southeast or north-south, and the resultant sub-basins filled with an average of 1000–2000 m of Cretaceous through Eocene prograded rift sediments. The stretched and thinned plateau subsided steadily during the Paleogene, and an early late Eocene marine transgression over basement is documented in Deep Sea Drilling Project (DSDP) Site 281 on the STR, 150 km to the southeast (Kennett, Houtz, et al., 1975). By the late Oligocene the sub-basins had filled, most of the high blocks were covered by sediment, detrital sedimentation had ceased, and pelagic sedimentation could no longer keep up with the subsidence, so much of the STR subsided to bathyal depths. Plate reconstructions show that the Tasmanian Gateway began to open during the Eocene–Oligocene transition, initially at shallow depths as a result of subsidence of the rise, and in deeper waters later in the Oligocene as the southern tip of the STR finally cleared Antarctica (Cande et al., 2000; S.C. Cande et al., unpubl. data; Royer and Rollet, 1997) (see Figs. F24, p. 90, F25, p. 91, F26, p. 92, in the "Leg 189 Summary" chapter).

DSDP Site 281 was drilled on a basement high of quartz-mica schist of latest Carboniferous age southwest of the tip of the STR in water 1591 m deep. The thin (169 m) sequence includes upper Eocene basement, conglomerate and glauconitic sandy mudstone, upper Oligocene glauconite-rich detrital sand, Miocene foraminifer-nannofossil ooze, and Pliocene–Pleistocene foraminifer-nannofossil ooze. Evidence from the recovered intervals suggests that the site had subsided into deep (bathyal) waters by the Miocene. The upper Neogene carbonate sequence and associated microfossil preservation were of sufficiently high quality to be incorporated into a widely used Cenozoic oxygen isotopic curve (Shackleton and Kennett, 1975).

Site 1170 is located at the intersection of multichannel seismic profiles *Sonne* SO36B-58 and *Tasmante* 125-14 (Fig. F2), in an area of flat-

F2. A portion of seismic line *Tasmante* 125-14 through Site 1170, p. 61.

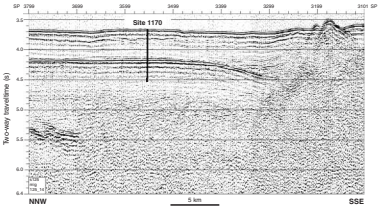

lying Cenozoic sediments, 10 km west of a structural low in the Cretaceous sequence caused by the subsidence of the structurally higher central block of the STR along the bounding north-south fault (Fig. **F3**). This movement apparently caused rollover into the fault in Oligocene times. The fault scarp to the east rises as much as 500 m above the present seafloor of the western block and was a source of detritus in the early Cenozoic when it was subject to subaerial erosion. A wedge of sediment derived from the eastern block overlies a strong reflector 0.51 s below the seafloor (sbsf) at the site. The top of the Lower Cretaceous is possibly at ~2.4 sbsf two-way traveltime (TWT), the top of the Cretaceous is possibly at ~1.4 sbsf, and the presumed Eocene/Oligocene boundary is at ~0.51 sbsf. A 3.5-KHz echo-sounder profile shows that the site is in an area of slightly irregular seabed (with a relief of 10 m), perhaps caused by scouring.

The site was designed to penetrate 0.51 s (460 m) of Oligocene through upper Neogene ooze and chalk above a strong reflector believed to represent the Eocene/Oligocene boundary. Below this reflector, we planned to drill 0.3 s (310 m) of Eocene sediments. In seismic profiles the wedge of young transparent ooze at the deeper water western Site 1169 apparently pinches out eastward toward Site 1170, where a weakly well-bedded sequence apparently reaches to the surface. Drilling proved this to be a facies change—from soupy nannofossil ooze to firmer foraminifer-nannofossil ooze—rather than an age change. The bedding in the upper sequence at Site 1170 is a little hummocky and appears to downlap slightly onto the Eocene/Oligocene reflector in places. The inferred Eocene through Paleocene sediments below the Eocene/Oligocene unconformity are weakly well bedded, and the underlying Cretaceous sequence is prograded.

Site 1170 is one of two southern sites drilled deeply during Leg 189, especially to advance understanding of circumpolar oceanographic and climatic evolution as a result of the opening of the Tasmanian Seaway and the development of the Southern Ocean. This site was selected, because of its location in middle bathyal depths near the southwestern margin of the STR, to investigate paleoenvironmental conditions in the extreme southeastern part of the Australo-Antarctic Gulf before and during this early opening of the Tasmanian Gateway in the Paleogene, and the history and consequences of subsequent Southern Ocean expansion. We expected to recover sedimentological evidence of a highly restricted, poorly ventilated gulf at the location of Site 1170 during the late Eocene, followed by the development through the Oligocene of more open ocean circulation.

Plate reconstructions show that Site 1170 was at a high latitude (~65°S) in the late Eocene (Cande, 2000; S.C. Cande et al., unpubl. data) and was immediately adjacent to the East Antarctic margin (see Figs. **F24,** p. 90, **F25,** p. 91, **F26,** p. 92, in the "Leg 189 Summary" chapter). The site, therefore, appeared to be well located to record early development of the antarctic cryosphere in the Paleogene. The early evolution of the antarctic cryosphere during the Eocene–Oligocene transition is not well known and it is possible that the antarctic cryosphere then was restricted to certain sectors of the continent. A major, but temporary, expansion of the East Antarctic Ice Sheet is well documented in the lowermost Oligocene (Breza and Wise, 1992; Zachos et al., 1992) for the antarctic sector in the Indian Ocean adjacent to the Kerguelen Plateau. Site 1170 is expected to allow comparison with these records in the region south of Tasmania, assuming that the opening of the gateway did not create a hiatus during this critical interval.

F3. Regional cross section through time across Site 1170, p. 62.

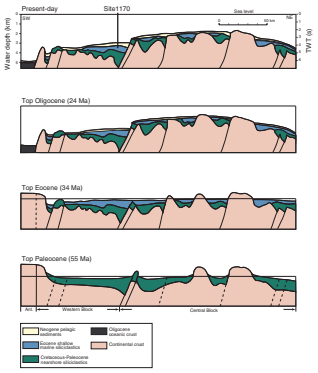

OPERATIONS

Transit to Site 1170

The transit from Site 1169 to Site 1170 required 3 hr at an average speed of 11.3 kt. Approximately 1 mile from location the vessel slowed, the thrusters were lowered, and a beacon was deployed at 1230 hr on 31 March, initiating operations at the site.

Hole 1170A

After settling on location, an APC/XCB BHA was made up and run close to the estimated depth of 2716.4 mbrf calculated from the precision depth recorder. Hole 1170A was spudded with the APC at 2030 hr on 31 March. The seafloor depth of 2715.5 mbrf, or 2704.7 mbsl, was calculated from the amount of recovery of the first core. Piston coring advanced to 163.2 mbsf with an average recovery of 98%. Piston cores were oriented starting with Core 3H, continuing through to Core 18H. Because of the 3.3-m vessel heave, no heat flow measurements were attempted.

The XCB system was used to deepen Hole 1170A from 163.2 to 464 mbsf with an average recovery of 73%. The rate of penetration slowed to nearly 1 m/hr in a hard nannofossil-limestone interval, which clearly signaled that this was the refusal depth of the XCB system. As XCB coring was concluding, the growing swell was now pushing the vessel heave over 6 m, which was outside the operating limits of the *JOIDES Resolution*. After the bit was pulled clear of the seafloor at 0545 hr on 3 April, coring operations were suspended for 4.3 hr while we waited for the swell to abate.

Hole 1170B

At 1000 hr on 2 April, the vessel was offset in dynamic positioning mode 20 m north of Hole 1170A. To obtain a stratigraphic overlap with the initial hole of the site, the bit was positioned 3 m shallower before starting Hole 1170B, which was spudded with the APC at 1145 hr on 2 April. The estimated seafloor depth was calculated to be 2715.7 mbrf, or 2704.7 mbsl, from the recovery of the first core. Piston coring advanced to 175.8 mbsf (Table T1) with an average recovery of 102%. Cores were oriented starting with Core 3H. Because of a growing swell that pushed the vessel heave over 4.5 m, the Tensor orientation tool was removed subsequent to the recovery of Core 14H to prevent damage to critical hardware. The bit was pulled clear of the seafloor at 0800 hr on 4 April, and the vessel was offset 20 m north of Hole 1170B.

T1. Coring summary, p. 115.

Hole 1170C

At 0945 hr, Hole 1170C was spudded with the APC. The stratigraphic overlap required lowering the bit 6 m from the spud-in depth of Hole 1170B. The seafloor depth estimated from recovery of the first core was 2714.4 mbrf, or 2703.3 mbsl. Piston coring advanced without incident to the depth objective of 180.1 mbsf, with an average recovery of 99.7%. Cores were oriented beginning with Core 3H, and one Adara deployment was made on Core 19H.

Hole 1170D

The ship was offset 20 m north of Hole 1170C, and a rotary core barrel (RCB) BHA was made up and deployed to 2668 mbrf. Hole 1170D was spudded with the RCB at 2000 hr on 4 April and drilled ahead with a center bit to 425 mbsf at an average rate of 55 m/hr. At 0745 hr on 6 April, RCB coring was initiated in Hole 1170D and advanced with increasing recovery (mean = 81%) to the depth objective of 779.8 mbsf (Table T1). The recovery below 529 mbsf to the bottom of the hole averaged nearly 100%. There were no stability problems encountered while drilling and coring in this hole.

At the conclusion of coring, the contrast in hole conditions between the upper and lower section of the hole was discussed among the relevant personnel. Logging difficulties were expected at a depth of 474–529 mbsf, where indurated limestone horizons were present above a zone of partially consolidated glauconitic sandstones and siltstones. It was agreed that it would be difficult for a logging tool to easily make the transition from the upper 425 m of the hole into the bottom 355 mbsf because of the likelihood that there would be washed out sections overlying a relatively narrow 10- to 12-in-diameter hole into the limestone capped lower section. Hence, it was decided to log the hole in two stages, with the end of the pipe placed initially at 529 mbsf to log the base of the hole then raised to ~200 mbsf to log the top of the hole.

Following a routine wiper trip and displacement of the hole with a 200-bbl sepiolite solution, the bit was dropped and the end of the drill string was placed at 529 mbsf. At 1730 hr on April 9, the first logging tool was deployed. Three tool-string runs were made with the pipe at 529 mbsf; the triple combo, the GHMT-sonic, and the FMS. The borehole was smooth with a relatively uniform diameter (~11–12 in), and high-quality data were obtained. All the logs came within 6 m of the bottom of Hole 1170D.

At 1700 hr on April 10, the first part of the logging program was completed and the drill crew made preparations to reposition the end of the pipe at 200 mbsf. After pulling the drill string back from 529 mbsf while encountering increasing drag, the drill string stuck firmly at 468 mbsf. The top drive was picked up and the drill string was subjected to overpulls as large as 200 kilopounds in an attempt to free the pipe. After attempts to move the pipe from 1715 to 2130 hr met with no progress, it was decided to sever the drill string just above the BHA.

An explosive charge was made up and deployed on the logging line to 3033 mbrf, which corresponded to the position of the first 5-in drill pipe joint above the BHA. At 0415 hr on April 10, the charge was detonated and severed the pipe. The drill string was then recovered, as were the two beacons. The vessel departed for Site 1171 at noon on 11 April 2000.

F4. Summary of biozonation, lithostratigraphic units, and physical properties, p. 63.

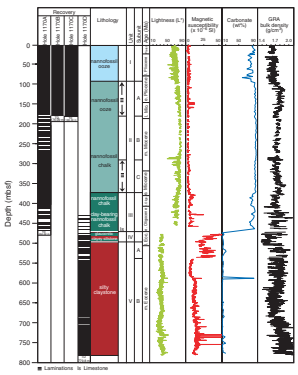

LITHOSTRATIGRAPHY

Introduction

Site 1170 consisted of four holes that produced a nearly continuous 779.8-m-thick section of Holocene to middle Eocene sediments (Fig. F4). Nannofossil oozes and chalks characterize the upper interval from 0 to 472 mbsf (Cores 189-1170A-1H through 52X and Cores 189-1170D-1R through 5R), followed by a distinct shift to glauconite-rich,

sandy to clayey siltstones between 472 and 497 mbsf (Cores 189-1170D-6R through 9R). This relatively coarse siliciclastic interval overlies relatively finer silty claystones that comprise the remainder of the section (497–779.8 mbsf; Cores 189-1170D-10R through 38R).

The Site 1170 section is divided into five lithostratigraphic units (Units I–V) based on core features, smear slides, thin sections, coulometric-based carbonate content, spectrophotometry, and magnetic susceptibility from Holes 1170A and 1170D (Fig. F5). Units II and V are divided into three and two subunits, respectively. Compositional and textural percentages define the primary lithology of each unit and subunit (Figs. F6, F7). Coulometric-based carbonate content was generally lower than smear slide–based carbonate estimates but did not significantly affect recognition of the major lithostratigraphic units. As demonstrated for Site 1168, Site 1170 spectrophotometric lightness (L*) and carbonate content appear strongly positively correlated. The lithostratigraphic units of Site 1170 are chronostratigraphically correlated to those of ODP Site 1168 (this volume) and DSDP Site 281 (Kennett, Houtz, et al., 1975) (see Table T2).

Unit I (Holocene to early Pliocene) is a light-colored nannofossil ooze that increases downsection in minor modifiers (10%–25%) of clays, foraminifers, and diatoms. Unit II (early Pliocene to early Miocene) is also a nannofossil ooze but contains significantly higher and more consistent carbonate content and spectrophotometric lightness values. Unit III (early Miocene to early Oligocene/late Eocene) is a light-colored clay-bearing nannofossil chalk that increases in clay content downsection, with isolated centimeter- to decimeter-scale gray silicified limestone beds near its base. Unit III marks the transition between the biogenic calcareous regime of Units I and II and the siliciclastic regime of Units IV and V. Unit IV (early Oligocene–late Eocene) is a dark gray glauconitic clayey siltstone with elevated magnetic susceptibility and lower carbonate content. Unit V (middle Eocene) is a finer, dark gray silty claystone with stepped changes in magnetic susceptibility and oscillations in spectrophotometric lightness, carbonate content, and quartz and glauconite content. Site 1170 sediments recovered by the APC and XCB ranged in drilling disturbance from none to severe flow-in because of the high ship heave during heavy weather. To aid in evaluation of physical properties and other data, mean drilling disturbance for each core section in Hole 1170A was rated on a qualitative scale (see "Lithostratigraphy," p. 5, in the "Explanatory Notes" chapter).

Lithostratigraphic Units

Unit I

Depth: 0 to 93 mbsf
Age: Holocene to early Pliocene
Intervals: Cores 189-1170A-1H to 11H; Cores 189-1170B-1H to 11H; and Cores 189-1170C-1H to 10H
Thickness: 93 m

Unit I is a white (N 8) to light greenish gray (5G 8/1, 5GY 7/1, 10Y 8/1 to 7/1, and 10GY 8/1 to 7/1) nannofossil ooze. Nannofossil abundance decreases downsection, with increasing proportions of minor modifier clays, foraminifers, and diatoms (10%–25% each). Light greenish gray (5G 8/1) to light bluish gray (10B 7/1) laminae and thin beds are common. Bioturbation intensity ranges from absent to common, and pyrite

F5. Detailed summary of biozonation, lithostratigraphic units, and physical properties, p. 64.

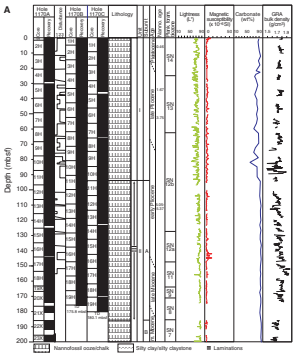

F6. Smear slide–based lithologic composition of Hole 1170A sediments, p. 68.

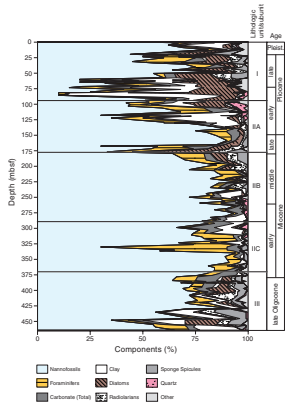

F7. Smear slide–based lithologic composition of Hole 1170D sediments, p. 69.

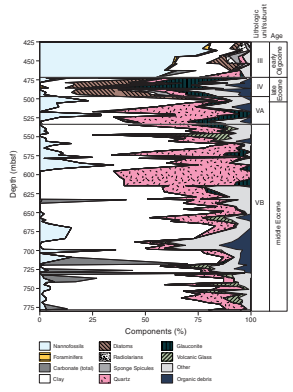

T2. Summary of Site 1170 lithology and corresponding lithostratigraphic units for Site 1168 and DSDP Site 281, p. 118.

staining is present throughout. Carbonate content ranges between 57 and 93 wt% with an average of 81 wt% (N = 31). A distinct moderately bioturbated light greenish gray (10Y 7-8/1) to light olive-gray (5Y 6/2) interval at ~81 mbsf (Section 189-1170A-10H-3) consists of diatom- and clay-dominated lithologies, with ~10%–30% nannofossils. Unit I is Holocene to early Pliocene in age and likely corresponds to Subunit IA of Site 1168 (see "Lithostratigraphy," p. 8, in the "Site 1168" chapter) and the upper portion of Subunit IA of DSDP Site 281 (Kennett, Houtz, et al., 1975).

Unit II

Depth: 93 to 373 mbsf
Age: early Pliocene to early Miocene
Intervals: Cores 189-1170A-11H to 41X; Cores 189-1170B-11H to 19H; and Cores 189-1170C-11H to 19H
Thickness: 280 m

Unit II is a white to light greenish gray nannofossil ooze with variable minor modifiers (10%–25%) of clay, foraminifers, and diatoms. The upper unit boundary is based on pronounced increases in carbonate content, spectrophotometric lightness, and bulk density. The unit is divided into three subunits based on color, laminations, minor modifier components, and carbonate content. Pyrite staining and rare pyrite nodules are throughout. Unit II is early Pliocene to early Miocene in age and likely corresponds to the lower portion of Subunits IB and IIA of Site 1168 (see "Lithostratigraphy," p. 8, in the "Site 1168" chapter) and the lower portion of Subunit IA and Subunit IB of DSDP Site 281 (Kennett, Houtz, et al., 1975).

Subunit IIA

Depth: 93 to 185.9 mbsf
Age: early Pliocene to middle Miocene
Intervals: Cores 189-1170A-11H to 21X; Cores 189-1170B-11H to 19H; and Cores 189-1170C-11H to 19H
Thickness: 92.9 m

Subunit IIA is a foraminifer-bearing white (N 8) nannofossil ooze. Clays and diatoms are common as minor modifiers (10%–25%) in the upper portion (Cores 189-1170A-11H through 15H). Distinct to diffuse, light greenish gray (5G 8/1) to light bluish gray (10B 7/1) laminations of variable thickness (millimeters to centimeters) decrease in overall abundance but increase in localized concentration downsection. Visible bioturbation is difficult to identify because of the subunit's homogeneous composition. Levels with bioturbation ranging from rare to present in intensity are restricted to ~107–123 mbsf and 135–139 mbsf (Cores 189-1170A-13H, 14H, and 16H). Carbonate content ranges between 90 and 96 wt%, with an average of 93 wt% (N = 26) and no stratigraphic trend. Isolated meter-scale intervals of light greenish gray and light bluish gray intervals are found in Cores 189-1170A-12H and 20X, respectively. Subunit IIA is early Pliocene to middle Miocene in age and likely corresponds to Subunit IB of Site 1168 (see "Lithostratigraphy," p. 8, in the "Site 1168" chapter) and lower portion of Subunit IA of DSDP Site 281 (Kennett, Houtz, et al., 1975).

Subunit IIB

Depth: 185.9 to 290 mbsf
Age: middle Miocene
Interval: Cores 189-1170A-22X to 32X
Thickness: 104.1 m

Subunit IIB is a massive white (N 8) nannofossil ooze with minor modifiers (10%–25%) of foraminifers and clays in Cores 189-1170A-23X, 28X, and 32X. In contrast to Subunits IIA and IIC, laminations are extremely rare and a very diffuse light bluish gray (~10B 8/1). Carbonate content increases markedly by ~3 wt% at the top of the subunit and ranges between 93 and 96 wt%, with an average value of 95 wt% (N = 25) and no stratigraphic trend. Visible bioturbation is absent, even where laminations provide contrast. Subunit IIB is middle Miocene in age and likely corresponds to the upper portion of Subunit IIA of Site 1168 (see **"Lithostratigraphy,"** p. 8, in the "Site 1168" chapter) and middle portion of Subunit IB of DSDP Site 281 (Kennett, Houtz, et al., 1975).

Subunit IIC

Depth: 290 to 373 mbsf
Age: middle Miocene to early Miocene
Interval: Cores 189-1170A-33X to 41X
Thickness: 83 m

Subunit IIC is a nannofossil ooze to chalk that fluctuates at the meter scale from predominately light greenish gray (5GY 8/1 to 10Y 8/1) to predominately white (N 8) downsection. Minor modifiers (10%–25%) of foraminifers and clays are more prevalent in the upper portion (290–335 mbsf; Cores 189-1170A-32X through 37X). In contrast to Subunit IIB, faint light greenish gray (5GY 7/1) laminations of variable thickness and concentration are relatively common in appearance and prominence, particularly as overall whiteness increases. Carbonate content decreases markedly by ~3 wt% at the top of the subunit, ranges between 91 and 95 wt% with an average of 93 wt% (N = 26), and shows a slight decreasing trend downsection. Visible bioturbation is generally absent, with rare to present levels between ~301 and 310 mbsf and ~330–357 mbsf (Cores 189-1170A-34X and 1170A-37X through 39X). Pyrite staining is less common than in previous subunits. Subunit IIC is middle Miocene to early Miocene in age and likely corresponds to Subunit IIA of Site 1168 (see **"Lithostratigraphy,"** p. 8, in the "Site 1168" chapter) and lower portion of Subunit IB of DSDP Site 281 (Kennett, Houtz, et al., 1975).

Unit III

Depth: 373 to 472 mbsf
Age: early Miocene to early Oligocene/late Eocene
Intervals: Cores 189-1170A-41X to 52X and Cores 189-1170D-1R to 5R
Thickness: 99 m

Unit III is a light greenish gray (10GY 8/1 to 7/1, 10Y 8/1 to 7/1, 10GY 8/1, and 5GY 8/1) to occasionally white (N 8) nannofossil chalk, with a general downsection increase in clays and decrease in biogenic carbon-

ate. Carbonate content decreases markedly by ~8 wt% at the top of the unit and ranges between 78 and 93 wt%, with an average of 85 wt% (*N* = 26). The top of the unit is also marked by high magnetic susceptibility and a slight decrease in GRA bulk density. Abundances of diatoms, radiolarians, and sponge spicules are greater overall than in Subunit IIC, occasionally to minor modifier level (10%–25%). Visible bioturbation ranges from absent to abundant in intensity. Distinct grayish green (5G 4/2) to light bluish gray (5B 7/1) laminae are below ~419 mbsf (Core 189-1170A-46X). Isolated intervals of hard limestone greatly reduced core recovery below ~459 mbsf (Cores 189-1170A-51X and 189-1170D-4R). Diagenetic dissolution pressure solution seams enriched in clay are found in Core 189-1170D-5R. Subunit IIIA is early Miocene to early Oligocene–late Eocene and likely corresponds to Subunits IIB, IIC, and Unit III of Site 1168 (see **"Lithostratigraphy,"** p. 8, in the "Site 1168" chapter) and Unit II and uppermost Unit III of DSDP Site 281 (Kennett, Houtz, et al., 1975).

Unit IV

Depth: 472 to 497 mbsf
Age: early Oligocene/late Eocene to late Eocene
Interval: Cores 189-1170D-5R to 9R
Thickness: 25 m

Unit IV is a dark greenish gray (10Y 5/1 to 4/1) to greenish black (10GY 2.5/1 to 5G 2.5/1), slightly sandy to generally clayey siltstone, containing as much as 35% diatoms and 60% glauconite. High glauconite content is often present within distinct centimeter-scale layers that decrease in abundance and thickness downsection. Nannofossils are rare (<5%), organic matter is present (3%–15%), and bioturbation is generally extensive. Carbonate content decreases markedly at the top of Unit IV by >80 wt% and averages only 2 wt% (*N* = 7). This pronounced decrease is accompanied by a ~40% decrease in average spectrophotometric lightness (L*) and ~15-fold increase in magnetic susceptibility values compared to Units I to III. Spectrophotometric lightness is relatively constant throughout Unit IV; however, magnetic susceptibility decreases in three minor steps. Unit IV is early Oligocene/late Eocene to late Eocene in age and likely corresponds to Unit IV of Site 1168 (see **"Lithostratigraphy,"** p. 8, in the "Site 1168" chapter) and Units III to V of DSDP Site 281 (Kennett, Houtz, et al., 1975).

Unit V

Depth: 497 to 779.8 mbsf
Age: late Eocene to middle Eocene
Interval: Cores 189-1170D-9R to 38R
Thickness: 282.8 m

Unit V is a dark green to dark gray silty claystone. The upper boundary is defined by a marked decrease in biosiliceous sediments and increase in silt- to sand-sized quartz. The unit contains prominent long-term oscillations in carbonate content, quartz content, spectrophotometric lightness, and lithologic components. Unit V is middle to late Eocene and likely corresponds to Unit V of Site 1168 (see **"Lithostratigraphy,"** p. 8, in the "Site 1168" chapter).

Subunit VA

Depth: 497 to 539.1 mbsf
Age: late Eocene
Interval: Cores 189-1170D-9R to 13R
Thickness: 42.1 m

Subunit VA is a dark greenish gray (10Y 3/1 to 5Y 3/2) to dark olive-gray (5Y 3/1) glauconite-bearing silty claystone to rarely clayey siltstone (i.e., only Cores 189-1170D-11R and 12R), with occasional dark olive-gray (5Y 3/1), dark gray (2.5Y 6/1), and black (5Y 2.5/2) intervals. The majority of the silt-sized siliciclastic material is quartz, with less glauconite and more nannofossils relative to Unit IV. Decimeter-scale intervals of higher glauconite content decrease in thickness and frequency downsection. Carbonate content averages 5 wt% (N = 9) with a broad peak through the subunit, consistent with smear-slide nannofossil abundances. Relative to Unit IV, average spectrophotometric lightness (L*) decreases slightly downsection, whereas magnetic susceptibility contains a broad relative maximum and GRA bulk density generally increases. Subunit VA is late Eocene in age and likely corresponds to Unit V of Site 1168 (see **"Lithostratigraphy,"** p. 8, in the "Site 1168" chapter) and Units IV and V of DSDP Site 281 (Kennett, Houtz, et al., 1975). DSDP Site 281 records glauconitic silty clays, sand, and basal breccia in the upper Eocene above quartz-mica schists (Kennett, Houtz, et al., 1975).

Subunit VB

Depth: 539.1 to 779.8 mbsf
Age: middle Eocene
Interval: Cores 189-1170D-14R to 38R
Thickness: 240.7 m

Subunit VB is a very dark gray (5Y 3/1) to dark olive-gray (5Y 3/2) to dark greenish gray (10Y 3/1) and to very dark greenish gray (10Y 3/1) silty claystone. The upper boundary of the subunit is marked by a 50%–60% decrease in both quartz content and magnetic susceptibility. Notable features within, and exceptions to, this silty claystone lithology include (1) volcanic glass-bearing sediments centered around 549 mbsf (Core 189-1170D-15R), (2) light gray (N 7/1) to light olive-gray (5Y 6/2) decimeter-scale limestones at ~587, ~598, and ~634 mbsf (Cores 189-1170D-19R, 20R, and 23R), (3) a very dark gray (5Y 3/1) to dark olive-gray (5Y 3/2) to very dark gray (5Y 3/1), quartz-rich clayey siltstone from 588 to 615 mbsf (Cores 189-1170D-19R through 21R), (4) a very dark gray (5Y 3/1) to dark greenish gray (10Y 3/1) claystone from ~647 to 653 mbsf (Core 25R), and (5) organic matter-bearing sediments (up to 15% from smear-slide analysis; <3% from geochemical analysis) from 670 to 735 mbsf (Cores 27R through 34R).

Carbonate content averages 2 wt% (N = 73) with three broad maxima at 539–597 mbsf (Cores 189-1170D-14R through 20R), 647–689 mbsf (Cores 25R through 29R), and 727 mbsf to the base of the core (Cores 33R through 38R). This carbonate trend is also reflected in spectrophotometric lightness maxima centered at 580, 675, and 735 mbsf (Cores 189-1170D-18R, 28R, and 34R) and, to a lesser extent, smear slide nannofossil maxima. Magnetic susceptibility is stable within Subunit VB relative to Unit IV and Subunit VA, with only minor incremental in-

creases at ~583 and 686 mbsf (Cores 189-1170D-18R and 29R) and occasional order-of-magnitude higher spikes below 728 mbsf (Core 33R).

Horizontal ~1-mm-diameter hollow tubes of very fine sand- to silt-sized siliceous grains are common at densities of ~1–10/m. Solitary azooxanthellate corals (N = ~5), bivalves (N = ~4), and pyrite nodules are rare but generally are within carbonate-poor intervals. Bioturbation ranges from moderate to abundant in intensity, with larger burrows appearing more common within more carbonate-rich intervals. Faint diffuse laminations are present. Subunit VB is middle Eocene, with the older part constrained by only limited biostratigraphic data. Site 1168 (see "Lithostratigraphy," p. 8, in the "Site 1168" chapter) did not penetrate to equivalent-age sediments.

Paleoenvironmental Interpretation

Site 1170 is located in the Ninene Basin on the western block of the STR. The basin's boundary with the central block of the STR is a fault scarp ~10 km east of Site 1170. The basin originated as a complex of transtensional sub-basins produced by strike-slip faulting during the Late Cretaceous to Eocene divergence of Australia from Antarctica (Exon et al., 1997). A plate tectonic reconstruction (Royer and Rollet, 1997) suggests that the western block moved with Antarctica from ~95 Ma, colliding with the central block during the latest Cretaceous, and became welded to the central block during the middle Eocene (~43 Ma). Given this paleogeographic location along the southeasternmost part of the developing Australo-Antarctic Gulf, Site 1170 should provide important insights on both regional tectonism and circumpolar ocean-atmosphere evolution.

During the middle to early late Eocene (Subunit VB), silty claystone sediments were deposited at rates of ~10 cm/k.y. or higher. Bioturbation was common to extreme throughout the interval and indicates that bottom waters were generally oxic to dysoxic, supporting metazoans capable of producing millimeter- to centimeter-scale burrow diameters. Burrow cross section populations tend to lack circular end-members, implying that significant compaction and dewatering occurred after bioturbation. This intense bioturbation destroyed primary sedimentary structures, except for extremely rare, faint remnants of irregular bedding at the centimeter scale. Therefore, paleodepth estimates cannot be based on sedimentary structures. Benthic foraminiferal assemblages, although highly altered diagenetically, indicate middle neritic (~50–100 m) paleodepths with a progressively more "restricted" paleoenvironment through time (see "Biostratigraphy," p. 19).

Three long-term oscillations in carbonate content during the middle Eocene are indicated by both low-resolution carbonate contents (two per core) and high-resolution spectrophotometric lightness values (proxy for carbonate at 2-cm sampling intervals) (Fig. F8). Maxima in carbonate content coincide with smear-slide nannofossil maxima, as well as faunal peaks in the oligotroph dinoflagellate *Enneadoxysta partridgei*, (see "Biostratigraphy," p. 19). Conversely, carbonate minima are higher in clays and silts with quartz more abundant and glauconite appearing and increasing in the two later minima. The driving cause(s) of these long-term oscillations remains uncertain, but the predominance of chemical weathering–produced smectite through the interval does not support significant tectonism. At much higher resolution, gamma-ray logs, and potentially spectrophotometric lightness values, show very regular sedimentation cycles throughout most of the middle

F8. Eocene oscillations in carbonate content and spectrophotometric lightness, Hole 1170D, p. 70.

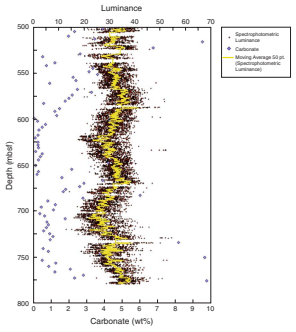

Eocene at the orbital frequency of either precession or obliquity (see "Downhole Measurements," p. 52), depending on the preferred age model (see "Biostratigraphy," p. 19).

In the uppermost Eocene (Unit IV), an environment shift to less restricted conditions is inferred from the pronounced increase in neritic diatoms but may be partially controlled by silica dissolution (see "Biostratigraphy," p. 19, and "Inorganic Geochemistry," p. 46). Also associated with this interval is an increase in sand-sized quartz and glauconite, the latter including sand-sized grains often concentrated in centimeter-scale beds. Organic matter also increases and is present throughout the unit, whereas clays show another illite peak and are more abundant overall.

Across the poorly recovered Eocene/Oligocene boundary (Units III/IV), the depositional environment fundamentally shifted from a siliciclastic to carbonate-dominated regime. This shift is best shown by a marked step increase in nannofossils and decrease in glauconite at the boundary, whereas diatoms are absent in the lowermost Unit III but later return as a more open marine fauna. Based on sedimentation rates and carbonate contents, the pronounced shift is driven mostly by increased productivity, particularly as preservation of carbonate microfossils appears consistently moderate to good through the event. This pronounced carbonate productivity increase, together with the paleodepth increase to middle bathyal depths (600–1000 m) based on benthic foraminifers, may reflect the ocean-atmosphere response to the opening of the eastern Tasmanian land bridge of the Australo-Antarctic Gulf to some critical size, shape, latitude, or orientation. Movement along the adjacent scarp was apparently not an integral part in this opening because of the lack of coarse beds at Site 1170, although that depends on the nature of the scarp's lithology.

Through the Oligocene (Unit III), nannofossil sedimentation predominated, whereas biosiliceous sediments were relatively common and clay content decreased through time to less than a few percent. No sedimentological evidence exists for the late early to early late Oligocene hiatus (see "Biostratigraphy," p. 19). Through the early to early middle Miocene (Subunit IIC), biosiliceous sediments decrease in abundance and laminations are common. Increased middle Miocene productivity and/or preservation is indicated by higher carbonate content and sedimentation rates. There is seismic evidence of middle Miocene scouring along the scarp to the northeast, which could have provided the quartz found at that level. Biosiliceous sediments began to increase again in the later middle Miocene (upper Subunit IIB) and reached a relative peak at the middle late Miocene boundary (Subunit IIA/IIB boundary). Above this boundary, carbonate content decreases and laminations reappear. The long hiatus in the late Miocene sequence is not recognized lithologically. Following a step increase in biosiliceous sediments, the Pliocene and Quaternary sediments (upper Subunit IIA and Unit I) show no pronounced lithologic patterns other than an apparent late Pliocene reduction in clay content.

Clay Mineralogy

X-ray diffraction (XRD) analyses were completed on 47 samples from Holes 1170A and 1170D (Fig. F9). The purpose of the clay mineral studies at Site 1170 was to recognize the major variations of the paleoenvironment as expressed by the clay mineral assemblages at a sampling interval of one every two cores and to compare the clay mineral assem-

F9. Clay mineral units, p. 71.

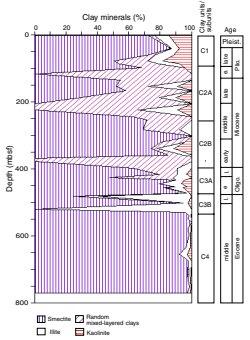

blages with those recognized at Site 1168, which was drilled at similar water depth on the western Tasmania margin and with sites in other areas of the Southern Ocean.

Results

The clay minerals identified include smectite, random mixed-layered clays, illite, and kaolinite. Chlorite has been recognized only in trace quantities in two samples and is not included in the percent estimates. Based on the relative abundance of the clay minerals, four units were identified for Site 1170. These were designated Units C1 to C4 (Fig. F9).

Unit C1, which extends from the seafloor to 100 mbsf, has a clay mineral assemblage that consists of very abundant smectite (50% to 85%) and common kaolinite (10% to 20%) accompanied by random mixed-layered clays and illite (0% to 20% each). Unit C1 ranges in age from the late Pliocene to the Pleistocene and correlates to lithostratigraphic Unit I. Unit C2 extends from 100 to 380 mbsf, is characterized by dominant smectite (50% to 85%) alternating with dominant random mixed-layered clays (0% to 100%), and correlates to lithostratigraphic Unit II. Because of the low clay content in most nannofossil oozes of lithostratigraphic Unit II, percentages of random mixed-layered clays >50% are probably overestimated. Unit C2 is divided into two subunits. Subunit C2A extends from 100 to 250 mbsf and is middle Miocene to early Pliocene in age. Subunit C2A shows decreased contents of smectite (<70%) and significant amounts of random mixed-layered clays (>20%) and illite (up to 25%). Subunit C2B extends from 250 mbsf to 380 mbsf and is early Miocene to middle Miocene in age. Subunit C2B shows increased contents of smectite (up to 100%), low amounts of illite (<10%), and sporadic kaolinite (up to 10%). With the exception of one sample with poor clay content, the random mixed-layered clays are <20%. Unit C3 extends from 380 to 530 mbsf, is characterized by significant occurrences of illite (up to 100%), and correlates to lithostratigraphic Units III and IV and Subunit VA. Unit C3 is divided into two subunits. Subunit C3A extends from 380 to 472 mbsf and is Oligocene in age. Subunit C3A contains abundant smectite (45% to 95%), with random mixed-layered clays (0% to 30%), illite (traces to 15%), and kaolinite (0% to 5%). Subunit C3B extends from 472 to 530 mbsf and ranges in age from the middle Eocene to the late Eocene. Subunit C3B exhibits alternations of dominant illite (5% to 100%) and smectite (25% to 95%), associated with traces of kaolinite (0% to 2%). Unit C4 is characterized by largely predominant smectite (90% to 100%), accompanied by rare illite (0% to 5%), and traces of kaolinite (0% to 2%). Unit C4 is middle Eocene in age and correlates to lithostratigraphic Subunit VB.

Paleoenvironmental Interpretation of Clay Assemblages

The extreme predominance of smectite in middle Eocene Unit C4 supports warm climatic conditions and intense chemical weathering in the sediment source areas. Smectite prevails in areas of low relief with alternating periods of precipitation and aridity, and its formation is enhanced on basic volcanic substrates (Chamley, 1989; Weaver, 1989). Site 1170 was located in a basin on the western block of the STR still attached to Antarctica (see "Background and Objectives," p. 6). Sedimentation rates are high, and the sediment is largely fine-grained siliciclastic particles (silty claystone and clayey siltstone). However, the high

smectite content at Site 1170 suggests that no significant tectonic activity occurred and that low-relief areas prevailed in adjacent continental areas during the middle Eocene. The clay mineral assemblage is very comparable to those of similar age observed off the passive Antarctic margins on the South Orkney Microcontinent and Maud Rise in the Weddell Sea (Robert and Maillot, 1990; Diester-Haass et al., 1996) and Kerguelen Plateau in the southernmost Indian Ocean (Ehrmann, 1991).

Subunit C3B, of middle and late Eocene age, features distinct increases in illite, which forms up to 100% of the clay fraction. This is indicative of strong physical weathering and erosion of substrates in the source area. Physical weathering and illite formation prevail in modern cold and/or dry environments. Illite is also characteristic of steep relief areas, where tectonic activity and mechanical erosion, together with cold conditions, prevent soil development (Chamley, 1989; Weaver, 1989). Such an occurrence of predominant illite has not been described before in other areas of the middle and late Eocene Southern Ocean and Tasman Sea, where the clay mineral assemblage consisted largely of smectite (Robert et al., 1985; Robert and Maillot, 1990; Ehrmann, 1991). It is therefore assumed that predominant illite in Unit C3 derives from physical weathering and erosion of substrates in adjacent continental areas, where steep relief may have developed during the stage of strike-slip tectonic activity that preceded the separation of the STR from Antarctica to the west. The strike-slip motion probably formed the great ridge of the Tasman Fracture Zone along the western margin of the STR at that time, on the basis of plate tectonic, seismic reflection, and dredge information (Exon et al., 1997). Similar intervals of abundant illite, often associated to significant amounts of kaolinite and random mixed-layered clays, have been observed during active early opening stages in the South Atlantic (Robert, 1987).

Increased contents of illite in Subunit C3B started during the latest middle Eocene at ~38 Ma, in nannofossil Zone NP17. At the same time, slight increases of illite and random mixed-layered clays in the Weddell Sea on Maud Rise (Robert and Maillot, 1990) occurred during an increasing trend in the $\delta^{18}O$ values of the benthic and planktonic foraminifers (Kennett and Stott, 1990; Stott et al., 1990). This evolution suggests local development of poorly weathered soils in response to a cooling of the Southern Ocean. Coeval extension of antarctic siliciclastics from the lower to the upper part of the intermediate water mass in the entire Atlantic sector of the Southern Ocean suggests a greater influence of the antarctic environment upon the water column at southern high latitudes (Robert and Kennett, 1992). From clay mineral data, it seems that the peak of tectonic activity in the western STR area was constrained within the latest middle to late Eocene interval. Moreover, Subunit C3B also contains cosmopolitan dinocysts and is limited by possible hiatuses at its lower and upper parts (see **"Biostratigraphy,"** p. 19). It is highly probable that the middle late Eocene episode of plate tectonic activity in the STR had significant consequences on the development of cooler conditions at southern high latitudes and expansion of cool antarctic waters.

Illite, random mixed-layered clays, and kaolinite account for 20% to 50% of the clay assemblage of Subunit C3A, which is typical of early Oligocene subantarctic areas (Robert and Chamley, 1992). The conspicuous illite is very similar to that observed in other areas of the Southern Ocean, on the Kerguelen Plateau (Ehrmann, 1991), and on the Maud Rise (Diester-Haass et al., 1993). The trend of illite in Subunit C3A expresses the progression of physical weathering on East Antarctica in re-

lation to the development of cold and/or dry conditions that followed the temporary growth of an ice sheet in the earliest Oligocene (Zachos et al., 1993; Robert and Kennett, 1997).

In Subunit C2B, of early to middle Miocene age, lower values of illite and random mixed-layered clays than in Subunit C3A and sporadic kaolinite suggest slightly decreased physical weathering in the source area. The ratio of the 001 peak intensities for kaolinite and illite (kaolinite/[kaolinite+illite]) provides additional information on Subunit C2B. The ratio is highest (indicative of increased kaolinite) from 350 to 310 mbsf in nannofossil Zones NN2 to NN4 of early Miocene age. This pattern is coeval with a significant increase of the percentage of kaolinite at Site 1168. The regional increase of kaolinite is indicative of increased warmth and intensified precipitation (see "Lithostratigraphy," p. 8, in the "Site 1168" chapter) and immediately precedes major expansion of the East Antarctic Ice Sheet at 14–15 Ma (Kennett, 1977). However, the clay assemblage of Site 1170 is significantly different from that of Site 1168 on the western Tasmania margin, which is marked by more kaolinite and less illite. As ocean opening progressed, the clay assemblage at Site 1170 most probably derived from a range of continental areas and expresses average weathering conditions on the emerged margins of the Southern Ocean. Further increase of illite and random mixed-layered clays (and less smectite) in Subunit C2A indicates enhanced erosion of poorly weathered substrates, following the expansion of the East Antarctic Ice Sheet during the middle Miocene.

Unit C1 of late Pliocene and Pleistocene age is marked by small increases of kaolinite percentages, whereas the clay content of the calcareous biogenic sediment also slightly increases (Unit I). Such a clay assemblage, containing as much as 20% kaolinite, has not previously been observed in other subantarctic areas (Robert and Maillot, 1983; Ehrmann, 1991), but it is very similar to that observed in late Pliocene sediments from the Lord Howe Rise in the Tasman Sea (Stein and Robert, 1986). Most clay particles of Unit C1 may have been transported southward from arid Australian regions by northwesterly winds (Pye, 1987). This pattern may have commenced during the late Pliocene, when eolian particles from Australian arid areas reached their maximum southward extension and abundance in the Tasman Sea (Stein and Robert, 1986). Unit C1 of Site 1170 is coeval to Unit C1 of Site 1168, but kaolinite is less abundant on the STR than on the west Tasman margin (see "Lithostratigraphy," p. 8, in the "Site 1168" chapter). Greater distance from the source and/or additional contribution from runoff on the west Tasman margin may account for this difference.

BIOSTRATIGRAPHY

Combined microfossil biostratigraphy indicates that the recovered sequence at Site 1170 represents the Paleocene to Quaternary. Calcareous nannofossils are abundant from the Quaternary to the upper Oligocene, absent in the Eocene/Oligocene boundary transition, and generally few to common in most of the samples downhole through the middle Eocene. Planktonic foraminifers are abundant from the Quaternary to the Oligocene but rare or absent below the lower Oligocene. The paucity or absence of calcareous microfossils in the Paleogene is not attributed to strong carbonate dissolution because nannofossils, where present, show generally good preservation with some delicate features intact. Diatoms and radiolarians are generally abundant in the

upper Neogene, and their abundances diminish toward the Oligocene. Dinoflagellate cysts are present in the upper Pliocene and Pleistocene, abundant in the Eocene, and absent in the lower Pliocene through the Oligocene samples analyzed.

The late Neogene has the best biostratigraphic resolution, as a large number of bioevents from various microfossil groups can be used. Biostratigraphic data from this site show a generally uniform sedimentation rate for the late Neogene (see **"Age Model and Sedimentation Rates,"** p. 35; Fig. **F10**), in contrast with the extremely high sedimentation rate (~24 cm/k.y.) for the early Pliocene at Site 1169. This suggests that the high sedimentation rate at Site 1169 was a local rather than a regional phenomenon.

A hiatus representing the late Miocene (between ~7 and 11 Ma) was recognized. This hiatus was also recognized at Site 1169 (where it has a longer duration) and thus appears to be of regional significance. Another hiatus was revealed near the lower Oligocene/upper Oligocene boundary.

A questionable hiatus is indicated in the Eocene–Oligocene transition interval based on nannofossil data. However, the interpretation hinges heavily on the use of one nannofossil datum (the last occurrence [LO] of *Reticulofenestra umbilica*) with the exclusion of dinocyst datums (the LOs of *Areosphaeridium diktyoplokum* and *Enneadocysta partidgei*). The use of the dinoflagellate datums in the exclusion of the nannofossil datum will result in a significantly different age model interpretation. The available data do not allow for an unambiguous conclusion as there are a number of uncertainties, including whether the biochronological ages calibrated elsewhere can be applied to the nannofossil and dinoflagellate datums at this site (cf. Figs. **F11, F12**). Shore-based studies of additional samples, detailed comparison of results from this site with those from other southern high-latitude sites, and examination of some samples from those sites should shed more light on the age assignments for the critical Eocene–Oligocene transition.

Another questionable hiatus is indicated in the middle Eocene based on the co-occurrence of two nannofossil datums—the LO of *Chiasmolithus solitus* (38.2 Ma) and the first occurrence (FO) of *Reticulofenestra reticulata* (41.2 Ma). The inference of a hiatus, however, appears to be in conflict with dinocyst datums and sedimentological studies. Further work is needed to clarify this problem as it is critical for other studies requiring reliable age information.

Benthic foraminiferal assemblages change dramatically between the shallow-water middle–upper Eocene and the deeper, well-oxygenated Oligocene and Neogene sediments. This transition in water depth, from neritic to bathyal/abyssal, coincides with a sequence of glauconitic siltstone (Cores 189-1170D-7R through 9R) that is devoid of benthic foraminifers. Furthermore, there are distinctly neritic diatom floras in Cores 189-1170D-9R through 7R (Eocene), mixed diatom floras from Cores 189-1170D-5R through 1R, which suggest a period of deepening in the earliest Oligocene, and fully open-ocean diatom floras in the late early Oligocene.

Noticeable reworking of dinocysts and radiolarians was observed in the middle Eocene sediments. In the case of radiolarians, the reworked specimens are dominantly of early Eocene age.

The quantitative dinocyst distribution in the lowermost Oligocene to middle middle Eocene generally indicates somewhat restricted, overall eutrophic, neritic marine conditions throughout the succession. Cross-correlation with the sedimentological (smear slide) data, and the dia-

F10. Age-depth plot and linear sedimentation rates, p. 72.

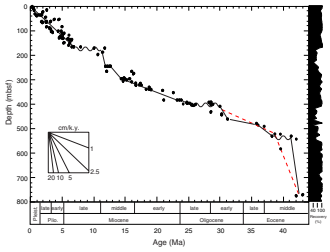

F11. Combined bioevents for the Eocene–Oligocene transition, Hole 1170D, p. 73.

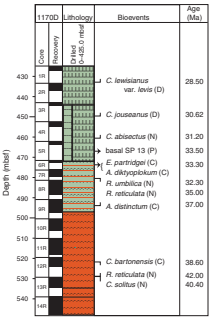

F12. Alternative age interpretations for the Eocene–Oligocene transition, Hole 1170D, p. 74.

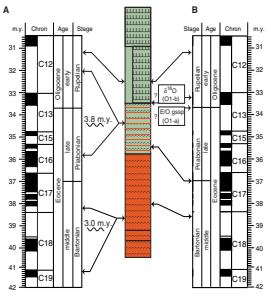

tom, radiolarian, and calcareous nannofossil distribution suggests (1) a positive correlation between maxima in *Deflandrea* spp. (dinocysts) with diatom maxima and most radiolarian maxima and (2) a positive correlation between maxima in calcareous nannoplankton content and *E. partridgei* (dinocysts) maxima. Optima in *Thalassiphora pelagica* (dinocysts) immediately follow an *E. partridgei* maximum. These correlations are tentatively interpreted to reflect changes in trophic levels of the water masses and are shown to have a cyclic nature.

Terrestrial palynomorphs are consistent in the Eocene, but in low relative abundances. The few identified taxa may be compared with established records from New Zealand and Australia and indicate cooling and increasing humidity from the middle middle Eocene into the late Eocene.

A discussion of each microfossil group studied is provided below.

Calcareous Nannofossils

All core-catcher samples from the four holes at Site 1170 were examined for calcareous nannofossils. Additional samples from some critical intervals were also examined to refine biostratigraphic resolution. Calcareous nannofossils are generally abundant and well preserved in the Neogene. Nannofossil abundance decreases downhole from generally abundant in the upper Oligocene to generally common or few in the middle Eocene, with a number of samples barren of nannofossils. Nannofossil datums recognized, and their ages, sample intervals, and depth intervals are listed in Table **T3.** The stratigraphic distribution of selected species is presented in Table **T4.** Most of this nannofossil biostratigraphic information in these five tables is self-explanatory. A few comments are made below for several nannofossil datums.

T3. Calcareous nannofossil datum levels, p. 119.

T4. Stratigraphic distribution of selected nannofossil species, p. 120.

Ceratoliths are very rare at this site. The FO and LO of *Ceratolithus acutus* (Table **T3**) were based on the rare occurrence of the species in one sample (189-1170A-12H-CC). The true FO is most likely to be stratigraphically lower and the true LO stratigraphically higher than recorded. Similarly, amauroliths are also very rare and sporadic at the site. The FO of *Amaurolithus delicatus* recorded between Samples 189-1170C-16H-CC and 17H-CC (Table **T3**) is likely to be stratigraphically higher than its true FO.

Sample 189-1170D-6R-CC contains an Oligocene nannofossil assemblage without *Cyclicargolithus abisectus* and *R. umbilica*. This suggests an age of ~31.3 Ma for this sample. Core 189-1170D-7R and the upper part of Core 189-1170D-8R are barren of calcareous nannofossils. Sample 189-1170D-8R-5, 50 cm, immediately below this barren interval, contains *R. umbilica* and *R. reticulata*. An age of 35.8 Ma can be assigned to this sample. The interval from Samples 189-1170D-8R-5, 50 cm, through 7R-CC thus appears to represent an ~4-m.y. duration. This would suggest a condensed section or, more likely, a major hiatus over the Eocene/Oligocene boundary.

Another hiatus is tentatively placed in Core 189-1170D-13R based on co-occurrence of two nannofossil datums—the LO of *Chiasmolithus solitus* (40.4 Ma) and the FO of *R. reticulata* (42.0 Ma). The duration of the hiatus would be >1.6 m.y. if the above ages are used. The inference of a hiatus in this core, however, appears to be in conflict with a dinocyst datum in Core 189-1170D-12R. Shore-based studies of additional samples, detailed comparison of results from this site with those from other southern high-latitude sites, and examination of samples from those

sites should help clarify whether a hiatus exists and its potential duration.

The FO of *R. umbilica* (43.7 Ma) was recorded between Samples 189-1170D-37R-CC and 38R-CC. This suggests a sedimentation rate of >30 cm/k.y. between ~529 and 774 mbsf. As the deepest sample from the site (189-1170D-38R-CC) contains only rare specimens of nannofossils, the FO of *R. umbilica* is considered tentative, and its true FO may be stratigraphically lower. This would indicate possibly even higher sedimentation rates assuming that the numerical age can be applied to this site.

The generally low abundance (and sometimes absence) of nannofossils in the Eocene interval is attributed to dilution by abundant clays and to a very shallow and restricted water environment rather than dissolution of carbonate, as nannofossils, where present, are generally well preserved with very fine structures intact.

As at Site 1168, the Eocene through lower Oligocene nannofossil assemblages at this site show warmer water characteristics than those from sites of comparable paleolatitude (e.g., Sites 689, 690, 744, and 748, which range from 52° to 65°S) as there are fewer high-latitude taxa (e.g., chiasmoliths and *Reticulofenestra daviesii*) at Site 1170.

Planktonic Foraminifers

Shipboard examination of planktonic foraminifers from all core-catcher samples disclosed that sediments ranging in age from middle Eocene to Quaternary were recovered at Site 1170 (see Table T5 for datum ages). The planktonic foraminiferal assemblages are typical of cool-temperate to subantarctic regions. The Neogene section is punctuated by two significant hiatuses, one in the upper Miocene and another in the lower middle Miocene. Given the low sample density, the absence of some of the planktonic foraminiferal zones may reflect condensed intervals because of slow sedimentation rates, as opposed to actual hiatuses.

Planktonic foraminifers provide little biostratigraphic control throughout much of the Paleogene sequence recovered at Site 1170. There are several intervals within the upper Eocene to lowermost Oligocene sequence in Hole 1170A that are barren of planktonic foraminifers (e.g., samples below Sample 189-1170A-52X-CC, 464.25 mbsf). In Hole 1170D, planktonic foraminiferal assemblages are depauperate and sporadic throughout the section spanning the middle Eocene to lowermost Oligocene (Samples 189-1170D-6R-CC to 38R-CC). Nonetheless, the middle Eocene to upper Oligocene record still appears incomplete with the lower upper Oligocene missing. The stratigraphic distributions of species are given in Table T6.

T5. Planktonic foraminiferal datums, Hole 1170A, p. 126.

T6. Range chart of planktonic foraminifers, p. 127.

Quaternary

Identification of the FO of *Globorotalia truncatulinoides* (~1.98 Ma), the datum that approximates the lower boundary of the Quaternary, has been problematic. Typically, specimens of *G. truncatulinoides* are relatively large and morphologically distinct. However, at Sites 1168, 1169, and 1170 only diminutive, juvenile *G. truncatulinoides* with thin, pregametogenic shells comprise the lowermost occurrences of this marker species. Matters are further complicated by the fact that these small *G. truncatulinoides* are rare. The sporadic stratigraphic occurrence of early *G. truncatulinoides* has given rise to apparent ages that are dis-

cordant with those derived from calcareous nannoplankton datums. Kennett (1970) has reported that *G. truncatulinoides* first immigrated into subantarctic waters as recently as 200 ka. Thus, it appears that environmental conditions during the early Pleistocene were unfavorable for supporting viable populations of *G. truncatulinoides* in the region. These observations suggest that the FO of *G. truncatulinoides* is an unreliable datum in the STR area. The FO of *G. truncatulinoides* is tentatively placed within the interval between Samples 189-1170A-3H-CC (20.75 mbsf) and 4H-CC (29.07 mbsf).

Significant changes in faunal compositions were also noted in the series of Quaternary core catchers examined. For instance, in Sample 189-1170B-3H-CC warm temperate-water species such as *Orbulina universa* and *Globigerinella aequilateralis* are rare to absent, whereas the cold-water species *Neogloboquadrina pachyderma* (sinistral) is quite abundant. The opposite is the case for Sample 189-1170B-4H-CC in which temperate species increase in abundance. These faunal responses likely reflect geographic shifts in water-mass boundaries and concomitant changes in water temperatures during the Quaternary.

Pliocene

The base of the *Globorotalia inflata* Zone (SN13) is demarcated by the FO of the nominate taxon. This datum is used to recognize the base of the upper Pliocene (3.2 Ma) and is constrained to the interval between Samples 189-1170A-7H-CC (58.25 mbsf) and 8H-CC (68.07 mbsf). Upper Pliocene assemblages are mostly temperate in character containing such species as *Globigerina bulloides, Globigerina quinqueloba, Globorotalia crassaformis, Globorotalia puncticulata,* and *Globorotalia puncticuloides*.

The early Pliocene is composed of two subzones, the *G. puncticulata* (SN12b) and the *Globorotalia pliozea* (SN12a) subzones. The boundary between the subzones is defined by the LO of *G. pliozea* (4.60 Ma), which is restricted to the interval bounded by Samples 189-1170A-14H-CC (123.73 mbsf) and 15H-CC (133.94 mbsf).

The lower boundary of Subzone SN12a coincides with the Miocene/Pliocene boundary and is delimited by the FO of *G. puncticulata* (5.30 Ma). The base of Subzone SN12a was constrained to the interval between Samples 189-1170A-16H-CC (143.75 mbsf) and 17H-CC (153.47). It is curious that Subzone SN12a, which is defined as the interval in which the ranges of *G. puncticulata* and *G. pliozea* overlap, was not recognized over the same depth interval in the other holes at Site 1170. This inconsistency is attributed to the rarity of *G. pliozea*.

Late Miocene

The uppermost zone of the upper Miocene, the *Globorotalia conomiozea* Zone (SN11), is delimited by the lower portion of the nominate taxon's stratigraphic range that predates the FO of *G. puncticulata*. The lowermost core catcher containing typical populations of *G. conomiozea* was determined to be Sample 189-1170A-18H-CC (163.70 mbsf). The next sample down examined (189-1170A-19X-CC, 167.13 mbsf) contains no specimens of *G. conomiozea,* but abundant *Paragloborotalia continuosa,* indicating Zone SN9. This pattern of faunal succession suggests that the base of Zone SN11 is truncated by a hiatus and/or that the 3.43-m section separating Samples 189-1170A-18H-CC and 19X-CC is stratigraphically condensed. The *Globorotalia miotumida* Zone (SN10), as defined as the stratigraphic gap between the ranges of *P. continuosa* and

G. conomiozea, was not recognized. In fact, Zone SN10 was not identified in any of the holes at Site 1170. A similar, but stratigraphically more extensive, hiatus was documented at Site 1169.

The upper portion of the *P. continuosa* Zone is most likely truncated by the hiatus at the Miocene/Pliocene boundary as well. The base of this zone, which is defined by the LO of *Paragloborotalia nympha* (10.10 Ma), is confined to the interval between Samples 189-1170A-19X-CC (167.13 mbsf) and 20X-CC (174.54 mbsf).

The downhole stratigraphic sequence continues with presence of the *P. nympha* Zone (SN8), which straddles the upper/middle Miocene boundary. The base of Zone SN8 is demarcated by the LO of *Paragloborotalia mayeri* (11.4 Ma). This datum has been constrained to the interval bounded by Samples 189-1170A-21X-CC (180.91 mbsf) and 22X-CC (192.05 mbsf). As at Site 1168, assemblages spanning the upper Miocene to Pliocene are dominated by temperate species belonging to the *G. conomiozea* lineage, as well as the *Globoturborotalita woodi/Globoturborotalita decoraperta/Globoturborotalita apertura* plexus.

Middle Miocene

The *P. nympha* Zone (SN8) is followed by the *P. mayeri* Zone (SN7). The base of Zone SN7 is defined by the FO of *P. mayeri* (12.1 Ma). Sediments within the interval spanning Samples 189-1170A-22X-CC and 29X-CC are assigned to Zone SN7. Given that the *P. mayeri* Zone encompasses only 700 k.y., its thickness (~80 m) at Site 1170 is remarkable.

The *Orbulina suturalis* Zone (SN6) is defined as the interval that contains the nominate taxon but predates the FO of *P. mayeri*. The base of Zone SN6 is delineated by the FO of *O. suturalis* (15.1 Ma). The *O. suturalis* Zone was not recognized at Site 1170, which differs from the more temperate Site 1168 where this same zone was nearly 47 m thick. The absence of Zone SN6 at Site 1170 suggests the presence of a hiatus or a sharp reduction in sedimentation rates so that the *O. suturalis* Zone is confined within a single core and therefore not sampled. Alternatively, the paleogeographic position of Site 1170 may have been at, or near, the edge of the biogeographic range of *O. suturalis;* therefore, Zone SN6 is not well represented at this location.

The *Praeorbulina curva* Zone (SN5) was identified only in Sample 189-1170A-30X-CC, so its maximum thickness cannot exceed 22.3 m. This biozone (SN5) was not recognized at Site 1168, yet another difference between Site 1170 and the more northerly Site 1168. The lower/middle Miocene boundary coincides with the base of Zone SN5, which, in turn, is denoted by the FO of *P. curva* (16.30 Ma).

Early Miocene

The uppermost part of the lower Miocene appears to be an expanded sequence as reflected by the estimated thickness (57.03 m) of the *Globigerinoides trilobus* Zone (SN4). The lower boundary of Zone SN4 is defined by the FO of its nominate taxon (18.80 Ma). This datum is placed between Samples 189-1170A-36X-CC (327.22 mbsf) and 37X-CC (338.80 mbsf).

The *Globoturborotalita connecta* Zone (SN3) is defined as that part of the nominate taxon's range, which predates the FO of *G. trilobus*. Thus, the base of Zone SN3 is marked by the FO of *G. connecta* (20.90 Ma).

This datum has been constrained to the interval embraced by Samples 189-1170A-37X-CC (338.80 mbsf) and 38X-CC (347.18 mbsf).

The downhole succession of early Miocene biozones continues uninterrupted with the identification of the *G. woodi* Zone (SN2) in Sample 189-1170A-38X-CC. Zone SN2 is defined as the interval in which *G. woodi* is present prior to the FO of *G. connecta*. The lower boundary of the *G. woodi* Zone (22.60 Ma) is therefore restricted between Samples 189-1170A-38X-CC (347.18 mbsf) and 39X-CC (356.53 mbsf).

The *Globoquadrina dehiscens* Zone (SN1) is the lowermost biozone of the early Miocene. The base of Zone SN1 is by definition the FO of *G. dehiscens* (23.20 Ma). For practical purposes, this datum is also used to approximate the Oligocene/Miocene boundary. The lowermost occurrence of *G. dehiscens* was observed in Sample 189-1170A-41X-CC, thereby confining this datum between Samples 189-1170A-41X-CC (376.53 mbsf) and 42X-CC (387.17 mbsf).

Late Oligocene

The presence of the *Turborotalia euapertura* Subzone (SP14b), the uppermost biozone of the late Oligocene, suggests that the transition from the lower Miocene to the upper Oligocene is relatively complete. Foraminiferal assemblages lacking both *G. dehiscens* and *Chiloguembelina cubensis* in Samples 189-1170A-42X-CC (387.17 mbsf) to 44X-CC (405.83 mbsf) are indicative of this gap zone. The presence of Subzone SP14b constrains the age of this series of samples from 23.20 to 28.50 Ma, so the actual completeness of the uppermost Oligocene is difficult to assess.

It is noteworthy that, at Site 1170, Subzone SP14b is very thin in comparison with Site 1168. Furthermore, Subzone SP14b directly overlies Zone SP13. The absence of the *C. cubensis* Subzone (SP14a) is consistent with the presence of a significant hiatus separating the upper from the lower Oligocene. The moderately diverse assemblages are well preserved, with little or no evidence of secondary infilling.

Early Oligocene

Relative to the late Oligocene, the early Oligocene faunas at Site 1170 are marked by a reduction in diversity. The *C. cubensis* Subzone (SP14a) straddles the boundary between the lower and upper Oligocene. It is defined as the stratigraphic interval below the LO of *C. cubensis* (28.5 Ma), but above the LO of *Subbotina angiporoides* (30.0 Ma). However, at Site 1170, *C. cubensis* was invariably found to coexist with *S. angiporoides,* making Subzone SP14a unrecognizable. This faunal pattern, combined with the observed thinness of Subzone SP14b, suggests the presence of a hiatus separating the upper lower Oligocene from the lower upper Oligocene.

The upper boundary of the *S. angiporoides* Zone (SP13) is delimited by the LO of the nominate taxon. The highest stratigraphic occurrence of *S. angiporoides* is in Sample 189-1170A-45X-CC (410.05 mbsf), marking the top of the lower Oligocene at this site. Thus, sediments assigned to the late Oligocene Subzone SP14b unconformably overlie those of the early Oligocene Zone SP13. Specimens ascribed to the taxon *S. angiporoides* range down to Sample 189-1170A-51X-CC. Hole 1170A terminated at 464.27 mbsf. This sample (189-1170A-52X-CC) contained no *S. angiporoides* but was still assigned to Zone SP13 based on the presence

of *Globigerina labiacrassata,* a species that has not been recorded below Zone SP13 elsewhere (Hornibrook et al., 1989).

Eocene/Oligocene Boundary

Coring in Hole 1170D commenced within the *S. angiporoides* Zone (~427.27 mbsf) and overlaps with the lower Oligocene record recovered at the bottom of Hole 1170A. The *S. angiporoides* Zone ranges down into Sample 189-1170D-5R-CC (464.21 mbsf). The stratigraphic interval spanning Samples 189-1170D-6R-CC to 14R-CC is barren of planktonic foraminifers. Calcareous nannofossil assemblages indicate that the Eocene/Oligocene boundary falls within this same barren interval (472.72–548.46 mbsf). This would account for the absence of the *Subbotina brevis* Zone (SP12) at Site 1170. Zone SP12 straddles the Eocene/Oligocene boundary. Confident delineation of Zone SP12 is further hampered by the nondescript shell morphology and general paucity of *S. brevis* in the region. Thus, planktonic foraminifers were of little value to studying the Eocene/Oligocene boundary at Site 1170.

Eocene

Much of the middle and upper Eocene is characterized by poor preservation and a general scarcity of planktonic foraminifers. The sporadic record appears to be largely a function of paleoenvironmental conditions. Only rare specimens of *Subbotina linaperta* and *S. angiporoides* are found in Samples 189-1170D-15R-CC (558.49 mbsf) and 17R-CC (577.77 mbsf). The LO of *S. linaperta* has been dated at 37.7 Ma (Berggren et al., 1995), although Hornibrook et al. (1989) report this species as ranging up to the topmost Eocene. In either case, the presence of *S. linaperta* is clear evidence for assigning these samples to the late Eocene, tentatively to Zone SP11.

Sample 189-1170D-18R-CC (585.10 mbsf) contains *Acarinina aculeata,* which ranges from the top of Zone SP10 to within Zone SP9; this supports the notion that the section immediately below the upper barren interval is no older than late middle Eocene. The interval between Sample 189-1170D-20R-CC (606.55 mbsf) and 32R-CC (722.15 mbsf) is barren with the exception of a single specimen of *S. linaperta* in Sample 189-1170D-28R-CC. Rare specimens of *S. linaperta* are also found from Samples 189-1170D-33R-CC to 38R-CC. Finally, Sample 189-1170D-37R-CC (768.73 mbsf) was found to contain small specimens of *Turborotalia pomeroli,* suggesting a maximum age of Zone SP8 (middle Eocene). A striking difference between the middle to upper Eocene assemblages at Site 1170 and those at other Southern Ocean locales is the conspicuous absence of *Globigerinatheka index.* As with the lower Oligocene, the low-diversity assemblages are only moderately preserved, showing signs of recrystallization in the lowermost samples.

Benthic Foraminifers, Ostracodes, and Bolboforma

Benthic foraminiferal assemblages at this site change dramatically between the shallow-water Eocene and the deeper Oligocene and Neogene (Fig. F13). This transition in paleodepth, from neritic to bathyal/abyssal, coincides with a sequence of glauconitic siltstone at the Eocene/Oligocene boundary, which is devoid of benthic foraminifers. Diatoms from this sequence, however, indicate neritic depths also for the bottom part of this interval and open-ocean conditions for the top-

F13. Evolution of the depositional setting, p. 75.

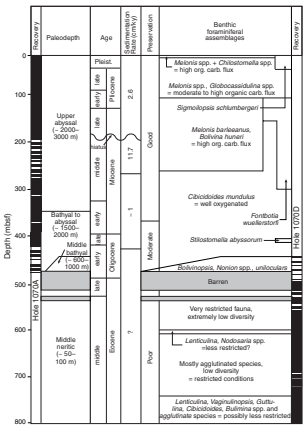

most part (see "Diatoms, Silicoflagellates, and Sponge Spicules," p. 29). This indicates that subsidence at this site is a much more rapid event than at Site 1168. Whereas the Neogene assemblages at both of these sites are rather similar, there are clearly strong differences in the Paleogene. At Site 1168, the Oligocene assemblages exhibit distinctly changing depth zonations and clearly were still shallower than the Neogene assemblages; whereas at Site 1170, the Oligocene assemblages are similar to those of the lower Neogene and are inferred to represent similar water depths.

The Eocene exhibits a transition from less restricted faunas, which are represented by a diverse assemblage of calcareous (e.g., *Lenticulina, Vaginulina, Guttulina, Cibicidoides,* and *Bulimina* spp.) and agglutinating species (Samples 189-1170D-38R-CC to 33R-CC) via a nondiverse, mostly agglutinated assemblage (Samples 189-1170D-32R-CC to 19R-CC) to an extremely restricted assemblage of traces of calcareous (e.g., *Elphidium* and *Lenticulina* spp.) and agglutinating species (Samples 189-1170D-17R-CC to 12R-CC, plus 10R-CC). Sample 189-1170D-18R-CC forms an exception to this trend with relatively high abundances of nodosariids and lenticulinids. The presence of the extinct species *Elphidium saginatum* in most of these samples indicates neritic water depths (50–100 m). Both intervals of glauconitic siltstone over the Eocene–Oligocene transition (Samples 189-1170D-11R-CC and 9R-CC to 5R-CC) are devoid of benthic foraminifers. The second, prominent interval of glauconitic siltstone is followed by an open-marine, biogenic carbonate sequence of abundant planktonic and benthic foraminifers of early Oligocene age. Preservation in the Eocene varies. Although the preservation of surface structures, particularly in the calcareous tests may appear good, these are generally only retained as siliceous infillings. Signs of breakage and diagenetic staining are observed.

The top samples in Hole 1170D, the earliest carbonate sequence, are characterized by the presence of *Bolivinopsis* and *Nonion* spp., as well as increased numbers of unilocular species (Samples 189-1170D-4R-CC to 1R-CC). The faunal composition, together with the absence of *Cibicidoides mundulus,* indicates intermediate water depths (~600–1000 m). This observation stands in contrast to the suggested bathyal to abyssal paleodepth for the bottom samples recovered from Hole 1170A, which include *C. mundulus*. This discrepancy implies that the top section of Hole 1170D predates the bottom section of Hole 1170A. Sediment depth in mbsf, however, suggests an overlap between the two sections. Recovery at both sites during the interval in question is low, and only a high-resolution postcruise study of the recovered sediment will help solve the question of whether there is a faunal transition with a potential gap between the two holes or an overlap with alternating assemblages.

The entire Oligocene sequence in Hole 1170A is marked by high numbers of *C. mundulus,* suggesting bathyal to abyssal paleodepths (~1500–2000 m) and well-oxygenated bottom waters. In fact, this species is abundant throughout Samples 189-1170A-51X-CC to 16H-CC. Sample 189-1170D-43X-CC and, to a lesser extent, 42X-CC are additionally marked by the presence of *Stilostomella abyssorum*. The presence of larger numbers of unilocular species in the calcareous sequence at the top of Hole 1170D suggests equally good oxygenation. Preservation in the Oligocene and Neogene sections is generally good.

By the middle Miocene, paleodepths had deepened to 2000–3000 m (upper abyssal). *Fontbotia wuellerstorfi* is present in Samples 189-1170A-31X-CC (middle Miocene) to 11H-CC (early Pliocene) and only in

traces thereafter. The interval 189-1170A-27X-CC to 11H-CC contains abundant *Melonis barleeanus* and *Bolivina huneri,* indicating increased organic carbon flux. The remaining Samples 189-1170A-10H-CC to 1H-CC in the Pliocene–Pleistocene are marked by both *M. barleeanus* and *Melonis pompilioides,* with additional *Chilostomella oolina* in Sample 189-1170A-1H-CC, resembling the assemblage pattern at Site 1169. At Site 1169, however, abundances of *C. oolina* were much higher. Organic carbon flux during this interval is most likely high. The occurrence of *Sigmoilopsis schlumbergeri* is restricted to Samples 189-1170A-4H-CC to 1H-CC. The general trends in the Neogene sections at Sites 1168 and 1170 show similarities but different timing based on the age-depth models. Detailed study of the sediments has potential in developing regional trends.

Ostracodes were recorded from most core-catcher samples of Hole 1170A, with the exception of Samples 189-1170A-50X-CC to 52X-CC. They are also present in Samples 189-1170D-1R-CC to 3R-CC. In the Eocene section of Hole 1170D, they sporadically are present as trace occurrences. Traces of *Bolboformids* were found in the middle and upper Miocene. *Bolboforma aculeata* is the only species to reach significant numbers in one of the samples (189-1170A-25X-CC).

Radiolarians

Radiolarians are generally common and well preserved in the Quaternary through Oligocene and generally rare to common in the Eocene, where species cannot be identified because of the strong recrystallization. The faunas at Site 1170 are characterized by the lack of index species of the traditional zonations. Consequently, no standard zonations can be recognized at this site. All datums applied herein were tentatively selected from the species with consistent occurrences at this site. The radiolarian sequence of the site is potentially useful for establishing a new zonation for the subantarctic. The datums, ages, and sample intervals recognized at Site 1170 are shown in Table T7. Selected datums and radiolarian faunas are discussed below.

T7. Radiolarian datums, p. 135.

Samples 189-1170A-1H-CC through 15H-CC, 189-1170B-1H-CC through 15H-CC, and 189-1170C-1H-CC through 15H-CC are assigned to the Quaternary through Pliocene. The base of the Pliocene is generally approximated by the last abundant occurrence (LAO) of *Stichocorys delmontensis* at 5.18–6.9 Ma.

The upper Miocene *Stichocorys peregrina* abundance zone was recognized in Samples 189-1170A-15H-CC, 189-1170B-18H-CC, and 189-1170C-19H-CC. The boundary between the upper and middle Miocene is placed between Samples 189-1170A-19X-CC and 20X-CC based on the FO of *Dictyophimus splendens* at 11.8 Ma. The base of the middle Miocene is approximated between Cores 189-1170A-32X-CC and 36X-CC based on the LO of *Cenosphaera coronata* at 16.7 Ma (*Cenosphaera* sp. of Morley and Nigrini, 1995). The early Miocene radiolarian faunas in Hole 1170A are marked by an abundance of *C. coronata* and *Cenosphaera coronataformis*. These two species have been reported only from the high-latitude North Pacific (Shilov, 1995). The FO of *Cyrtocapsella tetrapera* (23.6 Ma) between Samples 189-1170A-41X-CC and 42X-CC approximates the base of the lower Miocene.

Sample 189-1170D-1R-CC is assigned to the Oligocene on the basis of the absence of *C. tetrapera* (FO at 23.6 Ma) and the presence of its unnamed ancestor. Previous studies have reported no useful datums within the Oligocene in the temperate through antarctic oceans in the

Southern Hemisphere so that the Oligocene cannot be divided into early and late Oligocene on radiolarian evidence. However, the abundance of *Stylosphaera radiosa* may be useful for dividing the Oligocene.

The Oligocene faunas in Hole 1170D are characterized by the presence of *Theocorys robusta, Lychnocanoma conica,* and *Lophophaena tekopua*. The Eocene/Oligocene boundary cannot be delineated using radiolarians because of the absence of marker species.

Radiolarians are poorly preserved and sometimes absent in Samples 189-1170D-5R-CC through 28R-CC, which are dated as Eocene age by nannofossils. Radiolarians extracted from Samples 189-1170D-12R-CC through 28R-CC are filled with silica, fragmented, and highly recrystallized. Samples 189-1170D-29R-CC through the deepest one, 38R-CC, are nearly barren. Some samples from the middle Eocene contain early Eocene reworked radiolarians such as *Spongatractus balbis* with an age range of 49.0–52.9 Ma.

Diatoms, Silicoflagellates, and Sponge Spicules

All core-catcher material from Holes 1170A and 1170D was analyzed for diatoms, silicoflagellates, and sponge spicules. Well-preserved, diverse, and abundant diatom assemblages are present in Samples 189-1170A-1H-CC through 11H-CC. Samples 189-1170A-18H-CC through 41X-CC contain generally less abundant and diverse assemblages of moderately to poorly preserved specimens. Within this interval, however, Samples 189-1170A-19X-CC (late Miocene) and 34X-CC (middle Miocene) contain notably abundant and well-preserved diatoms. In addition, abundant well-preserved Oligocene diatoms are present in Samples 189-1170A-42X-CC through 49X-CC. Thin-section analysis of the silicified limestone Sample 189-1170A-50X-CC (see **"Lithostratigraphy,"** p. 9) revealed few diatoms that could not be identified. The lowermost samples from Hole 1170A (189-1170A-51X-CC and 52X-CC) are barren of diatoms.

For Hole 1170D, Samples 189-1170D-1R-CC through 9R-CC contain few to abundant diatoms, except Sample 189-1170D-6R-CC where diatoms are present only in trace amounts. Samples below Sample 189-1170D-9R-CC generally contain trace to rare diatoms or are barren. Relative abundance data for diatoms, sponge spicules, and silicoflagellates from Hole 1170A are presented in Table **T8.** The relative abundance of diatoms in Hole 1170D are graphically presented in Figure **F14** along with the abundance of the dinocyst *Deflandrea phosphoritica* group (see **"Palynology,"** p. 30).

Twenty-one diatom bioevents are recognized in Holes 1170A and 1170D (see Table **T9**). As many as three bioevents within the same depth interval (e.g., the LO of *Thalassiosira complicata* [2.5 Ma], *Thalassiosira inura* [2.5 Ma], and *Fragilariopsis weaveri* [2.65 Ma] are present between Samples 189-1170A-7H-CC and 8H-CC). Onboard analysis of core material to constrain events was undertaken only for the FO of *Cavitatus jouseanus* (30.62 Ma), which is placed at 454.43 mbsf within an accuracy of 0.53 m (see Table **T9**). Reworking is not strongly apparent throughout Holes 1170A and 1170D.

In terms of paleobathymetry, Samples 189-1170A-1H-CC through 46X-CC contain wholly open-ocean floras. Samples 189-1170A-47X-CC through 49X-CC and Samples 189-1170D-1R-CC through 5R-CC contain moderately diverse early Oligocene mixed floras of dominantly open-ocean diatoms with a common component of neritic taxa. Samples 189-1170D-7R-CC through 9R-CC contain a distinctly more neritic

T8. Relative abundance of selected taxa, sponge spicules, and silicoflagellates, Hole 1170A, p. 136.

F14. Comparison of *Deflandrea* spp. and estimates of diatom abundance, Hole 1170D, p. 76.

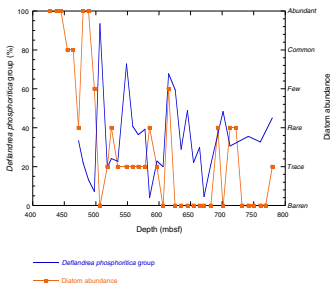

T9. Diatom bioevents identified, Holes 1170A and 1170D, p. 140.

flora. Below Sample 189-1170D-9R-CC, diatom abundance markedly falls; however, specimens recovered from these samples likewise suggest neritic water depths for the Eocene at Site 1170. The mixed diatom floras from Samples 189-1170D-5R-CC to 1R-CC suggest a period of deepening in the earliest Oligocene. Fully open-ocean conditions were attained in the late early Oligocene. Neritic diatoms at Site 1170 are considered to be in situ (i.e., not reworked) because of their high relative abundance and mostly good to moderate preservation. Such assemblages include heavily silicified resting spores of *Chaetoceros, Xanthiopyxis,* and *Stephanopyxis* plus benthic genera such as *Diploneis*. Species of the tychopelagic genus *Paralia* are also present.

Significantly high abundances of *Chaetoceros* resting spores in Samples 189-1170D-7R through 9R (the highest amounts for this site) strongly suggest enhanced eutrophic conditions for this interval. In a broad sense, the overall diatom signal throughout Hole 1170D positively correlates to that for the diatom-scavenging *Deflandrea phosphoritica* dinocyst group (Figs. **F14, F15;** see **"Paleoenvironment,"** p. 34 for discussion).

F15. Distribution of the organic walled dinocyst dominated taxa and indications of dominances of other (phyto)plankton groups, Hole 1170D, p. 77.

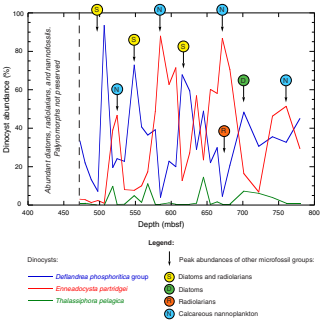

Palynology

Onboard palynological analysis included every fourth core-catcher sample taken from the cores of Hole 1170A and most of the core-catcher samples from Hole 1170D. In Hole 1170A, recovery of palynomorphs is good down to Sample 189-1170A-8H-CC, which is assigned to the lower Pliocene on the basis of calcareous microfossils. Unfortunately, below this horizon samples are palynologically barren. Recovery of palynomorphs is, in general, excellent in Hole 1170D, which is attributed to the middle Eocene to lower Oligocene on the basis of combined biostratigraphic information. Only the uppermost five core-catcher samples of Hole 1170D (189-1170D-1R-CC to 5R-CC) proved to be devoid of acid-resistant organic matter.

Hole 1170A

Dinoflagellate cysts (dinocysts) are the most abundant palynomorphs in Hole 1170A. Together with the record from Hole 1169A, these occurrences represent the southernmost late Neogene dinocysts found to date. Sporomorphs are also present in Samples 189-1170A-1H-CC and 4H-CC (Table **T10**). Foraminifer organic linings, common in age-equivalent samples from Holes 1168A and 1169A, are only present in trace abundances in productive samples from Hole 1170A.

T10. Distribution of organic walled dinocysts and sporomorph percentages, Hole 1170A, p. 141.

Pleistocene/uppermost Pliocene Sample 1169A-1H-CC yields a dinocyst assemblage dominated by *Nematosphaeropsis labyrinthea,* a cosmopolitan oceanic species. The few coexisting taxa are either indicative of the influence of relatively warm, oligotrophic water masses or of colder and more eutrophic water masses. The latter includes *Dalella chathamense,* a species endemic to the antarctic region. The underlying lower Pliocene Samples 189-1170A-4H-CC and 8H-CC, in contrast, yield poorly diversified dinocyst assemblages generally indicative of warm oligotrophic surface waters (abundant *Impagidinium aculeatum* and *I. paradoxum*). In Sample 189-1170A-8H-CC, some indications of the influence of colder water masses can be found in the occurrence of the cold to temperate *Corrudinium harlandii*. The range top of *Invertocysta tabulata* (2.65 Ma) between Samples 189-1170A-1H-CC and 4H-CC may assist the age assessment of this hole (Table **T11**). The consistent

T11. Useful stratigraphic dinocyst events, Holes 1170A and 1170D, p. 142.

occurrence of *C. harlandii* in the lower Pliocene in the region (cf. results from Sites 1168 and 1169), but distinct absence in the younger section, may prove to be a stratigraphically and palaeoenvironmentally useful event. The "mixed" assemblages, providing evidence for the varying influence of warmer and colder water masses, indicate a potential for future paleoceanographic studies involving dinocyst analysis; these may indicate former shifts in position of the subtropical convergence.

Hole 1170D

Palynomorphs are consistently present in great abundance from Sample 189-1170D-6R-CC down. Unfortunately, the uppermost three core-catcher samples are completely barren (189-1170D-1R-CC to 3R-CC), whereas samples from the silicified hard limestone of Samples 189-1170D-4R-CC and 5R-CC were not processed. Available smear slides and thin sections of these samples did not reveal the presence of palynomorphs. This aspect may indicate the inception of influence of well-oxygenated (bottom) water masses responsible for the oxidation of organic matter.

Dinocysts are the most abundant category of palynomorphs in productive samples from Hole 1170D and are assigned to the late middle Eocene to early Oligocene. In addition, pollen and spores, foraminifer organic linings, and acritarchs are present, albeit in low relative abundances, throughout Hole 1170D (Table T11). Palynomorphs are generally well preserved, and dinocyst concentrations are high, possibly in the order of >200,000 cysts/g in most samples. However, recovered assemblages are of relatively low diversity and are usually totally dominated by a single taxon. Terrestrial palynomorphs consistently are present in the middle Paleogene section (but in low relative abundances). The few identified taxa may be compared with established records from New Zealand and Australia and indicate cooling and increasing humidity from the middle middle Eocene into the late Eocene. Moreover, they are comparable to those reported by Mohr (1990) from ~age-equivalent sediments from across Antarctica.

The dinocyst assemblages throughout these sediments are indicative of the middle Eocene to earliest Oligocene (i.e., pre-O1b isotopic event of Zachos et al., 1996) and are composed of a mix of cosmopolitan and endemic taxa, with *Enneadocysta partridgei, Deflandrea phosphoritica,* allied morphotypes (including the presumed endemic *Deflandrea antarctica* and, occasionally, *Deflandrea cygniformis*), and/or *Thalassiphora pelagica* dominating the assemblages. High abundances of typical high-latitude Eocene representatives of *Vozzhennikovia, Alterbidinium,* and/or *Spinidinium* were increasingly found in the younger Eocene samples (cf. Wrenn and Hart, 1988) (Table T11). Such pulses of the latter taxa may indicate stepwise cooling of surface waters toward the Eocene–Oligocene transition.

Dinocyst Stratigraphy

As may be expected, Hole 1170D assemblages are quite comparable to those reported from the nearby upper middle to lower upper Eocene of Leg 29, Sites 280 and 281, and other sites on the STR (Haskell and Wilson, 1975; Crouch and Hollis, 1996; Truswell, 1997) and of western Tasmania continental margin sites (Truswell, 1997). They are also similar to those recorded from roughly age-equivalent sections from New Zealand (e.g., Wilson, 1985, 1988) and comparable to largely reworked

assemblages recorded from presumed Oligocene deposits in the CIROS-1 drill hole, McMurdo Sound, Antarctica (Wilson, 1989; Hannah, 1993). More surprisingly, the Hole 1170D assemblages are virtually identical to the approximate age-equivalent assemblages recorded by Mohr (1990) from Leg 113 drill sites from the opposite side of Antarctica (Weddell Sea) and from the outcrops in the Seymour Island region (Wrenn and Hart, 1988; Mao and Mohr, 1995). Moreover, they are similar to those reported by Goodman and Ford (1983) from the Eocene–Oligocene transitional strata from Leg 71 drill sites (Falkland Plateau). Furthermore, they bear a strong resemblance to coeval assemblages from Northern Hemisphere high-latitude sites like the Greenland Sea (Firth, 1996), Labrador Shelf, and Barents Sea (H. Brinkhuis, pers. observation).

Comparison of the dinocyst distribution in Hole 1170D with previous (Southern Ocean) studies, combined with the biostratigraphic compilation of Raine et al. (1997), indicates that the middle Eocene to lower(most) Oligocene succession is essentially continuous. The few age-diagnostic events in the relevant interval include the top and bottom of the *Enneadocysta* acme sensu Raine et al. (1997) (Samples 189-1170D-17R-CC and 36R-CC respectively; see Table **T11**). In addition, the LO of *Cerebrocysta bartonensis* and the first consistent occurrence of *Alterbidinium distinctum* appear to be stratigraphically useful events, occurring in Samples 189-1170D-12R-CC and 8R-CC, respectively. Age calibration of these events is, however, poor being based solely on high-latitude nannofossils. Despite this notion of stratigraphic usefulness, dinocyst datums are inconsistent with results from the calcareous nannofossil results in Hole 1170D.

On the basis of calcareous nannofossils, a hiatus of ~3.3 m.y. is inferred between Samples 189-1170D-12R-CC and 13R-CC. No breaks in the palynological record are apparent here; the horizon does coincide with the LO of *Pyxidinopsis waipawaense* (Sample 189-1170D-13R-CC), but otherwise, no change, either qualitative or quantitative, is recorded between these two samples. The range of *P. waipawaense* is poorly known; in its type area it first is present near the base of the middle Eocene (~49.5 Ma), whereas its extinction was not recorded (Wilson, 1988). Outside the type area, it has thus far only been recorded from Site 280 from the middle middle Eocene sediment; no calibration is available (Crouch and Hollis, 1996). In contrast to the nannofossils, the dinocysts indicate a nearly complete section from Sample 189-1170D-7R-CC downward. A minor hiatus may be recognized between Samples 189-1170D-6R-CC and 7R-CC, as discussed below.

Because the combined biostratigraphy of Hole 1170D indicates that the recovered succession is not older than ~43 Ma, the occurrences of *Wilsonidinium ornatum* and *Hystrichosphaeridium tubiferum* (including *H. truswelliae* morphotypes) are of interest. The (limited) available data indicate that these taxa have last occurrences at the base of the middle Eocene (at ~49.5 Ma; Wilson, 1988) or in the lower middle Eocene (at ~45 Ma), respectively (Bujak and Mudge, 1994). Occurrences of the former are, hence, taken to indicate a reworking of earliest Eocene materials into the middle Eocene. Records of *H. tubiferum* may indicate reworking of Upper Cretaceous to lower middle Eocene strata, because it first appears in the Upper Cretaceous. However, it may indicate that the taxon is longer ranging in the Southern Ocean than elsewhere. In addition, scattered occurrences of reworked lower and Upper Cretaceous dinocysts are recorded in samples from Hole 1170D (Table **T12**).

T12. Distribution of organic walled dinocysts and palynomorph group percentages, Hole 1170D, p. 143.

Eocene–Oligocene Transition

The combined shipboard biostratigraphies are also not in harmony where they come to the Eocene–Oligocene transition (viz., the interval from Samples 189-1170D-8R-CC to 6R-CC and higher [palynologically barren] samples [Figs. F11, F12]). In this case, potentially stratigraphically useful dinocyst criteria are the consistent occurrence throughout productive samples of Hole 1170D (and range tops) of *Enneadocysta partridgei* and the morphologically (extremely) similar *Areosphaeridium diktyoplokum*. It is surmised here that *E. partridgei* is, in fact, conspecific with *A. diktyoplokum,* which has a well-calibrated range top of 33.3 Ma (Brinkhuis and Biffi, 1993). *Enneadocysta partridgei* is here considered to represent a dorso-ventrally compressed variety of the latter (i.e., not partiform, as suggested by Stover and Williams [1995], but "compressed sexiform" as in *Areoligera* ["Gv"-cysts of Evitt, 1985]). The form appears to reflect an adaptation to conditions at higher latitudes since it also is present in Northern Hemisphere high-latitude Eocene strata (e.g., in the Barents Sea, H. Brinkhuis pers. observation). The present material has *E. partridgei* as the dominant morphotype. However, consistently, albeit in low abundances, the related taxa *A. diktyoplokum* and *Enneadocysta harrisii* are recorded as well. In the youngest productive samples from Hole 1170D, this group is joined by *Enneadocysta pectiniforme,* yet another related taxon, more typical for the lower Oligocene. The topmost productive sample yields representatives of all these taxa.

Since the LO of *A. diktyoplokum* is documented to be associated with the O1b isotopic event of Zachos et al. (1996) and calibrated to occur in Chron C13N in central Italy (Brinkhuis and Biffi, 1993), its demise was suggested to be linked to the onset of major antarctic glaciation (e.g., Brinkhuis and Visscher, 1995). The limited available data indicate that the *E. partridgei* morphotype has the same stratigraphic range as *A. diktyoplokum*. Reported post–33.3 Ma occurrences may be a result of reworking or should otherwise be suspect. Both bioevents may be useful to discriminate pre-O1b strata from younger sediments. Sample 189-1170D-6R-CC contains a few specimens of *E. partridgei, E. pectiniforme,* and *A. diktyoplokum,* which thus suggests either an age not younger than 33.3 Ma or that the specimens are reworked. This age (~33.3 Ma) contrasts with an age of ~31 Ma inferred from nannofossil assemblages in the same sample (see "Calcareous Nannofossils," p. 21).

There is a minor break in the palynological succession between Samples 189-1170D-6R-CC and 7R-CC. *Vozzhennikovia* spp. and *Spinidinium macmurdoense,* frequent in Sample 189-1170D-7R-CC, are not as abundant in Sample 189-1170D-6R-CC, whereas *Stoveracysta kakanuiensis* first appears in the latter sample. *Stoveracysta kakanuiensis* was described from the lower Oligocene of New Zealand (Clowes, 1985) but was suggested to range from the upper Eocene to lower Oligocene.

In summary, the present palynological information is difficult to reconcile with a presumed ~3-m.y. hiatus (including the marked cooling event of O1b over the Eocene–Oligocene transition). Furthermore, in sites around the Southern Ocean, where both nannofossil and dinocyst biostratigraphic information is available, the former consistently indicates an early Oligocene (implying post-O1b) age, whereas the palynology, including records of *A. diktyoplokum* and *E. partridgei,* would indicate an earliest Oligocene age at the youngest (cf. Goodman and Ford, 1983, with Wise, 1983, from Leg 29 and Mohr, 1990, with Wei and Wise, 1990, from Leg 113). Moreover, in all of these samples, and in other Southern Ocean cases, the overlying samples are conspicuously

barren of palynomorphs. It is proposed here that this absence of (acid resistant) organic matter is the result of the effects of well-oxygenated (bottom) waters associated with the development of the Antarctic Circumpolar Current, the cryosphere ("Icehouse" conditions), and the psychrosphere.

Paleoenvironment

The quantitative dinocyst distribution in the Eocene generally indicates somewhat restricted, eutrophic, neritic conditions throughout the succession. A generally eutrophic, restricted setting (possibly related to freshwater influences and/or coastal upwelling) may be indicated by (1) the relatively low species diversity (for middle Eocene times), (2) the high dominance of a single taxon in most samples, (3) the frequent dominance of peridinioid dinocysts like *Deflandrea phosphoritica, Vozzhennikovia* spp. (considered to represent mainly heterotrophic dinoflagellates; Brinkhuis et al., 1992), and (4) the near absence of typically open-marine coastal/neritic cysts like *Glaphyrocysta* spp., *Cordosphaeridium* spp., and so forth. The few open-marine taxa such as *Impagidinium* and *Spiniferites* spp. are quite rare.

From the combined onboard biostratigraphy, it appears that the succession below ~520 mbsf (from approximately Sample 189-1170D-12R-CC down) is unequivocally continuous and represents the interval between ~40/41? to 43 Ma. On the basis of the available core-catcher samples, an alternating pattern in the dominances of *E. partridgei* and *D. phosphoritica* group and common *T. pelagica* is apparent in this interval (Fig. **F15**). Interestingly, cross-correlation with the sedimentological (smear slide) data and the diatom, radiolarian, and calcareous nannofossil distribution suggests (1) a positive correlation between maxima in *Deflandrea* spp. with diatom maxima (see Figs. **F14, F15**) and most radiolarian maxima and (2) a positive correlation between maxima in calcareous nannoplankton content and *E. partridgei* maxima. Optima in *T. pelagica* immediately follow an *E. partridgei* maximum.

In addition, the Peridinioid/Gonyaulacoid (P/G) ratio (numbers of peridinioid cysts/numbers of gonyaulacoid cysts; not shown) mimics to a large extent the *Deflandrea* spp. percentage curve (Figs. **F14, F15**). The P/G ratio may be regarded to reflect the relative abundance of presumed heterotrophic dinoflagellates vs. the phototrophic ones: Extant *Protoperidinium* spp. feed primarily on diatoms; only few extant peridinioids have phototrophic lifestyles. The broadly positive correlation between the *Deflandrea* percentage maxima with the diatom abundance appears to support such a relationship. A similar result was obtained by Firth (1996), integrating dinocyst and diatom information from Hole 913B (Leg 151, Greenland Sea). In addition, all, except the lowermost, optima in radiolarian abundances also broadly correlate to these horizons (Fig. **F15**). Many representatives of this group also feed on diatoms. Most diatoms are noncolonial forms (C. Stickley, pers. comm., 2000).

The "*E. partridgei*-calcareous nannofossil" correlation may possibly be understood in terms of less eutrophic conditions, contrasting with highly eutrophic conditions associated with diatom and peridinioid maxima. *Thalassiphora pelagica* may be placed in an intermediate position in this scenario. There is evidence that *T. pelagica* represents dinoflagellates tolerant of strongly eutrophic conditions, often being found in conjunction with dysoxic and anoxic conditions ("black shales"; Köthe, 1990; Vonhof et al., 2000).

The record is likely to have a "third order" (~400–200 k.y.) resolution; the initial work demonstrates the potential for high-resolution quantitative palynology toward the paleoenvironmental interpretations of the middle to late Eocene of Hole 1170D and associated correlative strata in the area. Strong cyclicities are recorded as well in the physical properties record of this interval of Hole 1170D; these may well be compared and integrated with a future quantitative palynological record.

Age Model and Sedimentation Rates

The combined microfossil biostratigraphy at Site 1170 yielded 71 bioevents with age significance. Principal trends through this section are shown in Figure **F10.** Datums are from the combined microfossil bioevents from Holes 1170A and 1170D and 37 magnetic polarity datums (see **"Paleomagnetism,"** p. 36). The bioevents (Table **T13**) are comprised of 31 FO events, 39 LO events, and abundance events. All events are plotted according to their observed depths at Site 1170 and by their ages as defined in **"Biostratigraphy,"** p. 9, in the "Explanatory Notes" chapter. The FO events may have been placed too shallow and the LO events too deep because of the limited sampling interval. The stratigraphic positions of these datums may be refined with further study. More detailed bioevent data is provided in individual microfossil group discussions.

T13. Biostratigraphic events, p. 145.

Sedimentation at Site 1171 is punctuated by several hiatuses. Five clear hiatuses or condensed sections were encountered in the Neogene portion, and two possible hiatuses were seen in the Paleogene portion. The first 165 mbsf are well constrained by 29 bioevents and 19 magnetic polarity events. The average sedimentation rate is 2.6 cm/k.y. from the Pleistocene to the early late Miocene. Neogene event levels between microfossil groups agree fairly well, taking into consideration the large sampling interval. There are seven microfossil bioevents from three microfossil groups between 165 to 186 mbsf, indicating a condensed section in the upper Miocene. A condensed section was also present at Site 1169 in the upper Miocene and may represent a regional event.

High sedimentation rates (11.7 cm/k.y.) in the upper middle Miocene are truncated by a brief hiatus (~60 k.y.) marked by five closely spaced bioevents. Sedimentation through the remainder of the Miocene ranges from 1.0–2.6 cm/k.y. The sedimentation curve was based on the close agreement of 23 diatom, radiolarian, foraminifer, and paleomagnetic datums.

The Oligocene/Miocene boundary is marked by a 1-m.y. hiatus. The upper Oligocene is marked by a low sedimentation rate (0.88 cm/k.y.). A condensed section/hiatus encompasses the lower Oligocene/middle Oligocene boundary and is delineated by seven bioevents from three microfossil groups.

Sedimentation patterns from the lower Oligocene through the middle Eocene at the bottom of the hole have been interpreted in two ways. One interpretation (Figs. **F11, F12**) has two hiatuses, one within glauconitic clayey siltstones (lithostratigraphic Unit IV; see **"Lithostratigraphy,"** p. 9) across the Eocene/Oligocene boundary and one in the middle Eocene. The Eocene/Oligocene boundary interpretation is discussed in **"Calcareous Nannofossils,"** p. 21, and **"Palynology,"** p. 30. The middle Eocene hiatus is placed between Cores 189-1170D-12R to 14R based on calcareous nannofossil and dinocyst biostratigra-

phy. This hiatus corresponds to the subdivision between lithostratigraphic Subunits VA and VB (see "Lithostratigraphy," p. 9), and changes in physical properties are also seen in this interval (see "Physical Properties," p. 49). Sedimentation rates, based on the nannofossil interpretation, through the middle Eocene section are ~18.7 cm/k.y. The second interpretation of the dinoflagellate cyst biostratigraphy indicates a fairly continuous sequence through the lower Oligocene to middle Eocene (Figs. F11, F12). Sedimentation rates through the late Eocene–early Oligocene are 1.2 cm/k.y., increasing to 6.0 cm/k.y. in the middle Eocene (Fig. F10).

PALEOMAGNETISM

Introduction

After alternating-field (AF) demagnetization to 20 mT, the natural remanent magnetization (NRM) of whole-round sections from Site 1170 was measured at 5-cm intervals using the pass-through cryogenic magnetometer. An exception was made for cores whose liners or end caps were deformed, because these could damage the magnetometer. These cores were measured as archive-half cores. The nonmagnetic core barrel assembly was used for even-numbered cores in Holes 1170A and 1170C and for odd-numbered cores in Hole 1170B, starting with Core 3H. The comparison between results from cores collected with the nonmagnetic corer and with those from the standard corer is discussed the "Appendix" chapter, as are results of experiments investigating the effect of core splitting on magnetization and other coring-related magnetic experiments. However, it is noted here that (1) comparison of the NRM and 20-mT demagnetized whole-core results from Section 189-1170A-9R-1 revealed a strong downward-inclined drilling overprint and (2) comparison of Section 189-1170D-5R-1 before and after sawing revealed that the split archive-half had picked up a substantial moment that was not completely demagnetized by 20 mT. The Tensor tool is usually employed to orient the APC cores beginning with the third core at each hole, but the poor determination of the declination of the cores at this site precluded the orientation of cores.

Discrete oriented samples were routinely collected from Holes 1170A and 1170D. These were used to aid in the interpretation of the long-core record of magnetization by providing additional measurements of polarity and basic magnetic characterization. Most of the samples were demagnetized at 5, 10, 15, 20, 30, 40, and 50 mT to permit principal component analysis. For rock-magnetic characterization, anhysteretic remanent magnetization (ARM) was given in 0.2-mT DC and 200-mT AC fields and isothermal remanent magnetization (IRM) in a DC field of 1 T. Some discrete samples were progressively saturated up to 1.0 T to study the hardness of the IRM.

Results

Long-Core Measurements

The long-core measurements for the APC cores are presented in Figures F16, F17, and F18, which show inclination and intensity for Holes 1170A, 1170B, and 1170C. Strongly disturbed sections are indicated and can be recognized by their anomalously high negative inclination.

F16. Long-core measurements from 0 to 100 mbsf, p. 78.

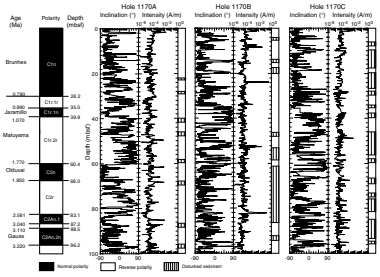

F17. Long-core measurements from 100 to 200 mbsf, p. 79.

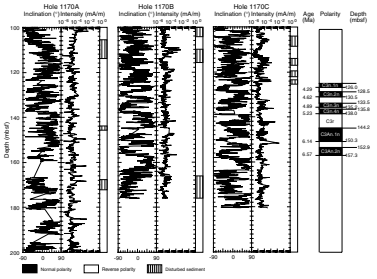

F18. Long-core measurements from 250 to 450 mbsf, p. 80.

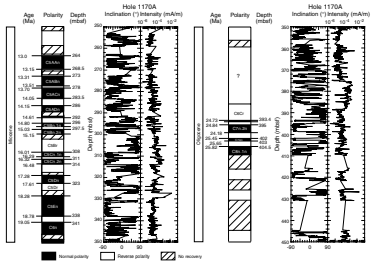

There are substantial lengths with an almost unbroken record of these high negative inclinations, which limited magnetostratigraphic work. The intensity of magnetization was between 10^{-5} and 10^{-4} mA/m. Even though measurements approached the background noise generated by core liners and the instrument's measurement threshold, a polarity record could be interpreted from distinctive patterns.

Hole 1170A was the least disturbed in the top 100 mbsf and afforded the best record of reversals. It was from this hole that the bulk of the magnetostratigraphy was interpreted. The Brunhes/Matuyama Chron boundary, the Jaramillo Subchron, the Olduvai Subchron, and the beginning of the Gauss Chron were all identifiable and provided a probable magnetostratigraphy for this first 100 mbsf (Fig. F16). Although individual features could be recognized in more than one hole, no consistent correlation between holes was achieved.

Below the first 100 mbsf in the APC cored interval, reversed inclinations in undisturbed sediments are seen in Cores 189-1170B-14H through 16H (Fig. F17). They appear to record the Gilbert Chron from 124 to 138 mbsf and below that the C3r Chron. Core 189-1170B-16H appears to contain the sequence of Subchrons C3An.1n to C3An.2n, which allowed the magnetostratigraphy to be established at this depth.

Below the APC cores, ~100 m of disturbed sediment with poor recovery precluded any further interpretation of magnetostratigraphy until a depth of ~250 mbsf was reached. There was better recovery below this depth with the improved coring conditions; hence, identification of a sequence of magnetozones from Subchron C5A.4n at 264 mbsf down to Chron C6n at 341 mbsf (Fig. F18) was possible. However, gaps in the record prevented the precise location of some chron boundaries. Near 400 mbsf, another section with recognizable magnetozones was found (Fig. F18). In Cores 189-1170A-43X and 44X, Subchrons C7n.1n, C7n.2n, C7An, and the termination of Subchron C8n.1n were identifiable.

Below 400 mbsf, identifiable chron boundaries were not observed. The core is dominantly normally magnetized over an interval of nearly 400 m. This suggests that either major remagnetization has taken place or there was a very high sedimentation rate. Comparison of the NRM and demagnetized results from Section 189-1170D-9R-1 demonstrated that the RCB coring imparts a steeply downward inclined moment, which is largely removed by 20-mT demagnetization (Fig. F19). Hence, the normal magnetization is not caused by the standard drill overprint. Another potential problem lies in the moment from the disturbed soft material between biscuits. To minimize this effect, the data were filtered and only sections which ranked <2 in the 0–5 scale of soft intervening material between the biscuits (see "Lithostratigraphy," p. 9) are shown in Figure F20. Even after this treatment, it was not possible to interpret this interval magnetostratigraphically. The origin of the normal moment bias remains unclear, but it is likely to come from the soft disturbed material between the biscuits, which carries a shallow normal magnetization.

Discrete Samples

The rock magnetic properties of the nannofossil oozes were similar over the depth of the APC coring. IRM intensities were on the order of 10^{-2} A/m, ARM intensities about one order less, and the NRM initially another order of magnitude lower at 10^{-4} A/m (Fig. F21). The ratio of ARM:IRM is not typical of single-domain grain sizes in magnetite;

F19. Long-core measurements for Section 189-1170D-9R-1 inclination and intensity before and after AF demagnetization, p. 81.

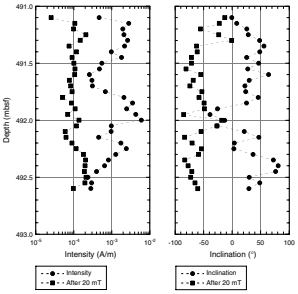

F20. Long-core measurements from 425 to 779.8 mbsf, p. 82.

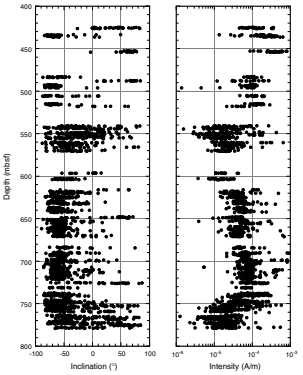

F21. Remanent magnetic characteristics of samples from nannofossil ooze, nannofossil chalk, and claystone, p. 83.

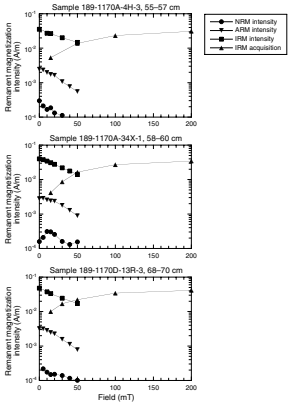

hence, we interpret that there is an important contribution from a detrital source rather than the dominantly biogenic magnetite found at Site 1168. The NRM was initially a downward-oriented drill moment, which was largely removed by 20 mT, revealing the polarity of the magnetization, although precise determinations of directions were precluded by the weak signal.

The rock-magnetic characteristics of the chalks obtained with XCB drilling were similar to those of the nannofossil ooze (Fig. F21), suggesting that lithification had not affected important changes in the magnetic fraction. The NRM was variable, with few samples showing analyzable results—largely because the small volume of the samples precluded good measurements.

The discrete samples from the silty claystone of Hole 1170D have consistent rock magnetic properties downcore. Moreover, they are similar to the characteristics of the nannofossil oozes and chalks (Fig. F21). This result suggests that they all have similar magnetic fractions, which in turn implies they all come from similar sources. It also suggests that the magnetic mineralogy is not likely to be varying substantially downhole, although this will have to be investigated during postcruise analysis.

There is some variation downhole that correlates roughly with magnetic susceptibility (see "Physical Properties," p. 49). Figure F22A shows the variation of ARM and IRM with depth, which peaks in lithostratigraphic Units IV and V. Parameters that serve as proxies for the coarse-and fine-grained magnetic fractions are shown as a function of depth in Figure F22B. The normalized fraction of IRM demagnetized between 0 and 20 mT is a measure of the coarsest fraction. In contrast, the normalized IRM acquired between 200 and 500 mT is a measure of the finest fraction. These two vary downhole, and the values cross at 300 m, reflecting a finer magnetic fraction in the upper part and a coarser fraction below.

F22. Variation of magnetic properties, Holes 1170A and 1170D, p. 84.

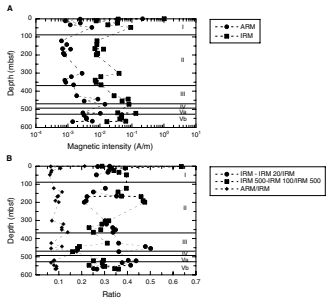

Magnetostratigraphy and Age-Depth Estimates

Using the reliable sections from Holes 1170A, 1170B, and 1170D, a magnetostratigraphy has been established (Table T14; Figs. F16, F17, F18). This has permitted an age-depth curve to be constructed (Fig. F23) that gives an estimate of sedimentation rates. It appears to indicate two different sedimentation rates—one from the Holocene down to the late Pliocene of 33 m/m.y. and a second of ~11 m/m.y. from the late Pliocene to the late Oligocene. A third, far greater sedimentation rate of 100 m/m.y. or more is likely in the Eocene section at the bottom of Hole 1170D, where we recorded a constant normal polarity corresponding presumably to a single polarity chron. From a purely magnetic viewpoint, this long magnetozone can be either Chron 20n or Chron 21n at ~45 Ma. Without a better sequence of reversals, we cannot determine the age reliably. If we accept the biostratigraphic constraints, it appears that the long normal magnetization is either Chron C20n or C21n. No matter which choice is made, it appears that sedimentation of ~100 m/m.y. is required. The final estimates of these sedimentation rates will be made in conjunction with the biostratigraphic data (see "Biostratigraphy," p. 19).

T14. Magnetostratigraphic results, p. 147.

F23. Age-depth relationship from paleomagnetic data, p. 85.

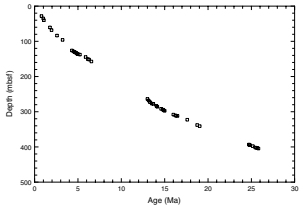

COMPOSITE DEPTHS

Multisensor track (MST) and spectral reflectance (L*) data collected from Holes 1170A, 1170B, and 1170C were used to align equivalent features between cores from different holes and determine the depth offsets in the composite section. Magnetic susceptibility, gamma-ray attenuation (GRA) bulk density, and spectral reflectance measurements were the primary parameters used for core-to-core correlation at Site 1170. GRA bulk density and magnetic susceptibility data were collected at 2-cm intervals on all APC cores recovered from Holes 1170A, 1170B, and 1170C. Spectral reflectance data were collected at 2-cm intervals on most of the APC cores from Holes 1170A, 1170B, and 1170C (see "Physical Properties," p. 49, and "Lithostratigraphy," p. 9, for details about MST and spectral reflectance data).

The data used to construct the composite section and determine core overlaps are presented on a composite depth scale in Figure F24. The depth offsets that comprise the composite section for the APC sections of Holes 1170A, 1170B, and 1170C are given in Table T15.

Many of the cores in the APC section in Holes 1170A, 1170B, and 1170C contain significant intervals of flow-in or are highly disturbed (See "Lithostratigraphy," p. 9, and the "Core Descriptions" contents page). This ubiquitous core disturbance, especially between 40 and 120 mcd (Cores 6H–13H in Holes 1170A, 1170B, and 1170C), made the construction of a composite APC section very difficult. Between 0 m composite depth (mcd) (top of the section) and 75 mcd (Core 8H in Holes 1170A, 1170B, and 1170C) all the cores could be placed into a composite framework, but often only one or two sections of a core could be utilized for the composite construction. In the lower portion of the APC section, all other cores were either too highly disturbed (e.g., Cores 12H and 13H in Holes 1170A, 1170B, and 1170C) or the MST and color reflectance data did not have sufficient or coherent signal amplitude to definitively tie features together between adjacent cores (e.g., Cores 14H–18H in Holes 1170A, 1170B, and 1170C). These cores were left in their original alignment with only a cumulative composite depth correction added to the original mbsf depth.

The construction of the composite section shows that, in general, cores from Hole 1170A were several meters shallower than equivalent cores in Hole 1170B (Table T15) and, thus, needed to be depth-shifted downward with respect to Hole 1170B. Cores from Hole 1170C, however, were several meters deeper than equivalent cores in Hole 1170B and were adjusted upward with respect to Hole 1170B (Table T15). Core 189-1170C-3H, although highly disturbed, appears to be a near duplicate of Core 189-1170C-2H and was depth shifted upward nearly 11 m in the composite section. Such duplication of section is not unexpected considering the rough sea state (large heave) during APC coring operations at this site (see "Operations," p. 8, for details) and the system of APC core extraction and advancement utilized by the drillers. Only after a third APC core does the drill pipe always remain in the original hole (especially in rough seas). The combination of a large heave and the pipe entering a new hole could easily result in the recoring of the upper sedimentary section.

The depth offsets determined for the upper 70 mcd of Holes 1170A, 1170B, and 1170C are consistent with paleontological evidence. Most nannofossil, radiolarian, and foraminiferal datums (see "Biostratigraphy," p. 19) present in all three APC holes fall within the same 9.5-m

F24. Smoothed spectral reflectance, magnetic susceptibility, and GRA bulk density data, Holes 1170A, 1170B, and 1170C, p. 86.

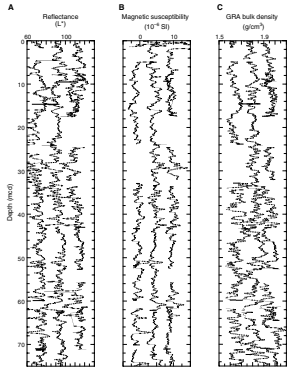

T15. Composite depth section for the APC interval, p. 148.

interval (the resolution of the datums) in the composite section. Exceptions include the FO of the radiolarian *Pseudocubus vema* and the FO of the foraminifer *Globorotalia truncatulinoides*. No amount of reasonable depth shifting of cores resulted in the alignment of these datums in the composite section. The FO of *G. truncatulinoides* is problematic at this site, though, often yielding ages that are discordant with the calcareous nannofossils. Specimens of *G. truncatulinoides* are very rare and, when present, are diminutive with thin, transparent shells (see "Biostratigraphy," p. 19).

Paleontological evidence also supports a rough composite section alignment for Cores 14H through 17H in Holes 1170A, 1170B, and 1170C (Table T15). Radiolarian (the last consistent occurrence of *Stichocorys delmontensis*), foraminiferal (the FO of *Globorotalia puncticulata*), and nannofossil (the LO of *Discoaster loeblichii*) datums present in cores in all three holes in this part of the section are in good agreement when the cores are aligned using the cumulative composite depth correction added to the original mbsf depth. Multisensor track data and spectral reflectance data, however, do not have sufficient signal amplitude or coherency to definitely tie the cores together. Thus, the alignment of cores in this section may be off by as much as 1–3 m.

Stretching and compression of sedimentary features in aligned cores indicate distortion of the cored sequence. Because significant distortion occurred within individual cores on depth scales of <9 m, it was not possible to align every feature in the MST and color reflectance records accurately by simply adding a constant to the mbsf core depth. Core-scale changes will require postcruise processing to align smaller sedimentary features. Only after allowing variable adjustments of peaks within each core can an accurate estimate of core gaps be made.

Following construction of the composite depth section for Site 1170, a noncontinuous spliced section was constructed for the upper 71 mcd. Cores from Hole 1170A were used as the backbone for the splice, with cores from Hole 1170B and, to a lesser extent, Hole 1170C used to cover intervals between gaps in cores from Hole 1170A. Intervals having significant disturbance or distortion were avoided when possible. The moderately disturbed portions of Core 189-1170B-3H, however, were used in the splice. Gaps between Cores 189-1170A-3H and 4H and between Cores 189-1170A-5H and 6H could not be spanned by cores from Holes 1170B and 1170C. Below 70 mcd, core disturbance or low signal variability precluded construction of a spliced section. The Site 1170 splice (Table T16) does not represent a continuous section and should only be used as a crude sampling guide for high-resolution studies conducted on the upper portion of the APC interval.

T16. Splice tie points, p. 149.

ORGANIC GEOCHEMISTRY

The shipboard organic geochemistry program at Site 1170 included studies of volatile hydrocarbons, total organic and inorganic carbon, total nitrogen, total sulfur, and hydrogen and oxygen indexes. Rock-Eval pyrolysis, CNS analysis, gas chromatography, and carbon coulometry were performed (see "Organic Geochemistry," p. 20, in the "Explanatory Notes" chapter).

Sedimentary Geochemistry

Results

Carbonate ($CaCO_3$) content values for the strata sampled at Site 1170 range from 0 to >95 wt% (Fig. F25; Table T17). In general, the carbonate distribution exhibits a two-tiered profile; sediments from 776 to ~470 mbsf commonly contain <2 wt% $CaCO_3$ (except for a distinct excursion with a value of ~90 wt% at ~590 mbsf), whereas values of $CaCO_3$ content abruptly increase to mostly >80 wt% above 470 mbsf. Within the upper high carbonate content strata, $CaCO_3$ content values fluctuate between 75 and 90 wt% from ~460 to 370 mbsf. From ~370 to 100 mbsf, carbonate content is mostly >90 wt%. From here, carbonate content values exhibit an overall decrease (ranging from ~<60 to 85 wt%) to ~20 mbsf; above 20 mbsf, values increase to ~80–90 wt%.

The total organic carbon (TOC) content for most intervals at Site 1170 is <1 wt%, although deposits below ~600 mbsf contain up to 2 wt% TOC (Fig. F25; Tables T17, T18). Note that TOC content values determined by Rock-Eval pyrolysis and CNS analysis provide similar TOC content profiles, although the absolute values differ for each method. Total nitrogen content ranges from 0 to 0.17 wt% (Fig. F25; Table T17), with the highest values occurring below ~600 mbsf; nitrogen content covaries with TOC content (Fig. F25). From ~754 to 476 mbsf, total sulfur content ranges from 0.25 to ~2.9 wt% (Fig. F26; Table T17). Above ~476 mbsf, the total sulfur profile shows an abrupt decrease, although no reliable data were obtained above ~425 mbsf. We calculated C/S ratios for the deepest strata at the site assuming that all of the sulfur exists as pyrite. The C/S values <2 are generally considered representative of marine environments, whereas the C/S values >5 indicate relatively freshwater environments (Berner and Raiswell, 1984). See "Discussion," p. 54, for the implications of these ratios.

Organic matter type was assessed using Rock-Eval pyrolysis and CNS analyses. In general, high hydrogen index (HI) (>~200) and low oxygen index (OI) (<~150) values from Rock-Eval pyrolysis are indicative of marine (Type II) or lacustrine (Type I) organic matter (Espitalié et al., 1977; Peters, 1986), whereas C/N ratios of ~5–8 are generally considered to indicate marine organic matter (Bordovskiy, 1965; Emerson and Hedges, 1988). The H/C ratios provide information similar to that provided by the Rock-Eval pyrolysis HI; H/C values >1 in this study indicate the presence of lipid-rich organic matter, likely of marine affinity. In contrast, terrestrially derived organic matter (Type III) exhibits relatively low HI and high OI values, C/N ratios of ~25–35, and relatively low H/C ratios. Oxidized Types I and II organic matter may show HI and OI values similar to Type III organic matter; very low HI and OI values are characteristic of Type IV highly oxidized organic matter.

The HI values from Rock-Eval pyrolysis range from 0 to 800 mg of hydrocarbon per gram of TOC at Site 1170 (Fig. F25; Table T18). The highest HI values are in sediments above 100 mbsf and from ~350 to 435 mbsf; horizons containing values >150 also exist between ~530 and 670 mbsf. The OI values vary between 0 and >10000 mg of CO_2 per gram of TOC. The T_{max} values obtained from Rock-Eval pyrolysis range from 300° to 590°C (Fig. F27), although the most reliable T_{max} values cluster between 420° and 435°C. The T_{max} provides an estimate of organic matter thermal maturity, with values <435°C indicative of immaturity relative to petroleum generation. The "oil window" is generally

F25. Plots of carbonate, total organic carbon, total nitrogen, C/N and H/C ratios, and hydrogen index values p. 87.

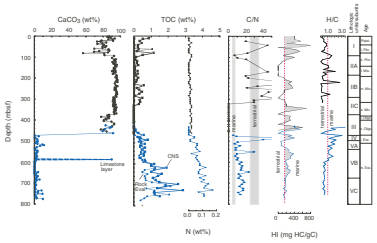

T17. Values for inorganic carbon, calcium carbonate, total carbon, total organic carbon, total nitrogen, total sulfur, and hydrogen in sediments, Hole 1170A, p. 150.

T18. Results of Rock-Eval pyrolysis analyses on sediments, Hole 1170A, p. 154.

F26. Total sulfur contents compared to C/S ratios, p. 88.

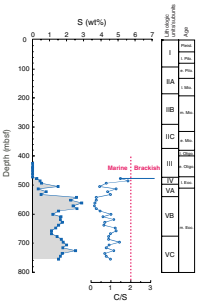

F27. T_{max} values generated from Rock-Eval pyrolysis analyses of organic matter, p. 89.

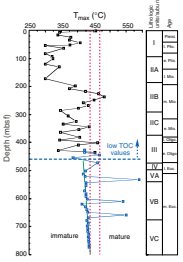

considered to range between T_{max} values of 435° and 465°C, whereas values >465°C are indicative of thermogenic gas zones (Espitalié et al., 1977; Peters, 1986).

The extremely low TOC content values obtained from Rock-Eval pyrolysis in the upper part of the sediment (to ~480 mbsf) at Site 1170 lower the reliability of HI and OI values in this interval. We performed replicate analyses on many of the samples to validate the results. The HI values and C/N ratios (discussed immediately below) exhibit similar trends, which suggests that most of our results are consistent. However, total nitrogen contents above ~480 mbsf in the core are very low, so C/N ratios must also be considered with care. The generally high OI values through much of the core are here attributed to the thermal degradation of calcium carbonate during pyrolysis and are not considered in this interpretation.

Discussion

The high carbonate content of the Oligocene through Holocene sediments at Site 1170 mainly reflects dominance of calcareous nannofossils (see **"Biostratigraphy,"** p. 19); this observation is similar to those made for Sites 1168 and 1169. The overall upward increase in carbonate content through the core is a direct consequence of a change from shallow marine to pelagic open-ocean conditions (also see **"Biostratigraphy,"** p. 19). However, although the transition from carbonate-poor to carbonate-rich sediments is gradual at Site 1168, the change is abrupt at Site 1170. This observation implies either a rapid change in depositional environments or, more likely, the presence of a hiatus(es) or condensed section(s) in the stratigraphic record here.

Two general modes of carbonate and TOC preservation are observable in the sediment from Site 1170 (Fig. **F25**). High carbonate content values generally correspond to sediments with low TOC content values, whereas low carbonate-content sediment contains a range of TOC content values including the highest values observed at the site. Middle Eocene sediments with high TOC and low $CaCO_3$ contents exist between ~460 mbsf and the base of Hole 1170A. Here, common to abundant ichnofossils (see **"Lithostratigraphy,"** p. 9) and Th/U ratios >2 (see **"Downhole Measurements,"** p. 52) suggest a dysoxic to oxic seafloor, so it is unlikely that anoxic conditions can be invoked to describe the higher sedimentary organic carbon content in this interval. At Site 1168, high TOC–low $CaCO_3$ sediments were suggested to represent preferential preservation (enhanced burial rate?) of organic matter, or enhanced organic matter delivery associated with higher clastic sediment flux (or both); these processes were most likely active in the middle Eocene at Site 1170.

The organic matter type encountered provides some insight into depositional processes. Sediments from ~690 to 776 mbsf (lithostratigraphic Subunit VB) contain a terrestrial component of preserved organic matter (HI values <130 and C/N ratios >20). As described above, this interval contains generally low $CaCO_3$ content and the highest TOC values from the site. These attributes likely were formed by enhanced clastic and terrestrial organic matter delivery to the site. Zones of increased carbonate content (up to 9 wt%) observable from ~730 mbsf to the base of the hole appear to contain some marine organic matter, and therefore, may represent episodes of marine-dominated sedimentation with lower terrestrial organic matter inputs to the seafloor. These characteristics are compatible with observations of di-

noflagellate cyst assemblages dominated by *Enneadocysta partridgei,* a dinoflagellate apparently often associated with nannofossils (see **"Biostratigraphy,"** p. 19). Of note are the lithologic descriptions of carbonate-rich horizons through the interval from ~710 to 740 mbsf (see **"Lithostratigraphy,"** p. 9). Total sulfur values and C/S ratios suggest dominantly marine conditions through this interval at Site 1170 (Fig. **F26**).

A shift from mixed terrestrial-marine to marine-influenced conditions is indicated by organic matter (type) and carbonate preservation between ~650 and 690 mbsf at Site 1170, as well as palynological studies (see **"Biostratigraphy,"** p. 19). Here, total sulfur and C/S values again suggest deposition under marine conditions. Note that TOC content decreases through this marine organic matter interval, supporting the suggestion that terrestrial organic matter delivery dominated total organic matter content in these sediments (including the underlying strata from 690 to 776 mbsf); *E. partridgei* again dominates the dinoflagellate cyst assemblage here (see **"Biostratigraphy,"** p. 19). From ~650 to 620 mbsf, TOC content increases to >1 wt%, corresponding to a shift to lower HI values indicating increased terrestrial organic matter delivery to the seafloor. From ~620 to 585 mbsf, TOC decreases to <0.5 wt%. Here, abundant glauconite was observed during lithologic descriptions of Site 1170 (see **"Lithostratigraphy,"** p. 9). Through this interval, a prominent limestone bed is observable on the carbonate content profile, and at least one horizon of increased carbonate content was noted in the lithologic descriptions between ~630 and 640 mbsf (see **"Lithostratigraphy,"** p. 9); the dinoflagellate assemblage in each of these horizons is again dominated by *E. partridgei* (see **"Biostratigraphy,"** p. 19). The presence of these relatively carbonate-rich horizons within a mostly carbonate-poor marine section (below ~460 mbsf at Site 1170) suggests the possibility of higher-frequency marine to terrestrially influenced fluctuations than those resolved by our analyses.

From ~585 to 460 mbsf, carbonate content displays a slight overall increase and marked fluctuations between ~0.5 and 5 wt% $CaCO_3$. These variations are likely attributable to variations in calcareous nannofossil content noted through this interval (see **"Lithostratigraphy,"** p. 9). The TOC values decline to ~0.5 wt% and are dominated by marine organic matter preservation. A horizon from ~585 to 530 mbsf displays the strongest marine signature based on organic matter type (highest HI values), the highest total sulfur content, and C/S ratios indicative of marine depositional conditions. This horizon overlies the prominent limestone bed at ~585 mbsf. Interestingly, the dinoflagellate cyst assemblage for this interval is dominated by deflandreoids, a group associated with the presence of diatoms (see **"Biostratigraphy,"** p. 19). Marine organic matter preservation is interrupted by an episode of reduced HI values from ~500 to 530 mbsf, suggestive of terrestrial organic matter preservation. This suggestion is not supported by C/N and H/C ratios, however. Again, abundant glauconite was noted in the lithologic descriptions (see **"Lithostratigraphy,"** p. 9) in this zone of apparent terrestrial organic matter preservation. The interval from ~500 to 520 mbsf also exhibits a relative increase in carbonate content (to >10 wt% $CaCO_3$), C/S ratios, *E. partridgei* content, and an overall decrease in total sulfur content, although sulfur values increase to >1.5 wt% at the top of the interval. A return to dominantly marine organic matter preservation is observed from ~500 to 460 mbsf. Here, the C/S values increase toward the brackish salinity realm. These observations suggest rapidly

changing environmental conditions during deposition and early diagenesis of this upper Eocene interval.

Above ~460 mbsf, the extremely high carbonate contents (up to 95 wt%) represent either a reduction in clastic input or enhanced carbonate preservation and may indicate enhanced biogenic productivity. The extremely low TOC content through this portion of the core may record settling of organic matter through a well-mixed water column and/or to a well-oxygenated seafloor. The HI values vary widely, and the C/N ratios show a wide range of values from 0 to >40. The apparent variations in organic matter type may record variations in seafloor redox conditions, although we cannot discount the possibility of limited terrestrial input to the system. Of note in this regard are the elevated TOC values (>1 wt%) at ~53 mbsf on the Rock-Eval pyrolysis profile and at ~72 mbsf on the CNS profile. Here, pyritized vitrain (i.e., "woody" material) was observed in the core; this observation is supported by a Type III organic matter characterization by Rock-Eval pyrolysis. Intervals containing high HI and low C/N values may record preservation of residual marine organic matter perhaps associated with carbonate producers (see **"Biostratigraphy,"** p. 19). Relatively high C/N and low HI intervals may represent oxidized marine organic matter in which N- and H-bearing functional groups have been cleaved to produce a more refractory, carbon-rich residuum. Alternatively, the high C/N and low HI units may represent total oxidation of labile marine organic matter and subsequent preservation of minor quantities of refractory terrestrial residuum.

The T_{max} values obtained from Rock-Eval pyrolysis are interpreted to represent mostly immature organic matter (Fig. **F27**). In the upper half of the core, T_{max} values fluctuate through the maximum possible range observed at Site 1170. This wide range is attributed to extremely low TOC content and the mixed marine-oxidized character of organic matter, which can generate an erroneously large range in T_{max} values. In the lower half of the core, by contrast, the T_{max} values gradually smooth out and exhibit a sloping linear trend from ~420° to 435°C with depth. We consider these values as valid because they were obtained from horizons containing at least 0.5 wt% TOC composed of Type I organic matter; note, however, that Type I organic matter can generate erroneously low T_{max} values.

Volatile Hydrocarbons

Results

Concentrations of volatile hydrocarbon gases were measured from every core using the standard ODP headspace-sampling technique and gas chromatographic analysis. Profiles of methane content and various methane and heavier volatile hydrocarbon ratios are presented in Figure **F28** (also see Table **T19**). Within the upper ~480 m of the cored sediment section, methane only occurred in minor concentrations (0 to 1027 ppmv). From 480 to ~545 mbsf, methane concentrations increased to a pronounced peak of ~32,200 ppmv. Below 545 mbsf, methane concentrations exhibited a pronounced decrease to values of <1000 at ~570 mbsf, and then they steadily increased to a high value of ~66,500 ppmv at a depth of ~700 mbsf. Relatively high methane concentrations (>20,000 ppmv) were observed from here to the base of Hole 1170D. The ratio of methane vs. ethane and propane (C_1/C_2+C_3) showed maximum values above ~500 mbsf and decreased gradually to

F28. Methane concentrations, methane vs. ethane and propane ratios, and percent wetness from headspace gas analysis, p. 90.

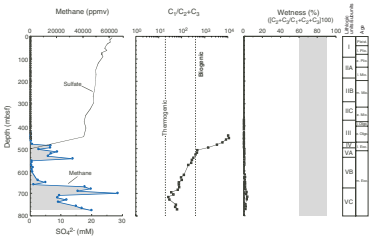

T19. Headspace gas composition, p. 156.

<30 at ~725 mbsf. The percent wetness is below 4% through the core, thus falling below the range of values typical for economically viable gas reservoirs.

Discussion

The low gas content of the uppermost 480 m of Site 1170 is nearly identical to those in the stratigraphically equivalent headspace-gas profiles generated for Sites 1168 and 1169. At those sites, the low gas content was suggested to be a function of two characteristics of the sediment that also partially explain the gas profiles at Site 1170. First, the sediments contain very little organic matter as a source of natural gas. Second, pore-water profiles show that appreciable SO_4^{2-} exists in Oligocene and younger strata, so sulfate reduction processes may be limiting the onset of methanogenesis at these sites.

Below ~480 mbsf at Site 1170, methane content increases to a broad multipeaked zone of high concentrations through to the base of the hole. The C_1/C_2+C_3 ratios above ~545 mbsf indicate that this gas has a biogenic origin. This abrupt change from low to high methane-containing sediment corresponds to a sharp gradient to zero pore-water sulfate (Fig. **F28**). These observations suggest the presence of a barrier to diffusional pore-water processes (see **"Inorganic Geochemistry,"** p. 46). Lithologic descriptions indicate the presence of lithified glauconitic sands and an abrupt upward change from these "greensands" to limestone and chalk through this section of the core (see **"Lithostratigraphy,"** p. 9); each of these lithologies could serve as a permeability barrier. The presence of small amounts of methane within the zone of relatively high pore-water sulfate concentrations (between ~425 and 480 mbsf) suggests that minor quantities of methane are migrating across this barrier.

Beneath the zone of relatively elevated biogenic methane content, methane concentrations and C_1/C_2+C_3 values show an overall decrease, followed by an increase in methane content with correspondingly low C_1/C_2+C_3 values. The C_1/C_2+C_3 ratios approach the thermogenic range near the base of Hole 1170D. Headspace samples analyzed on the natural gas analyzer from ~670 mbsf to the base of the hole, include butane (C_4), pentane (C_5), and hexane (C_6), indicative of a thermogenic origin for this gas (Hunt, 1996). Hinz et al. (1986) postulated an early to middle Eocene source rock for thermogenic gas observed on the western Tasmania continental slope, which is consistent with the middle Eocene age (see **"Biostratigraphy,"** p. 19) of the thermogenic gas-containing strata at Site 1170.

The T_{max} values approaching 435°C at the base of Hole 1170D are indicative of the top of the "oil window." Of further import to the thermal maturity of the strata in Hole 1170D is the observation of double S_2 peaks (attributed to the presence of bitumen [Clementz, 1979]) on most Rock-Eval pyrograms from ~530 mbsf to the base of the hole. Fluorescence observed in core material treated with acetone near the base of Hole 1170D suggests the presence of liquid hydrocarbons (Shipboard Scientific Party, 1995), although the fluorescence was more likely derived from acetone soluble portions of the bitumen. The likely presence of bitumen and thermogenic gases suggests that the lower portions of Hole 1170D have been subject to some thermal maturation. The core depths at which maturation is postulated to have occurred are low, suggesting an alternate heat source to burial maturation.

INORGANIC GEOCHEMISTRY

A total of 41 whole-round samples were collected at Site 1170 (30 from Hole 1170A and 11 from Hole 1170D) for interstitial water (IW) analysis at the following frequency: three per core in the upper 60 m, one per core from 60–100 mbsf, and one every third core to total depth. Only 33 of the IW samples were used for shipboard analyses; the balance of samples from the upper 60 mbsf of the hole were archived for shore-based analyses. Results of the IW analyses are reported in Table T20 and Figure F29.

T20. Interstitial water data, p. 158.

F29. Concentration-depth profiles for interstitial water chemistry, p. 91.

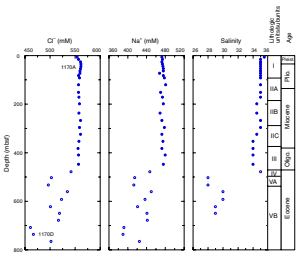

Chloride, Sodium, and Salinity

Chloride (Cl^-), sodium (Na^+), and salinity concentrations show little variation in the upper ~450 mbsf at Site 1170 (Fig. F29A). The exception is a 1.4% increase in Cl^- from 556 mM in the uppermost sample to 562 mM centered at ~40 mbsf. This increase in Cl^- is followed by a decrease to ~557 mM at ~80 mbsf. Below ~450 mbsf, Cl^- concentration profiles are highly variable and less than seawater values. Chlorinity values reach a minimum of 461 mM at 707 mbsf, a 17% decrease from mean seawater values.

The sharp boundary in the concentration profiles between ~450 and 470 mbsf is coincident with the base of lithostratigraphic Unit III, near the Eocene–Oligocene transition (see "Biostratigraphy," p. 19, and "Lithostratigraphy," p. 9). The Unit III/IV boundary is defined by the transition from glauconitic sandstones to overlying well-lithified nannofossil limestones. The apparent chemical decoupling of the Cl^- and Na^+ profiles above and below the boundary, as well as with other porewater constituents, suggests a lack of diffusional communication across this boundary. Based on the location of the chemical discontinuity, which will be referred to informally as the "boundary" throughout the remainder of this section, we infer that the very hard limestones, which are also a major excursion on the velocity profile (see "Physical Properties," p. 49), are acting as a diffusional barrier.

The existence of low-Cl^- waters at depth on the STR, as well as on the western Tasmania margin ~400 km to the north of Site 1170, has implications for the origin of these fluids. If the source of the low-Cl^- fluid at the two sites is related, then it is unlikely that the fluid is derived externally (i.e., advection of meteoric fluids) because of the large distances between the sites and, in particular, the distal location of Site 1170 relative to any reasonable meteoric source. Instead, the presence of low-Cl^- fluids at both sites suggests similar internal processes. Previously, we postulated that the following were possible internal sources for low-Cl^- fluid: (1) gas hydrate dissociation, (2) dehydration reactions of hydrous minerals, such as clays and biogenic opal, and (3) clay membrane ion filtration. At both Sites 1168 and 1170, the presence of low-Cl^- fluids coincides with older parts of the sedimentary section (connate fluids?) and, in particular, with the onset of methanogenesis and, hence, may be linked, perhaps by water expelled during the organic matter maturation process. However, at present we cannot eliminate any of the aforementioned hypotheses.

Sulfate, Ammonium, Alkalinity, and pH

Sulfate decreases gradually from seawater values to 17.4 mM, an ~40% reduction. Below the boundary, sulfate has been completely consumed, whereas methane displays a corresponding increase (Fig. F29B). Alkalinity increases to a maximum of 5.6 mM in the upper 450 mbsf and is highly variable below the boundary, varying from 2.2 to 5.7 mM. The pH decreases downcore in the upper 300 mbsf but increases slightly to the boundary. Below the boundary, pH varies conversely with alkalinity, reaching a maximum of 8.0 at 707 mbsf. Ammonium steadily increases downcore to 450 mbsf, below which the trend continues to increase to a maximum of ~1600 µM but is more variable than above 450 mbsf.

The major changes in the SO_4^{2-}, NH_4^+, and alkalinity profiles are largely a function of microbially mediated organic matter degradation. The higher TOC content of the Eocene sediments below the boundary (see "Sedimentary Geochemistry," p. 41), combined with the diffusional barrier above, leads to complete sulfate reduction, methanogenesis, and continued production of NH_4^+ in this interval. The dramatically sharp break in the sulfate and methane profiles between 450 and 470 mbsf provides excellent evidence for a diffusional barrier near the Eocene–Oligocene transition.

Silica

Dissolved silica concentrations range from 561 to 1235 µM in the upper 450 mbsf with distinct shifts at 120 (negative) and 295 mbsf (positive) (Fig. F29B). Below the boundary, $H_4SiO_4^0$ drops precipitously to <200 µM, decreasing to a minimum of 23 µM at the base of the hole.

The distinct shifts in $H_4SiO_4^0$ in the pore fluids correspond to shifts in biogenic silica abundance in the sediments (see "Biostratigraphy," p. 19, and "Lithostratigraphy," p. 9). The rapid decrease across the boundary is likely a response to the overall decrease in biogenic silica associated with the dramatic shift in depositional environments across the boundary. In addition, opal-CT was noted in many of the XRD patterns of samples below 450 mbsf. Therefore, the lower $H_4SiO_4^0$ values in the lower 470 mbsf may also be the result of recrystallization of opal-A to opal-CT as previously observed (e.g., Baker, 1986), although Gieskes (1981) noted that a significant decrease in $H_4SiO_4^0$ content usually does not occur until the opal-CT to quartz transition.

Calcium and Strontium

Calcium and Sr^{2+} increase with depth in the upper 400 mbsf, reaching a maximum of 15.5 mM and 969 µM, respectively, between 300 and 400 mbsf (Fig. F29C). Below the boundary at ~450 mbsf, Sr^{2+} sharply decreases to a uniform value of ~325 µM. Conversely, Ca^{2+} concentrations remain elevated relative to standard seawater below the boundary, varying between 13.2 and 14.6 mM.

The increase in Sr^{2+} and Ca^{2+} values with depth in the upper part of the sedimentary section, where the sediments are composed principally of nannofossil ooze, is likely the result of dissolution and/or recrystallization of calcite. If the profiles are solely the result of calcite dissolution, then we would not expect the observed increase in Sr^{2+}/Ca^{2+} ratios because the proportion of Ca^{2+} input would be much greater (Fig. F30)

F30. Concentration-depth profile of Sr^{2+}/Ca^{2+} and interstitial water Ca^{2+} plotted vs. weight percent $CaCO_3$, p. 94.

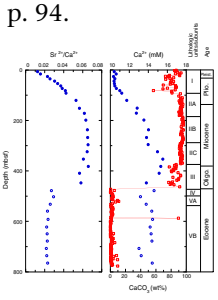

(Baker et al., 1982). Unlike most of the other IW constituents, Ca^{2+} does not show a shift across the diffusional barrier, which suggests dissolution of a Ca-rich phase(s) or exchange reactions occurring both above and below the boundary. Because there is very little carbonate in the sediments and pore-water Sr^{2+} is low below the boundary (Fig. F29C), it seems unlikely that the elevated Ca^{2+} in the lower part of the cored interval is derived from calcite dissolution. Elevated pore-water Ca^{2+} content (and decreasing Mg^{2+} and K^+; see "Magnesium, Potassium, and Lithium," p. 48,) has been previously attributed to volcanic matter alteration (e.g., Lawrence et al., 1975). Smear-slide analysis noted the presence of volcanic glass in various stages of preservation in Hole 1170D, (see "Lithostratigraphy," p. 9), and alteration of this glass may be the source of Ca^{2+} in these carbonate-poor sediments.

Magnesium, Potassium, and Lithium

Magnesium (Mg^{2+}) and potassium (K^+) concentrations decrease steadily from the topmost sample to the base of lithostratigraphic Unit III at ~460 mbsf (Fig. F29C). At the boundary, the Mg^{2+} and K^+ profiles are marked by an abrupt decrease (36.5 to 22.4 mM for Mg^{2+} and 8.8 to 5.0 mM for K^+). Below the boundary, Mg^{2+} and K^+ continue to decrease to the base of the hole reaching minimums that are ~73% less than normal seawater. Lithium (Li^+) concentrations are uniformly low (<60 µM) in the upper 450 mbsf, decreasing to <10 µM between ~50 and 200 mbsf. Below the boundary, Li^+ concentrations sharply increase to ~400 µM and remain uniform at this concentration to the base of the cored interval.

As at the previous sites, the decreases in Mg^{2+} and K^+ are highly correlated ($r = 0.995$). We interpreted the decreasing concentration profiles at Sites 1168 and 1169 to indicate that Mg^{2+} and K^+ were being consumed at depth, likely associated with silicate reactions. The sharply decreasing profiles across the boundary generally support that hypothesis. However, Mg^{2+} and K^+ do increase significantly (28% and 20%, respectively) above the boundary within the largely pelagic sediments. Because there appears to be virtually no diffusional communication across the boundary, the decrease in Mg^{2+} and K^+ suggests there is a sink, presently unrecognized, for these elements in the upper 450 mbsf. A typical Mg^{2+} sink in carbonate-rich sediments is dolomitization; however, no dolomite has been observed in smear-slide or XRD analyses. In addition, we do not expect significant dolomitization in pore fluids with appreciable SO_4^{2-} and low alkalinities (Baker and Kastner, 1981; Compton, 1988).

The presence of a diffusion barrier provides insights into the location of sources and sinks for Li^+ that were not apparent in the profiles from the previous sites. The decrease in Li^+ concentration to values lower than seawater between ~50–200 mbsf indicates that an active Li^+ sink exists in this depth interval, although the nature of the sink is unknown. In contrast to the smooth Li^+ profile observed at Site 1168, the much higher Li^+ contents below the diffusional boundary at Site 1170 suggest that the major source of Li^+ to the IW is likely from silicate phases and not from biogenic carbonates. This observation is also compatible with silicate reactions consuming Mg^{2+} and K^+ below the boundary, which also may be related to volcanic matter alteration.

Summary

The fortuitous location of the diffusional boundary near the transition between the siliciclastic and pelagic sediments provides important insights into the location of sources and sinks for many of the porewater constituents that were not apparent at the previous sites. In essence, the diffusional barrier isolates reactions occurring in the siliciclastic sediments and the section below the cored interval vs. the younger pelagic sediments. The Eocene organic-rich, clayey glauconitic siltstones and sandstones are the major source for Li^+ and probably the low-Cl^- fluids. In addition, Mg^{2+} and K^+ are being consumed by reactions in these same sediments and/or the section below the cored interval. The bulk of sulfate reduction in the sedimentary sequence occurred in these Eocene organic-rich siliciclastics. Not surprisingly, the primary source for dissolved silica and Sr^{2+} are the pelagic sediments. A Li^+ sink is also present within the nannofossil ooze and chalks. Calcium is being released to the waters from the pelagic sediments and, surprisingly, from the siliciclastics as well. Another surprise provided by the presence of the boundary is the considerable sink for Mg^{2+}, K^+, and Li^+ in the pelagic sediments. The origin of these unexpected sources and sinks is unknown at present.

PHYSICAL PROPERTIES

The physical properties program at Site 1170 included MST and thermal conductivity measurements of whole-round cores and compressional wave (*P*-wave) velocity, moisture and density (MAD), and vane shear-strength measurements of split cores. The Adara tool was deployed once in Hole 1170C for in situ temperature measurements.

Multisensor Track

All core sections from Holes 1170A, 1170B, 1170C, and 1170D were measured on the MST (for magnetic susceptibility, *P*-wave velocity, GRA density, and natural gamma ray) at 2-cm intervals. *P*-wave velocities were recorded at 2-cm intervals in Hole 1170A to a depth of ~163.8 mbsf. *P*-wave velocities were not recorded in the XCB-cored sections. Natural gamma-ray emission was measured at 20-cm intervals in Hole 1170D only.

The downcore changes in magnetic susceptibility (Fig. **F31A**) correlate well with the lithostratigraphic units (see **"Lithostratigraphy,"** p. 9). The glauconite-rich sediments of Unit IV and Subunit VA have the highest values in the magnetic susceptibility curve. The natural-gamma radiation record (Fig. **F31C**) also shows a good correlation with the magnetic susceptibility profile (especially for the lithostratigraphic Subunit VB), reflecting the increased terrigenous fraction deeper in the section recovered at Site 1170. Magnetic susceptibility (Fig. **F31A**) is negatively correlated with GRA and discrete bulk density (Fig. **F31B**) in both carbonate-rich and clay-rich intervals of the hole, except the lower 120 m of lithostratigraphic Subunit VB.

Discrete and GRA density data correlate well, with both data sets reflecting the sediment compaction and dewatering associated with increased overburden (Fig. **F31B**). All first-order features of density variations correlate with other physical parameters and lithostratigraphic units. GRA values are higher than discrete density values in carbonate-

F31. Magnetic susceptibility, GRA density, wet bulk density, and natural gamma ray vs. depth, Holes 1170A and 1170D, p. 95.

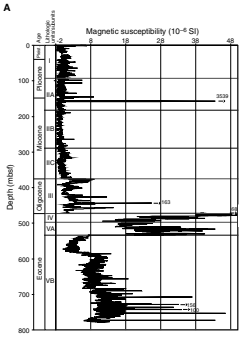

rich sections (between ~93 and 373 mbsf). The calibration procedure for the GRA density is optimized for mixed sediments and thus overestimates densities in carbonate-rich sediments. GRA density is lower than discrete density in the RCB cores from Hole 1170D (425 mbsf to total depth [TD]). The GRA density data reduction software assumes a full core liner. RCB cores do not generally fill the liner, and thus, the GRA density in RCB cores is underestimated.

The GRA density profile has a good first-order correlation with the *P*-wave velocities in the upper part of the hole (Fig. **F32**). *P*-wave velocity, however, decreases at 120 mbsf and remains particularly low to 300 mbsf (cf. Figs. **F31B, F32**). This decline in velocity may be a result of the changes from APC to XCB coring and from wire cutting to the sawing of the core. The latter process introduces water into the core, lowering its *P*-wave velocity. When sediments become more lithified, they are influenced less by additional water from core splitting and values are more representative.

Acoustic Velocity

Compressional velocities were obtained on the split-core sections at a sampling interval of one per section in cores from Holes 1170A and 1170D to a depth of ~754 mbsf (PWS3; x-direction) (Figs. **F32, F33;** Tables **T21, T22**). Wherever possible, discrete velocity was measured in longitudinal directions (PWS1; z-direction down to ~80 mbsf for Hole 1170A); transverse directions were recorded in some cores only (PWS2; y-direction between 77 and 116 mbsf for Hole 1170A).

A comparison of the continuous MST velocity profile and the discrete values for the interval between 0 and 165 mbsf is shown in Figure **F32.** All data sets correlate well and reflect the normal increase in density with depth. Within lithostratigraphic Unit I, acoustic velocity increases with depth below seafloor from values slightly higher than seawater velocity to average values of 1600 m/s (PWS1) (Figs. **F32, F33**). Velocity is variable within Unit I, with high values associated with relatively darker, clay-bearing layers, and low values associated with lighter, carbonate-rich layers. In the upper 200 m of Unit II (Subunits IIA and IIB), velocity increases slightly with depth. Acoustic velocity increases by 150 m/s across the ooze–chalk transition at 300.8 mbsf. Over this transition a slight increase in magnetic susceptibility and a decrease in carbonate content (see **"Organic Geochemistry,"** p. 40) is also observed. The well-lithified limestone at the base of lithostratigraphic Unit III near the Eocene–Oligocene transition (see **"Lithostratigraphy,"** p. 9) is characterized by acoustic velocities as high as 3790 m/s. The relatively loose and less lithified glauconite-rich green silts and sands of lithostratigraphic Unit IV (see **"Lithostratigraphy,"** p. 9) have lower *P*-wave velocities. Measurements of sediment cubes cut from the limestone horizons within lithostratigraphic Unit V have velocities of ~3900 m/s (Fig. **F33**).

Thermal Conductivity

Thermal conductivity was measured on Section 3 of each core in Hole 1170A to a depth at which induration prevented insertion of the needles (~170 mbsf) (Fig. **F34;** Table **T23**). Values generally increase with depth, corresponding to a downhole decrease in porosity (Fig. **F35**).

F32. *P*-wave velocities measured for discrete samples and in whole cores vs. depth, Hole 1170A, p. 98.

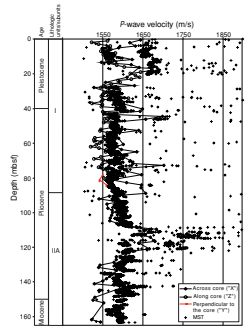

F33. *P*-wave velocities (PWS3) measured for discrete samples vs. depth, Holes 1170A and 1170D, p. 99.

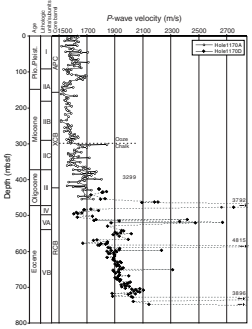

T21. *P*-wave velocities measured at discrete intervals, Hole 1170A, p. 159.

T22. *P*-wave velocities measured at discrete intervals across the core, Hole 1170D, p. 161.

F34. Thermal conductivity measured on whole cores vs. depth, Hole 1170A, p. 100.

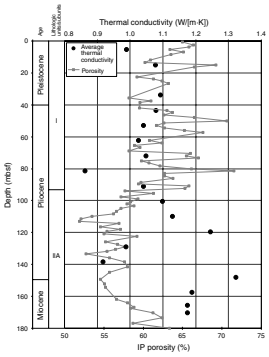

In Situ Temperature Measurements

The Adara tool was deployed once at Site 1170 and this deployment yielded an acceptable temperature record. The temperature at the seafloor (2.28°C) was determined using the mudline stops. Examination of the penetration temperature records indicates a normal deployment.

Heat Flow

The geothermal gradient was determined using the two points of the temperature profile (Fig. F36). Although there are only two control points, the solution of the least-squares regression gives a geothermal gradient of 52°C/km, which is similar to the 58°C/km gradient at Site 1168 (see "Physical Properties," p. 45, in the "Site 1168" chapter). Data for both sites show higher values than the Cape Sorell No. 1 exploration well (27°C/km) on the continental shelf 100 km to the northeast (Willcox et al., 1989). The average of the thermal conductivities measured from 0 through 180 mbsf in Hole 1170C is 1.083 W/(m·K). Using the average conductivity and the geothermal gradient, a heat flow of 56 mW/m² is calculated. This heat-flow value is nearly twice that of values reported from sedimentary basins and slopes near western Tasmania (north of the site) and Mesozoic continental margins in the mid-Atlantic (~40 mW/m²; see "Physical Properties," p. 45, in the "Site 1168" chapter).

Undrained Shear Strength

One measurement of vane shear strength was taken per section in Hole 1170A to the depth at which induration prevented insertion of the vane (~310 mbsf at the ooze–chalk transition). The results are displayed in Figure F37 and Table T24. Undrained shear strength increases with depth in the upper 60 mbsf from 20 to 30 kPa. The shear strength data show an overall increase with depth, but with high variability. In sediments where carbonate controls the deformation behavior (>50 wt% $CaCO_3$; Lee, 1982), shear strength increases with carbonate content. Variations in shear strength between 93 and 310 mbsf reflect the varying carbonate content of the nannofossil oozes with a good overall correlation to the GRA density (Fig. F37).

Moisture and Density

Bulk density generally increases with depth below seafloor, whereas porosity and water content decrease (Fig. F35; Table T25). These general trends vary in the sediment section with changes in the slope of the property-depth functions that are associated either with changes in sedimentation rates, diagenetic boundaries, or unconformities. The data for the discrete wet bulk density (Fig. F35) correlate very well with the GRA data and can be used to calibrate and correct GRA density (see "Multisensor Track," p. 49; Fig. F31B).

Summary

Major variations in physical properties were used to assist in defining the lithostratigraphic boundaries. For example, the carbonate-rich lithostratigraphic Unit II is characterized by an upper subunit (IIA) with relatively high density, *P*-wave velocity, shear strength, and thermal

T23. Thermal conductivity measured on whole core sections, Hole 1170A, p. 162.

F35. Wet bulk density, water content, and porosity measured at discrete intervals vs. depth, p. 101.

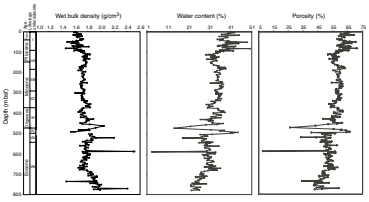

F36. Temperature vs. depth, p. 102.

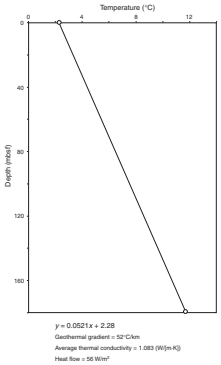

F37. Undrained shear strength from miniature vane-shear measurements and GRA density vs. depth, Hole 1170A, p. 103.

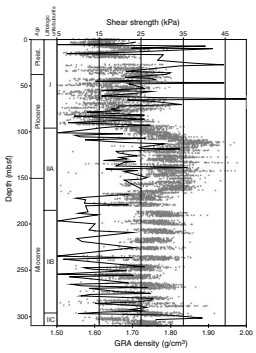

T24. Undrained shear strength from miniature vane-shear measurements, Hole 1170A, p. 163.

T25. Index properties measured at discrete intervals, p. 164.

conductivity but low porosity and water content, and a lower subunit (IIB) with low density, *P*-wave velocity, shear strength, and thermal conductivity but high porosity and water content. The lowermost subunit (IIC) in Unit II is characterized by relatively high density, *P*-wave velocity, shear strength, and thermal conductivity but lower porosity and water content (cf. Figs. **F31A, F33A, F34, F37, F35**). Water content and porosity correlate well and mirror the pattern of the magnetic susceptibility curve for the Eocene Subunit VA and for the upper part of Subunit VB.

DOWNHOLE MEASUREMENTS

Logging Operations

Downhole logging was conducted in Hole 1170D after it had been drilled to a depth of 780 mbsf with a 9.785-in drill bit. The basal 355 m was cored, whereas the upper 425 m of the hole was drilled ahead with a center bit (see **"Operations,"** p. 8). The presence of indurated limestone horizons above and below an unconsolidated glauconitic sand unit between 474 and 529 mbsf led to the decision to log the hole in two parts. The pipe was initially set at 529.2 mbsf to insure that TD was achieved by each of the tool strings. After a wiper trip (see **"Downhole Measurements,"** p. 47, in the "Site 1168" chapter) and displacing the hole with sepiolite mud, the RCB bit was released in preparation for logging.

Three tool-string configurations were run, the triple combo, the GHMT-sonic, and the FMS-sonic (see **"Downhole Measurements,"** p. 27, in the "Explanatory Notes" chapter). The dipole shear sonic imager (DSI) was run in combination with both the GHMT and the FMS in order to compare the quality of sonic data from different tool-string configurations. In combination with the GHMT, the DSI was run in P and S, upper and lower dipole mode (see Schlumberger, 1995). With the FMS-sonic tool string, the DSI was initially run in P and S, upper dipole mode. However, because of problems with data acquisition during this tool run, the DSI was discontinued after two aborted attempts to log the formation (see **"Results/Data Quality,"** p. 52). The weather was moderate and heave was typically between 3 and 4 m. Occasionally heave increased sufficiently to cause the wireline heave compensator to stroke out, which occurred once during each pass of the triple combo and GHMT-sonic tool strings.

Upon completion of logging operations in the bottom portion of the hole, the wireline tools were rigged down and the drillers attempted to raise the pipe to ~200 mbsf for the second stage of logging. However, after removing two stands of pipe, the drillers were unable to raise the drill string above 468 mbsf. After trying unsuccessfully to free the drill string, the pipe was severed at 317 mbsf, preventing any logging in the upper section of the hole (see **"Operations,"** p. 8). Details of the intervals logged, together with the position of the pipe and the depth of the seafloor, are shown in Figure **F38.**

Results/Data Quality

The principal results are shown in Figures **F39, F40, F41.** Borehole conditions were excellent. No ledges or obstructions were encountered and, with one exception, caliper readings from both the triple-combo

F38. Details of the logging operations, Hole 1170D, p. 104.

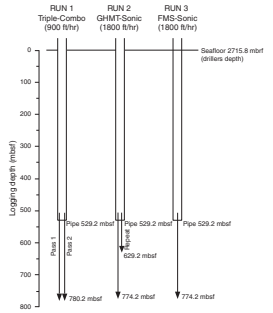

F39. Caliper, gamma-ray, resistivity, and magnetic susceptibility values, Hole 1170D, p. 105.

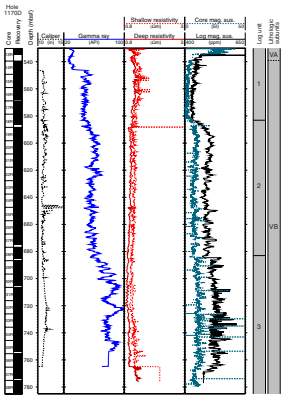

F40. Velocity, density, porosity, and photoelectric effect values, Hole 1170D, p. 106.

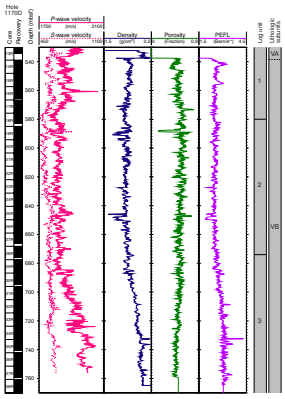

and FMS tool strings show a smooth borehole with a diameter typically between 10.5 and 12 in (Fig. F39). The one exception can be seen at ~645–650 mbsf, where the borehole width rapidly increased to a maximum value of 16.6 in. This washout corresponds to a decrease in natural gamma, resistivity, sonic velocity, and density values and to an increase in porosity values (Figs. F39, F40). The excellent hole conditions over the rest of the interval resulted in particularly good measurements in the contact tools such as density, porosity, and FMS.

Density and porosity values tend to increase and decrease respectively downhole, implying increased lithification with depth. A comparison between core and log density (Fig. F42) shows that log values are consistently higher than the core results and that this discrepancy increases with depth, perhaps because of core expansion when it is unloaded. Density porosity, neutron porosity, and core porosity values show generally good agreement downhole (Fig. F43). However, the slight offset between density porosity and neutron porosity increases below ~683 mbsf, at the log Unit 2/3 boundary (see "Log Units," p. 53). This may be caused by the increased influence of organic material and terrestrial clays (see "Discussion," p. 54) on the neutron porosity values because the neutron tool fails to differentiate between hydrogen in pore spaces and hydrogen bound in clays and organic matter.

Although heave was significant enough to shut down the heave compensator during each pass of the first two tool strings, subsequent passes of each string covered the intervals lacking active heave compensation during the original passes. Heave also affected the FMS raw data, resulting in apparently constant conductivity over depth intervals as the tool stalled its ascent; however, routine processing removed most of the problems.

The GHMT total field measurements were within the acceptable range, and the susceptibility log shows all of the same fine-scale structure as the core measurements from the MST track, which should allow a core-log correlation capable of determining more precisely the core gaps and postcoring expansion (see "Downhole Measurements," p. 47, in the "Site 1168" chapter).

The only major lithologic variation within the logged interval was a distinct limestone horizon at 589 mbsf, which is recognizable as a strong minimum in porosity and natural gamma radiation and a maximum in resistivity corresponding to a white stripe in the FMS image (Fig. F44). This limestone horizon can be clearly identified at 589 mbsf in both the neutron and core porosities (Fig. F43), indicating that there is very little depth mismatch between the two data sets at this point. The limestone is also evident in the core densities (Fig. F42) and core sonic velocities (Fig. F45), although it can not be identified in the log densities (Fig. F42) and log sonic velocities (Fig. F45). Log sonic velocities are typically 50–100 m/s below those measured in the core. The higher discreet sample values may be the result of a natural sampling bias toward consolidated (higher velocity) vs. unconsolidated (lower velocity) layers because they are less likely to biscuit or crack during coring and splitting, resulting in an overestimate of the mean core velocities.

Log Units

Log units have been differentiated mainly by using natural gamma-ray and magnetic susceptibility data, with sonic velocity, density, photoelectric effect (PEFL), and resistivity data showing similar but more

F41. Total gamma-ray and spectral gamma-ray values, Hole 1170D, p. 107.

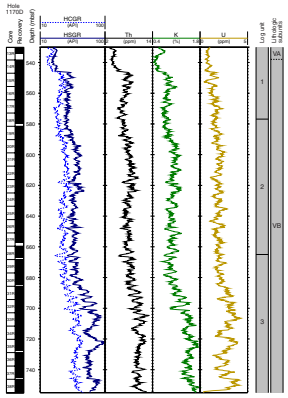

F42. Downhole log bulk density plotted with core bulk density, p. 108.

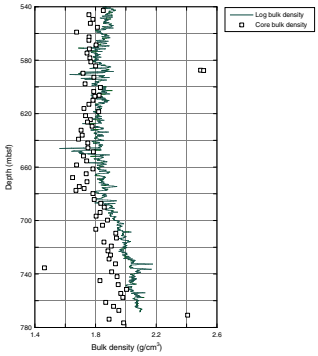

F43. Downhole density porosity and neutron porosity plotted with core porosity, p. 109.

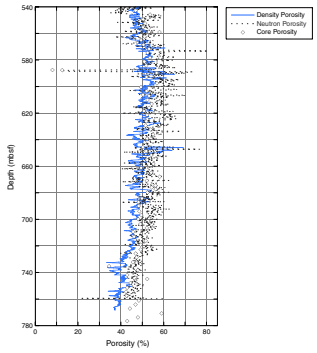

subtle changes over the unit boundaries. Three log units have been identified, even though the core results categorize all but the top 9 m of this interval as lithostratigraphic Subunit VB (see "Lithostratigraphy," p. 9).

Log Unit 1: Base of the Pipe (529 mbsf) to 583 mbsf

Magnetic susceptibility and natural gamma-ray values remain relatively low and show the smallest amplitude of variability within this unit (436 ± 9 ppm and 48 ± 2 API, respectively). In addition, resistivity and sonic velocities are generally higher than in Unit 2 below.

Log Unit 2: 583–683 mbsf

Magnetic susceptibility and natural gamma values increase between 583 and 595 mbsf, where they level off and vary about a mean of 492 ± 14 ppm and 58 ± 4 API, respectively, until the base of logging Unit 2. Porosity shows a strong minimum and spherically focused resistivity (SFLU) shows a distinct maximum at ~589 mbsf, near the top of Unit 2, correlative with the indurated limestone horizon recovered in the core (see "Results/Data Quality," p. 52).

Log Unit 3: 683 mbsf–Base of the Hole

The most marked change in log parameters is below 684 mbsf, where the mean and variance of magnetic susceptibility and gamma-ray values increase to 527 ± 21 ppm and 80 ± 8 API, respectively. Furthermore, mean density and PEFL values increase toward the base of this unit, whereas porosity shows a minor decrease downhole.

Discussion

The three log units described above appear to correlate with a general downhole trend toward a higher terrigenous component in the sediments. This trend is illustrated well by the magnetic susceptibility and Th log data (Fig. F46), both of which usually vary as a function of the detrital component. Fluctuations in the magnetic susceptibility and Th data also appear to correlate with downhole variations in the TOC of the sediment (Fig. F47), suggesting that the increases in TOC are associated with the input of terrigenous material. Increased magnetic susceptibility, Th, and TOC values also tend to correlate with Rock-Eval pyrolysis index values, indicative of mainly terrestrially derived organic carbon (see "Organic Geochemistry," p. 40) implying that the periodic increases in sediment TOC are caused by higher fluxes of terrestrial rather than marine organic matter. Interestingly, U values do not covary with the TOC above ~675 mbsf (Fig. F47). Uranium tends to be adsorbed by organic matter (Adams and Weaver, 1958) and, therefore, could be expected to show a correlation with TOC.

The spectral gamma-ray data from this site are also of considerable interest because they show a pronounced cyclicity, particularly between ~660 and 715 mbsf (Fig. F46). The Th data, which contain the clearest cyclicity, have a dominant peak with a wavelength centered on 4.1 m. Although it is tempting to relate such regular periodicity to an orbital frequency, preliminary biostratigraphic analyses from the base of Hole 1170D (see "Biostratigraphy," p. 19) indicate that sedimentation rates may have been as low as ~7.1 cm/k.y. (dinoflagellate dates) or as high as

F44. FMS image from the top of log Unit 2 with caliper, SGR, SFLU, and APLC data from the triple combo, p. 110.

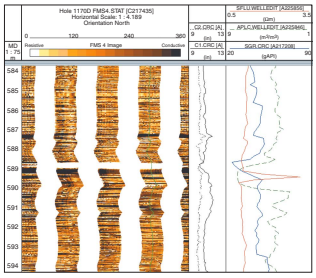

F45. Downhole *P*-wave velocities from the logs plotted with the *P*-wave velocities measured vertically on half cores, p. 111.

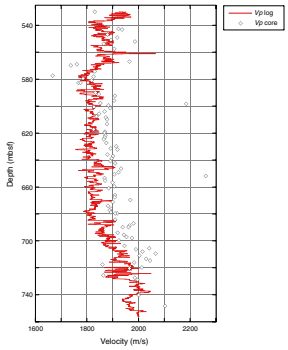

F46. Spectral gamma-ray data and preliminary spectral analysis from Hole 1170D, p. 112.

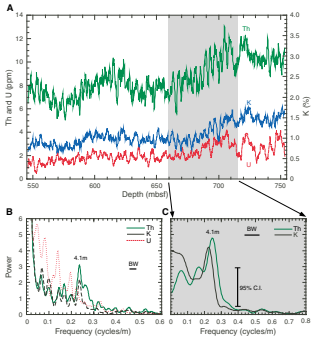

~23 cm/k.y. (nannofossil dates). Such a high range in possible sedimentation rates makes it impossible to assign a particular Milankovitch periodicity to the spectral gamma-ray cycles at this stage. For example, a 4.1-m cycle in the sediments could be related to obliquity if sedimentation rates were ~10 cm/k.y., or precession if sedimentation rates were closer to 20 cm/k.y.

The *P*-wave velocity data recorded by the DSI in Hole 1170D have been combined with *P*-wave velocities measured in the cores from Holes 1170A and 1170D to produce an integrated traveltime data set for this site. These data can be used to show a graph of increasing two-way traveltime vs. depth and also to plot the *P*-wave velocities against time, for comparison with the seismic section (Fig. **F48**). The two major spikes in *P*-wave velocity at ~474 and ~529 mbsf are caused by the presence of indurated limestone horizons (see **"Physical Properties,"** p. 49). These spikes probably correspond to the two main reflectors in the seismic section (Fig. **F48**). The fact that calculated traveltimes to these two spikes in *P*-wave velocity differ considerably from the traveltimes to the two reflectors in the seismic section (Fig. **F48**) suggests that the core measurements underestimate true sonic velocities over at least part of the interval. One explanation for this could be that the unconsolidated carbonate sediments from the uppermost ~350 m of the core have undergone considerable expansion or have been adversely affected by rotary coring and cutting with the saw during section splitting. The noticeable drop in core sonic velocities at the switch over to XCB drilling and saw splitting supports this hypothesis (see **"Physical Properties,"** p. 49).

F47. Magnetic susceptibility, Th, total organic carbon, hydrogen index value, and U data, Hole 1170D, p. 113.

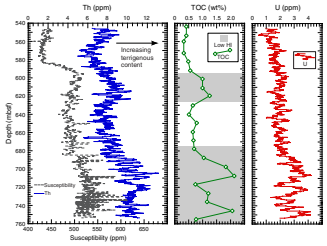

F48. Time/depth, sonic velocity, and seismic data, p. 114.

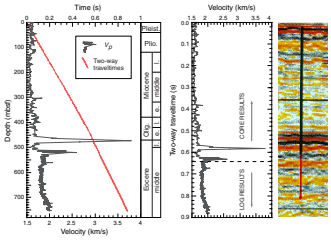

REFERENCES

Adams, J.A.S., and Weaver, C.E., 1958. Thorium-to-uranium ratios as indicators of sedimentary processes: example of concept of geochemical facies. *AAPG Bull.,* 42:387–430.

Baker, P.A., 1986. Pore-water chemistry of carbonate-rich sediments, Lord Howe Rise, Southwest Pacific Ocean. *In* Kennett, J.P., von der Borch, C.C., et al., *Init. Repts. DSDP,* 90 (Pt. 2): Washington (U.S. Govt. Printing Office), 1249–1256.

Baker, P.A., Gieskes, J.M., and Elderfield, H., 1982. Diagenesis of carbonates in deep-sea sediments: evidence from Sr^{2+}/Ca^{2+} ratios and interstitial dissolved Sr^{2+} data. *J. Sediment. Petrol.,* 52:71–82.

Baker, P.A., and Kastner, M., 1981. Constraints on the formation of sedimentary dolomite. *Science,* 213:215–216.

Berggren, W.A., Kent, D.V., Swisher, C.C., III, and Aubry, M.-P., 1995. A revised Cenozoic geochronology and chronostratigraphy. *In* Berggren, W.A., Kent, D.V., Aubry, M.-P., and Hardenbol, J. (Eds.), *Geochronology, Time Scales and Global Stratigraphic Correlation*. Spec. Publ.—Soc. Econ. Paleontol. Mineral. (Soc. Sediment. Geol.), 54: 129–212.

Berner, R.A., and Raiswell, R., 1984. C/S method for distinguishing freshwater from marine sedimentary rocks. *Geology,* 12:365–368.

Bordovskiy, O.K., 1965. Accumulation and transformation of organic substances in marine sediment, 2. Sources of organic matter in marine basins. *Mar. Geol.,* 3:5–31.

Breza, J.R., and Wise, S.W., Jr., 1992. Lower Oligocene ice-rafted debris on the Kerguelen Plateau: evidence for East Antarctic continental glaciation. *In* Wise, S.W., Jr., Schlich, R., et al., *Proc. ODP, Sci. Results,* 120: College Station, TX (Ocean Drilling Program), 161–178.

Brinkhuis, H., and Biffi, U., 1993. Dinoflagellate cyst stratigraphy of the Eocene/Oligocene transition in central Italy. *Mar. Micropaleontol.,* 22: 131–183.

Brinkhuis, H., Powell, A.J., and Zevenboom, D., 1992. High-resolution dinoflagellate cyst stratigraphy of the Oligocene/Miocene transition interval in north-west and central Italy. *In* Head, M.J., and Wrenn, J.H. (Eds.), *Neogene and Quaternary Dinoflagellate Cysts and Acritarchs*. Am. Assoc. Stratigr. Palynol. Found., 219–258.

Brinkhuis, H., and Visscher, H., 1995. The upper boundary of the Eocene Series: a reappraisal based on dinoflagellate cyst biostratigraphy and sequence stratigraphy. *In* Berggren, W.A., Kent, D.V., Aubry, M.-P., and Hardenbol, J. (Eds.), *Geochronology, Time Scales and Global Stratigraphic Correlation*. Spec. Publ.— Soc. Econ. Paleontol. Mineral. (Soc. Sediment. Geol.), 54:295–304.

Bujak, J.P., and Mudge, D.C., 1994. A high-resolution North Sea Eocene dinocyst zonation. *J. Geol. Soc. London,* 151:449–462.

Cande, S.C., Stock, J.M., Muller, R.D., and Ishihara, T., 2000. Cenozoic motion between east and west Antarctica. *Nature,* 404: 145–150.

Chamley, H., 1989. *Clay Sedimentology:* Berlin (Springer-Verlag).

Clementz, D.M., 1979. Effect of oil and bitumen saturation on source-rock pyrolysis. *AAPG Bull.,* 63:2227–2232.

Clowes, C.D., 1985. *Stoveracysta,* a new gonyaulacean dinoflagellate genus from the Upper Eocene and Lower Oligocene of New Zealand. *Palynology,* 9:27–35.

Compton, J.S., 1988. Degree of supersaturation and precipitation of organogenic dolomite. *Geology,* 16:318–321.

Crouch, E.M., and Hollis, C.J., 1996. Paleogene palynomorph and radiolarian biostratigraphy of DSDP Leg 29, Sites 280 and 281, South Tasman Rise. *Inst. Geol. Nucl. Sci., Sci. Rep,* 96/19.

Diester-Haass, L., Robert, C., and Chamley, H., 1993. Paleoceanographic and paleoclimatic evolution of the Wedell Sea (Antarctica) during the middle Eocene-late Oligocene, from coarse sediment fraction and clay mineral data (ODP Site 689). *Mar. Geol.,* 114:233–250.

————, 1996. The Eocene-Oligocene preglacial-glacial transition in the Atlantic sector of the Southern Ocean (ODP Site 690). *Mar. Geol.,* 131: 123–149.

Ehrmann, W.U., 1991. Implications of sediment composition on the southern Kerguelen Plateau for paleoclimate and depositional environment. *In* Barron, J., Larsen, B., et al., *Proc. ODP, Sci. Results,* 119: College Station, TX (Ocean Drilling Program), 185–210.

Emerson, S., and Hedges, J.I., 1988. Processes controlling the organic carbon content of open ocean sediments. *Paleoceanography,* 3:621–634.

Espitalié, J., Madec, M., and Tissot, B., 1977. Source rock characterization method for petroleum exploration. *Proc. Annu. Offshore Technol. Conf.,* 3:439–443.

Evitt, W.R., 1985. *Sporopollenin dinoflagellate cysts*. Am. Assoc. Stratigr. Palynol. Found.

Exon, N.F., Moore, A.M.G., and Hill, P.J., 1997. Geological framework of the South Tasman Rise, south of Tasmania, and its sedimentary basins. *Aust. J. Earth Sci.,* 44:561–577.

Firth, J.V., 1996. Upper middle Eocene to Oligocene dinoflagellate biostratigraphy and assemblage variations in Hole 913B, Greenland Sea. *In* Thiede, J., Myhre, A.M., Firth, J.V., Johnson, G.L., and Ruddiman, W.F. (Eds.), *Proc. ODP, Sci. Results,* 151: College Station, TX (Ocean Drilling Program), 203–242.

Gieskes, J.M., 1981. Deep-sea drilling interstitial water studies: implications for chemical alteration of the oceanic crust, layers I and II. *In* Warme, J.E., Douglas, R.G., and Winterer, E.L. (Eds.), *The Deep Sea Drilling Project: A Decade of Progress*. Spec. Publ.—Soc. Econ. Paleontol. Mineral., 32: 149–167.

Goodman, D.K., and Ford, L.N., Jr., 1983. Preliminary dinoflagellate biostratigraphy for the middle Eocene to Lower Oligocene from the Southwest Altantic Ocean. *In* Ludwig, W.J., Krasheninnikov, V.A., et al., *Init. Repts. DSDP,* 71: Washington (U.S. Govt. Printing Office), 859–977.

Hannah, M.J., 1993. A re-evaluation of the palynology of the CIROS-1 drillhole. McMurdo Sound, Antarctica. *In* Frogatt, P. (Ed.), *Geological Society of New Zealand 1993 Annual Conference Programme and Abstracts*. Geol. Soc. N. Z. Misc. Publ., 79A.

Haskell, T.R., and Wilson, G.L., 1975. Palynology of sites 280-284, DSDP Leg 29, off southeastern Australia and western New Zealand. *In* Kennett, J.P., Houtz, R.E., et al., *Init. Repts. DSDP, 29*: Washington (U.S. Govt. Printing Office), 731–741.

Hinz, K., Willcox, J.B., Whiticar, M., Kudrass, H.-R., Exon, N.F., and Feary, D.A., 1986. The West Tasmanian Margin: an underrated petroleum province? *In* Glenie, R.C. (Ed.), *Tech. Papers at 2nd South-Eastern Australia Oil Exploration Symposium,* Melbourne, November 14–15, 1985. Pet. Expl. Soc. Aust., 395–410.

Hornibrook, N. de B., Brazier, R.C., and Strong, C.P., 1989. Manual of New Zealand Permian to Pleistocene foraminiferal biostratigraphy. *Paleontol. Bull. N.Z. Geol. Surv.,* 56: 1–175.

Hunt, J.M., 1996. *Petroleum Geochemistry and Geology* (2nd. ed): New York (W.H. Freeman and Co.).

Kennett, J.P., 1970. Pleistocene paleoclimates and foraminiferal biostratigraphy in subantarctic deep-sea cores. *Deep-Sea Res. Part A,* 17: 125–140.

————, 1977. Cenozoic evolution of Antarctic glaciation, the circum-Antarctic Ocean, and their impact on global paleoceanography. *J. Geophys. Res.,* 82:3843–3860.

Kennett, J.P., Houtz, R.E., et al., 1975. *Init. Repts. DSDP, 29*: Washington (U.S. Govt. Printing Office).

Kennett, J.P., and Stott, L.D., 1990. Proteus and Proto-oceanus: ancestral Paleogene oceans as revealed from Antarctic stable isotopic results: ODP Leg 113. *In* Barker, P.F., Kennett, J.P., et al., *Proc. ODP, Sci. Results,* 113: College Station, TX (Ocean Drilling Program), 865–880.

Köthe, A., 1990. Paleogene dinoflagellates from Northwest Germany: biostratigraphy and paleoenvironment. *Geol. Jahrb., Reihe A,* 118:3–111.

Lawrence, J.R., Gieskes, J.M., and Broecker, W.S., 1975. Oxygen isotope and cation composition of DSDP pore waters and the alteration of Layer II basalts. *Earth Planet. Sci. Lett.,* 27: 1–10.

Lee, H.J., 1982. Bulk density and shear strength of several deep-sea calcareous sediments. *In* Demars, K.R., and Chaney, R.C. (Eds.), *Geotechnical Properties, Behavior, and Performance of Calcareous Soils*. ASTM Spec. Tech. Publ., 777:54–78.

Mao, S., and Mohr, B.A.R., 1995. Middle Eocene dinoflagellate cysts from Bruce Bank (Scotia Sea, Antarctica) and their palaeoenvironmental and palaeogeographic conclusions. *Rev. Palaeobot. Palynol.,* 86:235–263.

Mohr, B.A.R., 1990. Eocene and Oligocene sporomorphs and dinoflagellate cysts from Leg 113 drill sites, Weddell Sea, Antarctica. *In* Barker, P.F., Kennett, J.P., et al., *Proc. ODP, Sci. Results,* 113: College Station, TX (Ocean Drilling Program), 595–612.

Morley, J.J., and Nigrini, C., 1995. Miocene to Pleistocene radiolarian biostratigraphy of North Pacific Sites 881, 884, 885, 886, and 887. *In* Rea, D.K., Basov, I.A., Scholl, D.W., and Allan, J.F. (Eds.), *Proc. ODP, Sci. Results,* 145: College Station, TX (Ocean Drilling Program), 55–91.

Peters, K.E., 1986. Guidelines for evaluating petroleum source rock using programmed pyrolysis. *AAPG Bull.,* 70:318–329.

Pye, K., 1987. *Aeolian Dust and Dust Deposits:* London (Academic Press).

Raine, J.I., Askin, R.A., Crouch, E.M., Hannah, M.J., Levy, R.H., and Wrenn, J.H., 1997. Palynomorphs. *In* Hannah, M.J., and Raine, J.I. (Eds), *Southern Ocean Late Cretaceous/Early Cenozoic Biostratigraphic Datums*. Inst. Geol. Nucl. Sci., Sci. Rept., 97:25–33.

Robert, C., 1987. Clay mineral associations and structural evolution of the South Atlantic: Jurassic to Eocene. *Palaeogeogr., Palaeoclimatol., Palaeoecol.,* 58:87–108.

Robert, C., and Chamley, H., 1992. Late Eocene–early Oligocene evolution of climate and marine circulation: deep-sea clay mineral evidence. *In* Kennett, J.P., and Warnke, D.A. (Eds.), *The Role of the Southern Ocean and Antarctica in Global Change.* Antarct. Res. Ser., 56:97–117.

Robert, C., and Kennett, J.P., 1992. Paleocene and Eocene kaolinite distribution in the South Atlantic and Southern Ocean: Antarctic climatic and paleoceanographic implications. *Mar. Geol.,*103:99–110.

————, 1997. Antarctic continental weathering changes during Eocene-Oligocene cryosphere expansion: clay mineral and oxygen isotope evidence. *Geology,* 25:587–590.

Robert, C., and Maillot, H., 1983. Paleoenvironmental significance of clay mineralogical and geochemical data, Southwest Atlantic, DSDP Legs 36 and 71. *In* Ludwig, W.J., Krasheninnikov, V.A., et al., *Init. Repts. DSDP,* 71: Washington (U.S. Govt. Printing Office), 317–343.

————, 1990. Paleoenvironments in the Weddell Sea area and Antarctic climates, as deduced from clay mineral associations and geochemical data, ODP Leg 113. *In* Barker, P.F., Kennett, J.P., et al., *Proc. ODP, Sci. Results,* 113: College Station, TX (Ocean Drilling Program), 51–70.

Robert, C., Stein, R., and Acquaviva, M., 1985. Cenozoic evolution and significance of clay associations in the New Zealand region of the South Pacific, DSDP Leg 90. *In* Kennett, J.P., von der Borch, C.C., et al., *Init. Repts. DSDP,* 90: Washington (U.S. Govt. Printing Office), 1225–1238.

Royer, J.-Y., and Rollet, N., 1997. Plate-tectonic setting of the Tasmanian region. *In* Exon, N.F., and Crawford, A.J. (Eds.), *West Tasmanian Margin and Offshore Plateaus: Geology, Tectonic and Climatic History, and Resource Potential.* Aust. J. Earth Sci., 44:543–560.

Schlumberger, 1995. *DSI—Dipole Sonic Imager:* Houston (Schlumberger Wireline and Testing), SMP-5128.

Shackleton, N.J., and Kennett, J.P., 1975. Paleotemperature history of the Cenozoic and the initiation of Antarctic glaciation: oxygen and carbon isotope analyses in

DSDP Sites 277, 279, and 281. *In* Kennett, J.P., Houtz, R.E., et al., *Init. Repts. DSDP,* 29: Washington (U.S. Govt. Printing Office), 743–755.

Shilov, V.V., 1995. Miocene–Pliocene radiolarians from Leg 145, North Pacific. *In* Rea, D.K., Basov, I.A., Scholl, D.W., and Allan, J.F. (Eds.), *Proc. ODP, Sci. Results,* 145: College Station, TX (Ocean Drilling Program), 93–116.

Shipboard Scientific Party, 1995. Site 909. *In* Myhre, A.M., Thiede, J., Firth, J.V., et al., *Proc. ODP, Init. Repts.,* 151: College Station, TX (Ocean Drilling Program), 159–220.

Stein, R., and Robert, C., 1986. Siliciclastic sediments at Sites 588, 590 and 591: Neogene and Paleogene evolution in the Southwest Pacific and Australian climate. *In* Kennett, J.P., von der Borch, C.C., et al., *Init. Repts. DSDP,* 90 (Pt. 2): Washington (U.S. Govt. Printing Office), 1437–1455.

Stott, L.D., Kennett, J.P., Shackleton, N.J., and Corfield, R.M., 1990. The evolution of Antarctic surface waters during the Paleogene: inferences from the stable isotopic composition of planktonic foraminifers, ODP Leg 113. *In* Barker, P.F., Kennett, J.P., et al., *Proc. ODP, Sci. Results,* 113: College Station, TX (Ocean Drilling Program), 849–863.

Stover, L.E., and Williams, G.L., 1995. A revision of the Paleogene dinoflagellate genera *Areosphaeridium* Eaton 1971 and *Eatonicysta* Stover and Evitt 1978. *Micropaleontology,* 41:97–141.

Truswell, E.M., 1997. Palynomorph assemblages from marine Eocene sediments on the west Tasmanian continental margin and the South Tasman Rise. *Aust. J. Earth Sci.,* 44:633–654.

Vonhof, H.B., Smit, J., Brinkhuis, H., Moutanari, A., and Nederbragt, A.J., 2000. Global cooling accelerated by early-late Eocene impacts? *Geology,* 28:687–690.

Weaver, C.E., 1989. *Clays, Muds, and Shales:* Amsterdam (Elsevier).

Wei, W., and Wise, S.W., Jr., 1990. Middle Eocene to Pleistocene calcareous nannofossils recovered by Ocean Drilling Program Leg 113 in the Weddell Sea. *In* Barker, P.F., Kennett, J.P., et al., *Proc. ODP, Sci. Results,* 113: College Station, TX (Ocean Drilling Program), 639–666.

Willcox, J.B., Baillie, P., Exon, N.F., Lee, C.-S., and Thomas, B., 1989. The geology of western Tasmania and its continental margin—with particular reference to petroleum potential. *Bureau Mineral Resources (Australia),* Record 1989/13:27.

Williams, G.L., Brinkhuis, H., et al., 1998. Cenozoic dinocyst events. *In* De Graciansky, et al. (Eds.), *Sequence Stratigraphy of European Basins*. Spec. Publ.—Soc. Econ. Paleontol. Mineral., 60.

Wilson, G.J., 1985. Dinoflagellate biostratigraphy of the Eocene Hampden Section, North Otago, New Zealand. *N.Z. Geol. Surv. Rec.,* 8:93–101.

————, 1988. Paleocene and Eocene dinoflagellate cysts from Waipawa, Hawkes Bay, New Zealand. *N.Z. Geol. Surv. Paleontol. Bull.,* 57.

————, 1989. Marine palynology. *In* Barrett, P.J. (Ed.), *Antarctic Cenozoic History from the CIROS-1 Drillhole, McMurdo Sound.* N.Z. Dep. Sci. Ind. Res. Bull, 245: 129–133.

Wise, S.W., Jr., 1983. Mesozoic and Cenozoic calcareous nannofossils recovered by Deep Sea Drilling Project Leg 71 in the Falkland Plateau region, Southwest Atlantic Ocean. *In* Ludwig, W.J., Krasheninnikov, V.A., et al., *Init. Repts. DSDP,* 71 (Pt. 2): Washington (U.S. Govt. Printing Office), 481–550.

Wrenn, J.H., and Hart, G.F., 1988. Paleogene dinoflagellate cyst biostratigraphy of Seymour Island, Antarctica. *Mem.—Geol. Soc. Am.,* 169:321–447.

Zachos, J.C., Breza, J.R., and Wise, S.W., 1992. Early Oligocene ice-sheet expansion on Antarctica: stable isotope and sedimentological evidence from Kerguelen Plateau, southern Indian Ocean. *Geology,* 20:569–573.

Zachos, J.C., Lohmann, K.C., Walker, J.C.G., and Wise, S.W., Jr., 1993. Abrupt climate changes and transient climates during the Paleogene: a marine perspective. *J. Geol.,* 101: 191–213.

Zachos, J.C., Quinn, T.M., and Salamy, S., 1996. High resolution (10^4 yr) deep-sea foraminiferal stable isotope records of the Eocene-Oligocene climate transition. *Paleoceanography,* 11:251–266.

Figure F1. Postdrilling interpretation for local seismic profile AGSO 125-14, across Site 1170, showing broad ages and lithostratigraphic units. This shows the site's position just west of the high central block and the evidence of Miocene scouring that removed the Oligocene and late Eocene sequences. Note the thick Pliocene–Pleistocene and the reduced Oligocene sections at this site. TD = total depth.

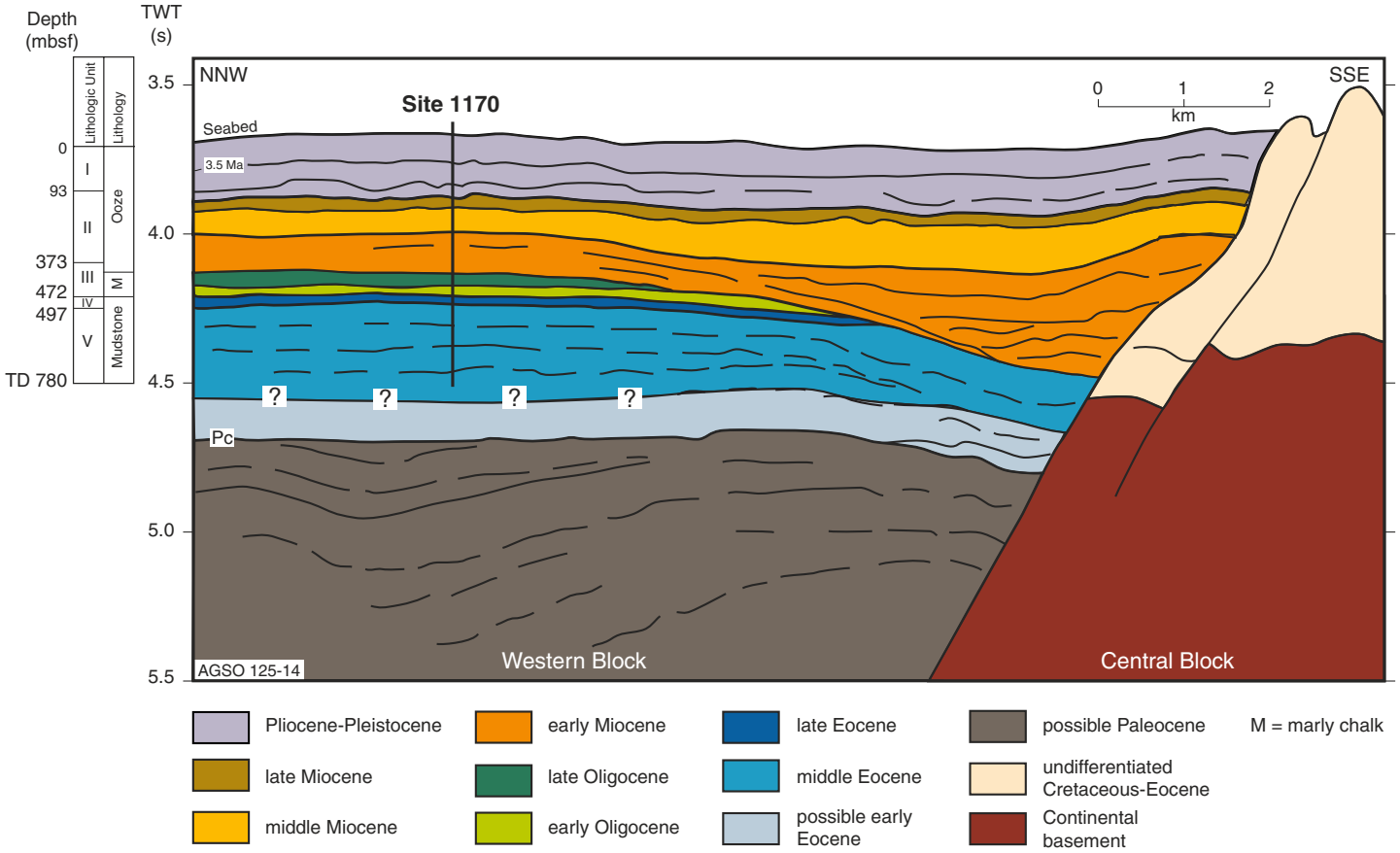

Figure F2. Portion of seismic line *Tasmante* 125-14 through Site 1170, including the approximate depth of penetration.

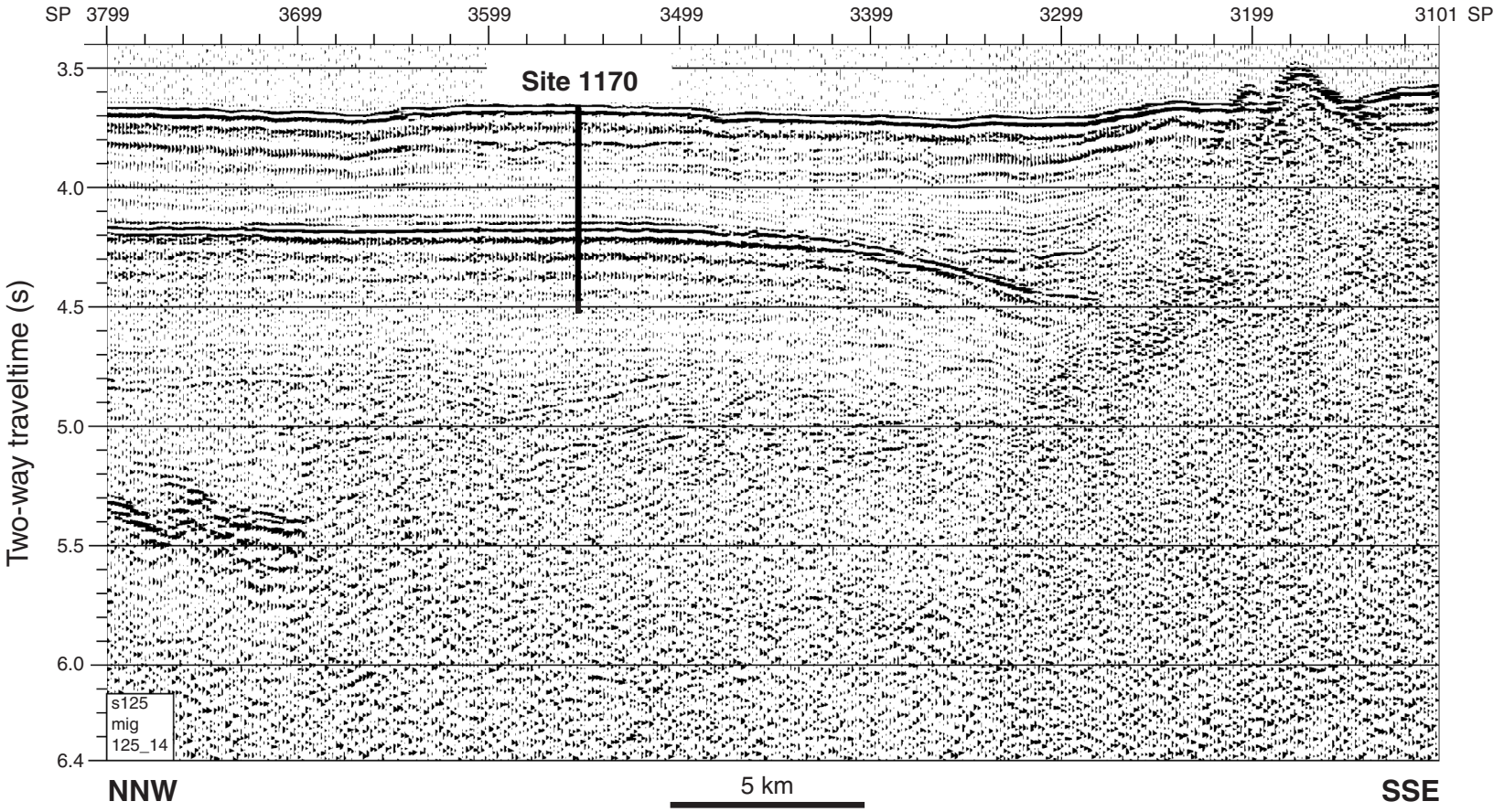

Figure F3. Regional cross section through time across Site 1170, southwest across the Tasmanian block, two blocks of the South Tasman Rise, and the abyssal plain, based on seismic profile SO36-58 and other geological information. The Eocene was marked by development of ridges by fast north-south strike-slip motion between Australia and Antarctica, and the Oligocene by departure of Antarctica by strike-slip motion, emplacement of oceanic crust, collapse of the western block, and development of the saddle between the South Tasman Rise and Tasmania. TWT = two-way traveltime. Ant. = Antarctica.

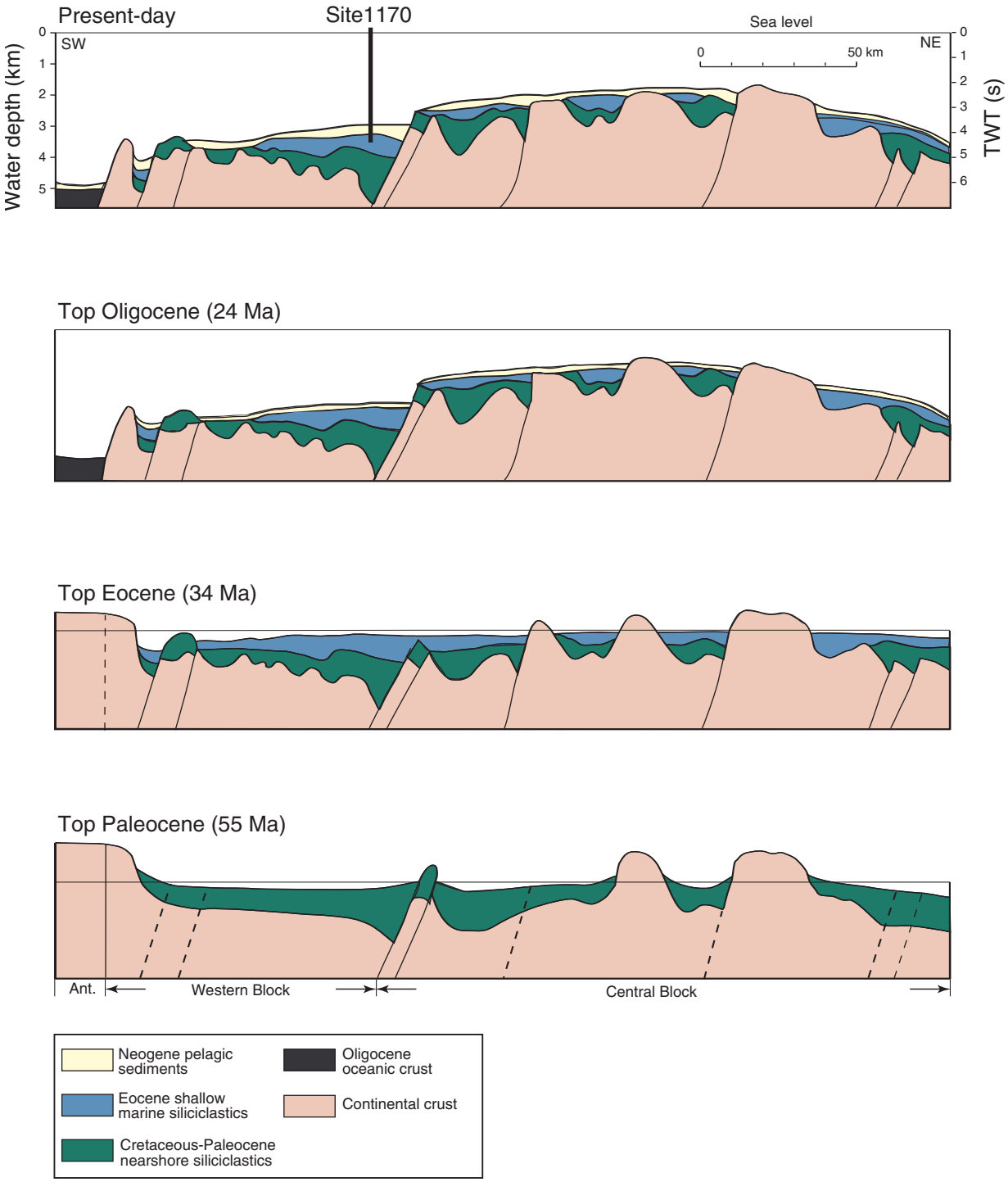

Figure F4. Summary of Site 1170 biozonation, lithostratigraphic units, and physical properties. TD = total depth.

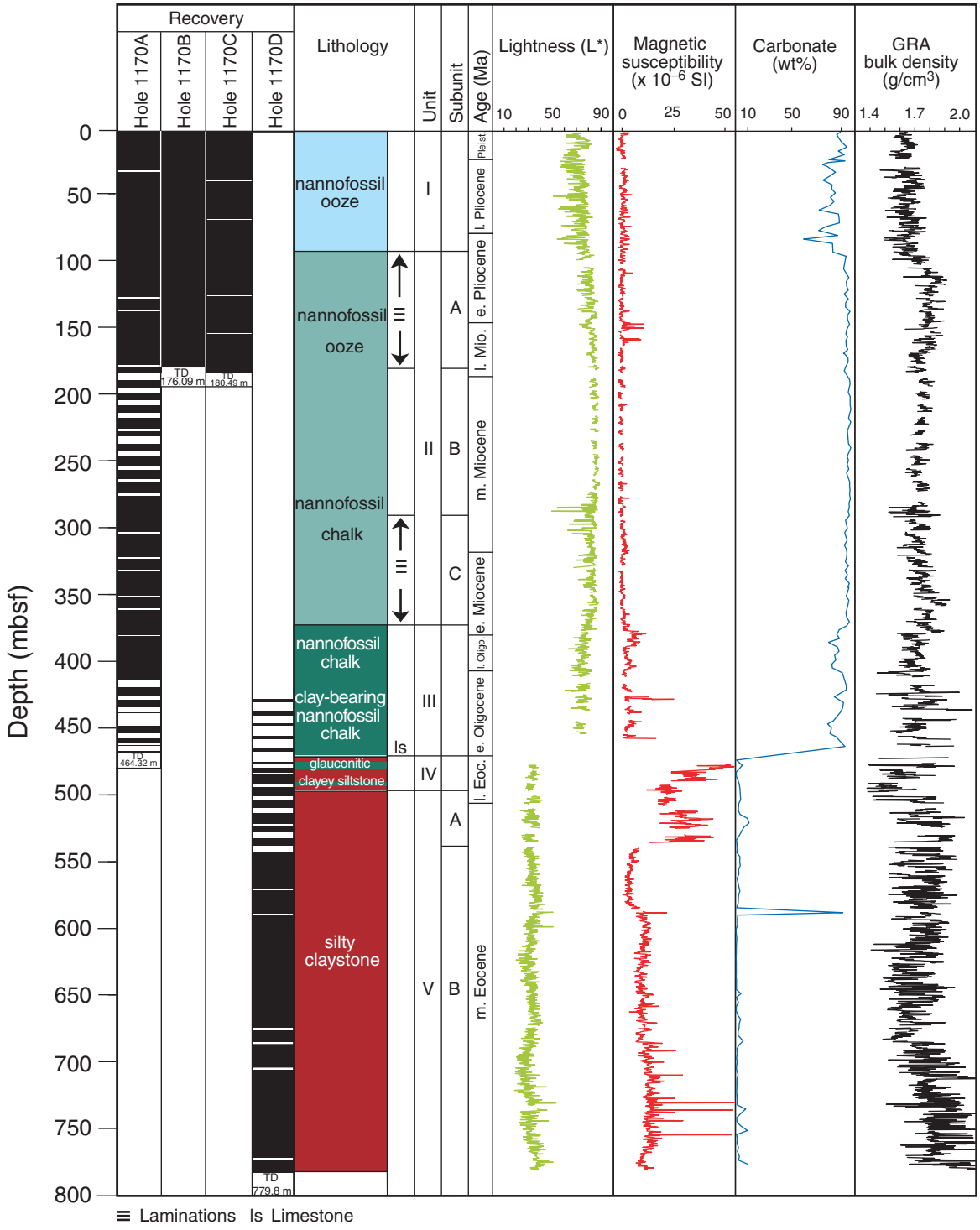

Figure F5. Detailed summary of Site 1170 biozonation, lithostratigraphic units, and physical properties for intervals of (**A**) 0–200 mbsf, (**B**) 200–400 mbsf, (**C**) 400–600 mbsf, and (**D**) 600–779.8 mbsf. Drilling disturbance ratings for the relatively soft sediments of Hole 1170A (A, B) consist of F0 (undisturbed sediments with only minor "edge effect"), F1 (bowing upward of up to approximately one-third core width [~2.2 cm vertical stretching] or 30° inclination of sediments), F2 (extreme bowing upward of approximately one-third to one-half core width [~2.2–3.4 cm vertical stretching] or 30°–60° inclination), F3 (onset of minor flow-in beyond that of F2), and F4 (massive flow-in). Drilling disturbance ratings for Hole 1170D (C, D) consist of B0 (>98%), B1 (97%–91%), B2 (90%–85%), B3 (84%–70%), and B4 (<70%). The minimum estimated percentage observed for Hole 1170D was ~50%. Physical properties data should be considered suspect for F3 and B3 and not considered robust for F4 and B4 categories. TD = total depth. (Continued on next three pages.)

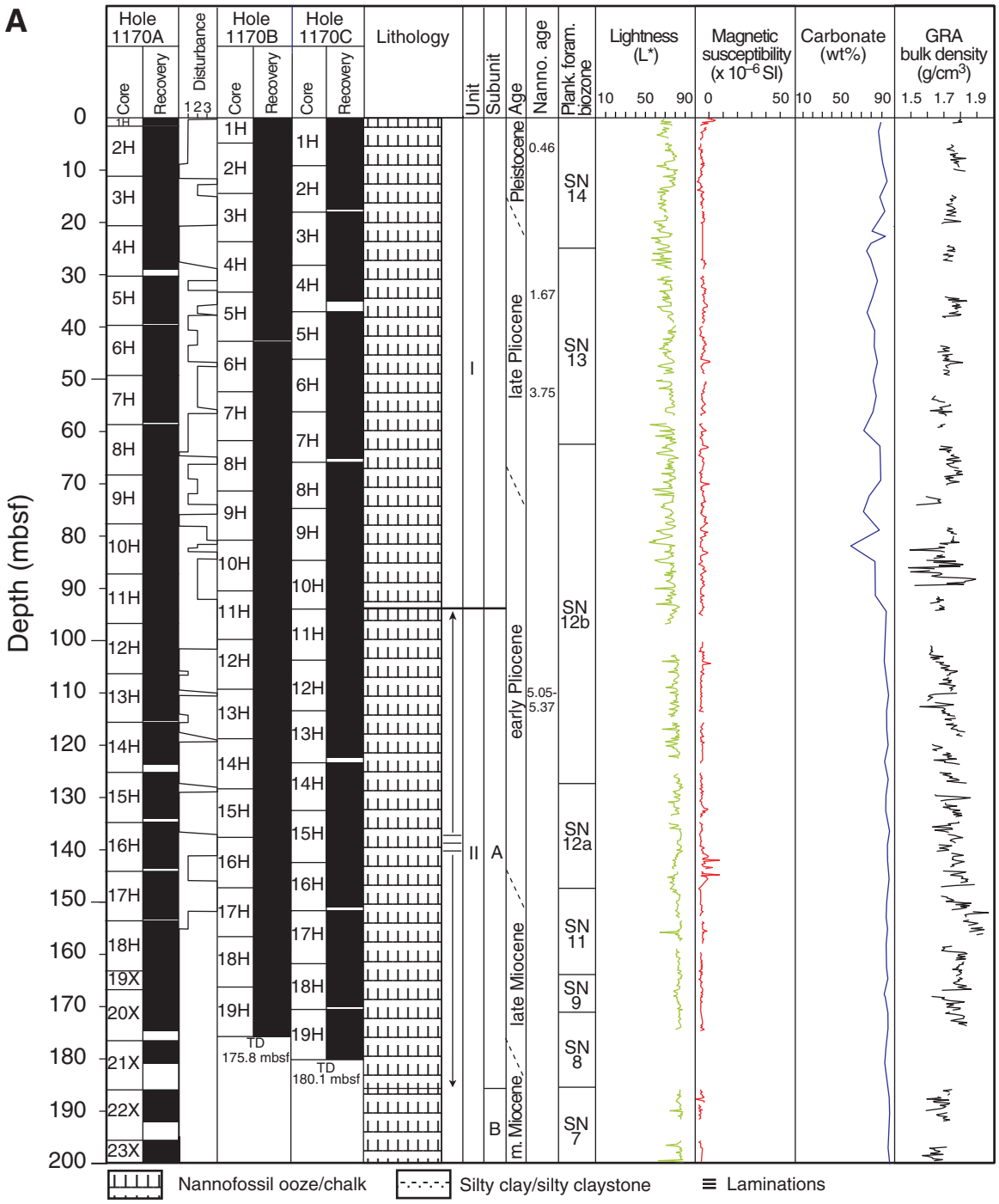

Figure F5 (continued).

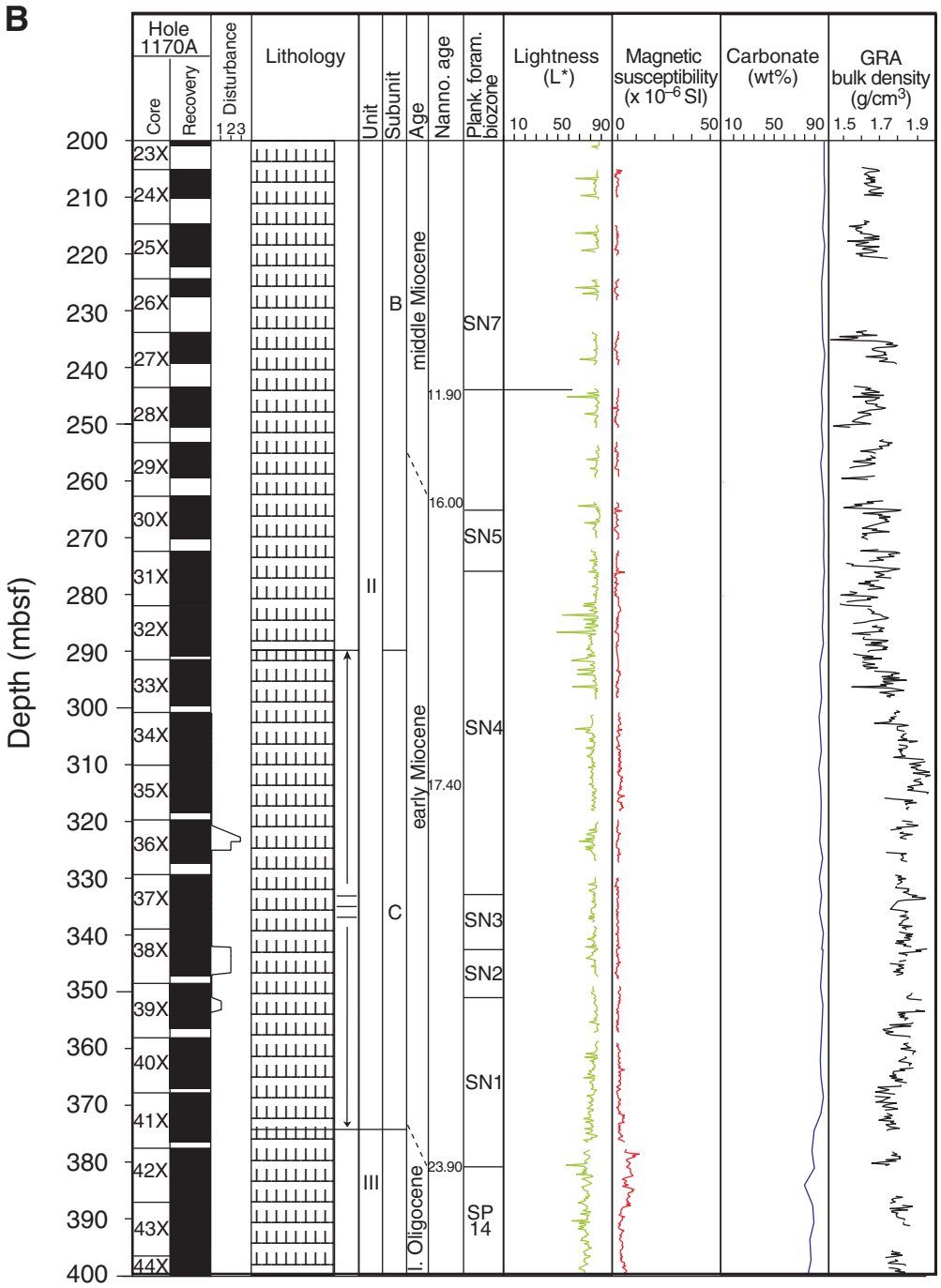

Figure F5 (continued).

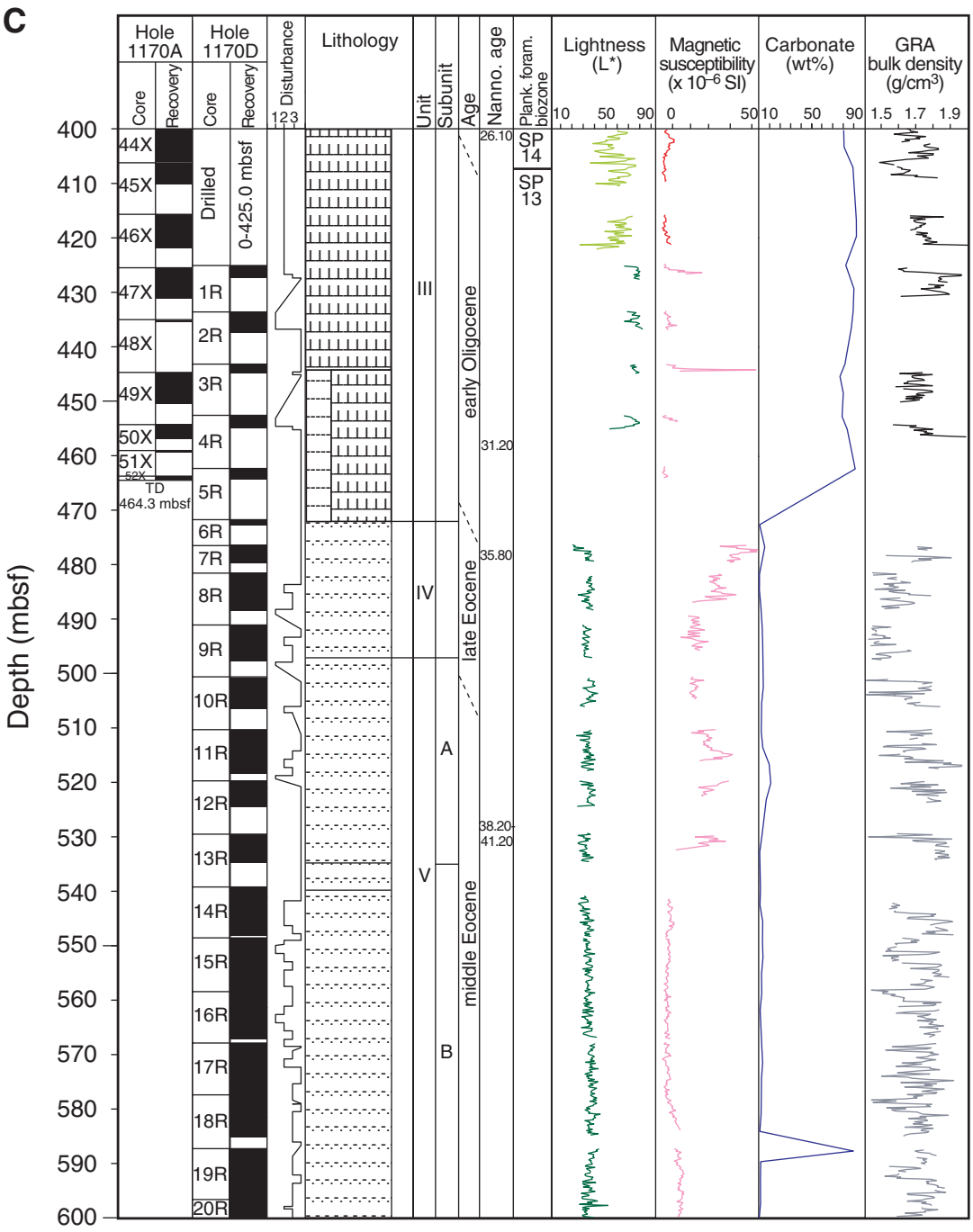

Figure F5 (continued).

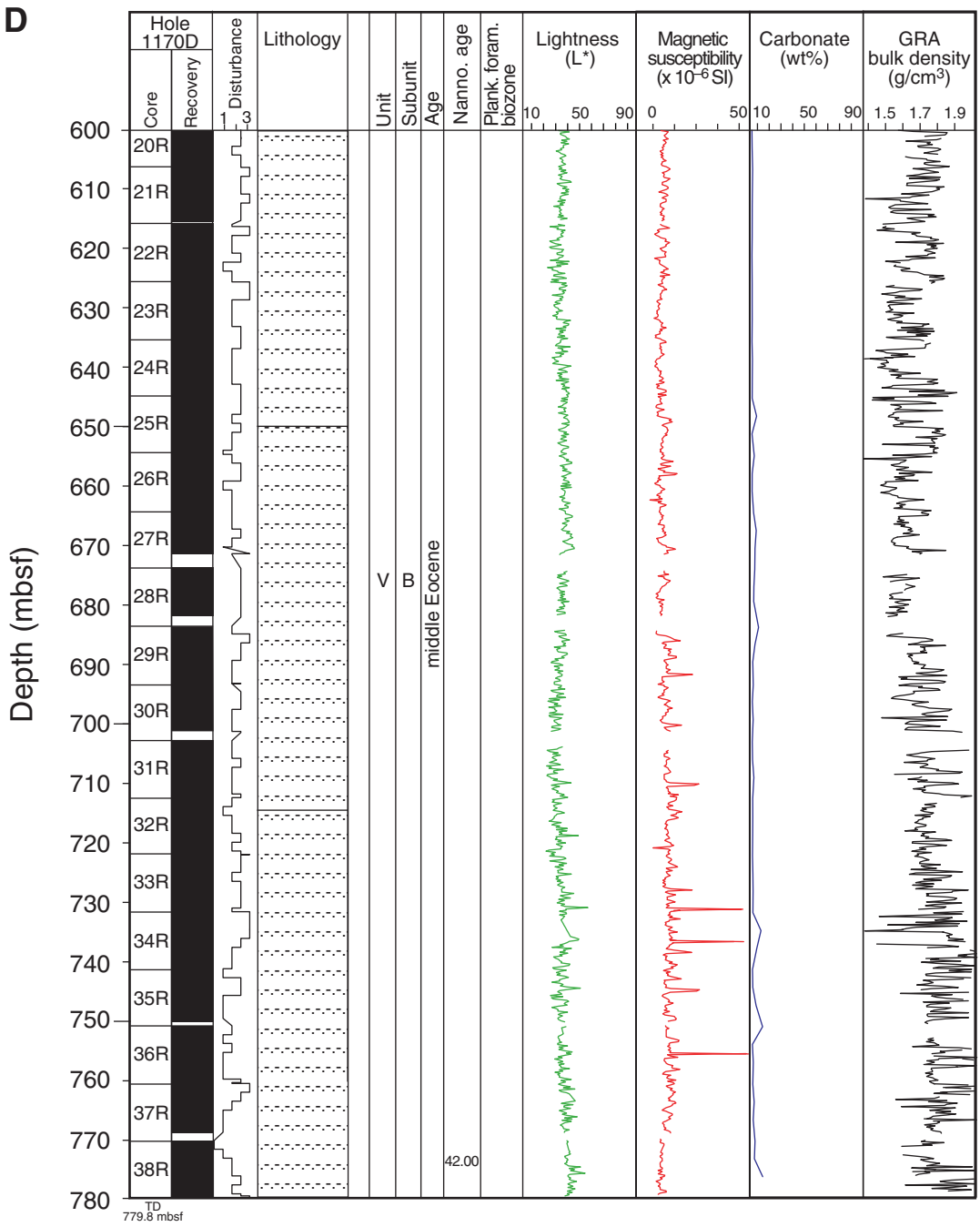

Figure F6. Smear slide–based lithologic composition of Hole 1170A sediments.

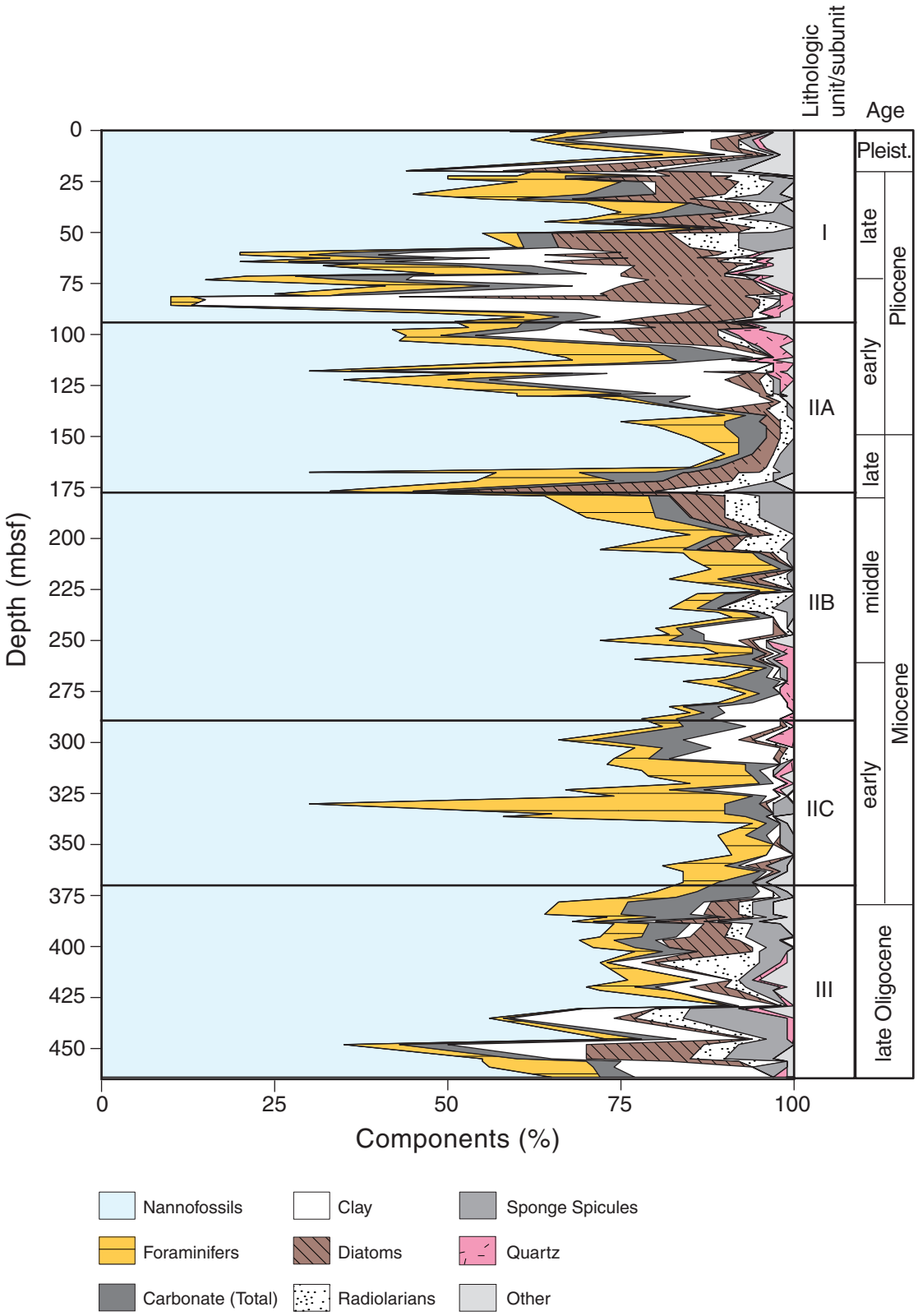

Figure F7. Smear slide–based lithologic composition of Hole 1170D sediments.

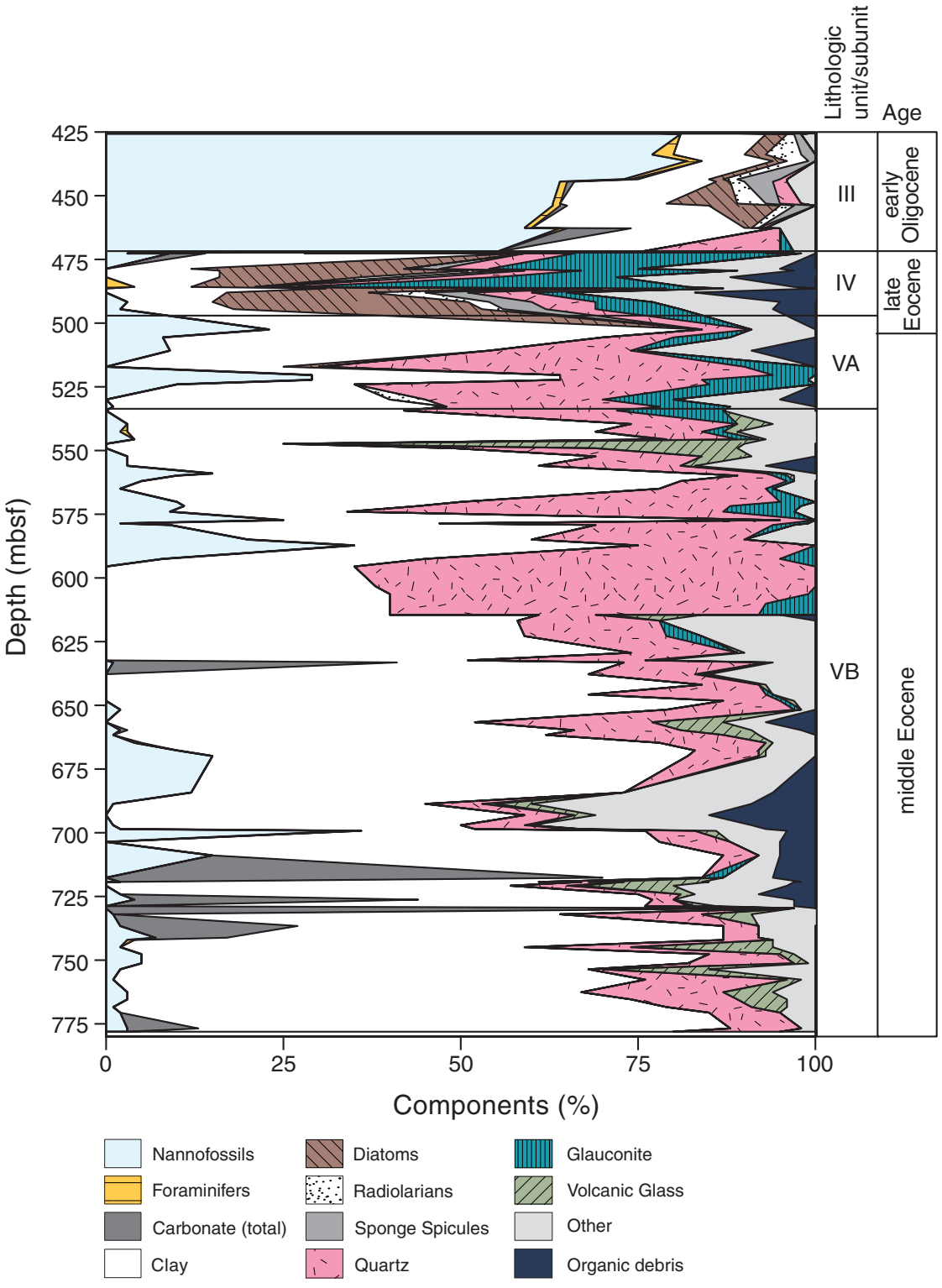

Figure F8. Eocene oscillations in carbonate content and spectrophotometric lightness for Hole 1170D.

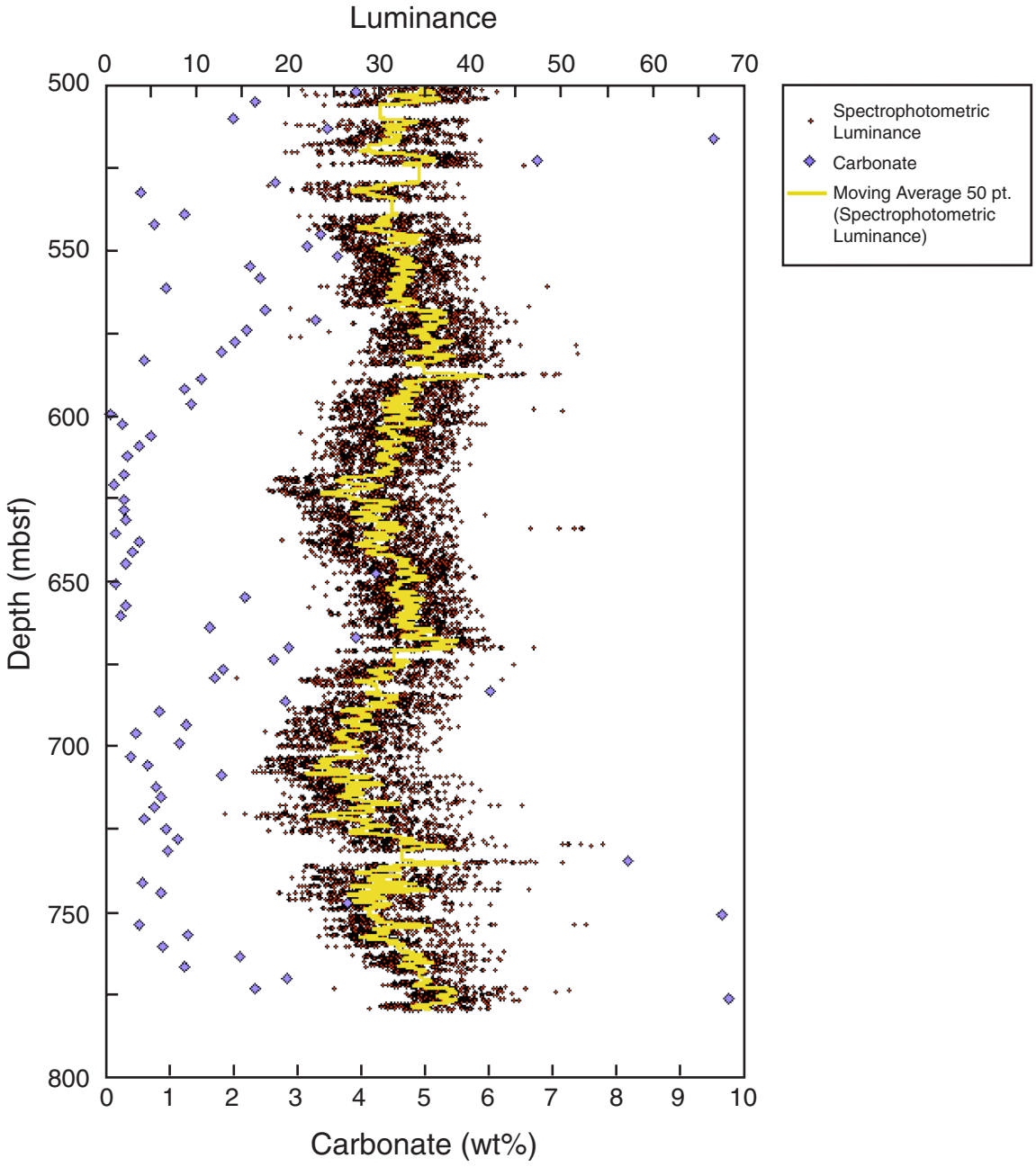

Figure F9. Clay mineral units of Site 1170, western South Tasman Rise.

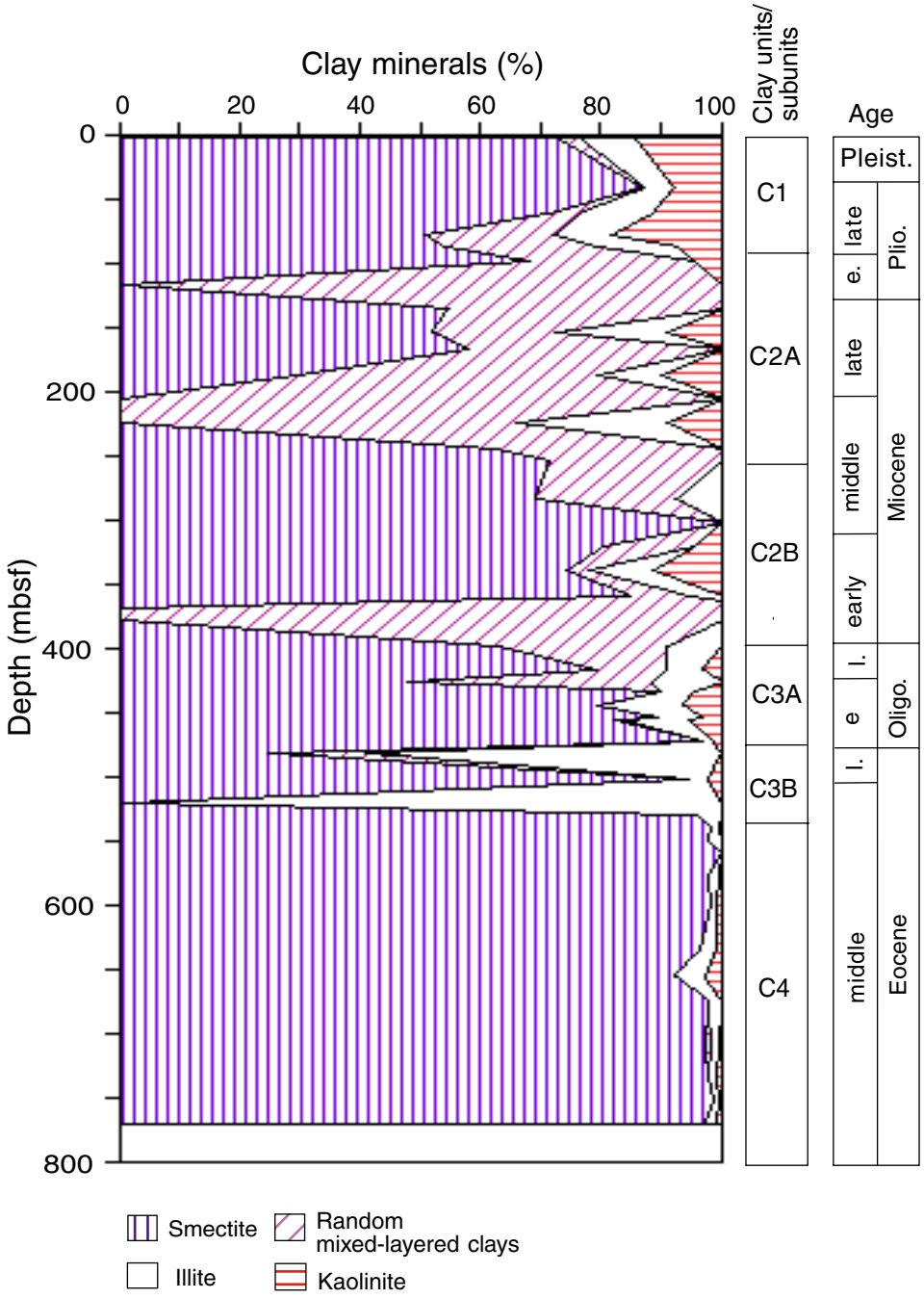

Figure F10. Site 1170 age-depth plot and linear sedimentation rates. The age-depth curve uses multiple microfossil and paleomagnetic datums for Site 1170. Events used are listed in Table T8, p. 136, and "Paleomagnetism," p. 36.

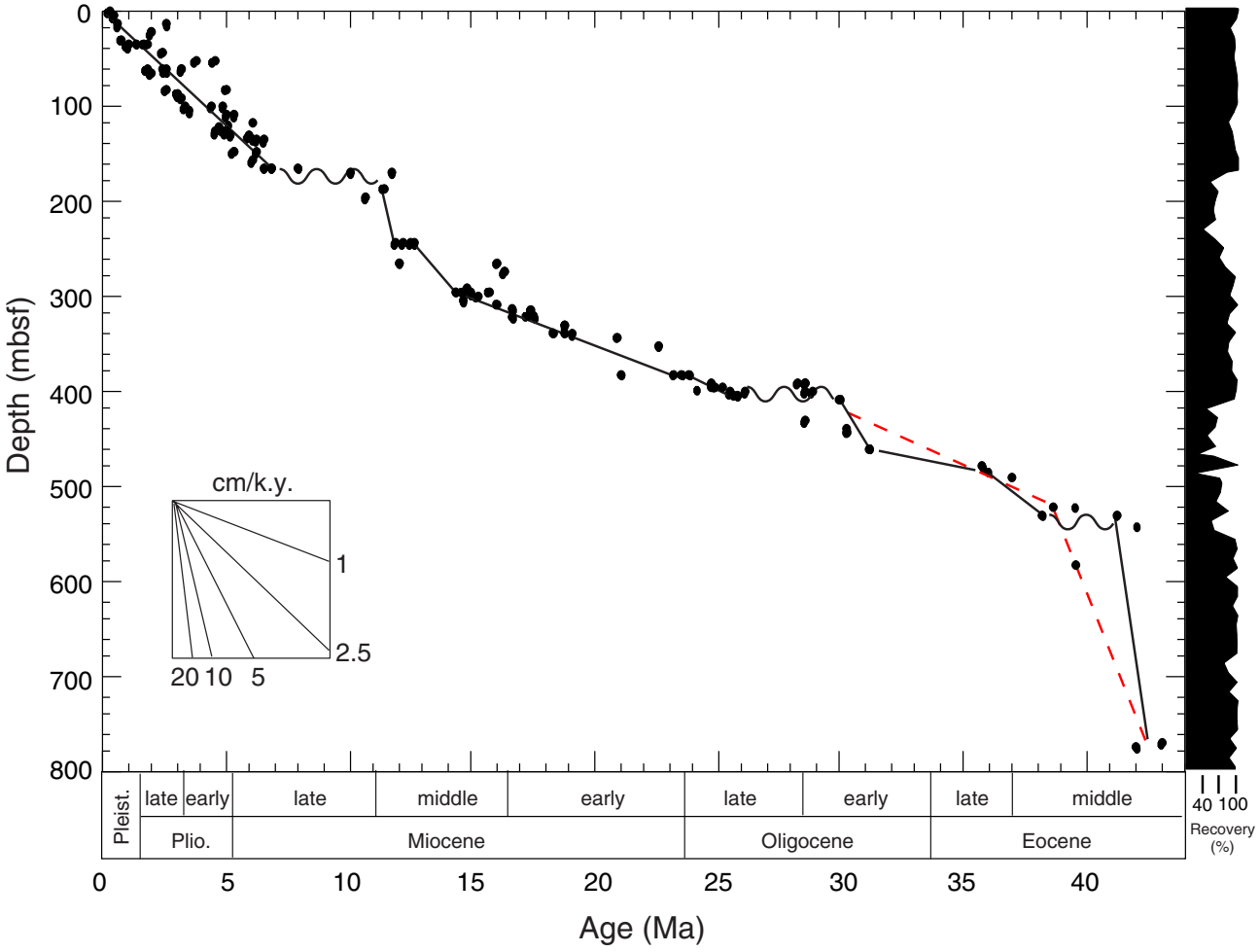

Figure F11. Combined bioevents for the Eocene–Oligocene transition in Hole 1170D. For lithostratigraphy key, see Fig. F3, p. 40, in the "Explanatory Notes" chapter. D = diatom, N= nannofossil, C = dinocyst, P = planktonic foraminifer.

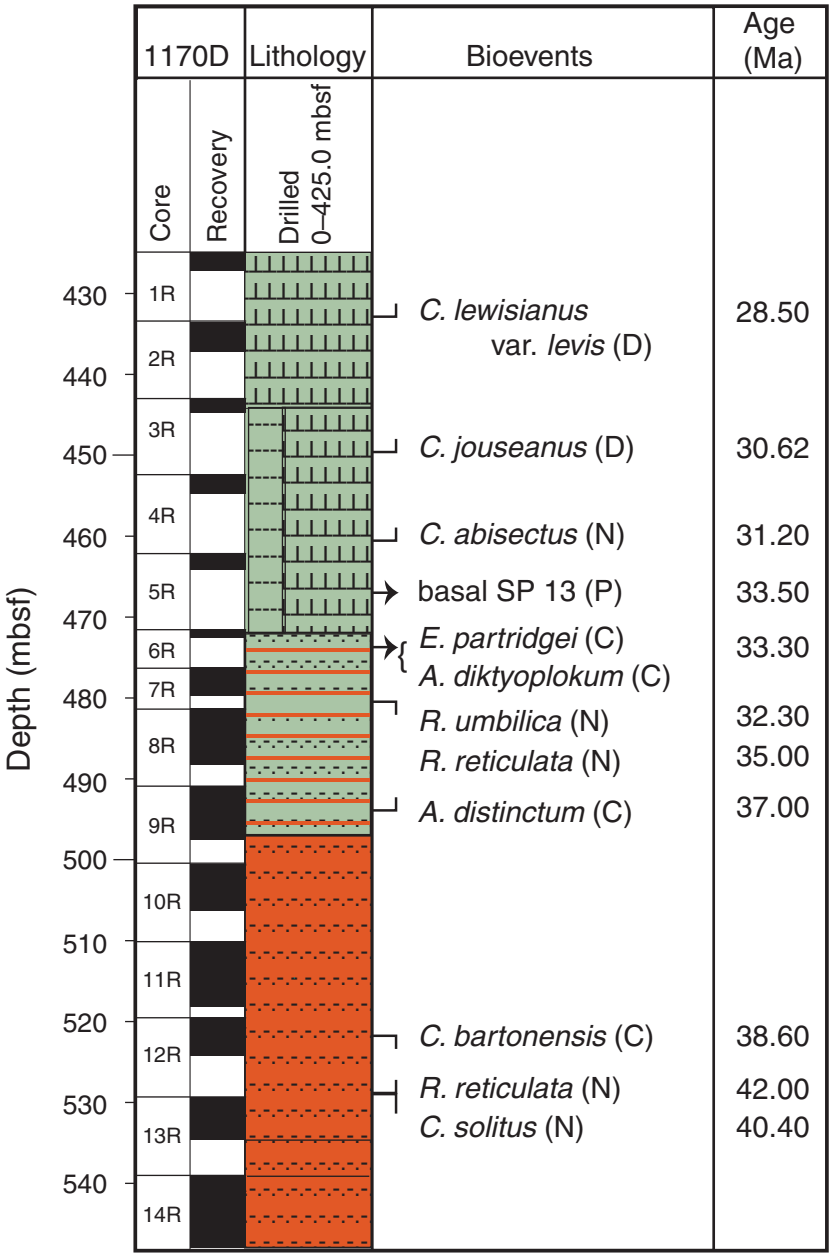

Figure F12. Alternative age interpretations for the Eocene–Oligocene transition in Hole 1170D. **A.** nannofossil solution. **B.** Palynological/diatom/foraminifer solution. For lithostratigraphy key, see Fig. F3, p. 40, in the "Explanatory Notes" chapter. δ^{18}, (01-a), (01-b) = isotopic events of Zachos et al., 1996. E/O gssp = Eocene/Oligocene global stratotype section and point.

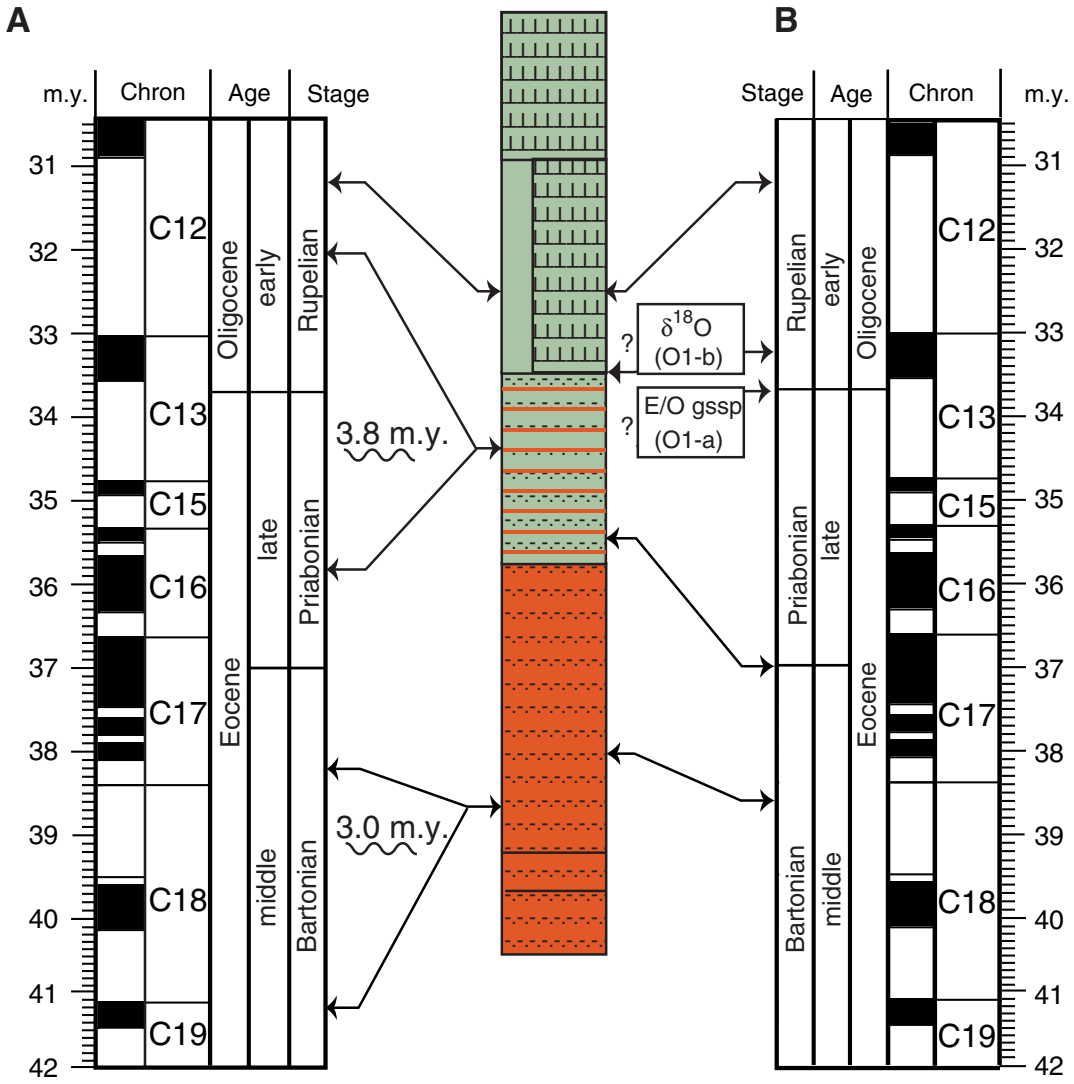

Figure F13. Evolution of the depositional setting at Site 1170, based on the benthic foraminifers in Holes 1170A and 1170D.

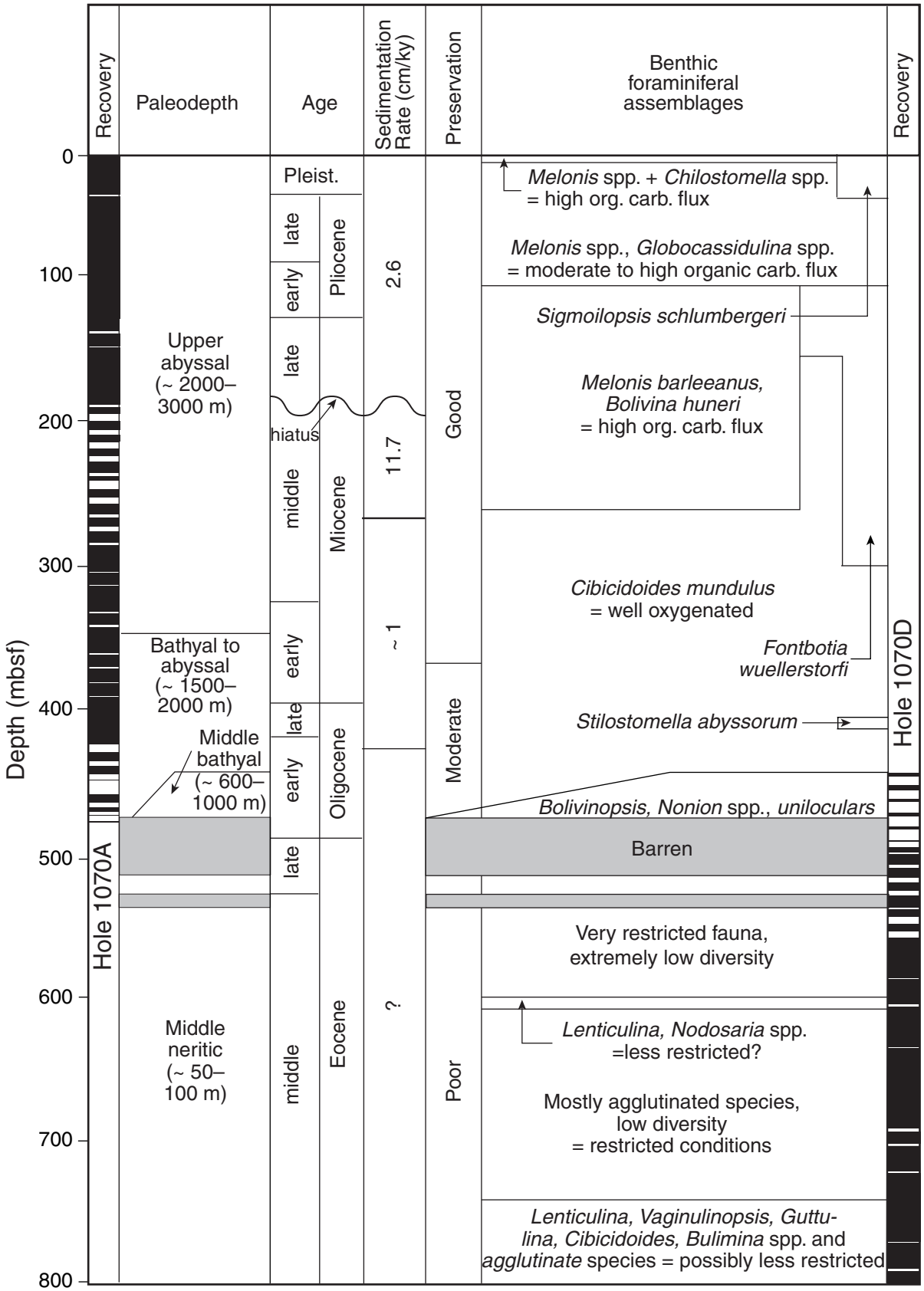

Figure F14. Comparison of *Deflandrea* spp. (dinocysts) and estimates of diatom abundance in Hole 1170D.

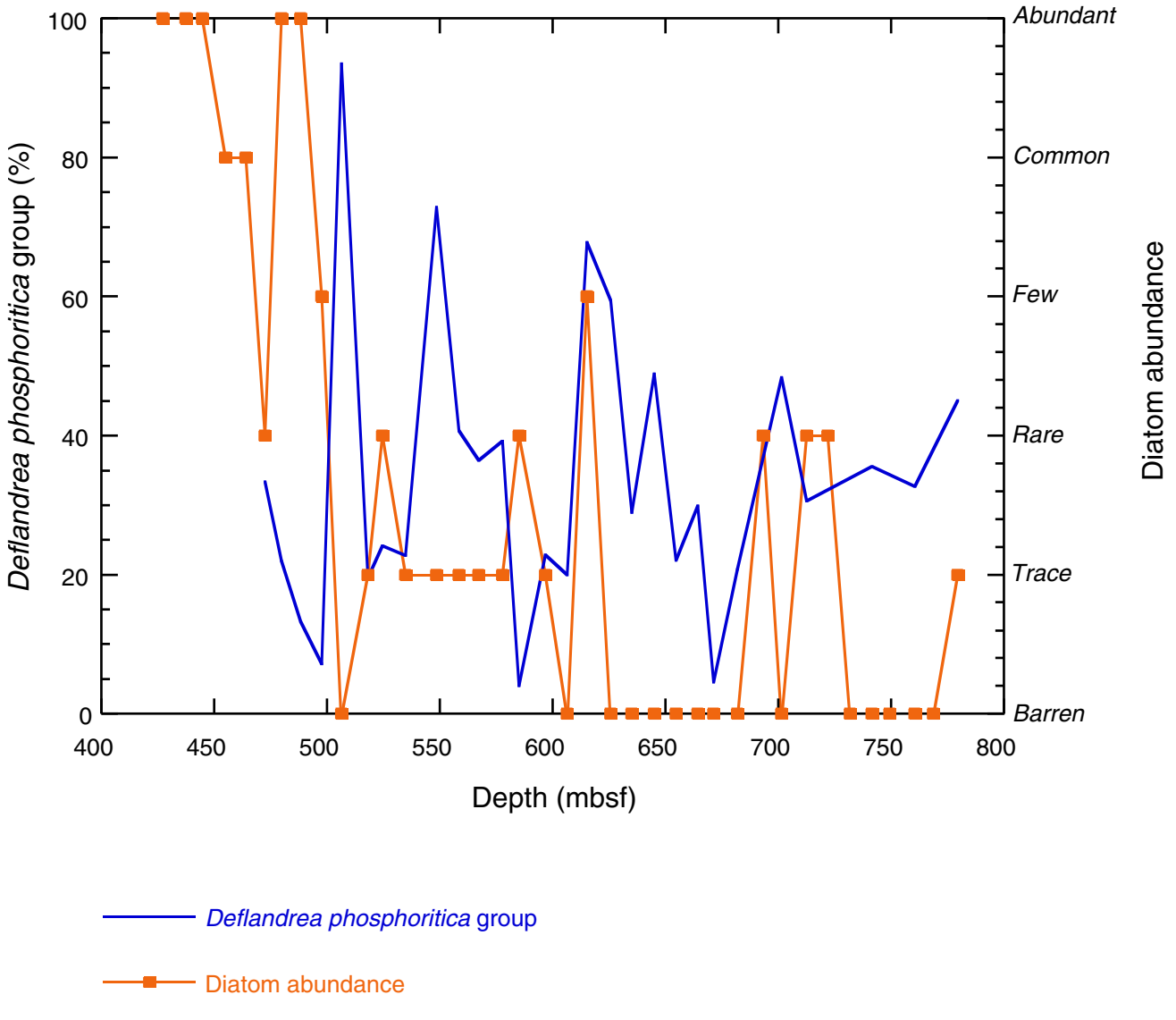

Figure F15. Distribution of the taxa dominating the organic walled dinocyst assemblages and indications of dominances of other (phyto)plankton groups in Hole 1170D. Note the correlation of peaks in *Deflandrea* spp., the optima in siliceous groups (S), and *E. partridgei* with calcareous nannofossils (N).

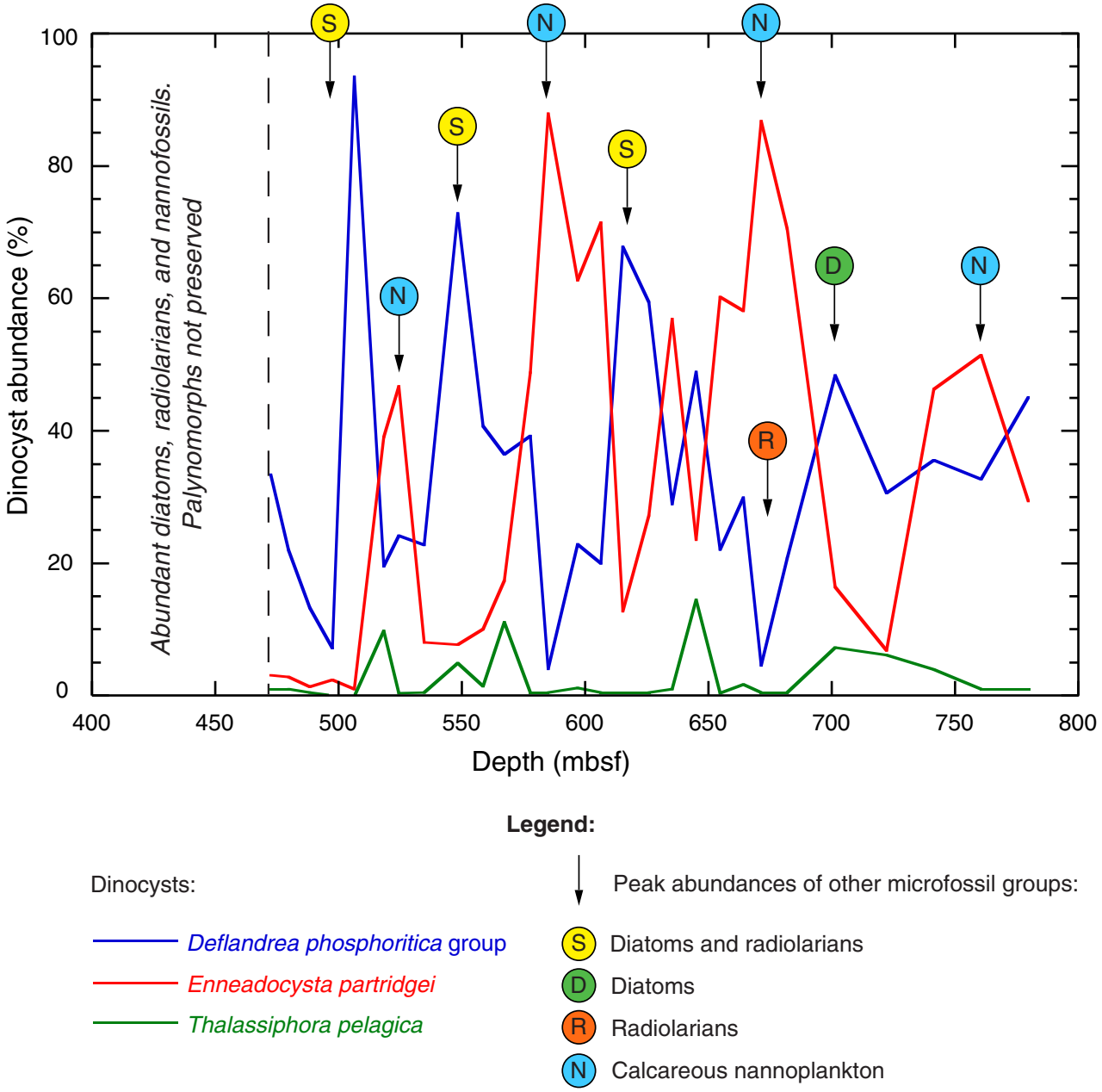

Figure F16. Long-core measurements from 0 to 100 mbsf for Holes 1170A, 1170B, and 1170C showing inclination, intensity, and interpreted magnetostratigraphy.

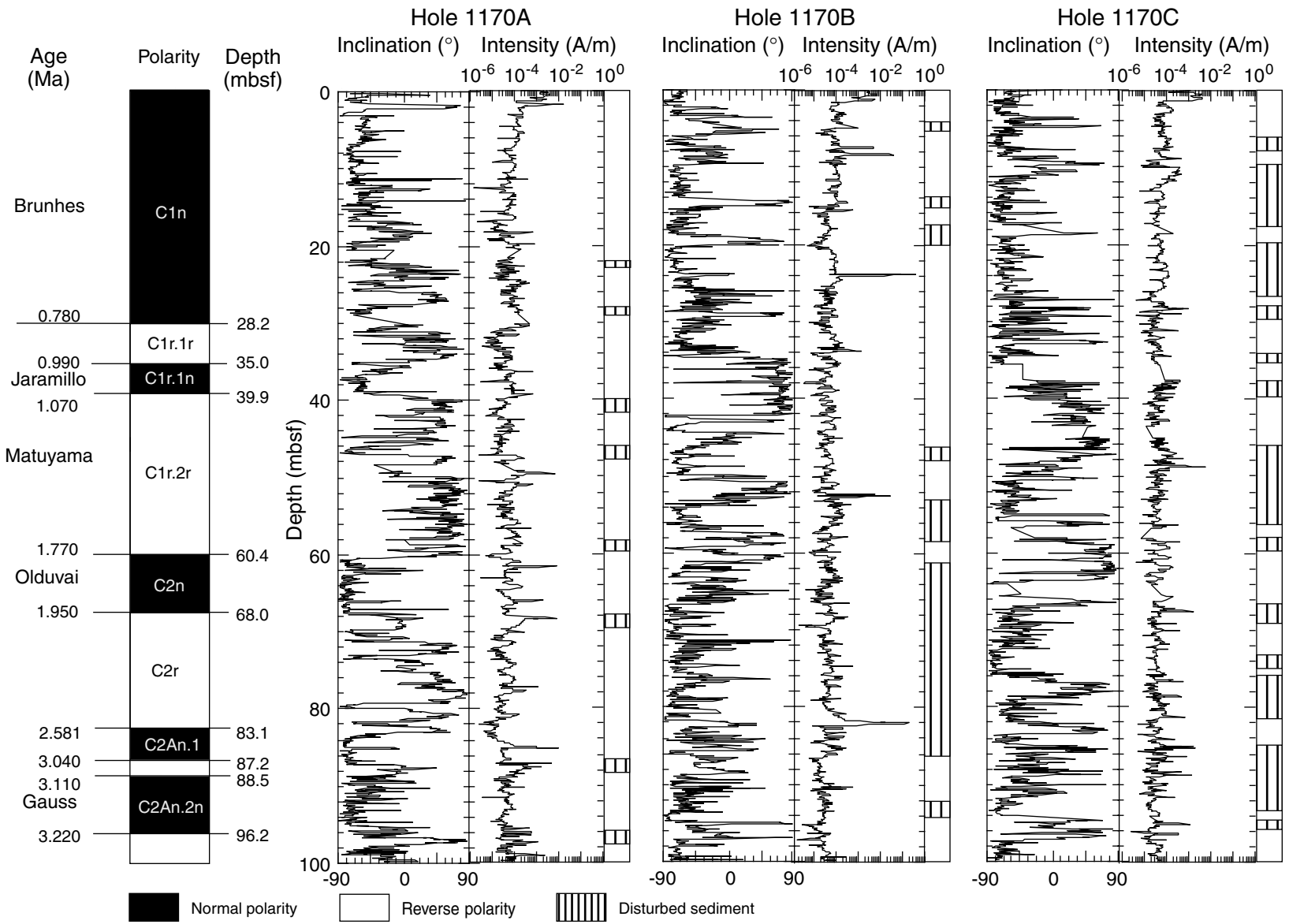

Figure F17. Long-core measurements from 100 to 200 mbsf for Holes 1170A, 1170B, and 1170C showing inclination, intensity, and interpreted magnetostratigraphy.

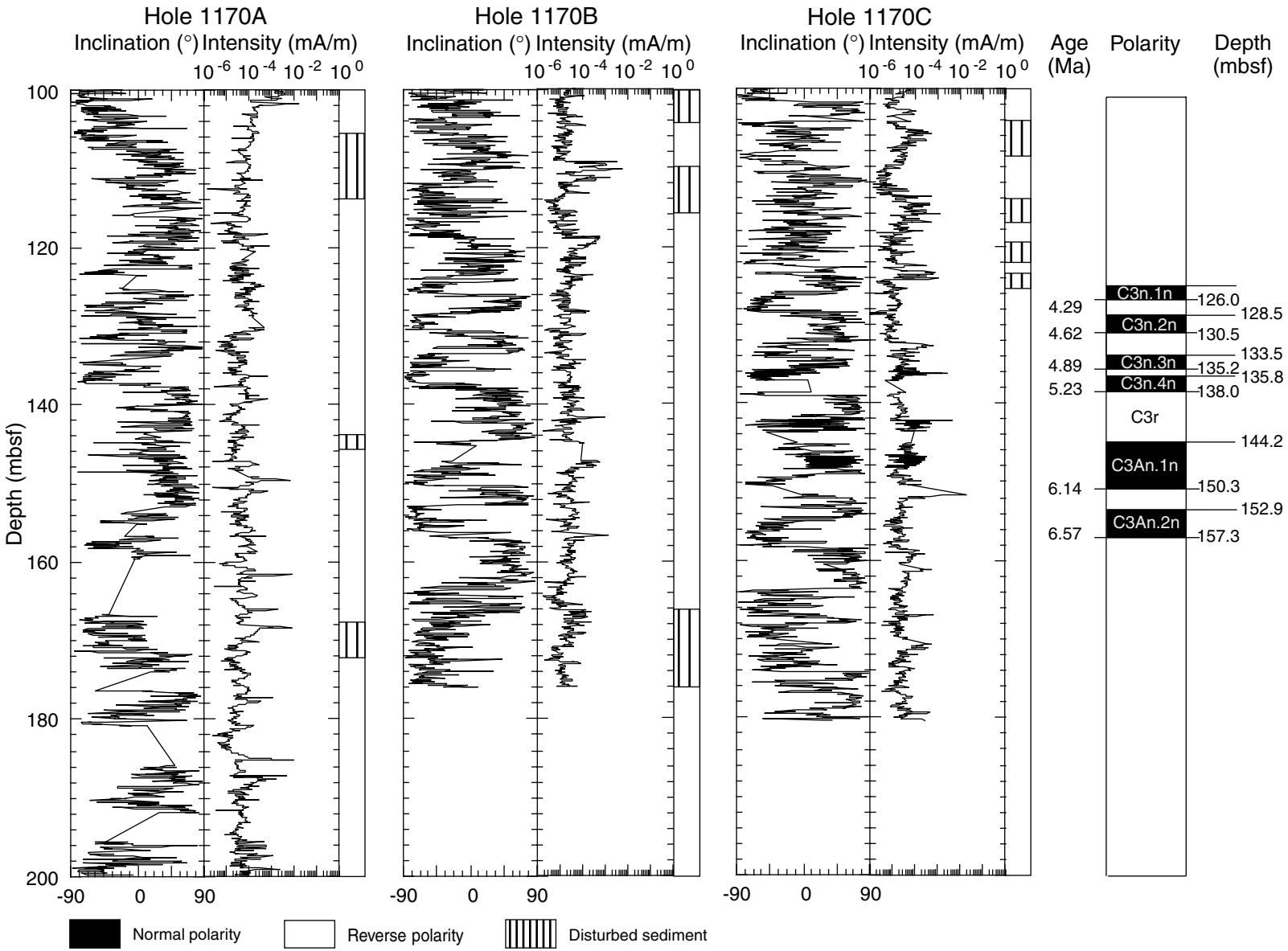

Figure F18. Long-core measurements from 250 to 450 mbsf for Hole 1170A showing inclination, intensity and interpreted magnetostratigraphy.

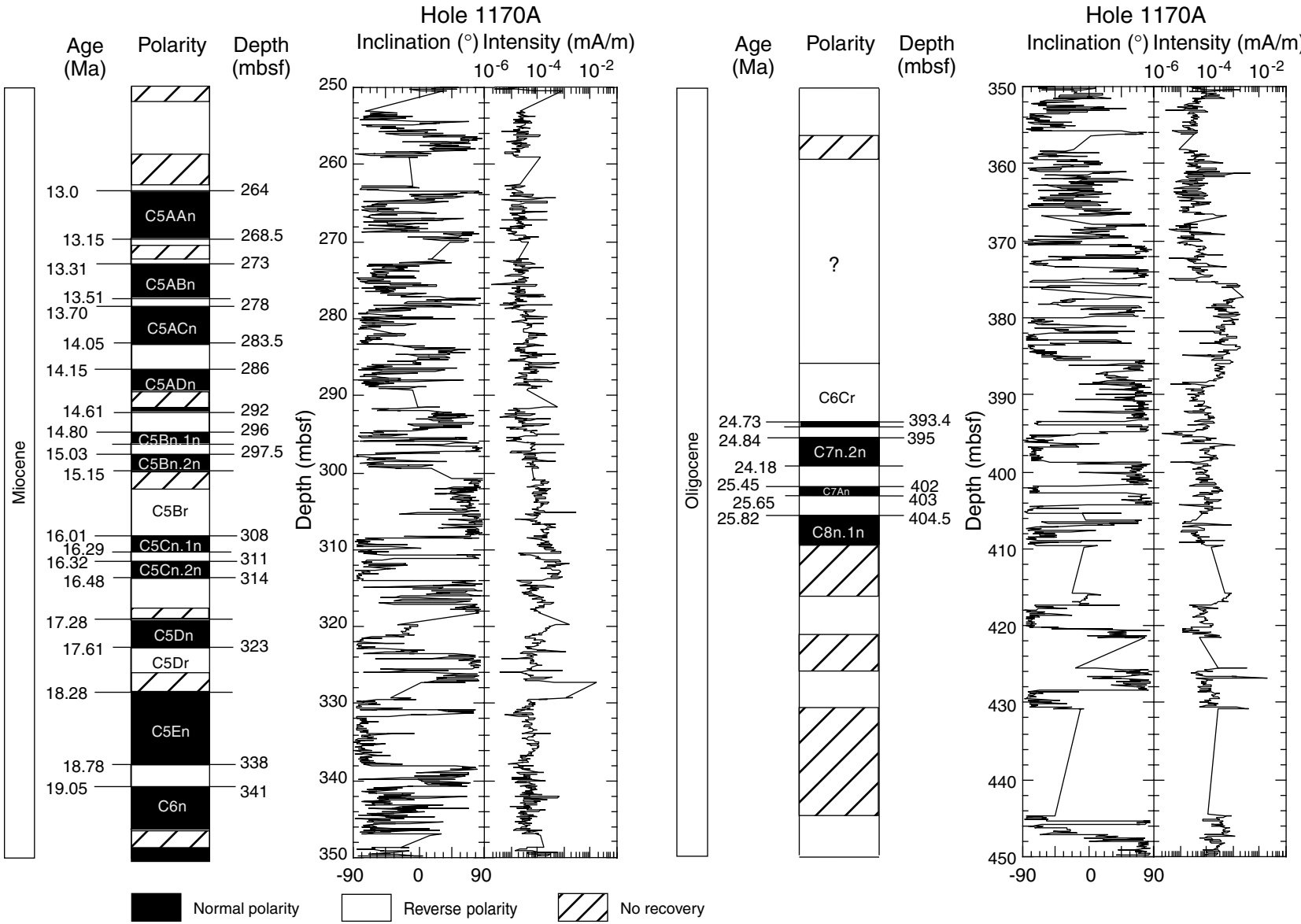

Figure F19. Long-core measurements for Section 189-1170D-9R-1 inclination and intensity before and after AF demagnetization to 20 mT. The intensity of magnetization decreases by about one order of magnitude, and the inclination changes polarity. There is therefore a strong downward drilling-induced moment in these sediments, which probably arises from the field of the drill bit in the bottom-hole assembly.

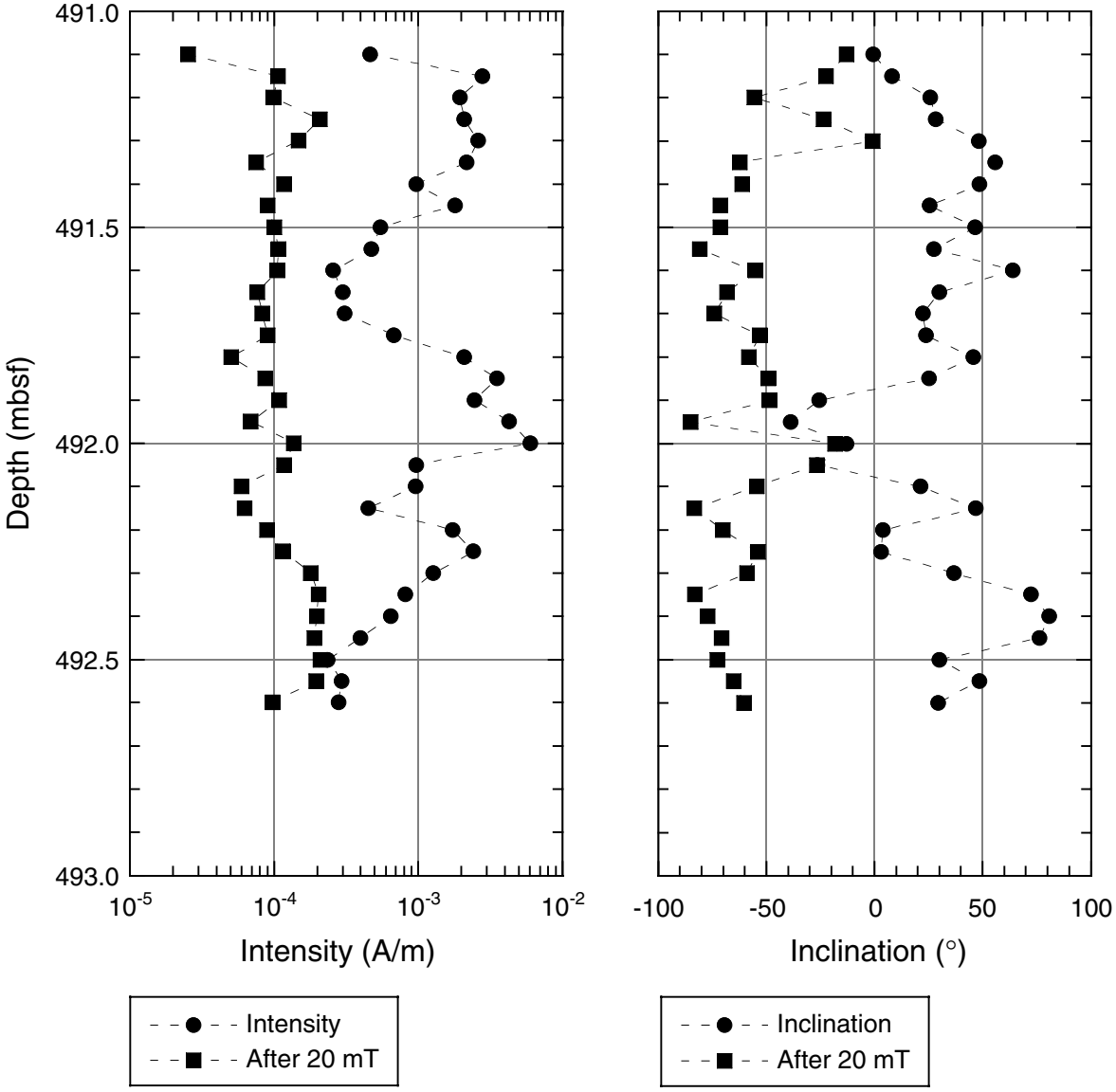

Figure F20. Long-core measurements for Hole 1170D from 425 to 779.8 mbsf after AC demagnetization to 20 mT and filtering to mitigate the effect of drill-mud contamination.

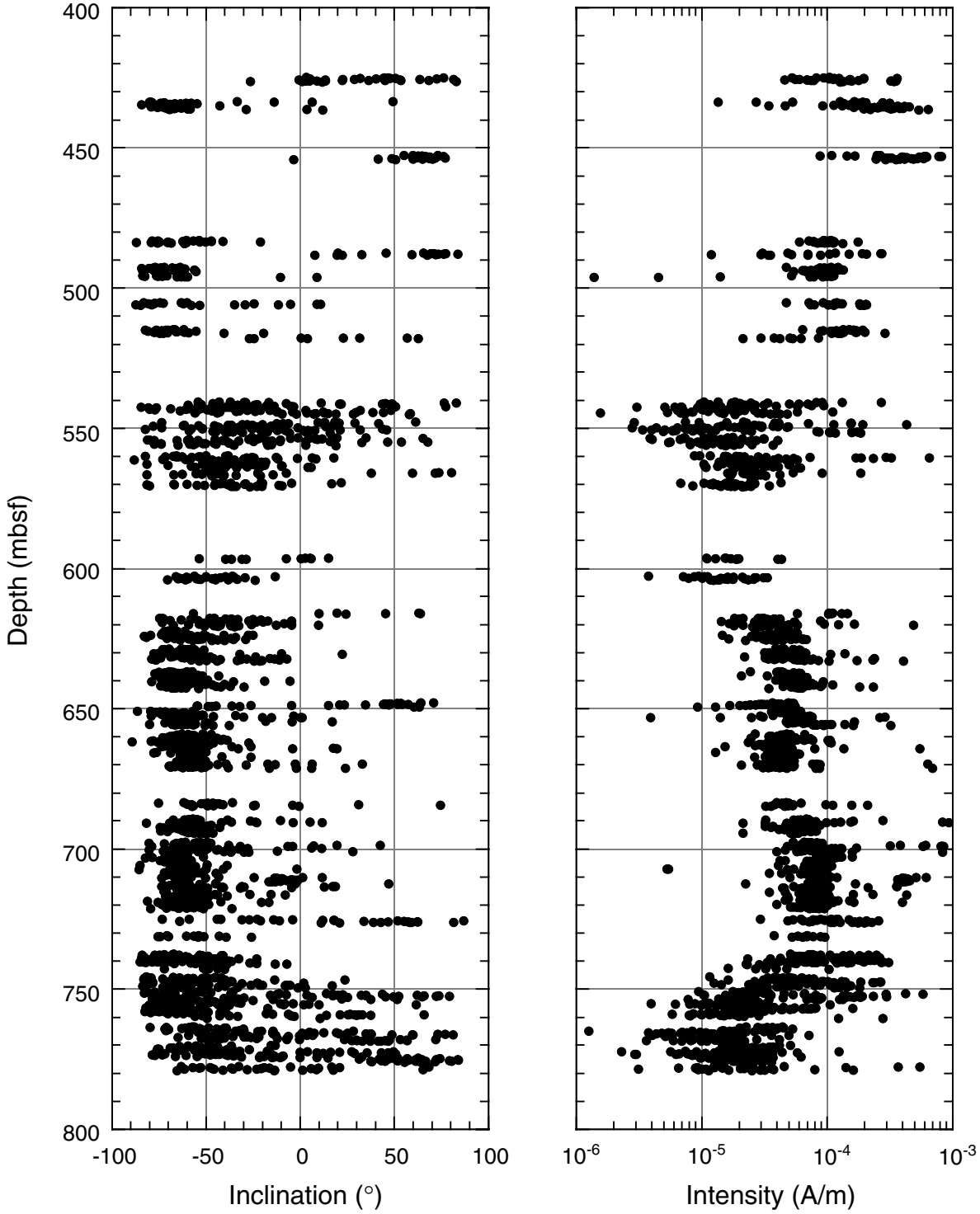

Figure F21. Remanent magnetic characteristics of samples from nannofossil ooze (Sample 189-1170A-4H-3, 55–57 cm), nannofossil chalk (Sample 189-1170A-34X-1, 58–60 cm), and claystone (Sample 189-1170D-13H-3, 68–70 cm).

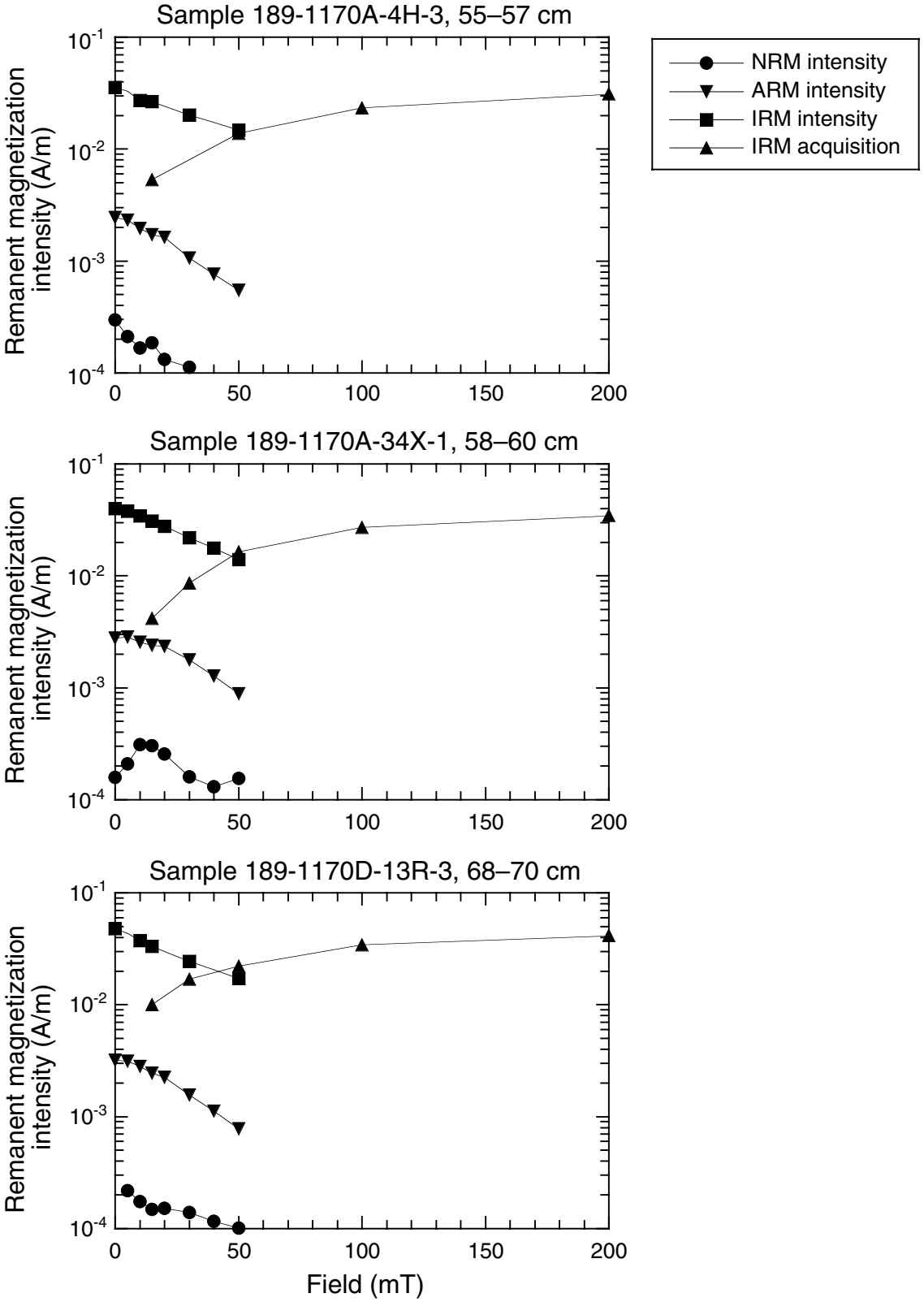

Figure F22. Variation of magnetic properties in Holes 1170A and 1170D. **A.** Variation of intensity of ARM and IRM. **B.** Variation of normalized IRM demagnetized between 0 and 20 mT and normalized IRM acquired between 200 and 500 mT.

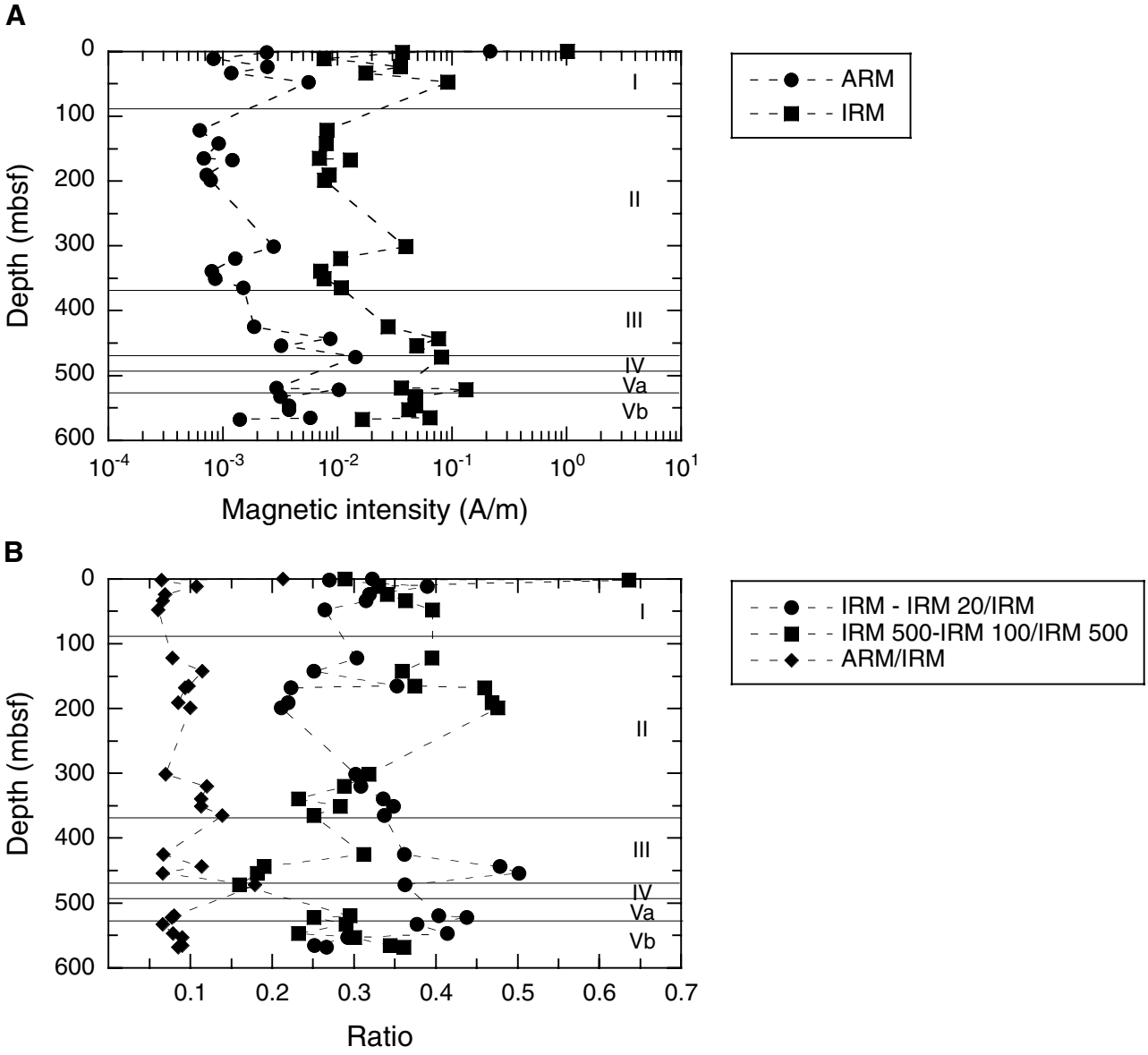

Figure F23. Age-depth relationship from paleomagnetic data.

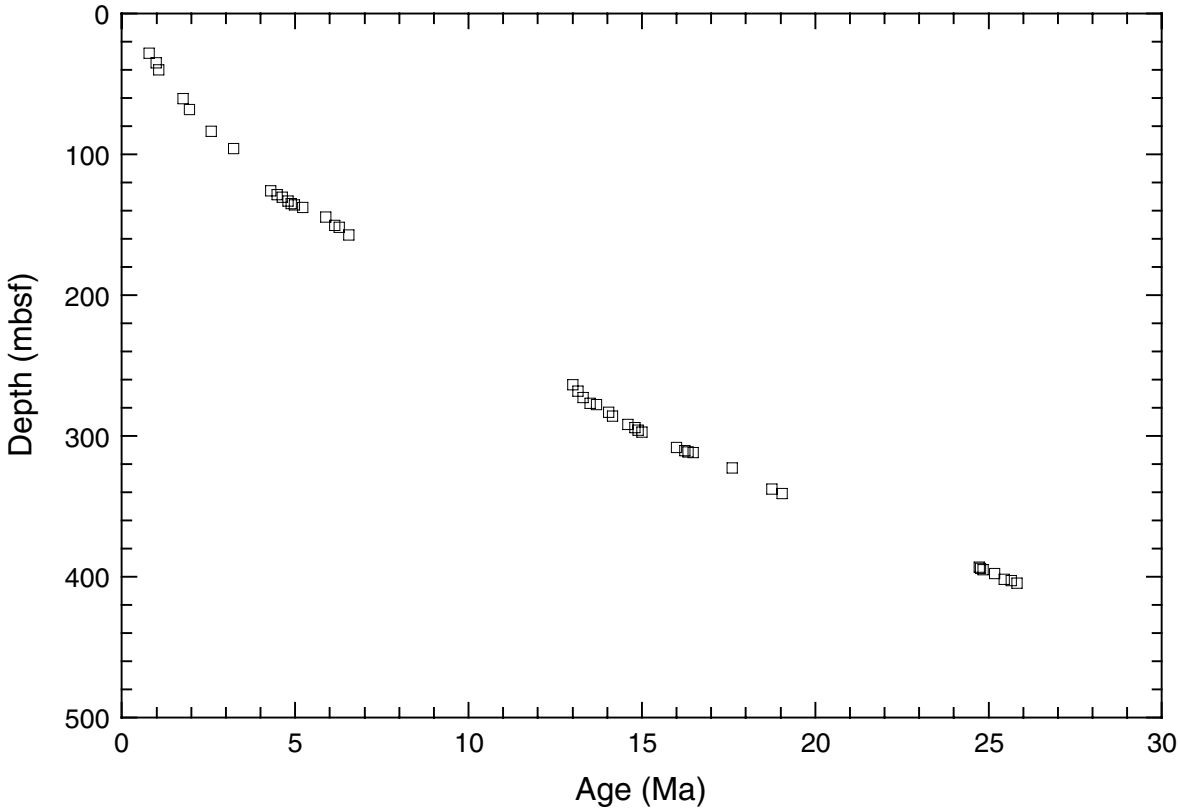

Figure F24. A. Smoothed (21-cm Gaussian) spectral reflectance (L*) data for the upper 75 mcd for Holes 1170A (left), 1170B (middle), and 1170C (right). Holes 1170B and 1170C are offset from Hole 1170A by a constant (20 and 40 L* units, respectively). **B.** Smoothed (21-cm Gaussian) magnetic susceptibility data for the upper 75 mcd for Holes 1170A (left), 1170B (middle), and 1170C (right). Holes 1170B and 1170C are offset from Hole 1170A by a constant (5×10^{-6} and 10×10^{-6}, respectively). **C.** Smoothed (21-cm Gaussian) GRA bulk density data for the upper 75 mcd for Holes 1170A (left), 1170B (middle), and 1170C (right). Holes 1170B and 1170C are offset from Hole 1170A by a constant (0.15 g/cm³ and 0.30 g/cm³, respectively).

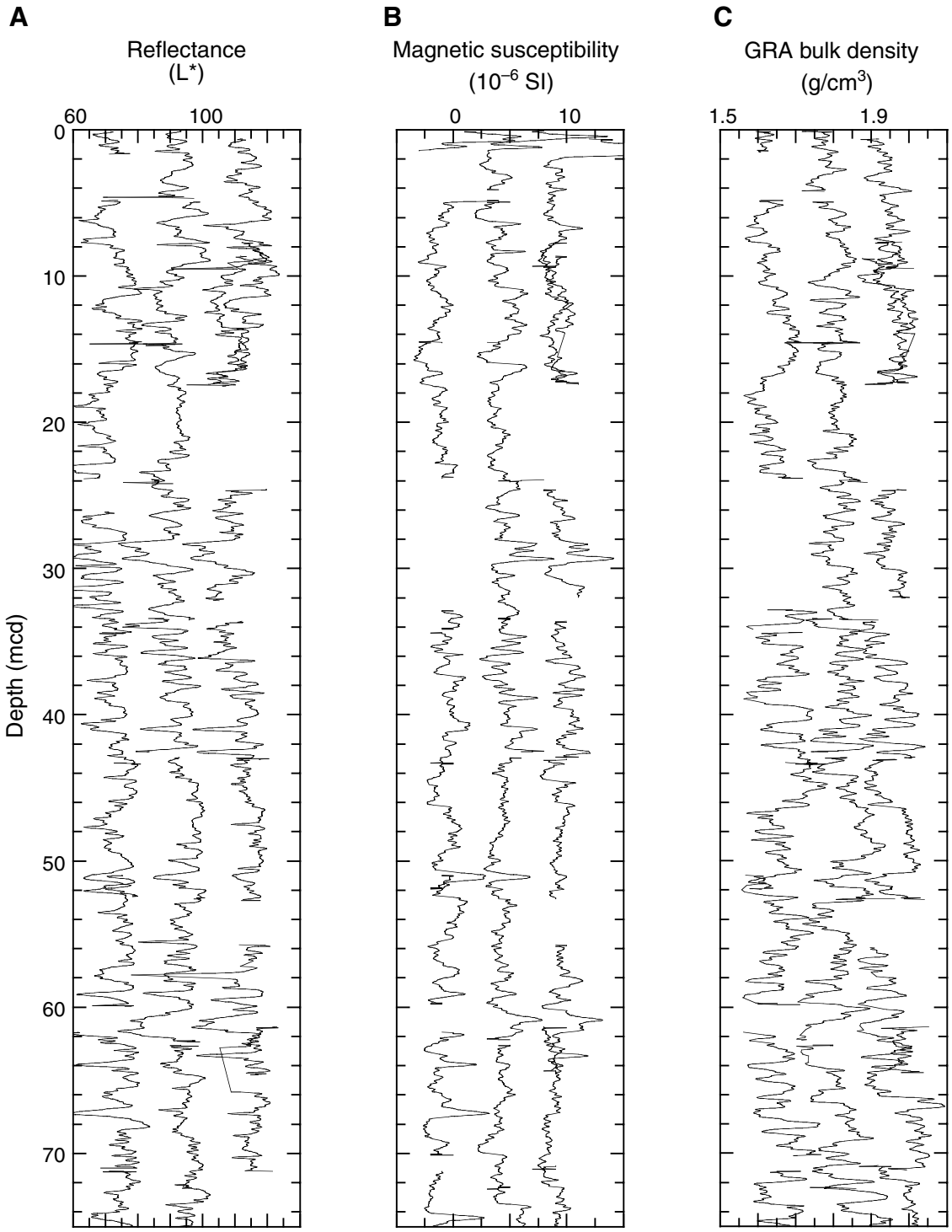

Figure F25. Plots of carbonate, total organic carbon (TOC) (squares = CNS analyzer data; dots = Rock-Eval pyrolysis values), total nitrogen, C/N and H/C ratios, and hydrogen index values for Site 1170. Data from Hole 1170A are presented in black, whereas Hole 1170D data are shown in blue. Shaded areas on the C/N ratio plot delineate typical marine and terrestrial organic matter fields. Lithostratigraphic and preliminary biostratigraphic units are shown on the right side of the figure.

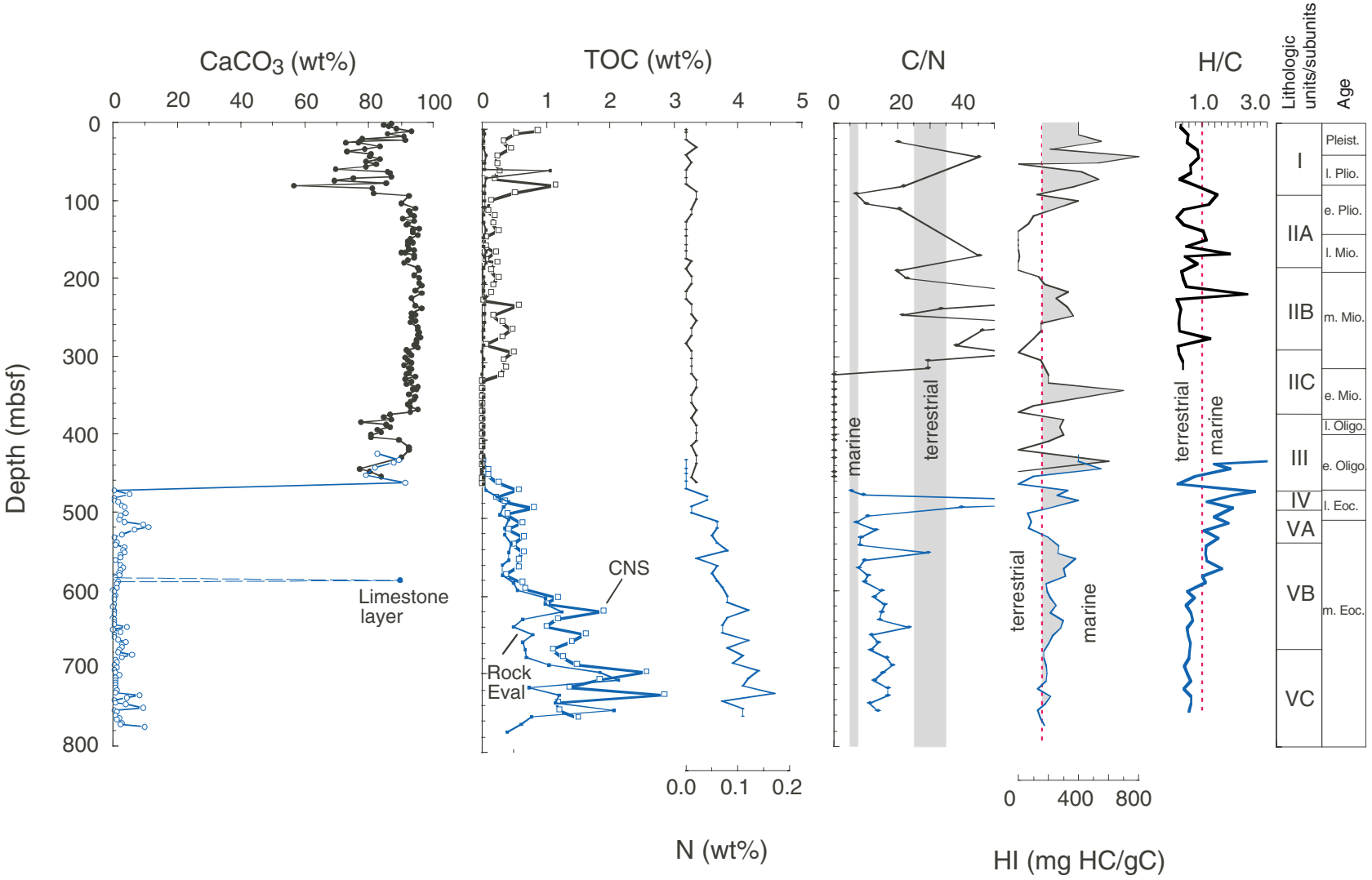

Figure F26. Total sulfur contents (squares) compared to the C/S ratios (circles) for Site 1170. Dashed lines indicate transitions between marine and brackish environments of formation. Lithostratigraphic units are indicated on the right side of the figure.

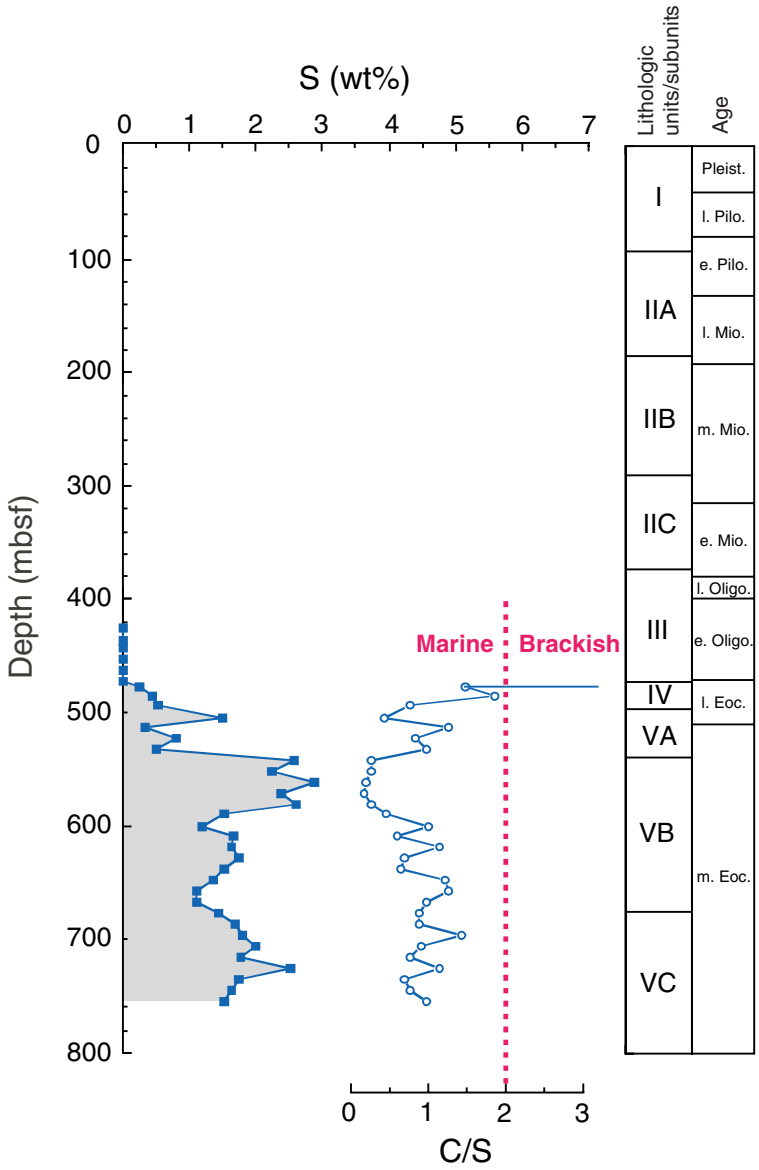

Figure F27. The T_{max} values generated from Rock-Eval pyrolysis analyses of organic matter for Site 1170. The high variability of values above ~460 mbsf is likely caused by the very low TOC values in these samples. Below 460 mbsf, the T_{max} values are indicative of immature organic matter relative to oil generation, although values approach the "oil window" (vertical dotted lines) at the base of the core.

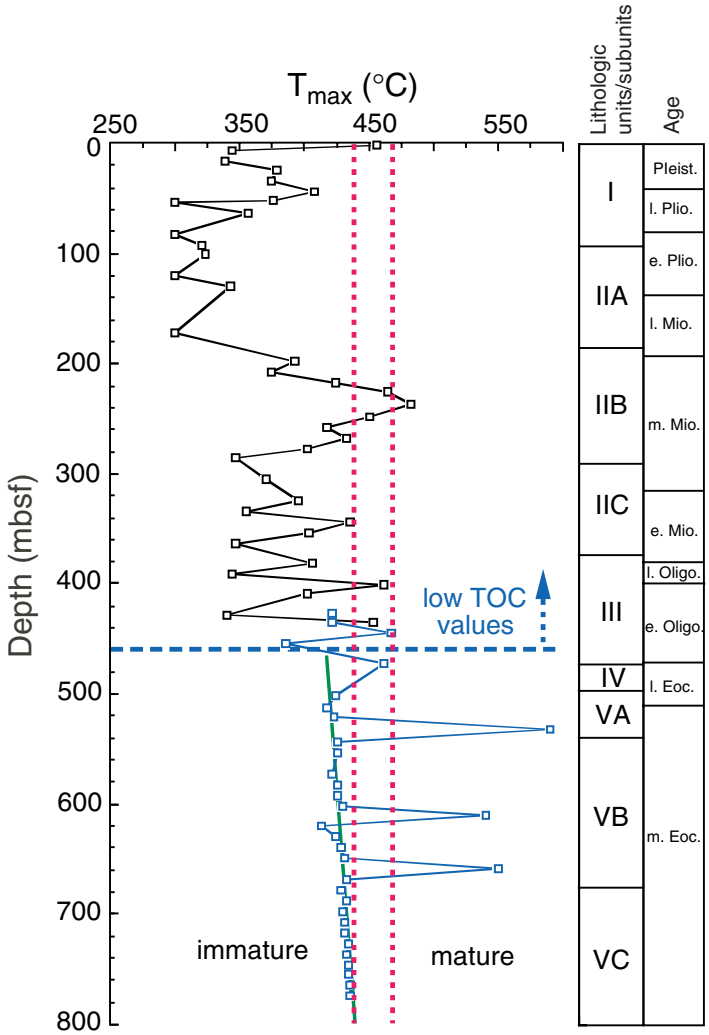

Figure F28. Methane (C_1) concentrations, methane vs. ethane and propane ratios (C_1/C_2+C_3), and percent wetness ($[C_2+C_3/C_1/C_2+C_3]100$) from headspace gas analysis at Site 1170. Dashed lines delineate biogenic and thermogenic fields on the C_1/C_2+C_3 plot (Hinz et al., 1986), whereas the shaded area on the percent wetness plot marks values typical for economically viable gas reservoirs.

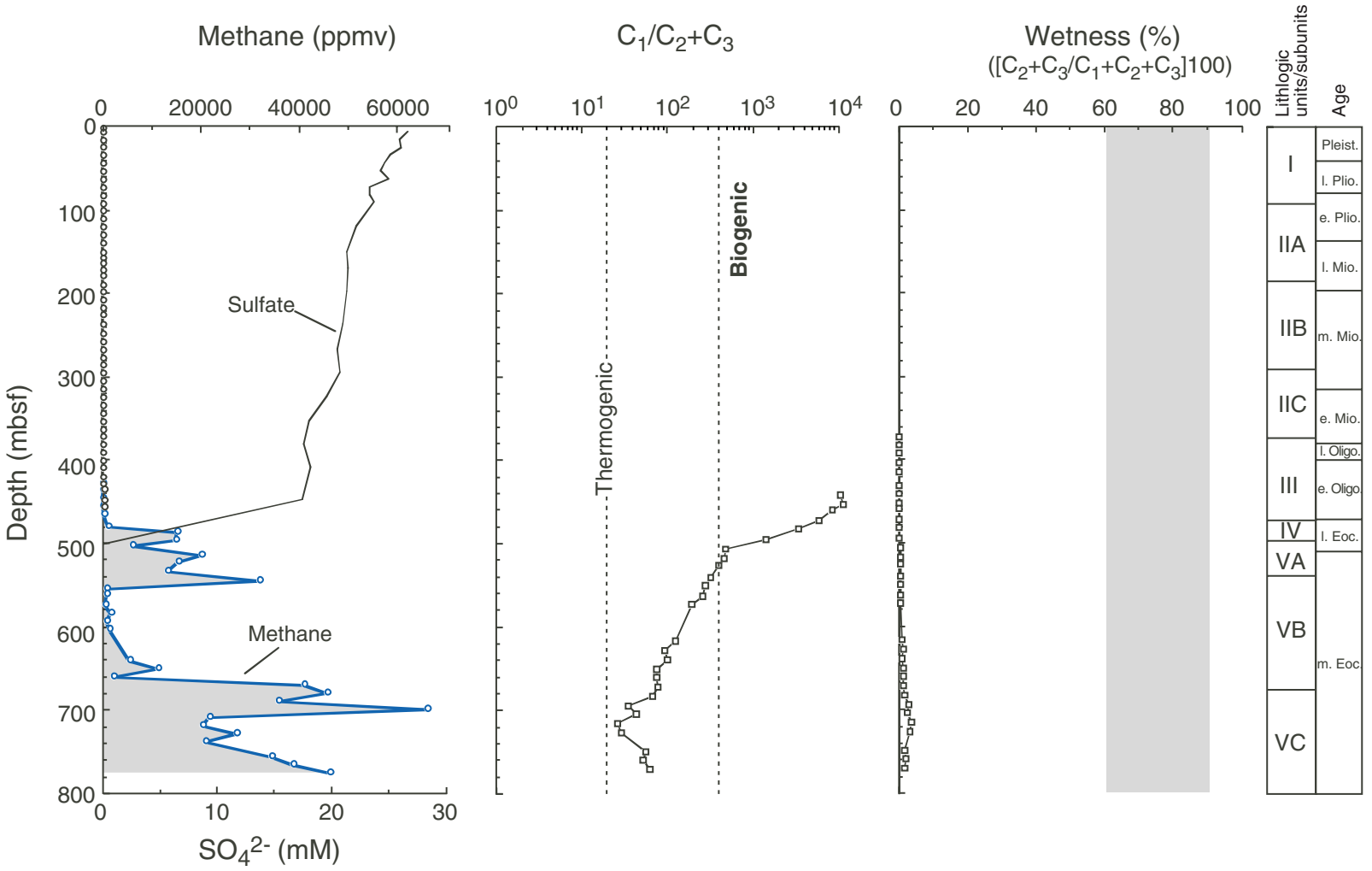

Figure F29. Concentration-depth profiles for interstitial water chemistry at Site 1170. Solid circles = samples collected from Hole 1170A. Open circles = samples from Hole 1170D. Approximate locations of lithostratigraphic boundaries and ages are also shown (see **"Lithostratigraphy,"** p. 9, and **"Biostratigraphy,"** p. 19). (Continued on next two pages.)

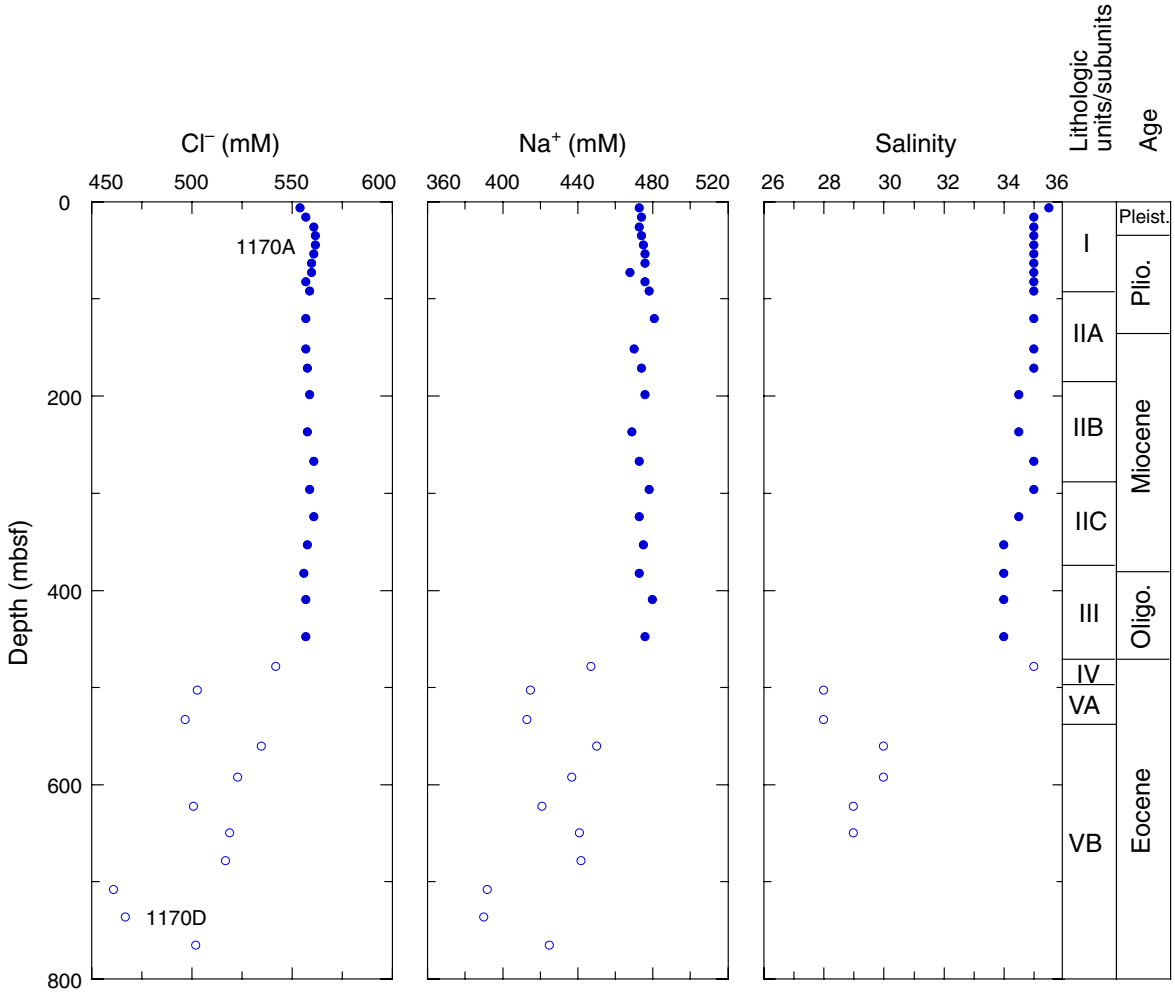

Figure F29 (continued).

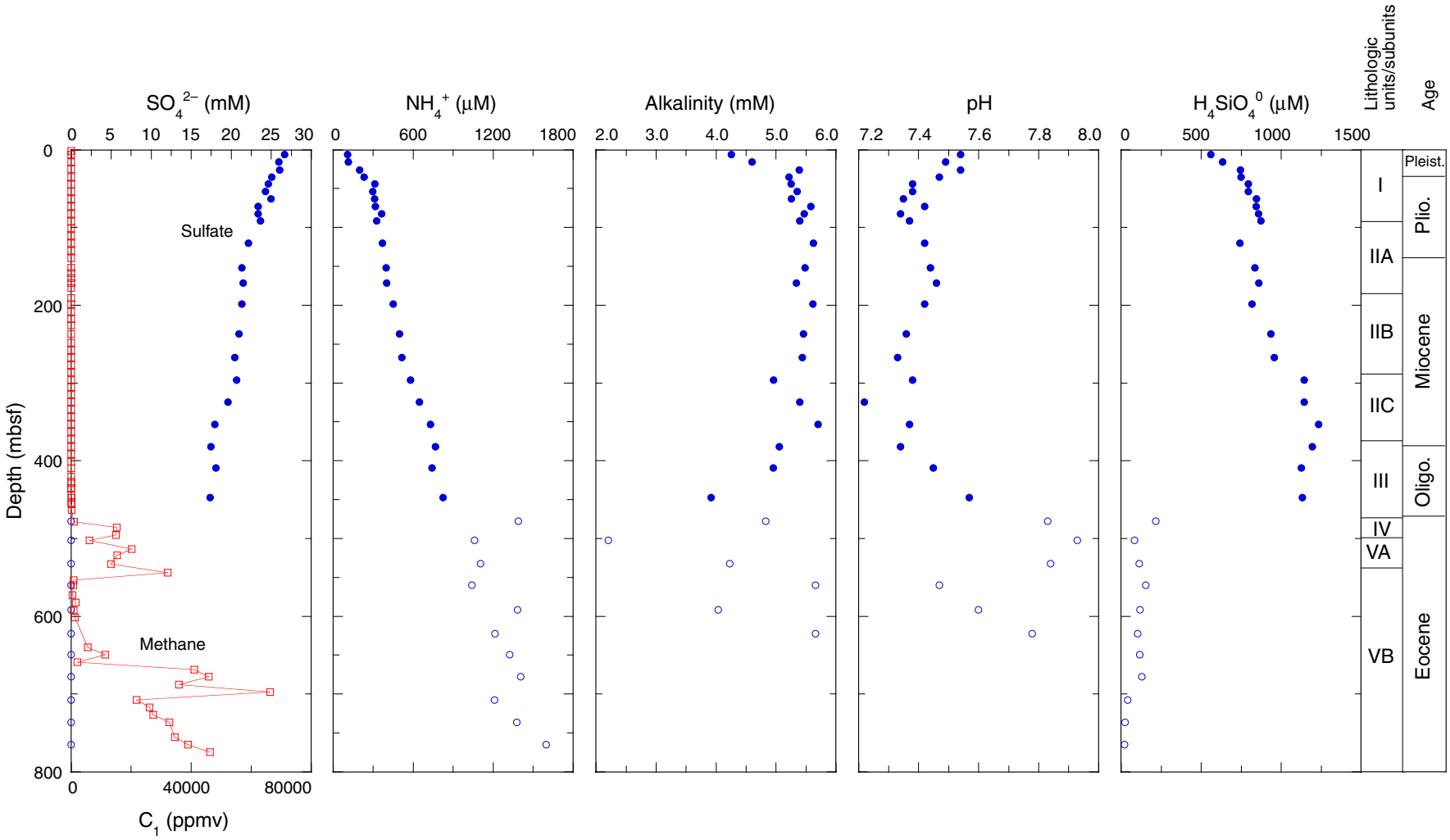

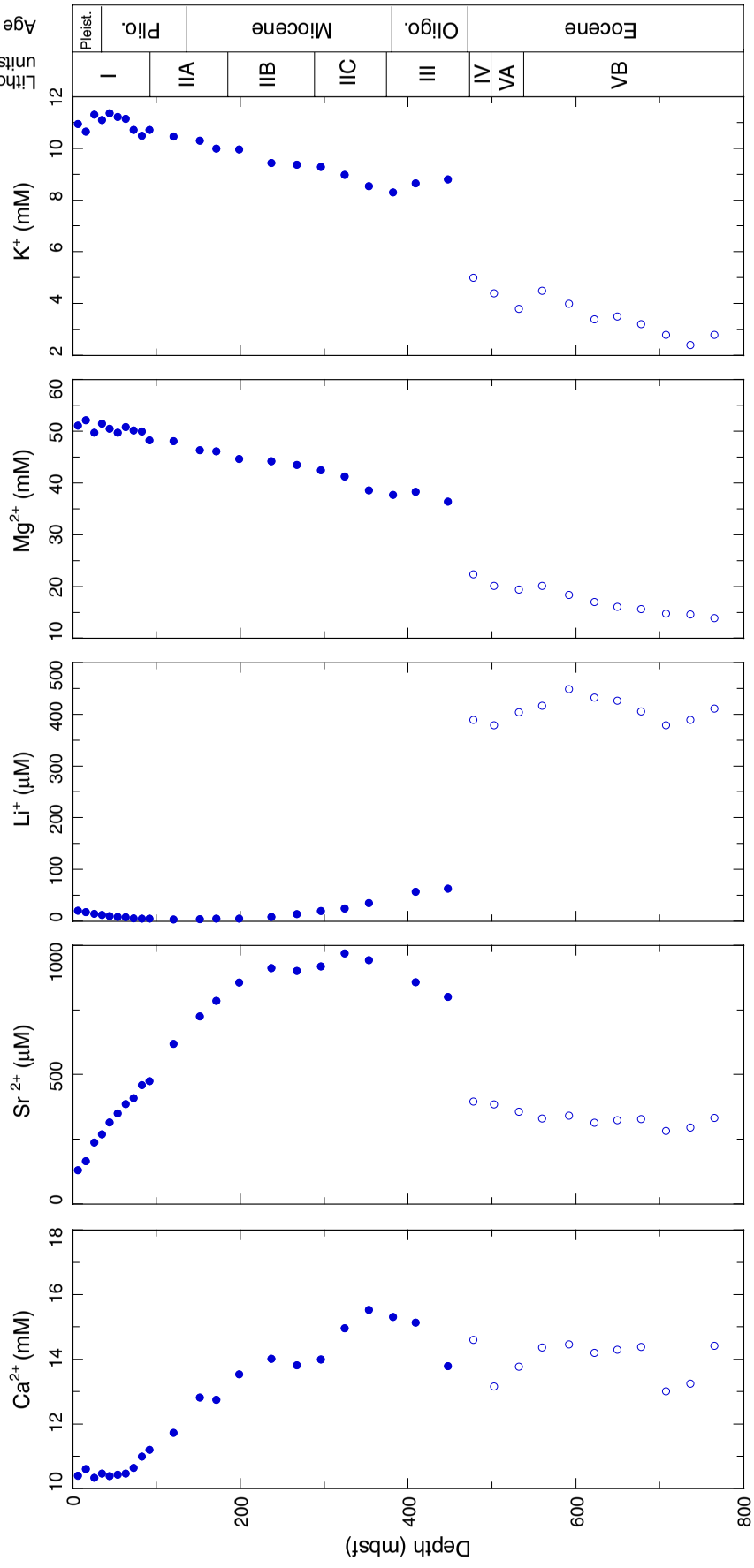

Figure F29 (continued).

Figure F30. Concentration-depth profile of Sr^{2+}/Ca^{2+} (solid circles = samples collected from Hole 1170A; open circles = samples from Hole 1170D). Interstitial water Ca^{2+} (solid blue circles = Holes 1170A; open circles = Hole 1170D) plotted vs. weight percent $CaCO_3$ (red squares). Approximate locations of lithostratigraphic boundaries and ages are also shown (see **"Lithostratigraphy,"** p. 9, and **"Biostratigraphy,"** p. 19).

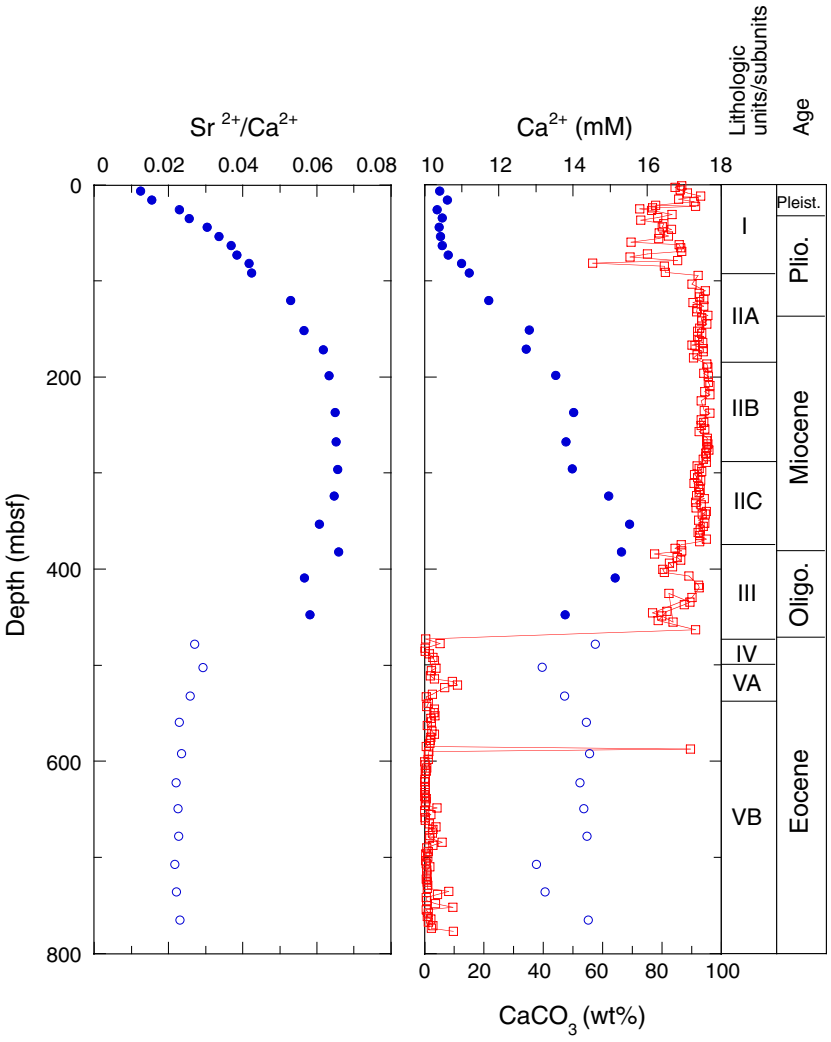

Figure F31. **A.** Magnetic susceptibility measured on whole cores by the MST vs. depth for Holes 1170A and 1170D. (Continued on next two pages.)

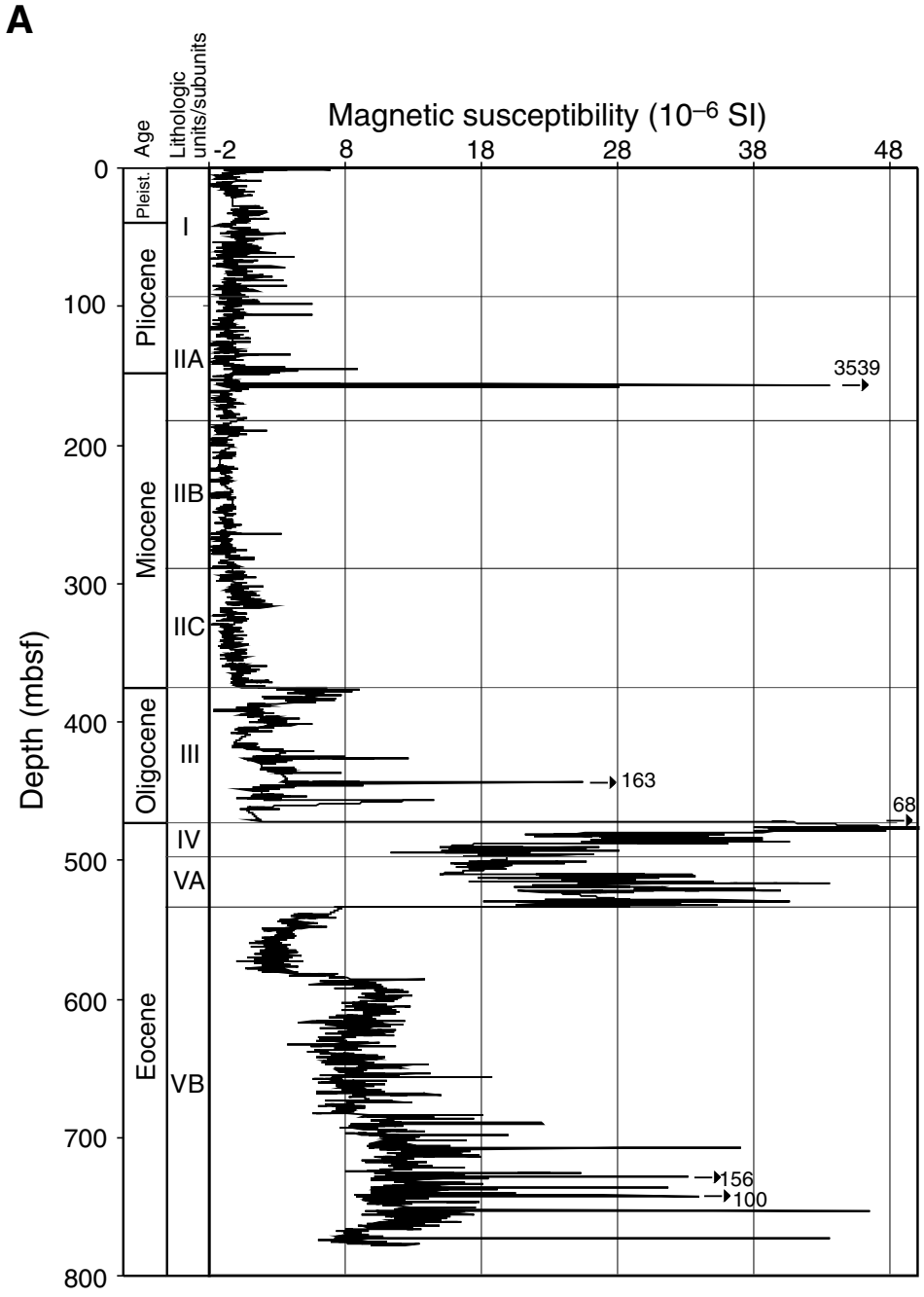

Figure F31 (continued). B. GRA density (dots) and wet-bulk density determined for discrete samples (open circles) vs. depth for Holes 1170A and 1170D.

B

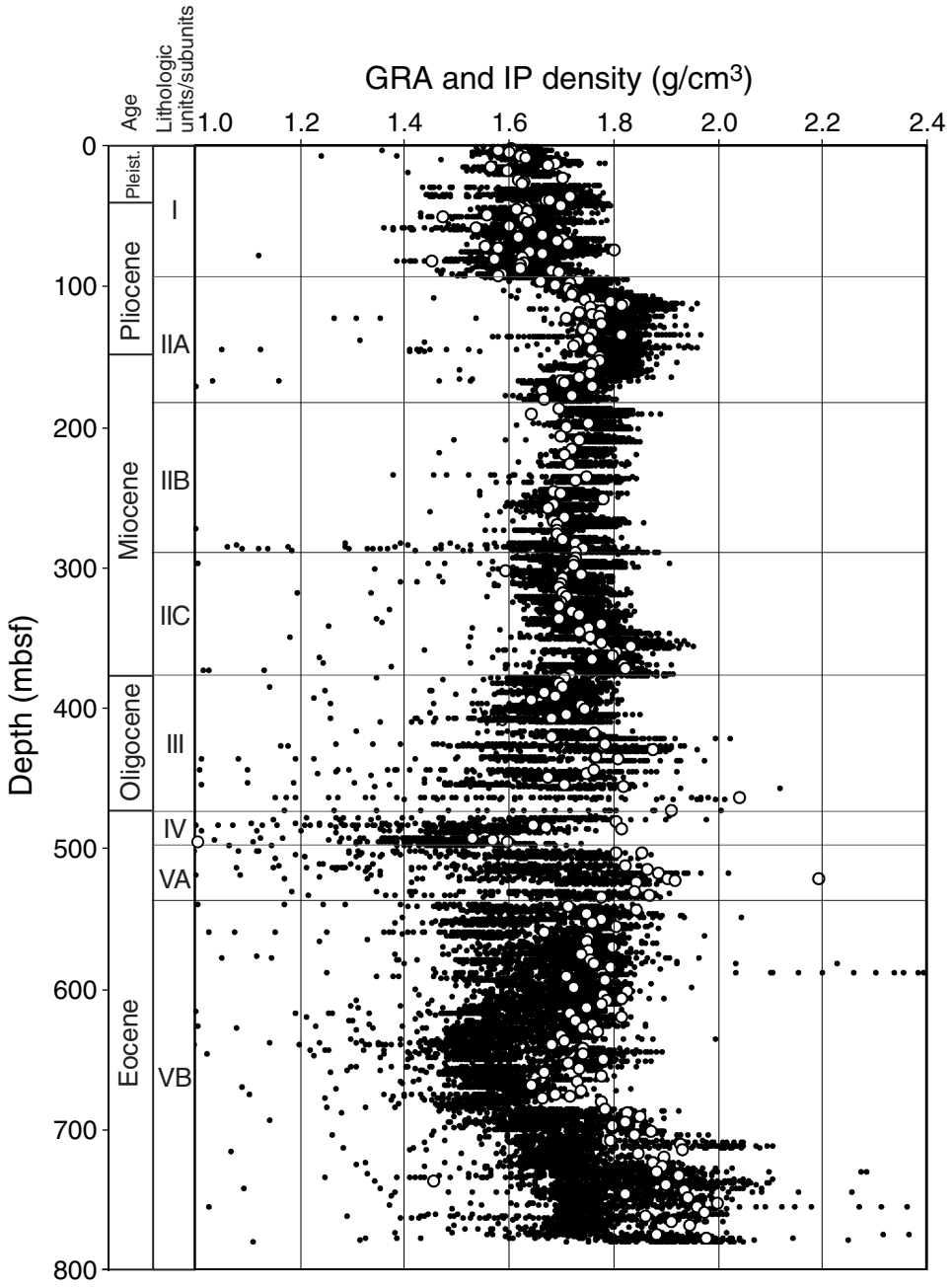

Figure F31 (continued). C. Natural gamma ray measured on whole cores by the MST vs. depth for Hole 1170A.

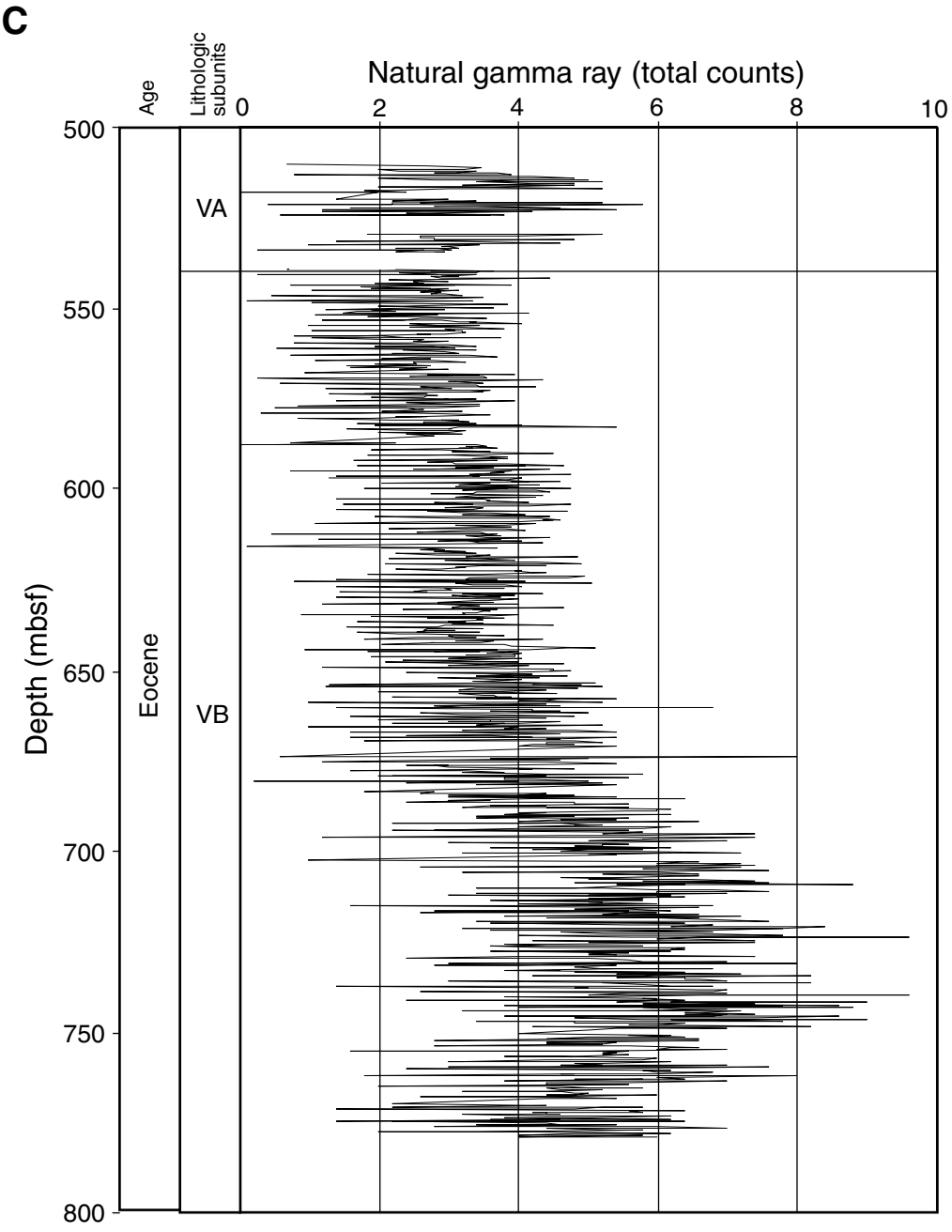

Figure F32. *P*-wave velocities (PWS1, PWS2, and PWS3) measured for discrete samples and *P*-wave velocities measured in whole cores (MST) vs. depth for the upper part of Hole 1170A. See Figure **F38B,** p. 102, in the "Site 1168" chapter for illustration of the three directions of measurement.

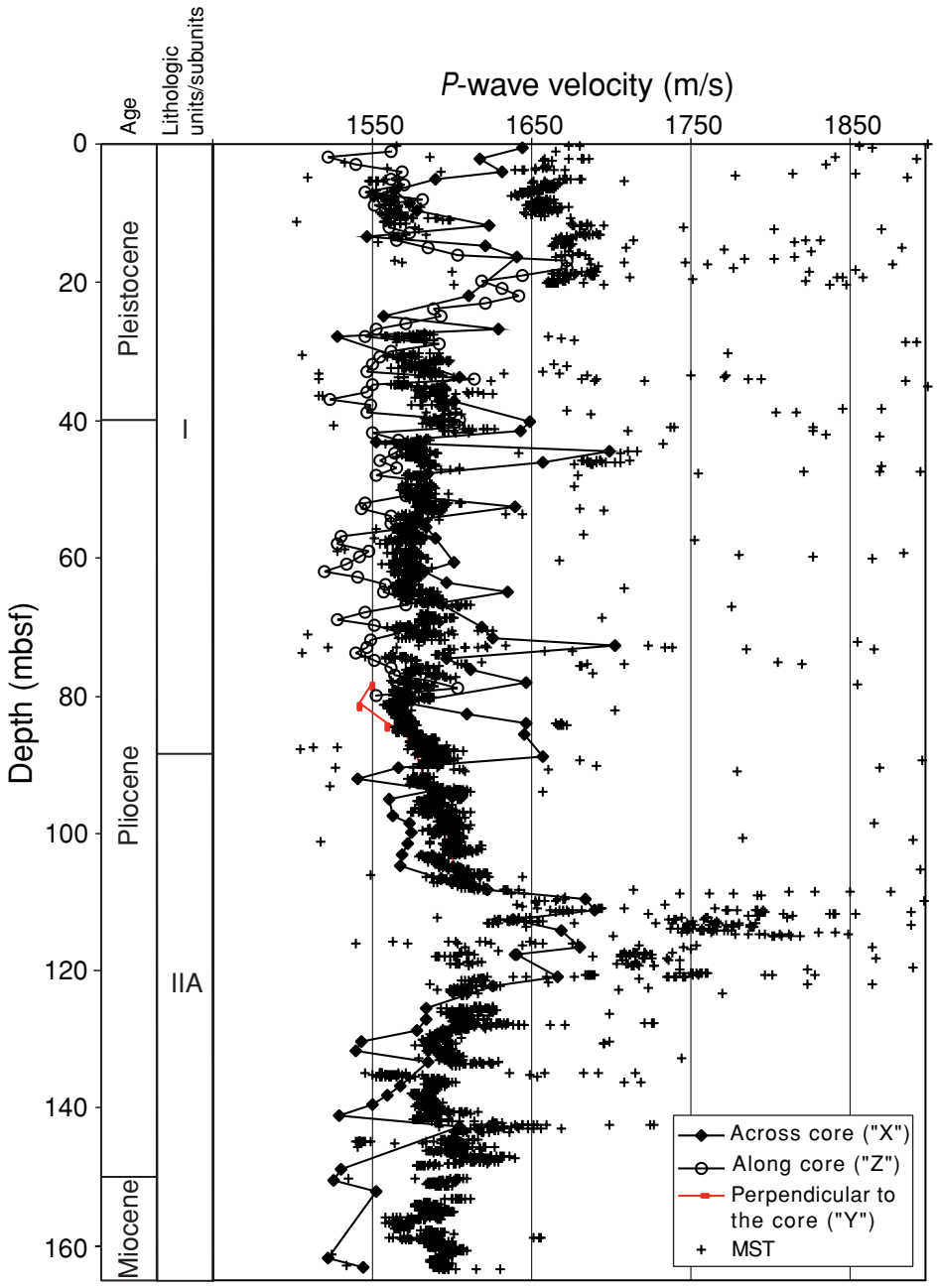

Figure F33. *P*-wave velocities (PWS3) measured for discrete samples vs. depth for Holes 1170A (open circles) and 1170D (solid diamonds). Measurements of sediment cubes cut from the limestone horizons within lithostratigraphic Unit V show peaks of relatively high velocity.

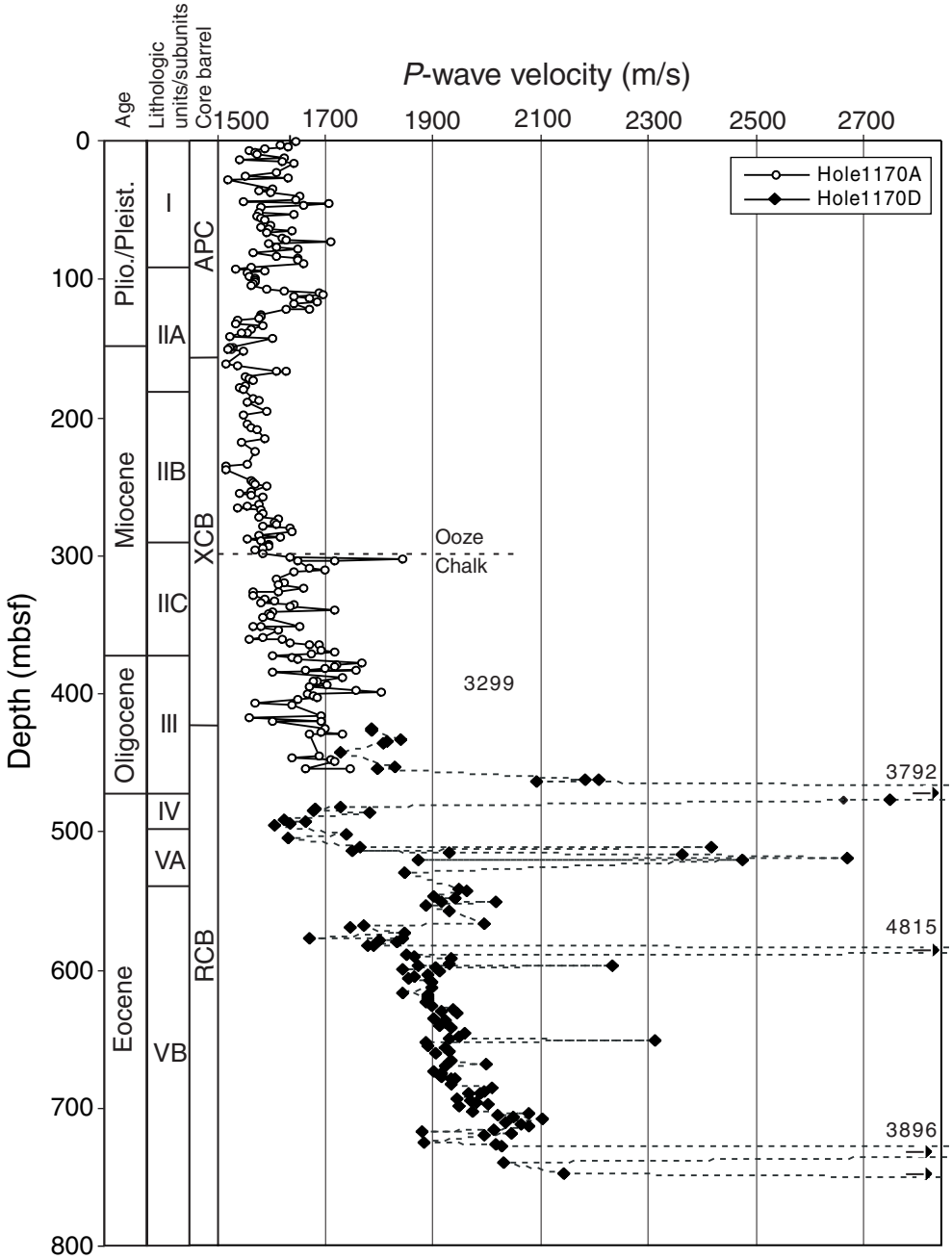

Figure F34. Thermal conductivity measured on whole cores vs. depth, Hole 1170A.

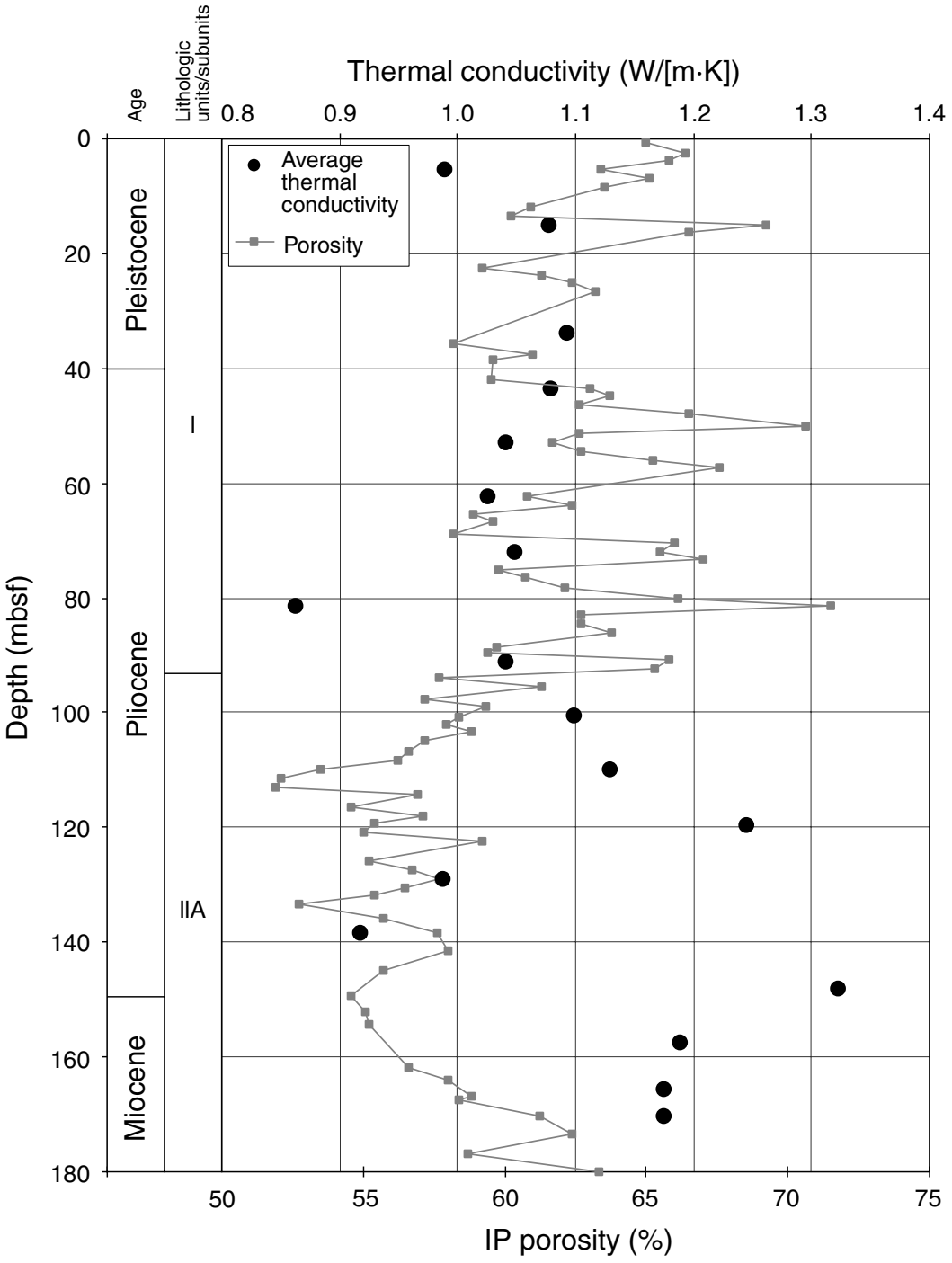

Figure F35. Wet bulk density, water content, and porosity measured at discrete intervals vs. depth, Site 1170.

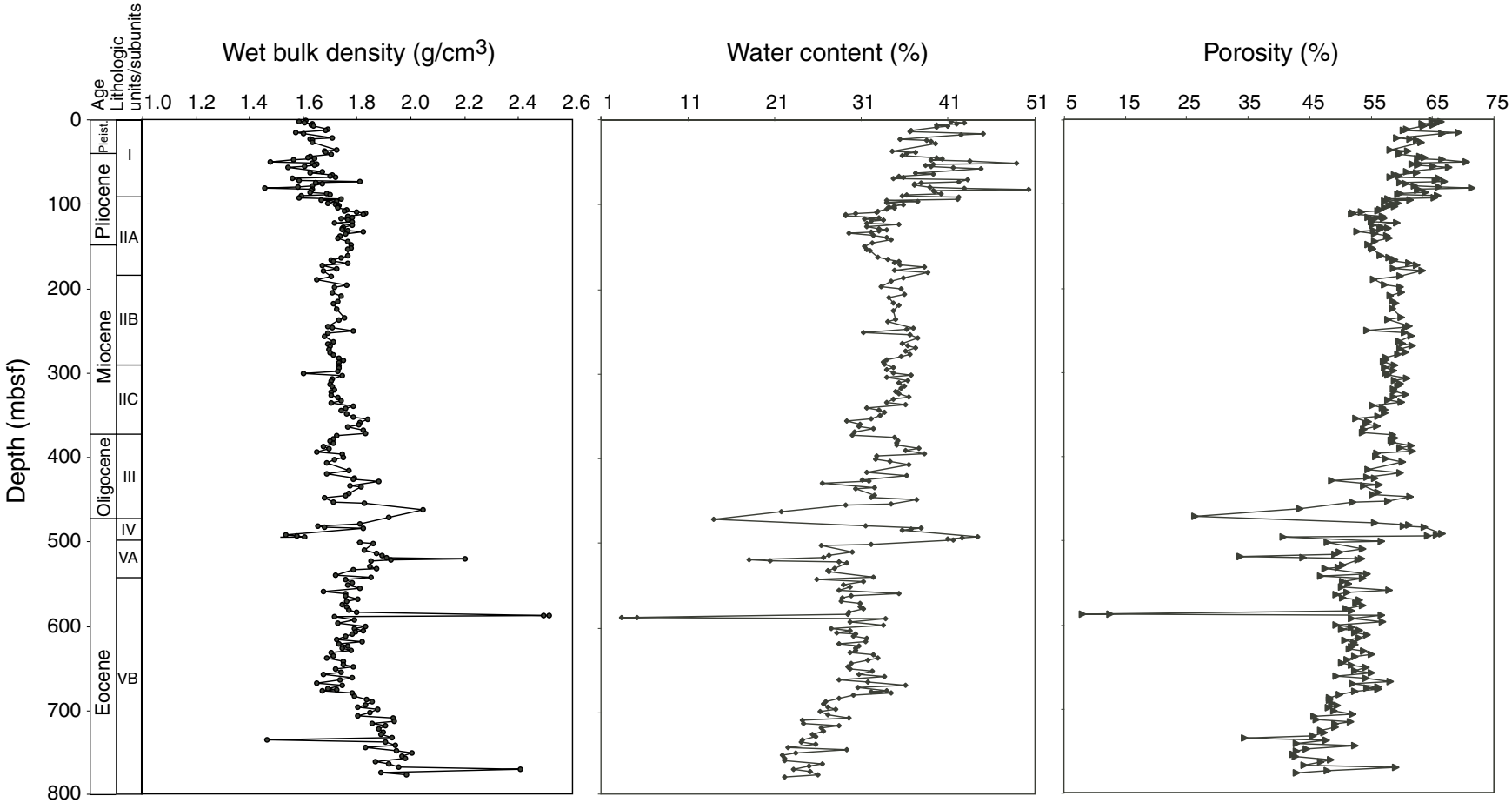

Figure F36. Temperature vs. depth, Site 1170.

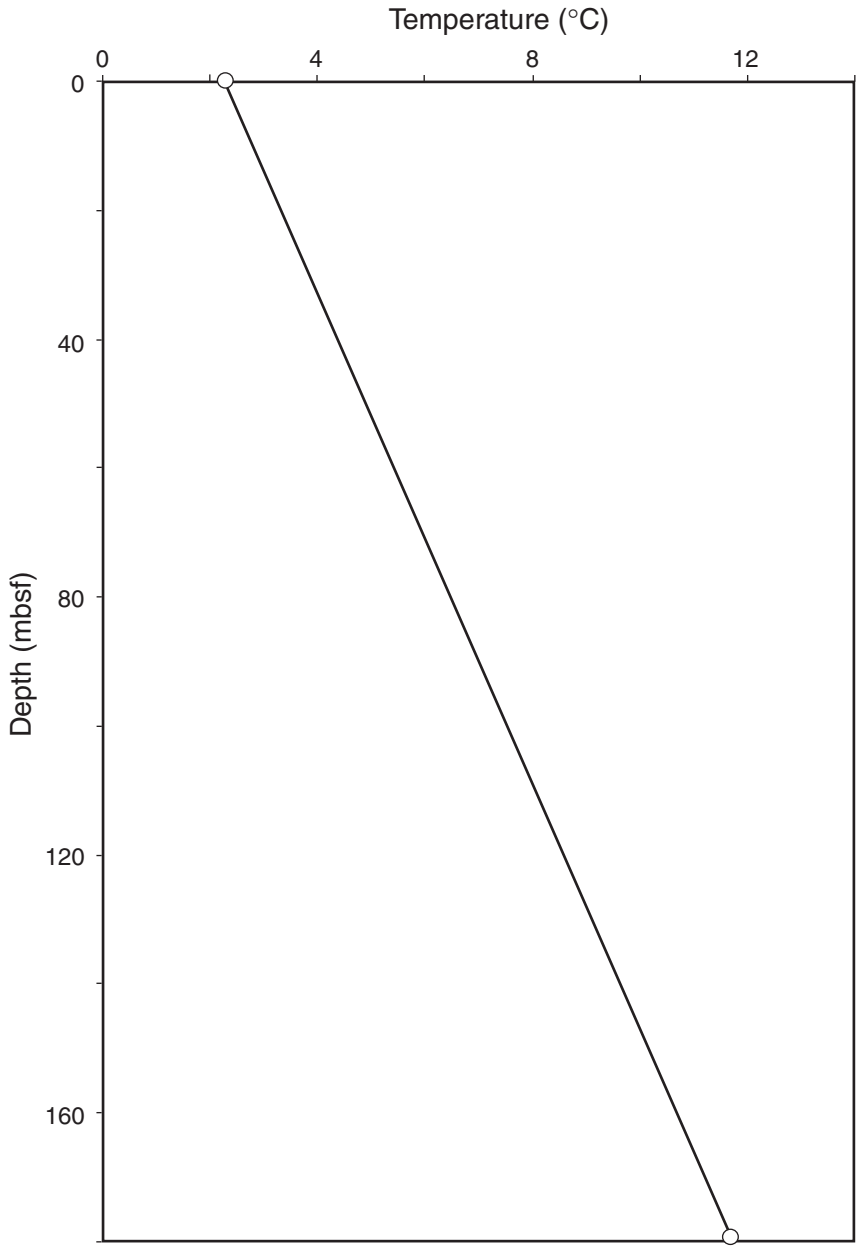

$y = 0.0521x + 2.28$

Geothermal gradient = 52°C/km

Average thermal conductivity = 1.083 (W/[m·K])

Heat flow = 56 W/m^2

Figure F37. Undrained shear strength from miniature vane-shear measurements (line) and GRA density (dots) vs. depth, Hole 1170A.

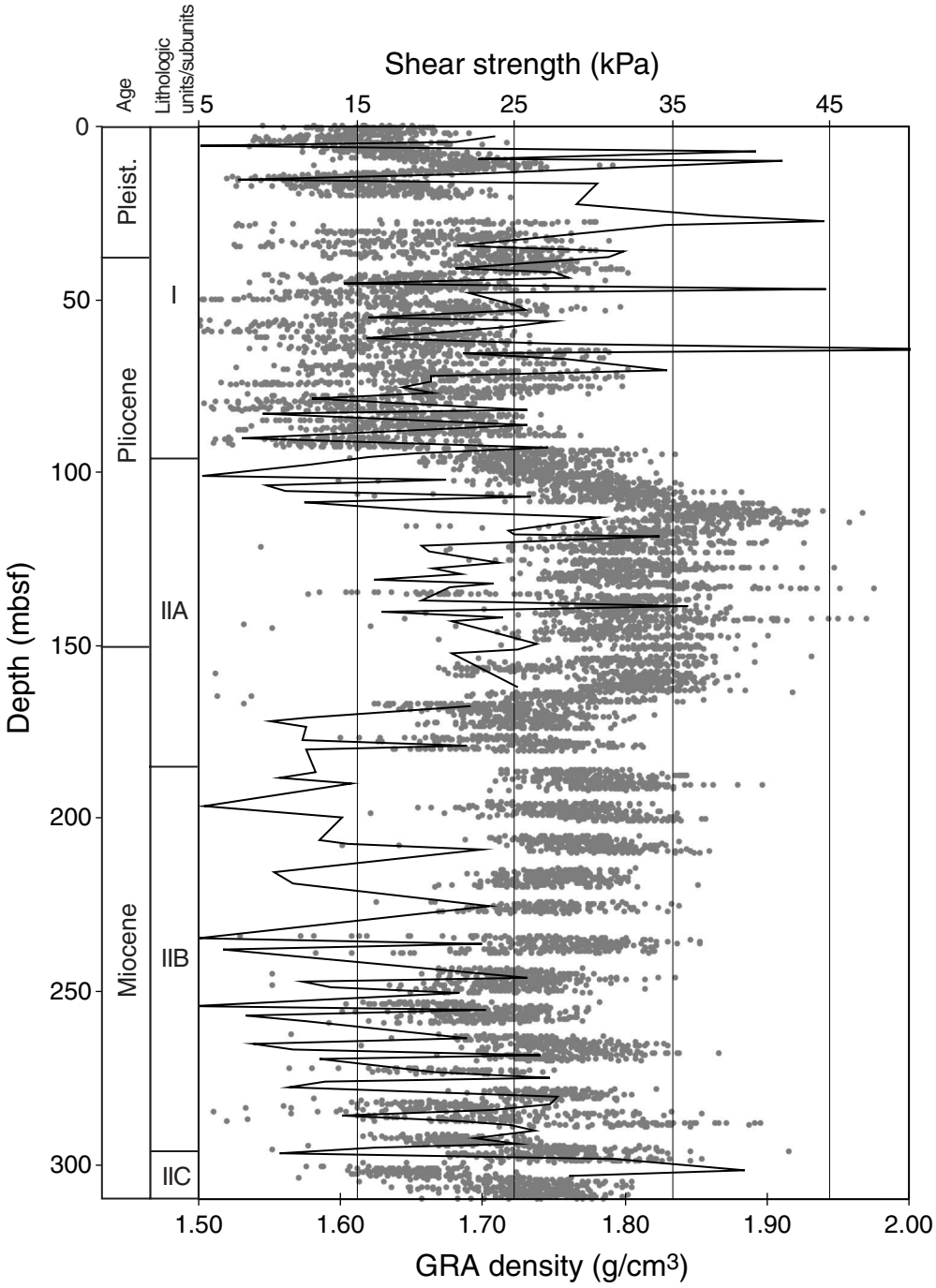

Figure F38. Details of the logging operations in Hole 1170D. Depths are shown in either meters below rig floor (mbrf) or meters below seafloor (mbsf). Run 3 was unsuccessful.

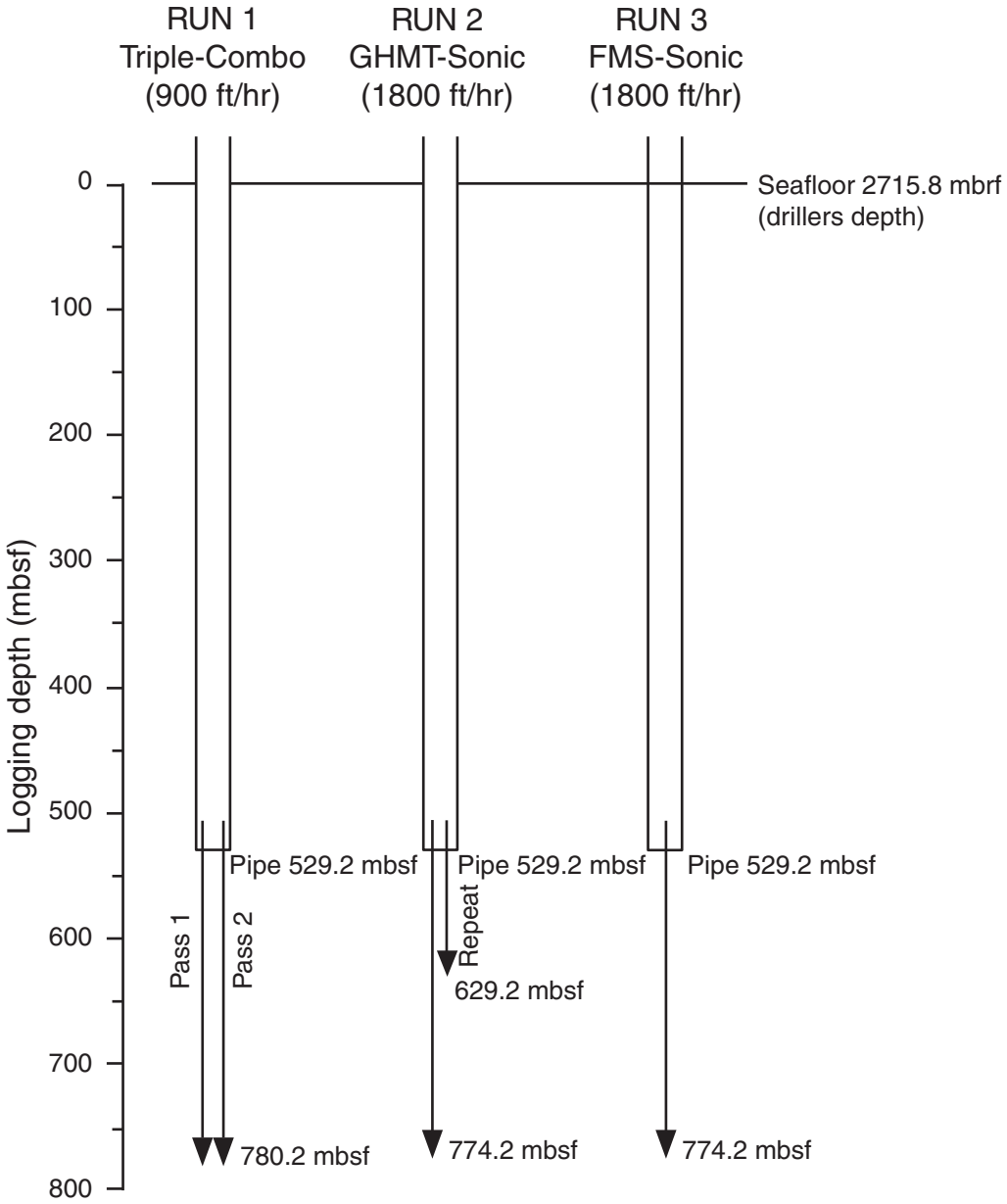

Figure F39. Caliper, gamma-ray, resistivity, and magnetic susceptibility (log and core) values from Hole 1170D.

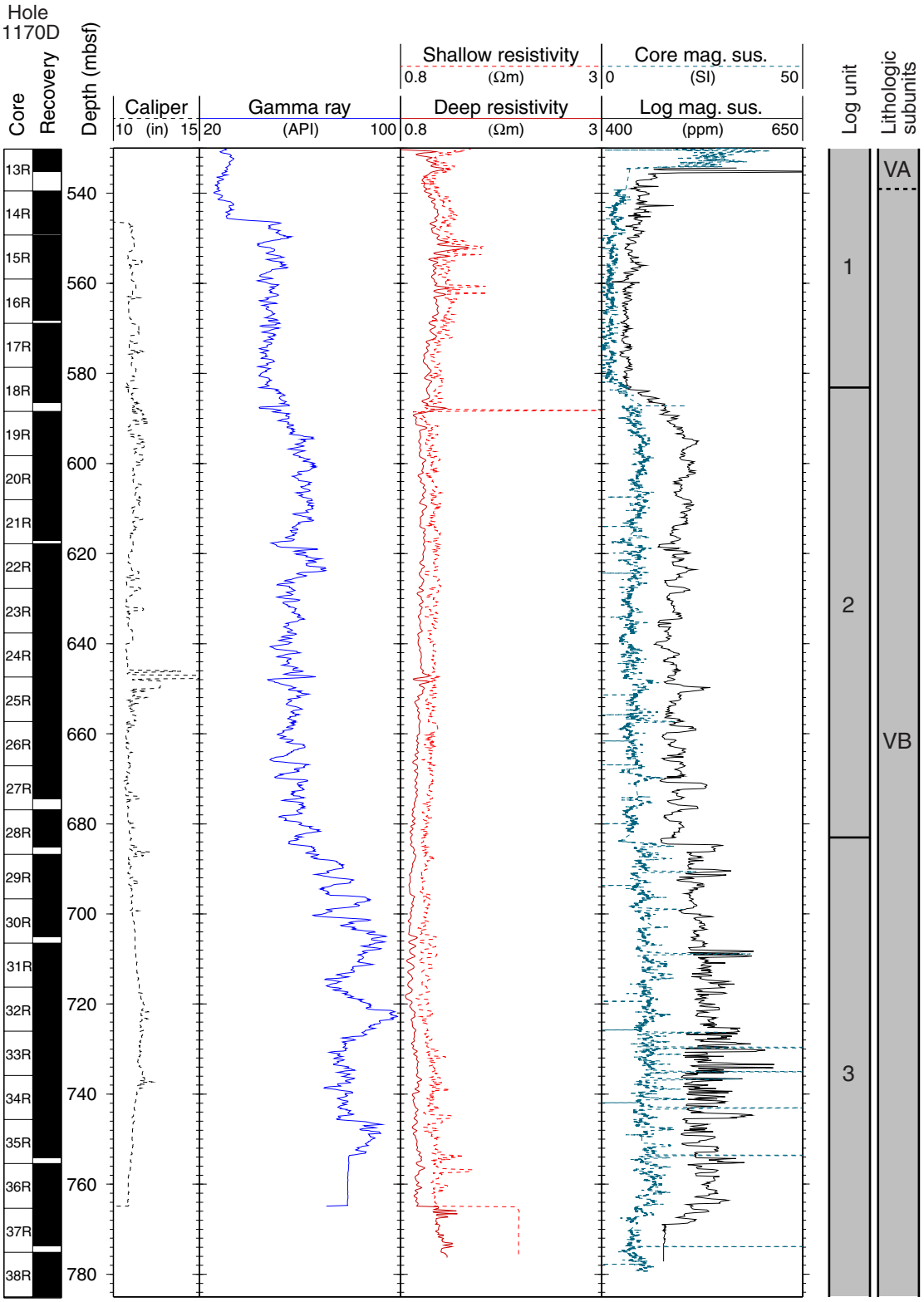

Figure F40. Velocity, density, porosity, and photoelectric effect (PEFL) values from Hole 1170D.

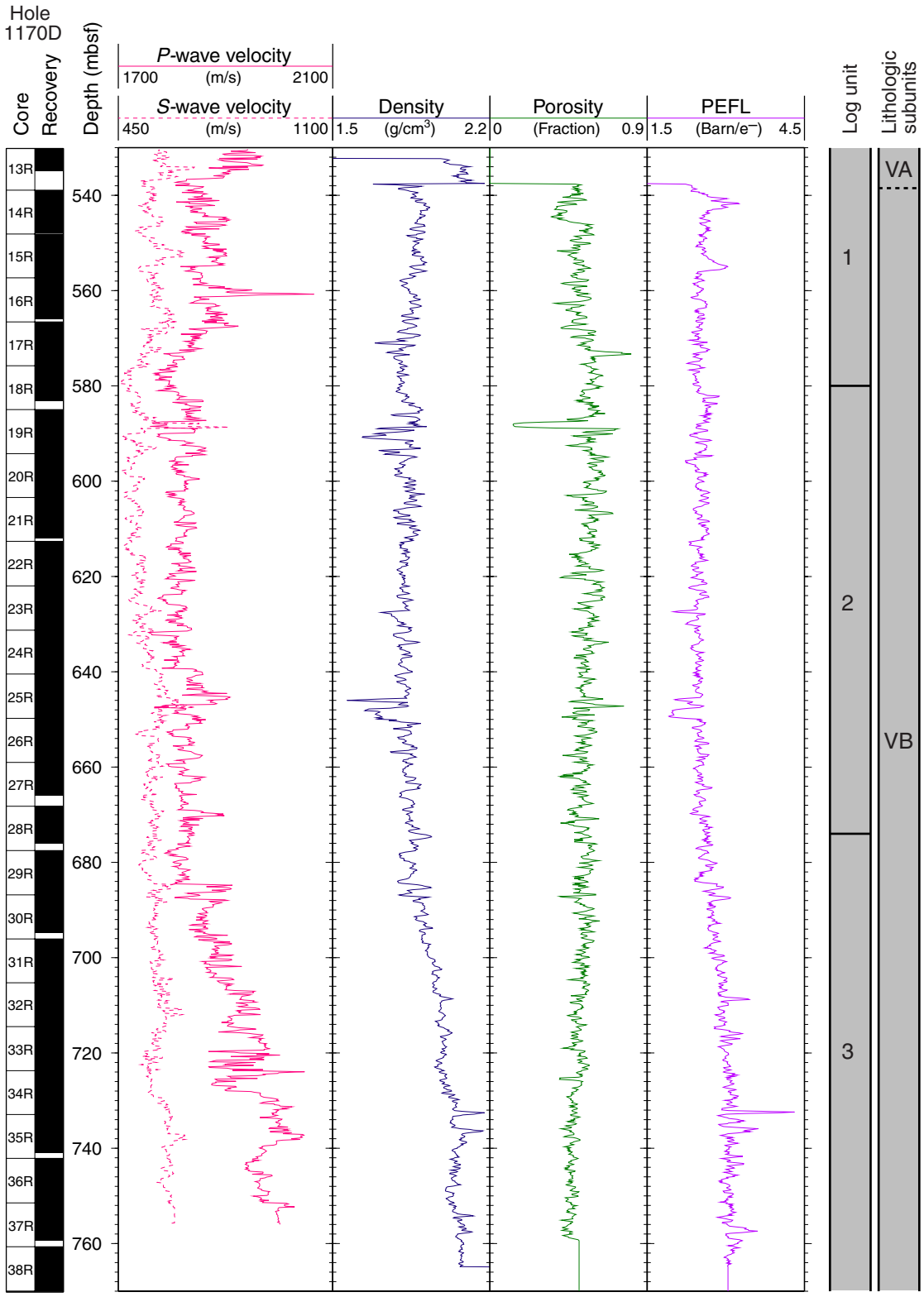

Figure F41. Total gamma-ray and spectral gamma-ray values from Hole 1170D. HSGR = total gamma radiation (from Th, K, and U). HCGR = gamma radiation from Th and K only.

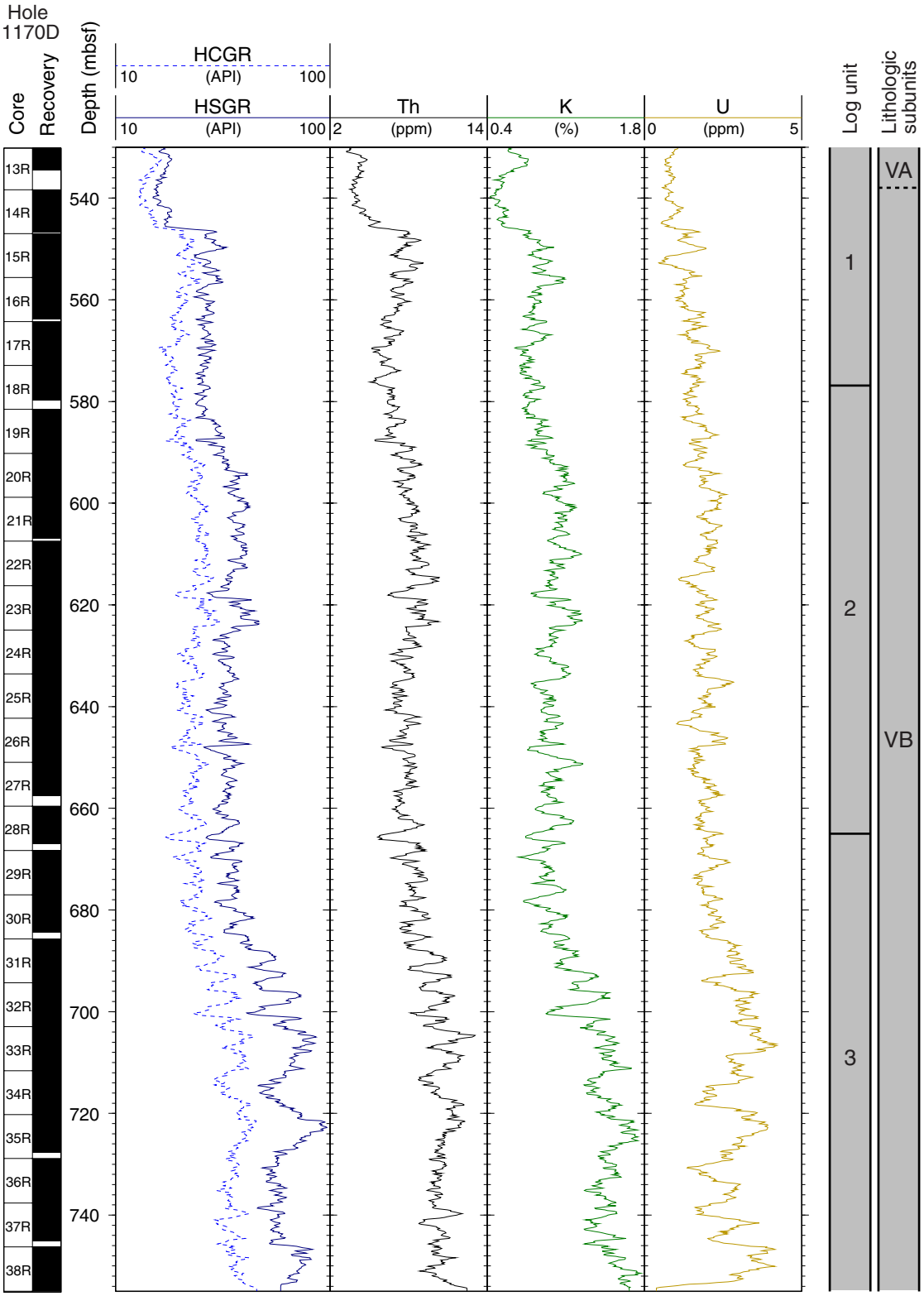

Figure F42. Downhole log bulk density plotted with core bulk density.

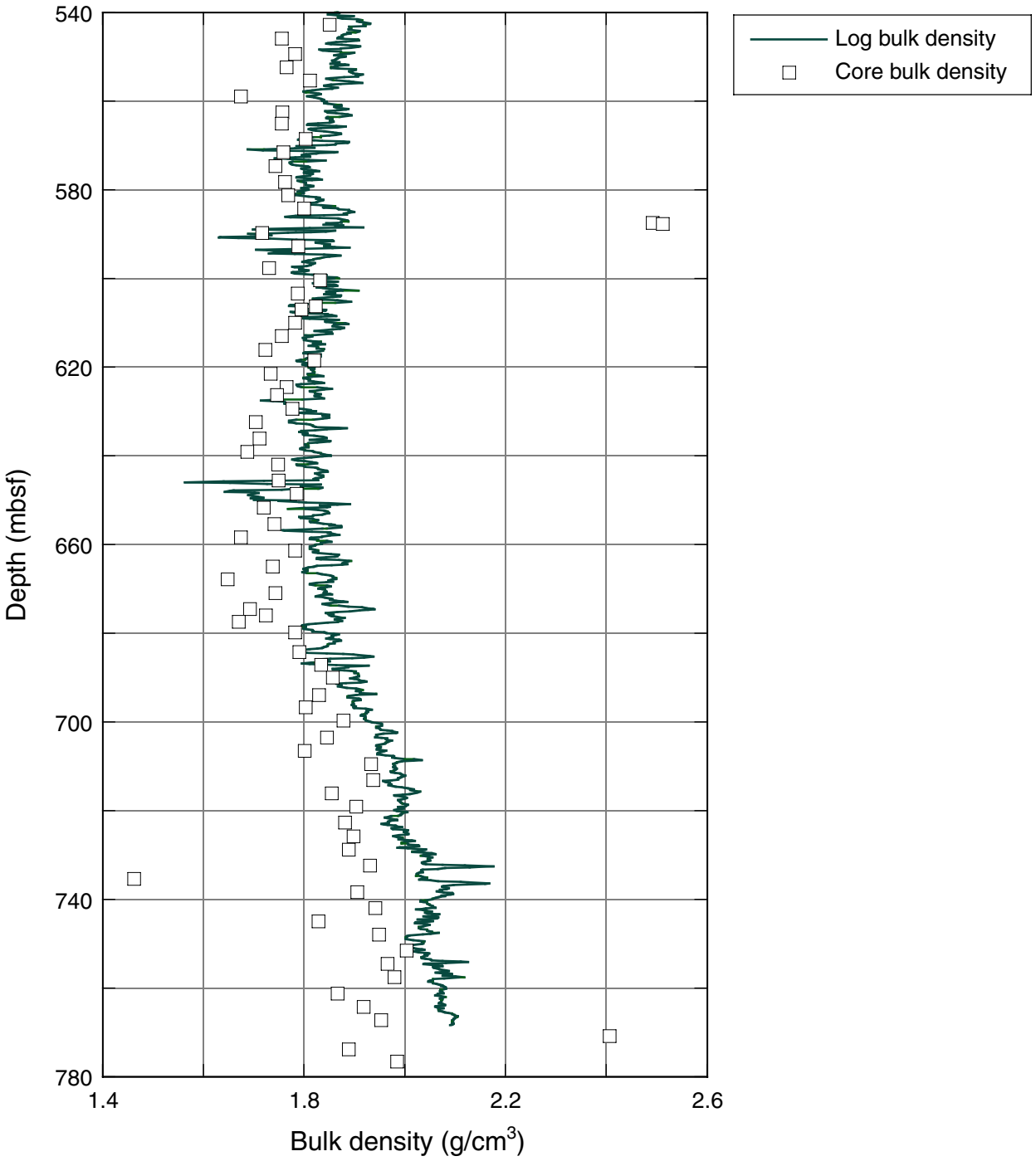

Figure F43. Downhole density porosity and neutron porosity plotted with core porosity.

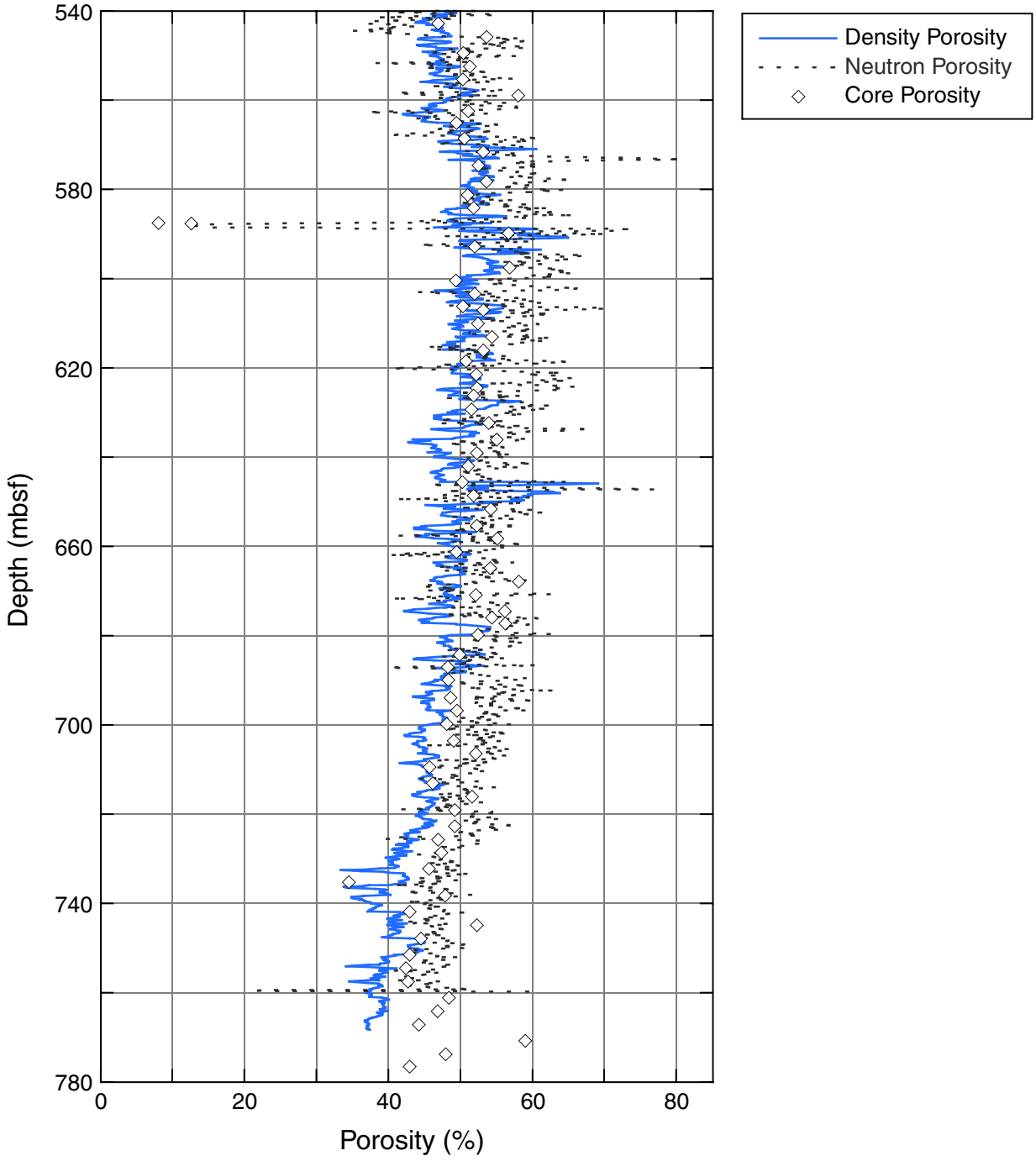

Figure F44. Formation MicroScanner (FMS) image from the top of log Unit 2. The caliper data (C1 and C2), the gamma-ray values (SGR) from this tool string, and the shallow resistivity (SFLU) and neutron porosity (APLC) from the triple-combo tool are also shown. An indurated limestone horizon can clearly be seen at 589 mbsf as a light stripe in the FMS, a decrease in the gamma and neutron porosity, and an increase in the shallow resistivity. There is a slight depth mismatch between the data from the two different tool strings.

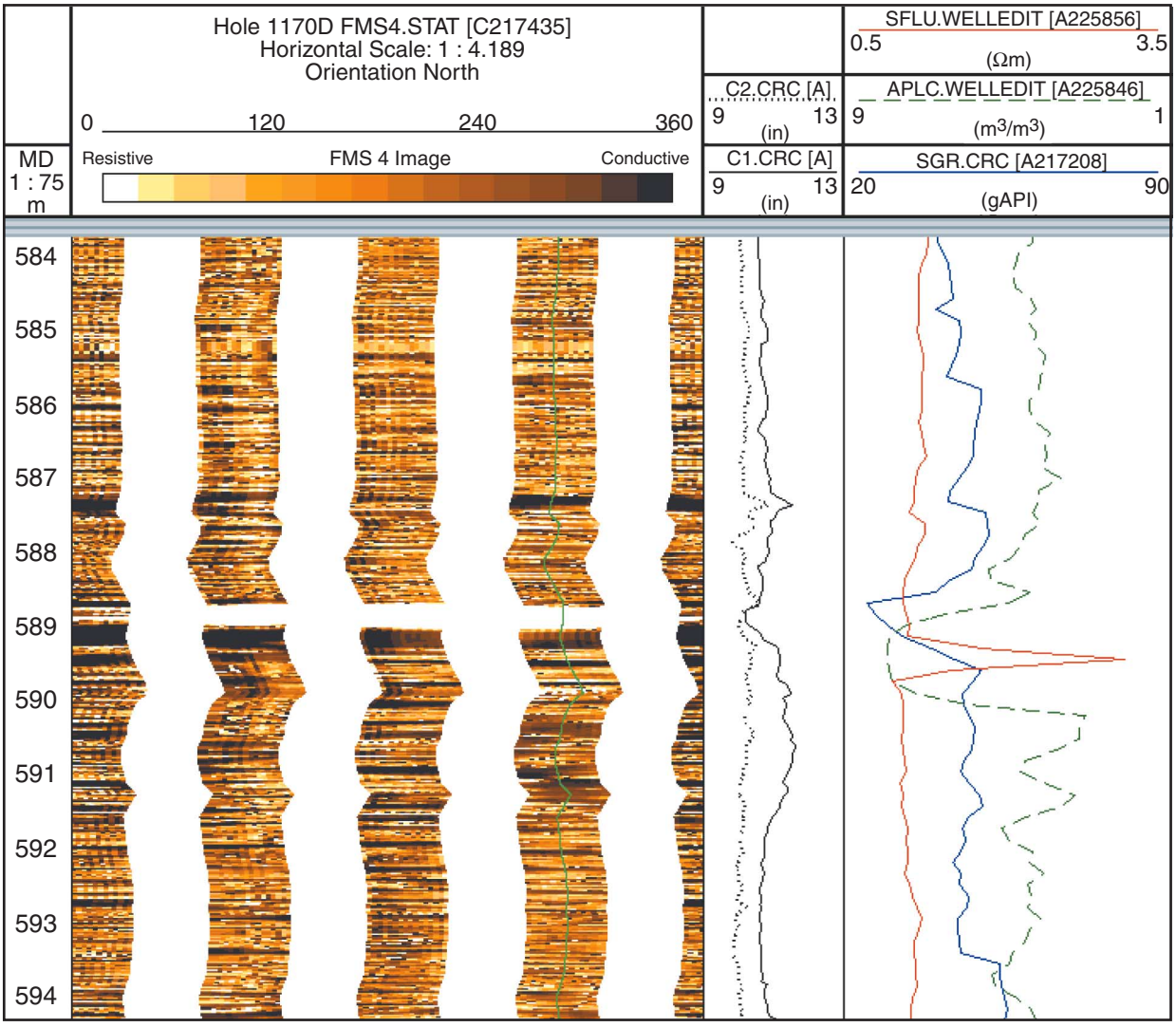

Figure F45. Downhole *P*-wave velocities (V_p) from the DSI logs plotted with the *P*-wave velocities measured vertically on half cores using the Hamilton frame.

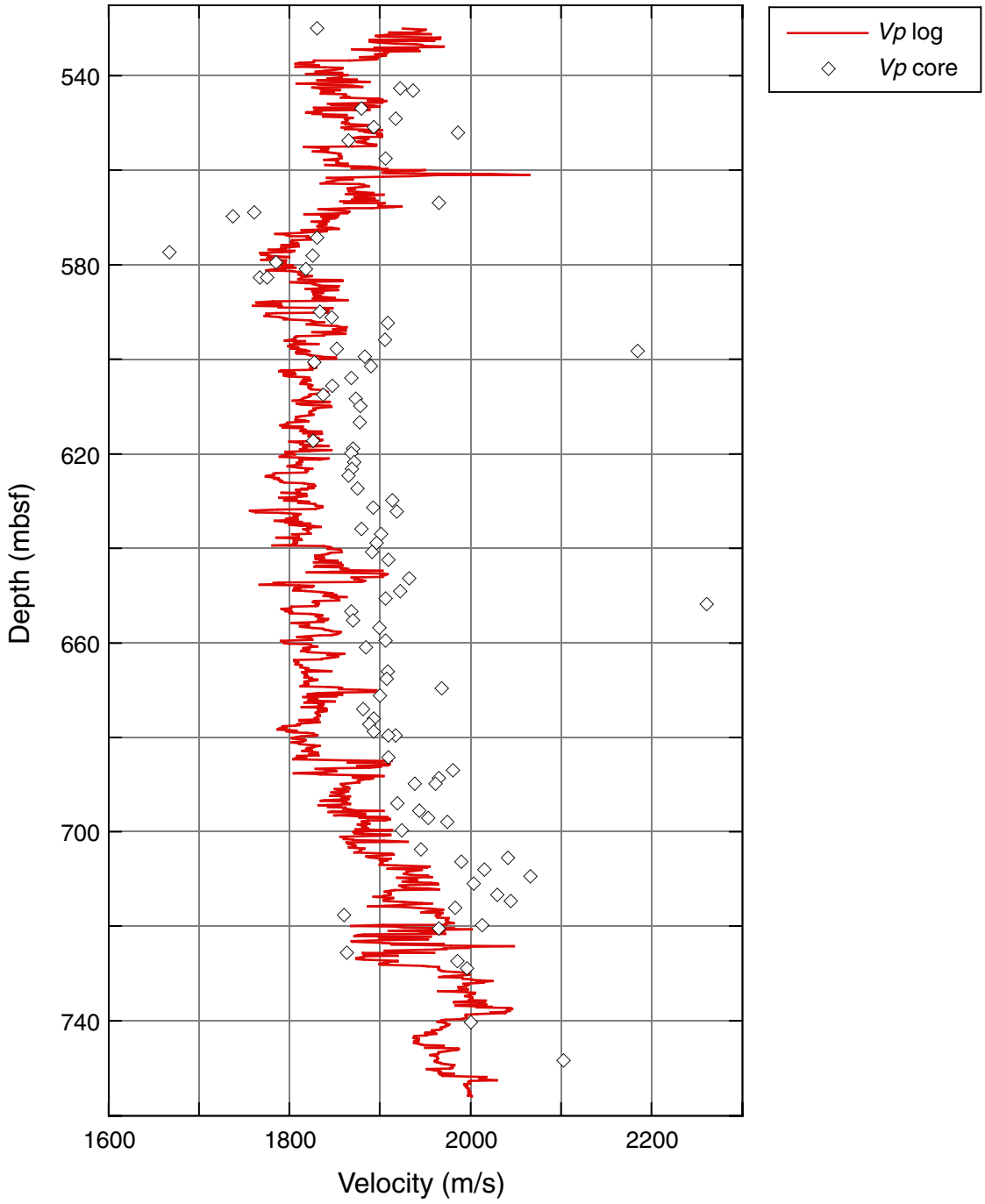

Figure F46. (A) Spectral gamma-ray data and (**B**, C) preliminary spectral analysis from Hole 1170D. The power spectrum shows the results of spectral analysis over (B) the entire logged section and (C) the interval where Th and K data show the most pronounced cyclicity (660–715 mbsf).

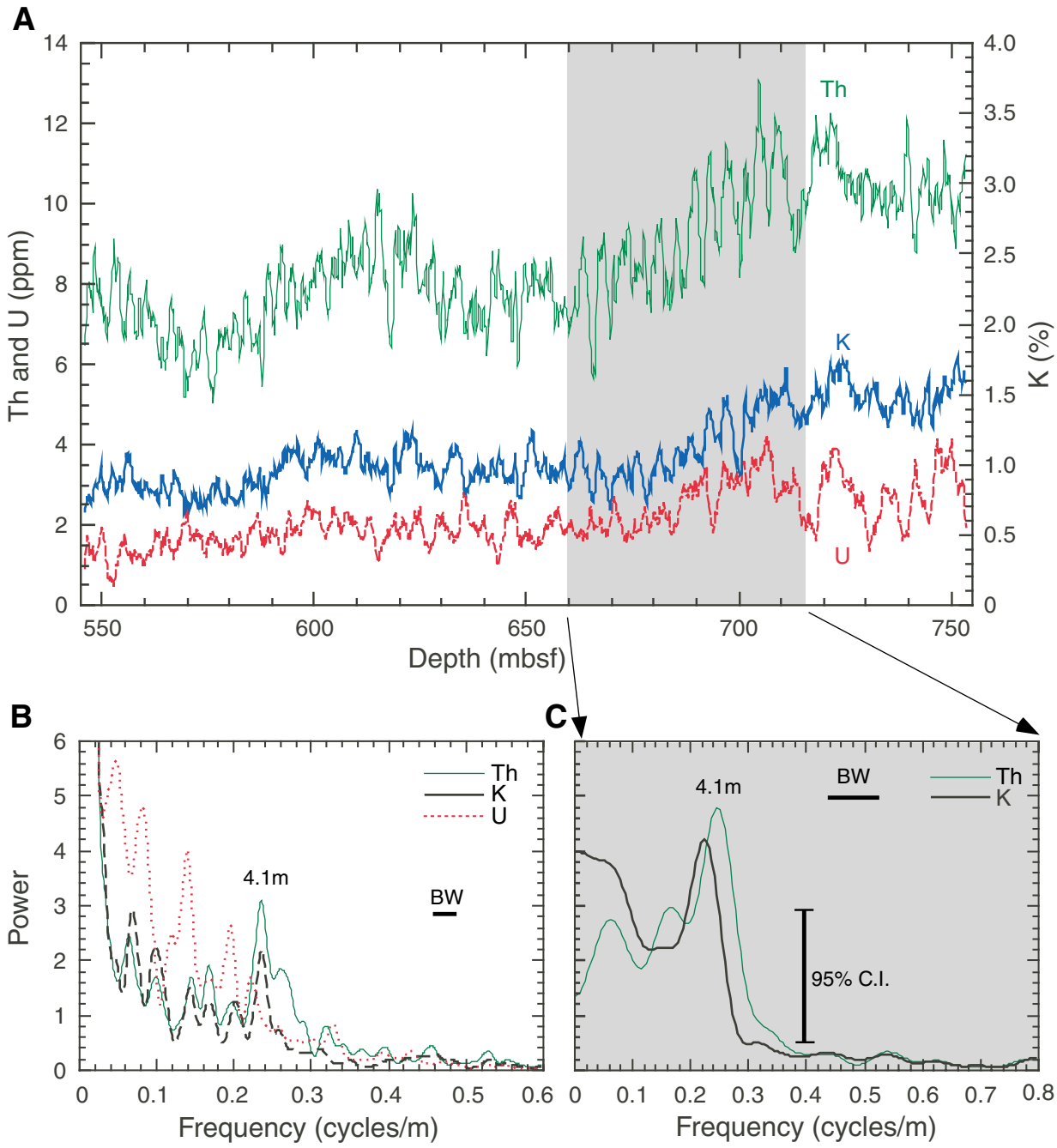

Figure F47. Magnetic susceptibility, Th, total organic carbon (TOC), hydrogen index (HI) value (see "Organic Geochemistry," p. 40), and U data from the basal 220 m of Hole 1170D. Higher TOC and lower HI values tend to correlate with increased magnetic susceptibility and Th values, which are assumed to result from increased terrigenous input. The U values, however, only seem to correlate with high TOC and low HI values below ~675 mbsf.

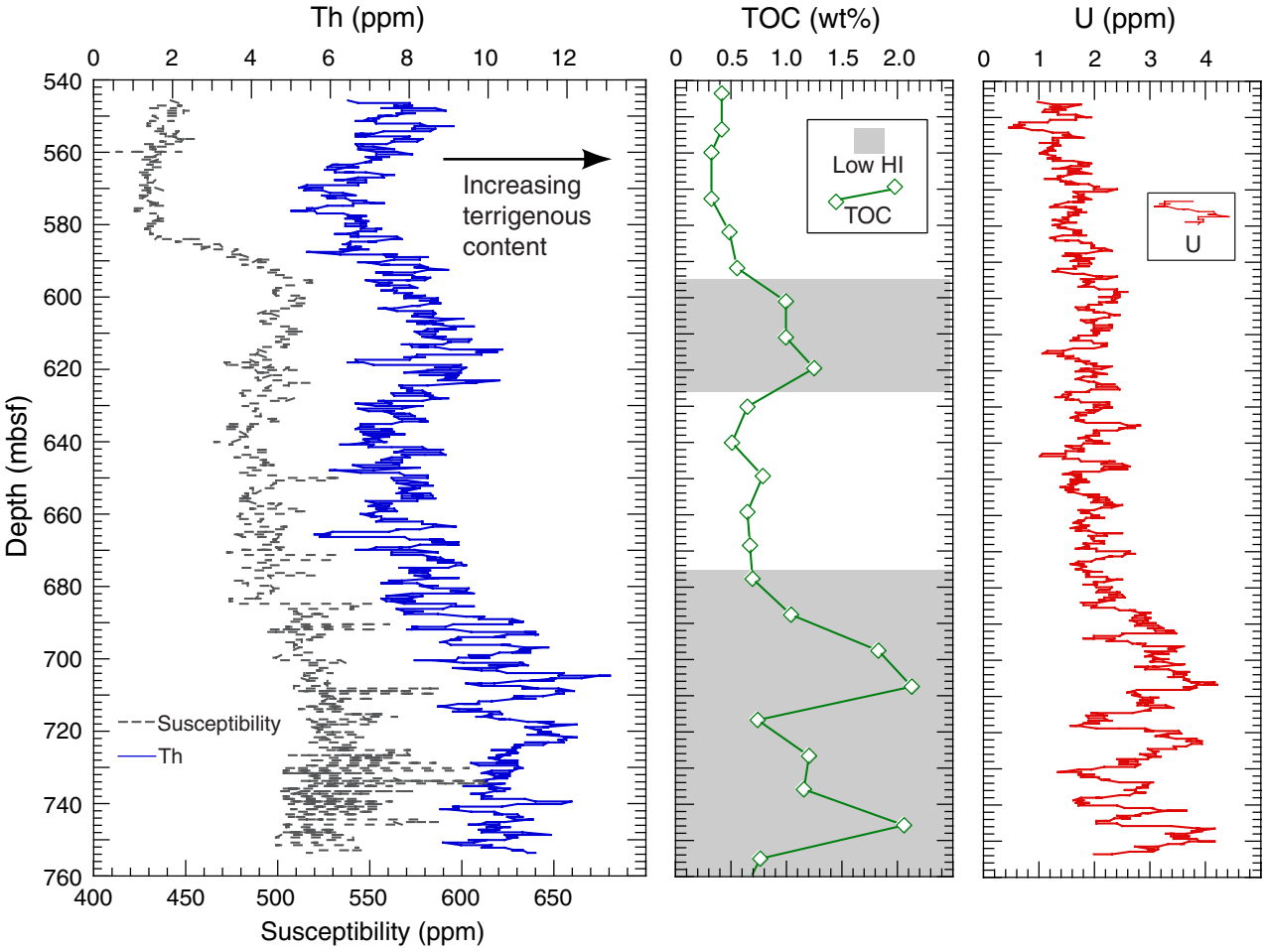

Figure F48. Time/depth, sonic velocity, and seismic data from Site 1170. The time/depth relationship was calculated using *P*-wave velocities (V_p) from the core and logs. The sonic velocities are plotted against both depth and time. The two main spikes in V_p are at a greater two-way traveltime than the two reflectors seen in the seismic section, indicating that some of the core-derived sonic velocities may be underestimated.

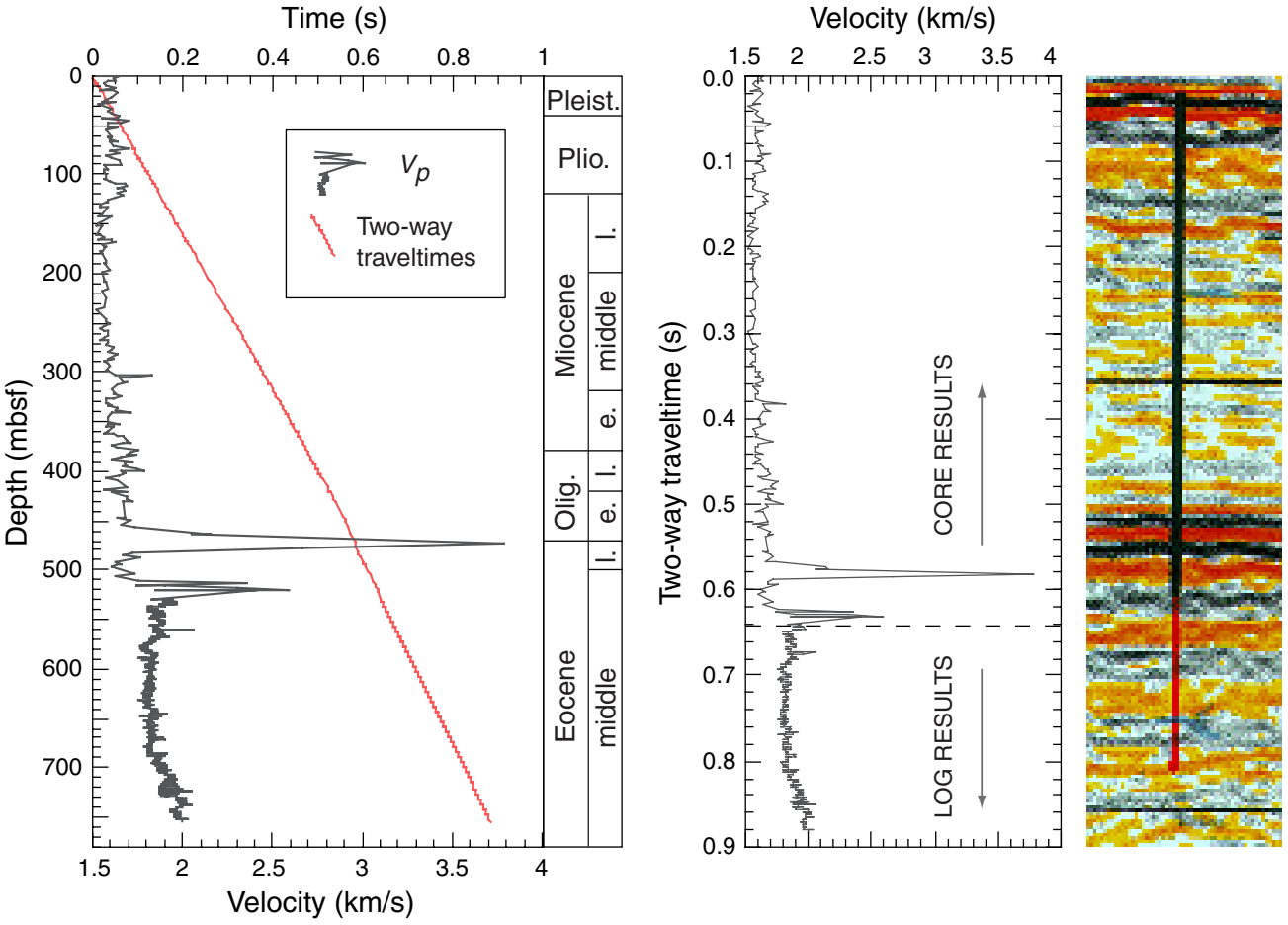

Table T1. Coring summary, Site 1170. (Continued on next two pages.)

Hole 1170A
Latitude: 47°9.0435′S
Longitude: 146°2.9881′E
Time on site: 263.5 hr (1200 hr, 31 March–1200 hr, 11 April 2000)
Time on hole: 41.25 hr; 1 day, 17 hr, 15 min (1220 hr, 31 March–0545 hr, 2 April 2000)
Seafloor (drill pipe measurement from rig floor, mbrf): 2715.8
Distance between rig floor and sea level (m): 11.1
Water depth (drill pipe measurement from sea level, m): 2704.7
Total depth (from rig floor, mbrf): 3180.1
Total penetration (mbsf): 464.3
Total length of cored section (m): 464.3
Total core recovered (m): 379.83
Core recovery (%): 81.8
Total number of cores: 52

Hole 1170B
Latitude: 47°9.0344′S
Longitude: 146°2.9846′E
Time on hole: 50.25 hr; 2 days, 2 hr, 15 min (0545 hr, 2 April–0800, 4 April 2000)
Seafloor (drill pipe measurement from rig floor, mbrf): 2715.7
Distance between rig floor and sea level (m): 11.0
Water depth (drill pipe measurement from sea level, m): 2704.7
Total depth (from rig floor, mbrf): 2891.5
Total penetration (mbsf): 175.80
Total length of cored section (m): 175.80
Total core recovered (m): 179.67
Core recovery (%): 102.2
Total number of cores: 19

Hole 1170C
Latitude: 47°9.0226′S
Longitude: 146°2.9871′E
Time on hole: 29 hr; 1 day, 5 hr (0800 hr, 4 April–1300 hr, 5 April 2000)
Seafloor (drill pipe measurement from rig floor, mbrf): 2714.4
Distance between rig floor and sea level (m): 11.1
Water depth (drill pipe measurement from sea level, m): 2703.3
Total depth (from rig floor, mbrf): 2894.5
Total penetration (mbsf): 180.1
Total length of cored section (m): 180.1
Total core recovered (m): 179.64
Core recovery (%): 99.7
Total number of cores: 19

Hole 1170D
Latitude: 47°9.0107′S
Longitude: 146°2.9829′E
Time on hole: 143 hr; 5 days, 23 hr (1300 hr, 5 April–1200 hr, 11 April 2000)
Seafloor (drill pipe measurement from rig floor, mbrf): 2715.8
Distance between rig floor and sea level (m): 11.1
Water depth (drill pipe measurement from sea level, m): 2704.7
Total depth (from rig floor, mbrf): 3495.6
Total penetration (mbsf): 779.8
Total length of cored section (m): 354.8
Total length of drilled intervals (m): 425.0
Total core recovered (m): 287.49
Core recovery (%): 81.0
Total number of cores: 38

Core	Date (2000)	Time (local)	Depth (mbsf) Top	Depth (mbsf) Bottom	Length (m) Cored	Length (m) Recovered	Recovery (%)
189-1170A-							
1H	31 March	2100	0.0	1.7	1.7	1.68	98.8
2H	31 March	2200	1.7	11.2	9.5	10.01	105.4
3H	31 March	2315	11.2	20.7	9.5	9.59	101.0
4H	1 April	0015	20.7	30.2	9.5	8.42	88.6
5H	1 April	0120	30.2	39.7	9.5	9.25	97.4
6H	1 April	0215	39.7	49.2	9.5	9.38	98.7
7H	1 April	0315	49.2	58.7	9.5	9.10	95.8
8H	1 April	0405	58.7	68.2	9.5	9.42	99.2
9H	1 April	0505	68.2	77.7	9.5	9.71	102.2
10H	1 April	0610	77.7	87.2	9.5	9.83	103.5

Table T1 (continued).

Core	Date (2000)	Time (local)	Depth (mbsf) Top	Depth (mbsf) Bottom	Length (m) Cored	Length (m) Recovered	Recovery (%)
11H	1 April	0705	87.2	96.7	9.5	9.73	102.4
12H	1 April	0800	96.7	106.2	9.5	9.80	103.2
13H	1 April	0845	106.2	115.7	9.5	9.09	95.7
14H	1 April	0945	115.7	125.2	9.5	8.08	85.1
15H	1 April	1045	125.2	134.7	9.5	8.79	92.5
16H	1 April	1135	134.7	144.2	9.5	9.10	95.8
17H	1 April	1240	144.2	153.7	9.5	9.41	99.1
18H	1 April	1410	153.7	163.2	9.5	10.05	105.8
19X	1 April	1525	163.2	166.7	3.5	3.99	114.0
20X	1 April	1615	166.7	176.3	9.6	7.89	82.2
21X	1 April	1700	176.3	185.9	9.6	4.66	48.5
22X	1 April	1800	185.9	195.5	9.6	6.20	64.6
23X	1 April	1850	195.5	205.1	9.6	5.64	58.8
24X	1 April	1945	205.1	214.7	9.6	5.26	54.8
25X	1 April	2035	214.7	224.3	9.6	5.69	59.3
26X	1 April	2130	224.3	233.9	9.6	3.30	34.4
27X	1 April	2215	233.9	243.5	9.6	5.53	57.6
28X	1 April	2315	243.5	253.1	9.6	7.25	75.5
29X	1 April	2355	253.1	262.7	9.6	6.39	66.6
30X	2 April	0130	262.7	272.3	9.6	7.57	78.9
31X	2 April	0210	272.3	281.9	9.6	9.49	98.9
32X	2 April	0300	281.9	291.5	9.6	9.04	94.2
33X	2 April	0340	291.5	300.8	9.3	8.15	87.6
34X	2 April	0420	300.8	310.1	9.3	9.64	103.7
35X	2 April	0510	310.1	319.7	9.6	8.38	87.3
36X	2 April	0555	319.7	329.3	9.6	7.87	82.0
37X	2 April	0705	329.3	338.9	9.6	9.55	99.5
38X	2 April	0750	338.9	348.6	9.7	8.33	85.9
39X	2 April	0900	348.6	358.2	9.6	7.98	83.1
40X	2 April	1005	358.2	367.8	9.6	8.88	92.5
41X	2 April	1100	367.8	377.4	9.6	8.78	91.5
42X	2 April	1205	377.4	387.0	9.6	9.82	102.3
43X	2 April	1305	387.0	396.6	9.6	9.68	100.8
44X	2 April	1405	396.6	406.2	9.6	9.28	96.7
45X	2 April	1525	406.2	415.8	9.6	3.90	40.6
46X	2 April	1645	415.8	425.4	9.6	6.07	63.2
47X	2 April	1800	425.4	435.0	9.6	5.60	58.3
48X	2 April	1940	435.0	444.6	9.6	0.31	3.2
49X	2 April	2120	444.6	454.2	9.6	5.70	59.4
50X	2 April	2300	454.2	459.0	4.8	2.67	55.6
51X	2 April	0100	459.0	463.8	4.8	0.38	7.9
52X	2 April	0400	463.8	464.3	0.5	0.52	104.0
				Totals:	464.3	379.83	81.8
189-1170B-							
1H	3 April	1210	0.0	4.8	4.8	4.80	100.0
2H	3 April	1310	4.8	14.3	9.5	9.90	104.2
3H	3 April	1415	14.3	23.8	9.5	9.82	103.4
4H	3 April	1515	23.8	33.3	9.5	9.84	103.6
5H	3 April	1610	33.3	42.8	9.5	9.41	99.1
6H	3 April	1705	42.8	52.3	9.5	9.82	103.4
7H	3 April	1820	52.3	61.8	9.5	9.93	104.5
8H	3 April	1920	61.8	71.3	9.5	10.03	105.6
9H	3 April	2020	71.3	80.8	9.5	9.71	102.2
10H	3 April	2120	80.8	90.3	9.5	10.03	105.6
11H	3 April	2220	90.3	99.8	9.5	9.99	105.2
12H	3 April	2320	99.8	109.3	9.5	9.96	104.8
13H	3 April	0045	109.3	118.8	9.5	9.67	101.8
14H	3 April	0145	118.8	128.3	9.5	9.86	103.8
15H	3 April	0240	128.3	137.8	9.5	9.98	105.1
16H	3 April	0335	137.8	147.3	9.5	7.55	79.5
17H	3 April	0425	147.3	156.8	9.5	9.63	101.4
18H	3 April	0525	156.8	166.3	9.5	9.95	104.7
19H	3 April	0630	166.3	175.8	9.5	9.79	103.1
				Totals:	175.8	179.67	102.2
189-1170C-							
1H	4 April	1005	0.0	9.1	9.1	9.07	99.7
2H	4 April	1105	9.1	18.6	9.5	8.99	94.6

Table T1 (continued).

Core	Date (2000)	Time (local)	Depth (mbsf) Top	Depth (mbsf) Bottom	Length (m) Cored	Length (m) Recovered	Recovery (%)
3H	4 April	1215	18.6	28.1	9.5	9.96	104.8
4H	4 April	1310	28.1	37.6	9.5	7.72	81.3
5H	4 April	1410	37.6	47.1	9.5	9.58	100.8
6H	4 April	1510	47.1	56.6	9.5	9.77	102.8
7H	4 April	1610	56.6	66.1	9.5	9.04	95.2
8H	4 April	1700	66.1	75.6	9.5	10.02	105.5
9H	4 April	1800	75.6	85.1	9.5	10.08	106.1
10H	4 April	1900	85.1	94.6	9.5	9.72	102.3
11H	4 April	2000	94.6	104.1	9.5	9.76	102.7
12H	4 April	2100	104.1	113.6	9.5	9.93	104.5
13H	4 April	2210	113.6	123.1	9.5	9.31	98.0
14H	4 April	2330	123.1	132.6	9.5	9.54	100.4
15H	5 April	0045	132.6	142.1	9.5	9.94	104.6
16H	5 April	0140	142.1	151.6	9.5	8.58	90.3
17H	5 April	0235	151.6	161.1	9.5	9.69	102.0
18H	5 April	0455	161.1	170.6	9.5	9.05	95.3
19H	5 April	0640	170.6	180.1	9.5	9.89	104.1
				Totals:	180.1	179.64	99.7
189-1170D-							
Drilled interval			0.0	425.0			
1R	6 April	0955	425.0	433.5	8.5	2.32	27.3
2R	6 April	1050	433.5	443.1	9.6	4.07	42.4
3R	6 April	1215	443.1	452.7	9.6	1.90	19.8
4R	6 April	1340	452.7	462.3	9.6	2.34	24.4
5R	6 April	1600	462.3	471.9	9.6	1.96	20.4
6R	6 April	1835	471.9	476.6	4.7	0.88	18.7
7R	6 April	2020	476.6	481.5	4.9	3.30	67.4
8R	6 April	2150	481.5	491.1	9.6	6.92	72.1
9R	6 April	2310	491.1	500.7	9.6	6.61	68.9
10R	7 April	0110	500.7	510.3	9.6	5.76	60.0
11R	7 April	0345	510.3	519.8	9.5	8.06	84.8
12R	7 April	0645	519.8	529.4	9.6	4.85	50.5
13R	7 April	0915	529.4	539.1	9.7	5.48	56.5
14R	7 April	1130	539.1	548.7	9.6	9.31	97.0
15R	7 April	1340	548.7	558.3	9.6	9.84	102.5
16R	7 April	1540	558.3	567.9	9.6	9.04	94.2
17R	7 April	1730	567.9	577.5	9.6	9.92	103.3
18R	7 April	1915	577.5	587.1	9.6	7.64	79.6
19R	7 April	2100	587.1	596.7	9.6	9.91	103.2
20R	7 April	2300	596.7	606.3	9.6	9.90	103.1
21R	8 April	0030	606.3	615.9	9.6	8.94	93.1
22R	8 April	0210	615.9	625.6	9.7	10.07	103.8
23R	8 April	0345	625.6	635.3	9.7	9.75	100.5
24R	8 April	0530	635.3	644.9	9.6	9.77	101.8
25R	8 April	0710	644.9	654.6	9.7	9.81	101.1
26R	8 April	0845	654.6	664.2	9.6	9.77	101.8
27R	8 April	1025	664.2	673.8	9.6	7.31	76.2
28R	8 April	1210	673.8	683.5	9.7	8.21	84.6
29R	8 April	1350	683.5	693.2	9.7	9.93	102.4
30R	8 April	1530	693.2	702.8	9.6	8.26	86.0
31R	8 April	1730	702.8	712.4	9.6	10.00	104.2
32R	8 April	1915	712.4	722.0	9.6	9.80	102.1
33R	8 April	2100	722.0	731.6	9.6	9.80	102.1
34R	8 April	2315	731.6	741.2	9.6	9.93	103.4
35R	9 April	0110	741.2	750.8	9.6	8.40	87.5
36R	9 April	0245	750.8	760.5	9.7	9.81	101.1
37R	9 April	0510	760.5	770.1	9.6	8.28	86.3
38R	9 April	0655	770.1	779.8	9.7	9.64	99.4
				Coring totals:	354.8	287.49	81.0
				Drilled totals:	425.0		
				Totals:	779.8		

Table T2. Summary of Site 1170 lithology and corresponding lithostratigraphic units for Site 1168 and DSDP Site 281.

Site 1170								
Lithologic unit	Subunit	Core intervals	Lithology	Depth (mbsf)	Thickness (m)	Age	Site 1168 corresponding lithologic unit/subunit	DSDP Site 281 corresponding lithologic unit/subunit
I		1170A-1H to 11H; 1170B-1H to 11H; 1170C-1H to 10H	White to light greenish gray nannofossil ooze	0.0-93.0	93	Holocene to early Pliocene	Subunit IA	Upper part of Subunit IA
II	IIA	1170A-11H to 21X; 1170B-11H to 19X; 1170C-11H to 19H	White, laminated nannofossil ooze	93.0-185.9	92.9	early Pliocene to middle Miocene	Subunit IB	Subunit IA
	IIB	1170A-22X to 32X	White, massive nannofossil ooze	185.9-290.0	104.1	middle Miocene	upper part of Subunit IIA	Middle part of Subunit IB
	IIC	1170A-33X to 41X	White, laminated nannofossil ooze	290.0-373.0	83	middle Miocene to early Miocene	Subunit IIA	Lower part of Subunit IB
III		1170A-41X to 52X; 1170D-1R to 5R	White to light greenish gray clay-bearing nannofossil chalk	373.0-472.0	99	early Miocene to early Oligocene/ late Eocene	Subunits IIB, IIC, Unit III	Unit II and uppermost part of Unit III
IV		1170D-5R to 9R	Dark greenish gray to black glauconitic clayey siltstone	472.0-497.0	25	early Oligocene/late Eocene to late Eocene	Unit IV	Units III to V
V	VA	1170D-9R to 13R	Dark green to dark gray silty claystone	497.0-539.1	42.1	late Eocene	Unit V	Units IV and V
	VB	1170D-14R to 38R		539.1-779.8	240.7	middle Eocene	Did not penetrate	Unit VI

Table T3. Calcareous nannofossil datum levels, Site 1170.

Datum	Age (Ma)	Interval Top	Interval Bottom	Depth (mbsf) Top	Depth (mbsf) Bottom	Mean (mbsf)	Error bar (m)
Hole 1170A							
FO *Emiliania huxleyi*	0.26	Top of core	1H-CC	0.00	1.64	0.82	0.82
LO *Pseudoemiliania lacunosa*	0.46	1H-CC	2H-CC	1.64	11.67	6.66	5.02
LO *Calcidiscus macintyrei*	1.67	4H-CC	5H-CC	29.07	39.40	34.24	5.17
LO *Reticulofenestra pseudoumbilica*	3.75	6H-CC	7H-CC	49.03	58.25	53.64	4.61
LO *Ceratolithus acutus*	5.05	12H-CC	13H-CC	106.45	115.24	110.85	4.40
FO *Ceratolithus acutus*	5.37	12H-CC	13H-CC	106.45	115.24	110.85	4.40
LO *Cyclicargolithus floridanus*	11.90	27X-CC	28X-CC	239.38	250.70	245.04	5.66
LO *Helicosphaera ampliaperta*	15.60	29X-CC	30X-CC	259.44	270.22	264.83	5.39
FO *Calcidiscus premacintyrei*	17.40	34X-CC	35X-CC	310.39	318.43	314.41	4.02
LO *Reticulofenestra bisecta*	23.90	41X-CC	42X-CC	376.53	387.17	381.85	5.32
LO *Chiasmolithus altus*	26.10	43X-CC	44X-CC	396.63	405.83	401.23	4.60
Hole 1170B							
LO *Pseudoemiliania lacunosa*	0.46	1H-CC	2H-CC	4.75	14.65	9.70	4.95
LO *Calcidiscus macintyrei*	1.67	4H-CC	5H-CC	33.59	42.66	38.13	4.54
LO *Reticulofenestra pseudoumbilica*	3.75	5H-CC	6H-CC	42.66	52.55	47.61	4.95
LO *Discoaster loeblechii*	7.40	16H-CC	17H-CC	145.30	156.88	151.09	5.79
Hole 1170C							
LO *Pseudoemiliania lacunosa*	0.46	2H-CC	3H-CC	18.04	28.51	23.28	5.24
LO *Calcidiscus macintyrei*	1.67	4H-CC	5H-CC	35.77	47.13	41.45	5.68
LO *Reticulofenestra pseudoumbilica*	3.75	5H-CC	6H-CC	47.13	56.82	51.98	4.85
FO *Amaurolithus delicatus*	6.90	16H-CC	17H-CC	150.63	161.24	155.94	5.31
LO *Discoaster loeblechii*	7.40	16H-CC	17H-CC	150.63	161.24	155.94	5.31
FO *Discoaster surculus*	7.30	17H-CC	18H-CC	161.24	170.09	165.67	4.42
Hole 1170D							
FO *Cyclicargolithus abisectus*	31.20	4R-CC	5R-CC	454.99	464.21	459.60	4.61
LO *Reticulofenestra reticulata*	35.00	6R-CC	8R-5, 50	472.72	486.35	479.54	6.82
LO *Chiasmolithus solitus*	40.40	12R-CC	13R-CC	524.59	534.83	529.71	5.12
FO *Reticulofenestra reticulata*	42.00	12R-CC	13R-CC	524.59	534.83	529.71	5.12
FO *Reticulofenestra umbilica*	43.70	37R-CC	38R-CC	768.73	779.69	774.21	5.48

Note: FO = first occurrence, LO = last occurrence.

Table T4. Stratigraphic distribution of selected nannofossil species, Site 1170. (**See table notes.** Continued on next five pages.)

Core, section, interval (cm)	Depth (mbsf)	Preservation	Group abundance	*Amaurolithus delicatus*	*Amaurolithus ninae*	*Braarudosphaera bigelowii*	*Calcidiscus leptoporus*	*Calcidiscus macintyrei*	*Calcidiscus premacintyrei*	*Ceratolithus acutus*	*Ceratolithus cristatus*	*Chiasmolithus altus*	*Chiasmolithus expansus*	*Chiasmolithus grandis*	*Chiasmolithus medius*	*Chiasmolithus solitus*	*Coccolithus pelagicus*	*Cyclicargolithus abisectus*	*Cyclicargolithus floridanus*	*Dictyococcites hesslandii*	*Discoaster adamanteus*	*Discoaster aulakos*	*Discoaster braarudii*	*Discoaster brouweri*	*Discoaster calcaris*	*Discoaster challengeri*	*Discoaster deflandrei*	*Discoaster formosus*	*Discoaster intercalaris*	*Discoaster loeblichii*	*Discoaster neorectus*	*Discoaster pentaradiatus*	*Discoaster surculus*	*Discoaster variabilis*
189-1170A-																																		
1H-CC, 18-22	1.64	G	A																															
2H-CC, 11-15	11.67	G	A																															
3H-CC, 12-16	20.75	G	A																															
4H-CC, 18-23	29.07	G	A				A				R						A																	
5H-CC, 8-13	39.40	G	A				A	C									A																	
6H-CC, 8-13	49.03	M	A					C									A																	
7H-CC, 10-15	58.25	M	A				A	C									A																	
8H-CC, 16-21	68.07	M	A				A	F									A						R									R		
9H-CC, 15-20	77.86	M	A				A	C									A																	
10H-CC, 12-17	87.48	M	A				A	C									A												F			R		
11H-CC, 12-17	96.88	M	A				A	C									A												R					
12H-CC, 10-15	106.45	M	A				A	C		R							A												C					
13H-CC, 12-17	115.24	M	A				A	C									A																	
14H-CC, 11-16	123.73	M	A				A	C									A																	
15H-CC, 12-17	133.94	M	A		R		A	C									A												F					
16H-CC, 12-17	143.75	M	A					R																										
17H-CC, 21-25	153.57	M	A	R																														
18H-CC, 23-28	163.70	M	A					C																										
19X-CC, 3-9	167.13	M	A																															
20X-CC, 21-26	174.54	M	A					C																										
21X-CC, 11-16	180.91	M	A																															
22X-CC, 12-17	192.05	M	A					C																										
23X-CC, 12-17	201.09	M	A					C																										
24X-CC, 16-21	210.31	M	A					C																										
25X-CC, 20-25	220.34	M	A					C																										
26X-CC, 10-15	227.55	M	A					C																										
27X-CC, 12-17	239.38	M	A					C																										
28X-CC, 20-25	250.70	M	A					F											R															
29X-CC, 10-15	259.44	M	A				C		C								A		A	R														
30X-CC, 9-14	270.22	M	A				A		C								A		C	F														R
31X-CC, 12-17	281.74	M	A				C		C								A		A		F							R						
32X-CC, 15-20	290.89	M	A				C		C								A		A		R						C	R						
33X-CC, 11-16	299.60	M	A					F	C								A		C															
34X-CC, 21-26	310.39	M	A				C		C								A		C		R	R												
35X-CC, 19-24	318.43	M	A				C										C		A															
36X-CC, 16-21	327.52	M	A				R										A		A								C							
37X-CC, 16-21	338.80	M	A																															
38X-CC, 13-18	347.18	M	A																															
39X-CC, 19-24	356.53	M	A														A		C		C						C							
40X-CC, 25-30	367.03	M	A														A	A	C															
41X-CC, 29-34	376.53	M	A														A	A	A								F							
42X-CC, 29-34	387.17	M	A																															
43X-CC, 14-19	396.63	M	A																															
44X-CC, 31-36	405.83	M	A									C																						
45X-CC, 30-35	410.05	M	A									C																						
46X-CC, 20-25	421.82	M	A									C																						
47X-CC, 10-15	430.95	M	A									C																						
48X-CC, 26-31	435.26	P	A									C																						
49X-CC, 10-15	450.25	P	A									C																						
50X-CC, 22-27	456.82	P	A									C																						
51X-CC, 33-38	459.33	P	A									C					F	C	A															
52X-CC, 47-52	464.27	P	A									C					F	C	A															
189-1170B-																																		
1H-CC, 13-18	4.75	G	A																															
2H-CC, 9-14	14.65	G	A																															
3H-CC, 13-18	24.07	G	A																															
4H-CC, 10-15	33.59	G	A																															
5H-CC, 13-18	42.66	G	A				A	F																										

Table T4 (continued).

Core, section, interval (cm)	Depth (mbsf)	Preservation	Group abundance	*Gephyrocapsa* >4.5 mm [µm?]	*Emiliania huxleyi*	*Gephyrocapsa caribbeanica*	*Gephyrocapsa* spp. (small)	*Helicosphaera ampliaperta*	*Helicosphaera kamptneri*	*Helicosphaera mediterranea*	*Helicosphaera sellii*	*Neococcolithes dubius*	*Pontosphaera* spp.	*Pseudoemiliania lacunosa*	*Reticulofenestra bisecta*	*Reticulofenestra daviesii*	*Reticulofenestra gelida*	*Reticulofenestra minuta*	*Reticulofenestra perplexa*	*Reticulofenestra pseudoumbilica*	*Reticulofenestra reticulata*	*Reticulofenestra samodurovii*	*Reticulofenestra* spp.	*Reticulofenestra umbilicus*	*Rhabdosphaera tenuis*	*Sphenolithus moriformis*	*Transversopontis pulcheroides*	*Transversopontis rectipons*	*Triquetrorhabdulus rugosus*	*Zygrhablithus bijugatus*	Comment
189-1170A-																															
1H-CC, 18-22	1.64	G	A		C	A																									
2H-CC, 11-15	11.67	G	A			A								F																	
3H-CC, 12-16	20.75	G	A	F		C																									
4H-CC, 18-23	29.07	G	A	F					F					C																	
5H-CC, 8-13	39.40	G	A								F			A																	
6H-CC, 8-13	49.03	M	A								F			F																	
7H-CC, 10-15	58.25	M	A								F									F											
8H-CC, 16-21	68.07	M	A															A		C											
9H-CC, 15-20	77.86	M	A															A		F											
10H-CC, 12-17	87.48	M	A						F		R							A		C											
11H-CC, 12-17	96.88	M	A															A		F											
12H-CC, 10-15	106.45	M	A						R									C		C											
13H-CC, 12-17	115.24	M	A						F																						
14H-CC, 11-16	123.73	M	A																	A											
15H-CC, 12-17	133.94	M	A																												
16H-CC, 12-17	143.75	M	A																												
17H-CC, 21-25	153.57	M	A																												
18H-CC, 23-28	163.70	M	A																	A									R		
19X-CC, 3-9	167.13	M	A																	A									R		
20X-CC, 21-26	174.54	M	A																	A											
21X-CC, 11-16	180.91	M	A																	A											
22X-CC, 12-17	192.05	M	A																	A											
23X-CC, 12-17	201.09	M	A																	A											
24X-CC, 16-21	210.31	M	A																	A											
25X-CC, 20-25	220.34	M	A																	A											
26X-CC, 10-15	227.55	M	A																	A											
27X-CC, 12-17	239.38	M	A																	A											
28X-CC, 20-25	250.70	M	A																	A											
29X-CC, 10-15	259.44	M	A														A		C												
30X-CC, 9-14	270.22	M	A					F		R							C									R					
31X-CC, 12-17	281.74	M	A					F		R																R					
32X-CC, 15-20	290.89	M	A					R																		F					
33X-CC, 11-16	299.60	M	A																												
34X-CC, 21-26	310.39	M	A														A									R					
35X-CC, 19-24	318.43	M	A														A									F					
36X-CC, 16-21	327.52	M	A																							R					
37X-CC, 16-21	338.80	M	A																												
38X-CC, 13-18	347.18	M	A																												
39X-CC, 19-24	356.53	M	A																							C					
40X-CC, 25-30	367.03	M	A																												
41X-CC, 29-34	376.53	M	A																												
42X-CC, 29-34	387.17	M	A												F																
43X-CC, 14-19	396.63	M	A												C																
44X-CC, 31-36	405.83	M	A												C																
45X-CC, 30-35	410.05	M	A												C																
46X-CC, 20-25	421.82	M	A												C																
47X-CC, 10-15	430.95	M	A												C																
48X-CC, 26-31	435.26	P	A												C																
49X-CC, 10-15	450.25	P	A												C																
50X-CC, 22-27	456.82	P	A												C																
51X-CC, 33-38	459.33	P	A												C																
52X-CC, 47-52	464.27	P	A												C																
189-1170B-																															
1H-CC, 13-18	4.75	G	A	C			A																								
2H-CC, 9-14	14.65	G	A				A							C																	
3H-CC, 13-18	24.07	G	A				A							F																	
4H-CC, 10-15	33.59	G	A				A							F																	
5H-CC, 13-18	42.66	G	A				A							F																	

Table T4 (continued).

Core, section, interval (cm)	Depth (mbsf)	Preservation	Group abundance	*Amaurolithus delicatus*	*Amaurolithus ninae*	*Braarudosphaera bigelowii*	*Calcidiscus leptoporus*	*Calcidiscus macintyrei*	*Calcidiscus premacintyrei*	*Ceratolithus acutus*	*Ceratolithus cristatus*	*Chiasmolithus altus*	*Chiasmolithus expansus*	*Chiasmolithus grandis*	*Chiasmolithus medius*	*Chiasmolithus solitus*	*Coccolithus pelagicus*	*Cyclicargolithus abisectus*	*Cyclicargolithus floridanus*	*Dictyococcites hesslandii*	*Discoaster adamanteus*	*Discoaster aulakos*	*Discoaster braarudii*	*Discoaster brouweri*	*Discoaster calcaris*	*Discoaster challengeri*	*Discoaster deflandrei*	*Discoaster formosus*	*Discoaster intercalaris*	*Discoaster loeblichii*	*Discoaster neorectus*	*Discoaster pentaradiatus*	*Discoaster surculus*	*Discoaster variabilis*
6H-CC, 0-7	52.55	G	A				A	C																										
7H-CC, 14-19	62.18	G	A				A	C																										
8H-CC, 10-15	71.78	G	A				A	C																										
9H-CC, 29-34	80.96	G	A				A	C																										
10H-CC, 18-23	90.78	G	A				A	C																										
11H-CC, 20-25	100.24	G	A				A	C																									R	
12H-CC, 17-22	109.71	G	A				A	C																										
13H-CC, 0-5	118.92	M	A				C	F									A																
14H-CC, 13-18	128.61	M	A	F			A	C									C																
15H-CC, 23-28	138.23	M	A	F	R		A	C									C								R	R							
16H-CC, 13-18	145.30	M	A				C	F									C																F
17H-CC, 13-18	156.88	M	A				C	F									A												R	F		F	
18H-CC, 16-21	166.70	M	A				F										A												R	F	R			F
19H-CC, 0-7	176.02	P	A														C										R		R		C			
189-1170C-																																		
1H-CC, 10-15	9.02	G	A				R										A																	
2H-CC, 20-25	18.04	G	A				A																											
3H-CC, 10-15	28.51	G	A				F																											
4H-CC, 17-22	35.77	G	A																															
5H-CC, 10-15	47.13	G	A					R																										
6H-CC, 9-14	56.82	G	A					R																										
7H-CC, 15-21	65.58	G	A					F																										
8H-CC, 9-14	76.07	G	A					F																										
9H-CC, 18-24	85.62	G	A					F																										
10H-CC, 0-6	94.76	G	A					F																										
11H-CC, 18-24	104.30	G	A					F																										
12H-CC, 22-27	113.98	G	A					F																										
13H-CC, 19-24	122.96	G	A					F																										
14H-CC, 16-21	132.59	G	A					F																										
15H-CC, 16-21	142.49	M	A		R		C	C									F												R					R
16H-CC, 16-21	150.63	M	A	R			A	F									C												F					C
17H-CC, 11-16	161.24	M	A				F										A							R					F	F			F	F
18H-CC, 7-13	170.09	M	A				F	F									F													F		R		F
19H-CC, 13-18	180.44	M	A				A	A									A							R		F			F	R				C
189-1170D-																																		
1R-CC, 11-16	427.27	M	A									A					C	F	F															
2R-CC, 14-21	437.50	M	A									C																						
3R-CC, 15-20	444.95	M	A									C																						
4R-CC, 19-24	454.99	M	A									C																						
5R-CC, 16-21	464.21	P	A									C																						
6R-CC, 21-27	472.72	P	C									C																						
7R-CC, 17-22	479.85		B																															
8R-CC, 0-7	488.35	P	R									R																						
9R-CC, 10-15	497.66	M	C									R																						
10R-CC, 10-15	506.41	P	F									R					R																	
11R-CC, 16-21	518.31	P	F														R																	
12R-CC, 16-22	524.59	P	C										F																						
13R-CC, 16-21	534.83	P	R													C																			
14R-CC, 0-5	548.46	M	C													F																			
15R-CC, 6-11	558.49	M	F													F																			
16R-CC, 20-25	567.29	G	R													R																			
17R-CC, 17-22	577.77	G	C													C																			
18R-CC, 0-4	585.10	M	F													R																			
19R-CC, 15-19	596.97	M	R													R																			
20R-CC, 12-17	606.55	M	R													R																			
21R-CC, 0-7	615.17	M	B													R																			
22R-CC, 18-23	625.92	P	R													R																			
23R-CC, 10-15	635.30		B																															
24R-CC, 11-16	645.02		B																															

Table T4 (continued).

Core, section, interval (cm)	Depth (mbsf)	Preservation	Group abundance	*Gephyrocapsa* > 4.5 mm?	*Emiliania huxleyi*	*Gephyrocapsa caribbeanica*	*Gephyrocapsa* spp. (small)	*Helicosphaera ampliaperta*	*Helicosphaera kamptneri*	*Helicosphaera mediterranea*	*Helicosphaera sellii*	*Neococcolithes dubius*	*Pontosphaera* spp.	*Pseudoemiliania lacunosa*	*Reticulofenestra bisecta*	*Reticulofenestra daviesii*	*Reticulofenestra gelida*	*Reticulofenestra minuta*	*Reticulofenestra perplexa*	*Reticulofenestra pseudoumbilica*	*Reticulofenestra reticulata*	*Reticulofenestra samodurovii*	*Reticulofenestra* spp.	*Reticulofenestra umbilicus*	*Rhabdosphaera tenuis*	*Sphenolithus moriformis*	*Transversopontis pulcheroides*	*Transversopontis rectipons*	*Triquetrorhabdulus rugosus*	*Zygrhablithus bijugatus*	Comment
6H-CC, 0-7	52.55	G	A				A													F											
7H-CC, 14-19	62.18	G	A																	A											
8H-CC, 10-15	71.78	G	A																	A											
9H-CC, 29-34	80.96	G	A																	A											
10H-CC, 18-23	90.78	G	A																	A											
11H-CC, 20-25	100.24	G	A																	C											
12H-CC, 17-22	109.71	G	A																	C											
13H-CC, 0-5	118.92	M	A						R		R							A		F											
14H-CC, 13-18	128.61	M	A															A		F											
15H-CC, 23-28	138.23	M	A															A		F											
16H-CC, 13-18	145.30	M	A														C	A		C											latest Miocene?
17H-CC, 13-18	156.88	M	A		F												C			F											
18H-CC, 16-21	166.70	M	A																										R		
19H-CC, 0-7	176.02	P	A														F														
189-1170C-																															
1H-CC, 10-15	9.02	G	A	A																											
2H-CC, 20-25	18.04	G	A																												
3H-CC, 10-15	28.51	G	A	F										F																	
4H-CC, 17-22	35.77	G	A	F										F																	
5H-CC, 10-15	47.13	G	A																	R											
6H-CC, 9-14	56.82	G	A																	R											
7H-CC, 15-21	65.58	G	A																	F											
8H-CC, 9-14	76.07	G	A																	R											
9H-CC, 18-24	85.62	G	A																	R											
10H-CC, 0-6	94.76	G	A																	R											
11H-CC, 18-24	104.30	G	A																	R											
12H-CC, 22-27	113.98	G	A																	F											
13H-CC, 19-24	122.96	G	A																	F											
14H-CC, 16-21	132.59	G	A																	F											
15H-CC, 16-21	142.49	M	A							R							A	A		F											
16H-CC, 16-21	150.63	M	A														A	C		F											
17H-CC, 11-16	161.24	M	A															A		F									C		
18H-CC, 7-13	170.09	M	A														C			F											
19H-CC, 13-18	180.44	M	A							R							C			F											
189-1170D-																															
1R-CC, 11-16	427.27	M	A												C																
2R-CC, 14-21	437.50	M	A												C																
3R-CC, 15-20	444.95	M	A												C																
4R-CC, 19-24	454.99	M	A												C																
5R-CC, 16-21	464.21	P	A												F																
6R-CC, 21-27	472.72	P	C												F																
7R-CC, 17-22	479.85		B																												
8R-CC, 0-7	488.35	P	R												R						R			R							
9R-CC, 10-15	497.66	M	C												F						C			C							
10R-CC, 10-15	506.41	P	F												F						F			R							
11R-CC, 16-21	518.31	P	F												R	F						F		C			R				
12R-CC, 16-22	524.59	P	C										R											R				R			
13R-CC, 16-21	534.83	P	R																					F							
14R-CC, 0-5	548.46	M	C																					F							
15R-CC, 6-11	558.49	M	F																												
16R-CC, 20-25	567.29	G	R																					R							
17R-CC, 17-22	577.77	G	C																					R							
18R-CC, 0-4	585.10	M	F																					F							
19R-CC, 15-19	596.97	M	R																												
20R-CC, 12-17	606.55	M	R																												
21R-CC, 0-7	615.17	M	B																												
22R-CC, 18-23	625.92	P	R																												
23R-CC, 10-15	635.30		B																												
24R-CC, 11-16	645.02		B																												

Table T4 (continued).

Core, section, interval (cm)	Depth (mbsf)	Preservation	Group abundance	*Amaurolithus delicatus*	*Amaurolithus ninae*	*Braarudosphaera bigelowii*	*Calcidiscus leptoporus*	*Calcidiscus macintyrei*	*Calcidiscus premacintyrei*	*Ceratolithus acutus*	*Ceratolithus cristatus*	*Chiasmolithus altus*	*Chiasmolithus expansus*	*Chiasmolithus grandis*	*Chiasmolithus medius*	*Chiasmolithus solitus*	*Coccolithus pelagicus*	*Cyclicargolithus abisectus*	*Cyclicargolithus floridanus*	*Dictyococcites hesslandii*	*Discoaster adamanteus*	*Discoaster aulakos*	*Discoaster braarudii*	*Discoaster brouweri*	*Discoaster calcaris*	*Discoaster challengeri*	*Discoaster deflandrei*	*Discoaster formosus*	*Discoaster intercalaris*	*Discoaster loeblichii*	*Discoaster neorectus*	*Discoaster pentaradiatus*	*Discoaster surculus*	*Discoaster variabilis*
25R-CC, 15-20	654.76	M	F												R	C																		
26R-CC, 8-13	664.32	M	R												R	R																		
27R-CC, 11-16	671.46	M	F																															
28R-CC, 9-14	681.96	P	F													F																		
29R-CC, 21-26	693.38	M	R													R																		
30R-CC, 17-22	701.41	M	R													F																		
31R-CC, 20-25	712.75		B																															
32R-CC, 18-23	722.15	M	R																															
33R-CC, 13-19	731.74	M	R													F																		
34R-CC, 21-26	741.48	M	C													F																		
35R-CC, 0-5	749.55	M	F													F																		
36R-CC, 19-24	760.56	M	F													F																		
37R-CC, 0-5	768.73	M	C			F								R		C																		
38R-CC, 25-30	779.69	M	R															R																

Notes: Preservation: G = good, M = moderate, P = poor. Abundance: A = abundant, C = common, F = few, R = rare, B = barren.

Table T4 (continued).

Core, section, interval (cm)	Depth (mbsf)	Preservation	Group abundance	*Gephyrocapsa* > 4.5 mm?	*Emiliania huxleyi*	*Gephyrocapsa caribbeanica*	*Gephyrocapsa* spp. (small)	*Helicosphaera ampliaperta*	*Helicosphaera kamptneri*	*Helicosphaera mediterranea*	*Helicosphaera sellii*	*Neococcolithes dubius*	*Pontosphaera* spp.	*Pseudoemiliania lacunosa*	*Reticulofenestra bisecta*	*Reticulofenestra daviesii*	*Reticulofenestra gelida*	*Reticulofenestra minuta*	*Reticulofenestra perplexa*	*Reticulofenestra pseudoumbilica*	*Reticulofenestra reticulata*	*Reticulofenestra samodurovii*	*Reticulofenestra* spp.	*Reticulofenestra umbilicus*	*Rhabdosphaera tenuis*	*Sphenolithus moriformis*	*Transversopontis pulcheroides*	*Transversopontis rectipons*	*Triquetrorhabdulus rugosus*	*Zygrhablithus bijugatus*	Comment
25R-CC, 15-20	654.76	M	F																				R							
26R-CC, 8-13	664.32	M	R																				R	R						
27R-CC, 11-16	671.46	M	F																											
28R-CC, 9-14	681.96	P	F																											
29R-CC, 21-26	693.38	M	R																											
30R-CC, 17-22	701.41	M	R																											
31R-CC, 20-25	712.75		B																											
32R-CC, 18-23	722.15	M	R																											
33R-CC, 13-19	731.74	M	R																											
34R-CC, 21-26	741.48	M	C																					R						
35R-CC, 0-5	749.55	M	F																			R	R	R						
36R-CC, 19-24	760.56	M	F										R									R	R							
37R-CC, 0-5	768.73	M	C									R										F		R	R	R				
38R-CC, 25-30	779.69	M	R																			C	C						F	

Table T5. Planktonic foraminiferal datums, Hole 1170A.

Datum	Age (Ma)	Interval Top	Interval Bottom	Depth (mbsf) Top	Depth (mbsf) Bottom	Mean (mbsf)	Error bar (m)
FO *Globorotalia truncatulinoides*	1.96	3H-CC	4H-CC	20.75	29.07	24.91	8.32
FO *Globorotalia inflata*	3.20	7H-CC	8H-CC	58.25	68.07	63.16	9.25
LO *Globorotalia pliozea*	4.60	14H-CC	15H-CC	123.73	133.94	128.84	10.21
FO *Globorotalia puncticulata*	5.30	16H-CC	17H-CC	143.75	153.47	148.61	9.72
FO *Globorotalia conomiozea*	6.90	18H-CC	19X-CC	163.70	167.13	165.42	3.43
LO *Paragloborotalia continuosa*	8.00	18H-CC	19X-CC	163.70	167.13	165.42	3.43
LO *Paragloborotalia nympha*	10.10	19X-CC	20X-CC	167.13	174.54	170.84	7.41
LO *Paragloborotalia mayeri*	11.40	21X-CC	22X-CC	180.91	192.05	186.48	11.14
FO *Paragloborotalia mayeri*	12.10	29X-CC	30X-CC	259.44	270.22	264.83	10.78
FO *Praeorbulina curva*	16.30	30X-CC	31X-CC	270.50	281.74	276.12	11.24
FO *Globigerinoides trilobus*	18.80	36X-CC	37X-CC	327.22	338.80	333.01	11.58
FO *Globoturborotalita connecta*	20.90	37X-CC	38X-CC	338.80	347.18	342.99	8.38
FO *Globoturborotalita woodi*	22.60	38X-CC	39X-CC	347.18	356.53	351.86	9.35
FO *Globoquadrina dehiscens*	23.20	41X-CC	42X-CC	376.53	387.17	381.85	10.64
FO *Chiloguembelina cubensis*	28.50	42X-CC	43X-CC	387.17	396.63	391.90	9.46
LO *Subbotina angiporoides*	30.00	44X-CC	45X-CC	405.83	410.05	407.94	4.22

Note: FO = first occurrence, LO = last occurrence.

Table T6. Range chart of planktonic foraminifers, Site 1170. (See table note. Continued on next seven pages.)

Hole, core, section	Depth (mbsf)	*Acarinina aculeata*	*Catapsydrax dissimilis*	*Catapsydrax unicavus*	*Chiloguembelina cubensis*	*Dentoglobigerina praedehiscens*	*Dentoglobigerina venezuelana*	*Globigerina bulloides*	*Globigerina cipercensis*	*Globigerina eamsi*	*Globigerina falconensis*	*Globigerina labiacrassata*	*Globigerina officinalis*	*Globigerina praebulloides*	*Globigerina quinqueloba*	*Globigerinella aequilateralis*	*Globigerinella obesa*	*Globigerinita glutinata*	*Globigerinita uvula*	*Globigerinoides primordius*	*Globigerinoides subquadratus*	*Globigerinoides trilobus*	*Globoquadrina dehiscens*	*Globorotalia cibaoensis*	*Globorotalia conomiozea*	*Globorotalia crassacarina*	*Globorotalia crassaconica*	*Globorotalia crassaformis* (sin)	*Globorotalia crassula*	*Globorotalia explicationis*	*Globorotalia hirsuta*	*Globorotalia inflata* (sin)	*Globorotalia juanai*	*Globorotalia margaritae*	*Globorotalia miotumida*	*Globorotalia miozea*	*Globorotalia panda*	*Globorotalia peripheroronda*	*Globorotalia pliozea*	*Globorotalia praescitula*	*Globorotalia pseudokugleri*
189-1170A-1H-CC	1.64							X			X				X			X													X								
1170B-1H-CC	4.75							X			X				X	X		X								X	X				X								
1170C-1H-CC	9.02							X			X				X	X		X								X	X				X								
1170A-2H-CC	11.67							X			X				X	X		X								X	X				X								
1170B-2H-CC	14.65							X			X				X	X		X								X	X		X		X								
1170C-2H-CC	18.04							X			X				X	X		X								X	X		X		X								
1170A-3H-CC	20.75							X			X				X	X		X	X							X	X		X		X	X								
1170B-3H-CC	24.07							X			X				X	X		X	X							X	X		X		X								
1170C-3H-CC	28.51							X			X				X	X		X								X	X		X		X								
1170A-4H-CC	29.07							X			X				X	X		X								X	X		X		X								
1170B-4H-CC	33.59							X			X				X	X		X								X	X		X		X								
1170C-4H-CC	35.77							X			X				X	X		X								X	X		X		X								
1170A-5H-CC	39.40							X			X				X	X		X								X	X		X		X								
1170B-5H-CC	42.66							X			X				X	X		X								X	X		X		X								
1170C-5H-CC	47.13							X			X				X	X		X								X	X		X		X								
1170A-6H-CC	49.03							X			X				X	X		X	X							X	X		X		X								
1170B-6H-CC	52.55							X			X				X	X		X								X	X		X		X								
1170C-6H-CC	56.82							X			X				X	X		X								X	X		X		X								
1170A-7H-CC	58.25							X			X				X	X		X	X							X	X		X		X								
1170B-7H-CC	62.18							X			X				X	X		X								X	X		X		X								
1170C-7H-CC	65.58							X			X				X	X		X								X	X		X		X								
1170A-8H-CC	68.07							X			X				X	X		X								X	X		X		X								
1170B-8H-CC	71.78							X			X				X	X		X								X	X		X		X								
1170C-8H-CC	76.07							X			X				X	X		X								X	X		X		X								
1170A-9H-CC	77.96							X			X				X	X		X	X							X	X		X		X								
1170B-9H-CC	80.96							X			X				X	X		X						?		X	X		X		X								
1170C-9H-CC	85.62							X			X				X	X		X								X	X		X		X								
1170A-10H-CC	87.48							X			X				X	X		X						?		X	X		X		X								
1170B-10H-CC	90.78							X			X				X	X								?			X		X		X								
1170C-10H-CC	94.76							X			X				X	X		X								X	X		X		X								
1170A-11H-CC	96.88							X			X				X	X		X						?		X	X		X		X								
1170B-11H-CC	100.24							X			X				X	X		X						?		X	X		X		X								
1170C-11H-CC	104.30							X			X				X	X		X	X							X	X		X		X								
1170A-12H-CC	106.45							X			X				X	X		X	X							X	X		X		X								
1170A-13H-CC	106.45							X			X				X	X		X	X							X	X		X		X								
1170B-12H-CC	109.71							X			X				X	X		X	X							X	X		X		X								
1170C-12H-CC	113.98							X			X				X	X		X	X							X	X		X		X								
1170B-13H-CC	118.92							X			X				X	X		X								X	X		X		X								
1170C-13H-CC	122.96							X			X				X	X		X								X	X		X		X								

Age	Zone/ Subzone
Pleistocene	SN14
Pliocene, late	SN13
Pliocene, early	SN12b

Table T6 (continued).

Hole, core, section	Depth (mbsf)	*Globorotalia puncticulata*	*Globorotalia puncticuloides*	*Globorotalia scitula*	*Globorotalia sphericomiozea*	*Globorotalia theyeri*	*Globorotalia tosaensis*	*Globorotalia triangula*	*Globorotalia truncatulinoides*	*Globorotalia ungulata*	*Globorotalia zealandica*	*Globoturborotalita suteri*	*Globoturborotalita apertura*	*Globoturborotalita brazieri*	*Globoturborotalita connecta*	*Globoturborotalita decoraperta*	*Globoturborotalita nepenthes*	*Globoturborotalita woodi*	*Indeterminable miliolines*	*Indeterminable textularines*	*Neogloboquadrina humerosa*	*Neogloboquadrina pachyderma* (sin)	*Orbulina universa*	*Paragloborotalia continuosa*	*Paragloborotalia mayeri*	*Paragloborotalia nana*	*Paraglobortalia nympha*	*Praeorbulina curva*	*Subbotina angiporoides*	*Subbotina eocaena*	*Subbotina linaperta*	*Tenuitella gemma*	*Tenuitella minutissima*	*Tenuitella munda*	*Tenuitellinata angustiumbilicata*	*Turborotalia euapertura*	*Turborotalia pomeroli*	Zone/ Subzone	Age		
189-																																									
1170A-1H-CC	1.64			X					X													X																			
1170B-1H-CC	4.75			X					X													X	X																		
1170C-1H-CC	9.02			X																		X																		
1170A-2H-CC	11.67			X			X		X													X	X																		
1170B-2H-CC	14.65			X					X													X	X																		
1170C-2H-CC	18.04			X																		X	X																		
1170A-3H-CC	20.75			X			X	X	X												?	X	X																		
1170B-3H-CC	24.07			X		X			X													X																			
1170C-3H-CC	28.51			X			X															X	X																		
1170A-4H-CC	29.07	X	X	X				X											X		?	X																			
1170B-4H-CC	33.59								X													X	X																		
1170C-4H-CC	35.77			X																		X	X																		
1170A-5H-CC	39.40	X	X	X				X														X	X																		
1170B-5H-CC	42.66	X		X			X															X	X																		
1170C-5H-CC	47.13	X	X	X																		X	X																		
1170A-6H-CC	49.03	X	X	X						X												X	X																		
1170B-6H-CC	52.55	X		X																		X	X																		
1170C-6H-CC	56.82	X	X	X				X														X	X																		
1170A-7H-CC	58.25	X	X	X																		X	X																		
1170B-7H-CC	62.18	X		X																		X	X																		
1170C-7H-CC	65.58	X	X	X				X														X	X																		
1170A-8H-CC	68.07	X	X																	X			X																		
1170B-8H-CC	71.78	X	X	X																		X	X																		
1170C-8H-CC	76.07	X	X	X																		X	X																		
1170A-9H-CC	77.96	X	X	X																		X	X																		
1170B-9H-CC	80.96	X	X	X																		X	X																		
1170C-9H-CC	85.62	X	X	X																		X	X																		
1170A-10H-CC	87.48	X	X																			X																		
1170B-10H-CC	90.78	X	X	X																		X																		
1170C-10H-CC	94.76	X	X	X																		X	X																		
1170A-11H-CC	96.88	X	X	X																			X																		
1170B-11H-CC	100.24	X	X	X																		X	X																		
1170C-11H-CC	104.30	X	X	X												?						X	X																		
1170A-12H-CC	106.45	X	X	X																		X	X																		
1170A-13H-CC	106.45	X	X	X																		X	X																		
1170B-12H-CC	109.71	X	X	X																		X	X																		
1170C-12H-CC	113.98	X	X	X												?						X	X																		
1170B-13H-CC	118.92	X	X	X																		X	X																		
1170C-13H-CC	122.96	X	X	X	?																	X	X																		

Table T6 (continued).

Hole, core, section	Depth (mbsf)	*Acarinina aculeata*	*Catapsydrax dissimilis*	*Catapsydrax unicavus*	*Chiloguembelina cubensis*	*Dentoglobigerina praedehiscens*	*Dentoglobigerina venezuelana*	*Globigerina bulloides*	*Globigerina cipercensis*	*Globigerina eamsi*	*Globigerina falconensis*	*Globigerina labiacrassata*	*Globigerina officinalis*	*Globigerina praebulloides*	*Globigerina quinqueloba*	*Globigerina aequilateralis*	*Globigerinella obesa*	*Globigerinita glutinata*	*Globigerinita uvula*	*Globigerinoides primordius*	*Globigerinoides subquadratus*	*Globigerinoides trilobus*	*Globoquadrina dehiscens*	*Globorotalia cibaoensis*	*Globorotalia conomiozea*	*Globorotalia crassacarina*	*Globorotalia crassaconica*	*Globorotalia crassaformis* (sin)	*Globorotalia crassula*	*Globorotalia explicationis*	*Globorotalia hirsuta*	*Globorotalia inflata* (sin)	*Globorotalia juanai*	*Globorotalia margaritae*	*Globorotalia miotumida*	*Globorotalia miozea*	*Globorotalia panda*	*Globorotalia peripheroronda*	*Globorotalia pliozea*	*Globorotalia praescitula*	*Globorotalia pseudokugleri*
1170A-14H-CC	123.73							X							X			X	X									X											
1170B-14H-CC	128.61							X			X				X			X	X									X	X										
1170C-14H-CC	132.89							X			X				X			X	X									X	X										
1170A-15H-CC	133.94							X			X				X			X										X											
1170B-15H-CC	138.23							X			X				X			X										X	X										
1170C-15H-CC	142.49							X							X			X										X	X				X						
1170A-16H-CC	143.75							X			X				X			X															X						
1170B-16H-CC	145.30							X							X			X															X						
1170C-16H-CC	150.63							X							X			X							X								X						
1170A-17H-CC	153.47							X							X			X															X						
1170B-17H-CC	156.88							X							X			X															X						
1170C-17H-CC	161.24							X							X			X								?							X						
1170A-18H-CC	163.70							X							X			X															X						
1170B-18H-CC	166.70							X							X			X																					
1170A-19X-CC	167.13							X							X			X																					
1170C-18H-CC	170.09							X			X				X			X																					
1170A-20X-CC	174.54							X							X		X	X																					
1170B-19H-CC	176.02							X			X				X			X								?													
1170C-19H-CC	180.44							X			X				X			X																					
1170A-21X-CC	180.91							X							X																								
1170A-22X-CC	192.05							X							X			X																					
1170A-23X-CC	201.09							X							X			X																					
1170A-24X-CC	210.31							X							X			X																					
1170A-25X-CC	220.34							X							X			X																					
1170A-26X-CC	227.55							X							X			X																					
1170A-27X-CC	239.38							X							X			X																					
1170A-28X-CC	250.70						?	X			X				X			X																					
1170A-29X-CC	259.44						X	X			X				X			X																					
1170A-30X-CC	270.22							X							X			X																					
1170A-31X-CC	281.74							X							X			X			X	X																	
1170A-32X-CC	290.89							X			X				X			X					X																
1170A-33X-CC	299.60							X							X			X																					
1170A-34X-CC	310.39							X							X			X																					
1170A-35X-CC	318.43							X							X			X																					
1170A-36X-CC	327.22		X			X		X							X			X					X	X															
1170A-37X-CC	338.80		X					X							X			X					X	X															
1170A-38X-CC	347.18		X												X			X			X		X	X															
1170A-39X-CC	356.53		X	X								X			X			X					X	X															
1170A-40X-CC	367.03		X	X							X	X			X			X					X	X															
1170A-41X-CC	376.53		X	X					X		X				X			X					X	X															

Age	Zone/ Subzone
Pliocene	
early	SN12b
early	SN12a
Miocene	
late	SN11
late	SN9
late	SN8
middle	SN7
early	SN5
early	SN4
early	SN3
early	SN2
early	SN1

Table T6 (continued).

Hole, core, section	Depth (mbsf)	*Globorotalia puncticulata*	*Globorotalia puncticuloides*	*Globorotalia scitula*	*Globorotalia sphericomiozea*	*Globorotalia theyeri*	*Globorotalia tosaensis*	*Globorotalia triangula*	*Globorotalia truncatulinoides*	*Globorotalia ungulata*	*Globorotalia zealandica*	*Globorotaloides suteri*	*Globoturborotalita apertura*	*Globoturborotalita brazieri*	*Globoturborotalita connecta*	*Globoturborotalita decoraperta*	*Globoturborotalita nepenthes*	*Globoturborotalita woodi*	*Indeterminable miliolines*	*Indeterminable textularines*	*Neogloboquadrina humerosa*	*Neogloboquadrina pachyderma* (sin)	*Orbulina universa*	*Paragloborotalia continuosa*	*Paragloborotalia mayeri*	*Paragloborotalia nana*	*Paraglobortalia nympha*	*Praeorbulina curva*	*Subbotina angiporoides*	*Subbotina eocaena*	*Subbotina linaperta*	*Tenuitella gemma*	*Tenuitella minutissima*	*Tenuitella munda*	*Tenuitellinata angustiumbilicata*	*Turborotalia euapertura*	*Turborotalia pomeroli*	Zone/ Subzone	Age	
1170A-14H-CC	123.73	X	X	X																		X																		
1170B-14H-CC	128.61	X	X	X	?																	X																SN12b	early	Pliocene
1170C-14H-CC	132.89	X	X	X	?																	X	X																
1170A-15H-CC	133.94	X	X	X	X																	X	X																
1170B-15H-CC	138.23	X	X		?																		X														SN12a		
1170C-15H-CC	142.49	X	X		?																	X	X																
1170A-16H-CC	143.75				X																	X	X																
1170B-16H-CC	145.30			X	X																	X	X																
1170C-16H-CC	150.63												X									X	X															SN11	late	
1170A-17H-CC	153.47				X																	X	X																
1170B-17H-CC	156.88																					X	X																
1170C-17H-CC	161.24												X										X	X			X												
1170A-18H-CC	163.70				?											X						X	X														SN9		
1170B-18H-CC	166.70			X																		X	X																
1170A-19X-CC	167.13												X			X	?						X	X															
1170C-18H-CC	170.09												X			X		X					X	X			X												
1170A-20X-CC	174.54												X			X							X	X			X												
1170B-19H-CC	176.02			X									X									?	X	X													SN8		
1170C-19H-CC	180.44												X			X		X					X																
1170A-21X-CC	180.91															X		X					X	X			X												
1170A-22X-CC	192.05												X					X					X	X	X		X												
1170A-23X-CC	201.09	?											X			X							X	X	X		X												
1170A-24X-CC	210.31												X			X							X		X														
1170A-25X-CC	220.34															X		X					X	X	X	X	X												
1170A-26X-CC	227.55															X		X					X	X	X	X	X												
1170A-27X-CC	239.38																						X	X	X	X	X												
1170A-28X-CC	250.70			X														X							X		X						X						
1170A-29X-CC	259.44			X																					X														
1170A-30X-CC	270.22										X							X					X			X			X				X					SN5		
1170A-31X-CC	281.74										X				X			X																					
1170A-32X-CC	290.89														X			X																					
1170A-33X-CC	299.60										X				X			X																			SN4		
1170A-34X-CC	310.39										X				X			X																					
1170A-35X-CC	318.43										X			X				X																					
1170A-36X-CC	327.22										X							X																	X				
1170A-37X-CC	338.80														X			X								X									X		SN3		
1170A-38X-CC	347.18																	X								X											SN2		
1170A-39X-CC	356.53											X																								X	X			
1170A-40X-CC	367.03																																			X	X	SN1		
1170A-41X-CC	376.53											X		?																						X				

Table T6 (continued).

Hole, core, section	Depth (mbsf)	*Acarinina aculeata*	*Catapsydrax dissimilis*	*Catapsydrax unicavus*	*Chiloguembelina cubensis*	*Dentoglobigerina praedehiscens*	*Dentoglobigerina venezuelana*	*Globigerina bulloides*	*Globigerina ciperoensis*	*Globigerina eamsi*	*Globigerina falconensis*	*Globigerina labiacrassata*	*Globigerina officinalis*	*Globigerina praebulloides*	*Globigerina quinqueloba*	*Globigerinella aequilateralis*	*Globigerinella obesa*	*Globigerinita glutinata*	*Globigerinita uvula*	*Globigerinoides primordius*	*Globigerinoides subquadratus*	*Globigerinoides trilobus*	*Globoquadrina dehiscens*	*Globorotalia cibaoensis*	*Globorotalia conomiozea*	*Globorotalia crassaformis*	*Globorotalia crassula*	*Globorotalia explicationis*	*Globorotalia hirsuta*	*Globorotalia inflata* (sin)	*Globorotalia juanai*	*Globorotalia margaritae*	*Globorotalia miotumida*	*Globorotalia miozea*	*Globorotalia panda*	*Globorotalia peripheroronda*	*Globorotalia pliozea*	*Globorotalia praescitula*	*Globorotalia pseudokugleri*	Zone/ Subzone	Barren	Age: Oligocene: late	Age: Oligocene: early	Age: Eocene: middle to late
1170A-42X-CC	387.17		X	X		X					X			X			X																					SP14b				
1170A-43X-CC	396.63		X	X						X	X			X				X																								
1170A-44X-CC	405.83		X	X								?	X	X				X																								
1170A-45X-CC	410.05			X	X					X			X	X				X																								
1170A-46X-CC	421.82		X	?	X					X			X	X																												
1170D-1R-CC	427.27		X	X	X							X	X	X				X																								
1170A-47X-CC	430.95		X	X	X					X			X	X																												
1170A-48X-CC	435.26		X	X	X	X				X			X	X																												
1170D-2R-CC	437.50				X	X						X	X					?																								
1170D-3R-CC	444.95			X	X	X				X		X	X	X																												
1170A-49X-CC	450.25		X	X	X	X						X	X	X																												
1170D-4R-CC	454.99		X	X	X	X						X	X	X																												
1170A-50X-CC	456.42			X	X	X						X	X																												
1170A-51X-CC	456.82				X							X																												
1170D-5R-CC	464.21			X									X																												
1170A-52X-CC	464.27		X	X									X	?																												
1170D-6R-CC	472.72																																								
1170D-7R-CC	479.85																																								
1170D-8R-CC	488.35																																								
1170D-9R-CC	497.66																																								
1170D-10R-CC	506.41																																								
1170D-11R-CC	518.31																																								
1170D-12R-CC	524.59																																								
1170D-13R-CC	534.83																																								
1170D-14R-CC	548.46																																								
1170D-15R-CC	558.49																																								
1170D-16R-CC	567.29																																								
1170D-17R-CC	577.77														X																										
1170D-18R-CC	585.10	X		X										X																											
1170D-19R-CC	596.97																																								
1170D-20R-CC	606.55																																								
1170D-21R-CC	615.17																																								
1170D-22R-CC	625.92																																								
1170D-23R-CC	635.30																																								
1170D-24R-CC	645.02																																								
1170D-25R-CC	654.76																																								
1170D-26R-CC	664.32																																								
1170D-27R-CC	671.46																																								
1170D-28R-CC	681.96																																								

Table T6 (continued).

Hole, core, section	Depth (mbsf)	*Globorotalia puncticulata*	*Globorotalia puncticuloides*	*Globorotalia scitula*	*Globorotalia sphericomiozea*	*Globorotalia theyeri*	*Globorotalia tosaensis*	*Globorotalia triangula*	*Globorotalia truncatulinoides*	*Globorotalia ungulata*	*Globorotalia zealandica*	*Globoturborotalita suteri*	*Globoturborotalita apertura*	*Globoturborotalita brazieri*	*Globoturborotalita connecta*	*Globoturborotalita decoraperta*	*Globoturborotalita nepenthes*	*Globoturborotalita woodi*	*Indeterminable miliolines*	*Indeterminable textularines*	*Neogloboquadrina humerosa*	*Neogloboquadrina pachyderma* (sin)	*Orbulina universa*	*Paragloborotalia continuosa*	*Paragloborotalia mayeri*	*Paragloborotalia nana*	*Paragloborotalia nympha*	*Praeorbulina curva*	*Subbotina angiporoides*	*Subbotina eocaena*	*Subbotina linaperta*	*Tenuitella gemma*	*Tenuitella minutissima*	*Tenuitella munda*	*Tenuitellinata angustiumbilicata*	*Turborotalia euapertura*	*Turborotalia pomeroli*	Zone/ Subzone	Age	
1170A-42X-CC	387.17											X		?																										
1170A-43X-CC	396.63											X		?																					X			SP14b	late	Oligocene
1170A-44X-CC	405.83																											?			X	X		X	X				
1170A-45X-CC	410.05											X																X						X	X				
1170A-46X-CC	421.82											X																X				X			X				
1170D-1R-CC	427.27											X																X				X			X				
1170A-47X-CC	430.95																											X				X			X				
1170A-48X-CC	435.26											X														X		X				X			X				
1170D-2R-CC	437.50											X																X				X							
1170D-3R-CC	444.95											X																X				X			X				
1170A-49X-CC	450.25																											X				X			X	X			
1170D-4R-CC	454.99																									X		X				X		X					
1170A-50X-CC	456.42											X																?											
1170A-51X-CC	456.82																											X							X				
1170D-5R-CC	464.21											X																X											
1170A-52X-CC	464.27																																						
1170D-6R-CC	472.72																																						
1170D-7R-CC	479.85																																						
1170D-8R-CC	488.35																																						
1170D-9R-CC	497.66																																						
1170D-10R-CC	506.41																																					ND	Barren	
1170D-11R-CC	518.31																																						
1170D-12R-CC	524.59																																						
1170D-13R-CC	534.83																																						
1170D-14R-CC	548.46																																						
1170D-15R-CC	558.49																												X		X							SP10+		
1170D-16R-CC	567.29																																					ND		
1170D-17R-CC	577.77																												X		X							SP10+		
1170D-18R-CC	585.10																									X			X		X									
1170D-19R-CC	596.97																														?									
1170D-20R-CC	606.55																																						
1170D-21R-CC	615.17																																						
1170D-22R-CC	625.92																																						
1170D-23R-CC	635.30																																					ND	middle to late	Eocene
1170D-24R-CC	645.02																																						
1170D-25R-CC	654.76																																						
1170D-26R-CC	664.32																																						
1170D-27R-CC	671.46																																						
1170D-28R-CC	681.96																														X							SP10+		

Table T6 (continued).

Hole, core, section	Depth (mbsf)	*Acarinina aculeata*	*Catapsydrax dissimilis*	*Catapsydrax unicavus*	*Chiloguembelina cubensis*	*Dentoglobigerina praedehiscens*	*Dentoglobigerina venezuelana*	*Globigerina bulloides*	*Globigerina ciperoensis*	*Globigerina eamsi*	*Globigerina falconensis*	*Globigerina labiacrassata*	*Globigerina officinalis*	*Globigerina praebulloides*	*Globigerina quinqueloba*	*Globigerinella aequilateralis*	*Globigerinella obesa*	*Globigerinita glutinata*	*Globigerinita uvula*	*Globigerinoides primordius*	*Globigerinoides subquadratus*	*Globigerinoides trilobus*	*Globoquadrina dehiscens*	*Globorotalia cibaoensis*	*Globorotalia conomiozea*	*Globorotalia crassacarina*	*Globorotalia crassaconica*	*Globorotalia crassaformis* (sin)	*Globorotalia crassula*	*Globorotalia explicationis*	*Globorotalia hirsuta*	*Globorotalia inflata* (sin)	*Globorotalia juanai*	*Globorotalia margaritae*	*Globorotalia miotumida*	*Globorotalia miozea*	*Globorotalia panda*	*Globorotalia peripheroronda*	*Globorotalia pliozea*	*Globorotalia praescitula*	*Globorotalia pseudokugleri*	Zone/ Subzone	Age	
1170D-29R-CC	693.38																																						ND	middle to late	
1170D-30R-CC	701.41																																								
1170D-31R-CC	712.75																																								
1170D-32R-CC	722.15																																								
1170D-33R-CC	731.74																																								
1170D-34R-CC	741.48																																								
1170D-35R-CC	749.55																																								
1170D-36R-CC	760.56																																								
1170D-37R-CC	768.73																																								
1170D-38R-CC	779.69																																							SP10 or older **[SP10+?]**	Eocene	

Note: X = present, ? = questionable identification, ND = not determined.

Table T6 (continued).

Hole, core, section	Depth (mbsf)	*Globorotalia puncticulata*	*Globorotalia puncticuloides*	*Globorotalia scitula*	*Globorotalia sphericomiozea*	*Globorotalia theyeri*	*Globorotalia tosaensis*	*Globorotalia triangula*	*Globorotalia truncatulinoides*	*Globorotalia ungulata*	*Globorotalia zealandica*	*Globoturborotalita suteri*	*Globoturborotalita apertura*	*Globoturborotalita brazieri*	*Globoturborotalita connecta*	*Globoturborotalita decoraperta*	*Globoturborotalita nepenthes*	*Globoturborotalita woodi*	*Indeterminable miliolines*	*Indeterminable textularines*	*Neogloboquadrina humerosa*	*Neogloboquadrina pachyderma* (sin)	*Orbulina universa*	*Paragloborotalia continuosa*	*Paragloborotalia mayeri*	*Paragloborotalia nana*	*Paragloborotalia nympha*	*Praeorbulina curva*	*Subbotina angiporoides*	*Subbotina eocaena*	*Subbotina linaperta*	*Tenuitella gemma*	*Tenuitella minutissima*	*Tenuitella munda*	*Tenuitellinata angustiumbilicata*	*Turborotalia euapertura*	*Turborotalia pomeroli*	Zone/Subzone	Age	
1170D-29R-CC	693.38																																					ND		
1170D-30R-CC	701.41																																						middle to late	
1170D-31R-CC	712.75																																							
1170D-32R-CC	722.15																																							
1170D-33R-CC	731.74																												?	X										
1170D-34R-CC	741.48																													X										
1170D-35R-CC	749.55											?																		X								SP10 or older [SP10+?]		
1170D-36R-CC	760.56											?																		X										
1170D-37R-CC	768.73																													X							?			
1170D-38R-CC	779.69											X																		X										

Table T7. Radiolarian datums, Site 1170.

Bioevent	Age (Ma)	Interval Top	Interval Bottom	Depth (mbsf) Top	Depth (mbsf) Bottom	Mean (mbsf)	Error (m)
Hole 1170A							
LO *Stylatractus universus*	0.45	1H-CC	2H-CC	1.64	11.67	6.66	10.03
LO *Pseudocubus vema*	2.4	5H-CC	6H-CC	39.40	49.03	44.22	9.63
FO *Pseudocubus vema*	4.5	6H-CC	7H-CC	49.03	58.25	53.64	9.22
LO *Lychnocanoma grande*	5.0	9H-CC	10H-CC	77.86	87.48	82.67	9.62
LCO *Stichocorys delmontensis*	5.18-6.9	13H-CC	14H-CC	115.24	123.73	119.49	8.49
LO *Amphymenium challengerae*	6.1	17H-CC	18H-CC	153.57	163.70	158.64	10.13
FO *Amphymenium challengerae*	6.6	18H-CC	19H-CC	163.70	167.13	165.42	3.43
FO *Dictyophimus splendeus*	11.8	19X-CC	20X-CC	167.13	174.54	170.84	7.41
LAO *Cyrtocapsella tetrapera*	12.5	27X-CC	28X-CC	239.38	250.70	245.04	11.32
LO *Lychnocanoma nipponica nipponica*	15.7	32X-CC	33X-CC	290.89	299.60	295.25	8.71
LO *Cenosphaera coronata*	16.7	35X-CC	36X-CC	318.43	327.52	322.99	9.09
FO *Cyrtocapsella tetrapera*	23.6	41X-CC	42X-CC	376.53	387.17	381.85	10.64
Hole 1170B							
LO *Pseudocubus vema*	2.4	5H-CC	6H-CC	42.66	52.55	47.61	9.89
FO *Pseudocubus vema*	4.5	9H-CC	10H-CC	80.96	90.78	85.87	9.82
LO *Lychnocanoma grande*	50.0	9H-CC	10H-CC	80.96	90.78	85.87	9.82
LCO *Stichocorys delmontensis*	5.18-6.9	13H-CC	14H-CC	118.92	128.61	123.77	9.69
Hole 1170C							
LO *Pseudocubus vema*	2.4	5H-CC	6H-CC	47.13	56.82	51.98	9.69
FO *Pseudocubus vema*	4.5	8H-CC	9H-CC	76.07	85.62	80.85	9.55
LO *Lychnocanoma grande*	5.0	10H-CC	11H-CC	94.76	104.30	99.53	9.54
LCO *Stichocorys delmontensis*	5.18-6.9	13H-CC	14H-CC	122.96	132.89	127.93	9.93

Note: LO = last occurrence, FO = first occurrence, LCO = last consistent occurrence, LAO = last abundant occurrence.

Table T8. Relative abundance of selected diatom taxa, sponge spicules, and silicoflagellates, Hole 1170A. (See table notes. Continued on next three pages.)

Core, section, interval (cm)	Depth (mbsf)	Preservation	Group abundance	*Actinocyclus actinochilus*	*Actinocyclus curvatulus*	*Actinocyclus dimorphus*	*Actinocyclus ingens*	*Actinocyclus ingens* var. *nodus*	*Actinocyclus ingens* var. *ovalis*	*Actinocyclus karstenii*	*Actinocyclus* cf. *karstenii*	*Actinocyclus* spp.	*Actinoptychus* spp.	*Asteromphalus parvulus*	*Asteromphalus* spp.	*Azpeitia gombosi*	*Azpeitia neocrenulata*	*Azpeitia nodulifer*	*Azpeitia* cf. *nodulifer*	*Azpeitia oligocenica*	*Azpeitia praenodulifera*	*Azpeitia tabularis* group	*Cestodiscus antarcticus*	*Cestodiscus pulchellus*	*Chaetoceros* resting spores	*Corethron criophilum*	*Coscinodiscus lewisianus* var. *levis*	*Coscinodiscus marginatus*	*Coscinodiscus rhombicus*	*Coscinodiscus* spp.	*Denticulopsis dimorpha*	*Denticulopsis hustedtii*	*Denticulopsis maccollumii*	*Diploneis bombus*	*Ethmodiscus rex*	*Eucampia antarctica*	*Fragilariopsis aurica*	*Fragilariopsis barronii*	*Fragilariopsis fossilis*	*Fragilariopsis kerguelensis*	*Fragilariopsis lacrima*	*Fragilariopsis reinholdii*	*Fragilariopsis* spp.	*Fragilariopsis weaveri*	*Hemiaulus* spp.	*Hemidiscus cuneiformis*	*Hemidiscus karstenii*	*Nitzschia evenescens*
189-1170A-																																															
1H-CC, 18-22	1.64	MG	C		R												R	R				C		F										R		R						R				
2H-CC, 11-15	11.67	M	C			R											R					A																		A							
3H-CC, 12-16	20.75	MG	A	F			F					F												F																A							
4H-CC, 18-23	29.07	MG	C	R	F		C					F												R																C				R			
5H-CC, 8-13	39.40	G	A				C																	R											R		F		F			R	F		
6H-CC, 8-13	49.03	MG	A				R											R						R	R		F									C	C	R		R					
7H-CC, 10-15	58.25	G	A				R							R													A								R		C			R		C	R		
8H-CC, 16-21	68.07	G	A				F							C				F																	R		R			R		D		C		
9H-CC, 15-20	77.86	G	C				R																		R			C									C	R						R		
10H-CC, 12-17	87.48	G	A															F					R											R	R		C			R		F	R		
11H-CC, 12-17	96.88	MG	A				D											C																			C			F	R	C		C	C		
12H-CC, 10-15	106.45	P	F															F					R																		R			F		
13H-CC, 12-17	115.24	MP	F				R											A																												
14H-CC, 11-16	123.73	M	F				R											A									F														R					
15H-CC, 12-17	133.94	P	T											T																T																
16H-CC, 12-17	143.75	P	T																								T																			
17H-CC, 21-25	153.57	P	F				F		C																R		R											F			R	R		R		
18H-CC, 23-28	163.70	MP	T				R		R														R																					R		
19X-CC, 3-9	167.13	MG	A				D																				C					R					C					R			
20X-CC, 21-26	174.54	MG	C						F																		C								R										
21X-CC, 11-16	180.91	P	R						R																		R					R													
22X-CC, 12-17	192.05	M	C									F											F				C																		
23X-CC, 12-17	201.09	P	R				R			R																					R												R		
24X-CC, 16-21	210.31	M	C				C			R																				R															
25X-CC, 20-25	220.34	MP	R				R					R																																		
26X-CC, 10-15	227.55	M	R				R																				R					R													
27X-CC, 12-17	239.38	P	R				R																																						
28X-CC, 20-25	250.70	P	R				C	C																			C																		
29X-CC, 10-15	259.44	M	F				F																																						
30X-CC, 9-14	270.22	P	T				T																								T	T													
31X-CC, 12-17	281.74	P	T																												T														
32X-CC, 15-20	290.89	G	F				F	C			F									F																										
33X-CC, 11-16	299.60	P	T				T																																						
34X-CC, 21-26	310.39	G	A				C																				R	R					A		R										R
35X-CC, 19-24	318.43	P	R				R																										R										T			
36X-CC, 16-21	327.52	P	T																																										

Table T8 (continued).

Core, section, interval (cm)	Depth (mbsf)	Preservation	Group abundance	*Nitzschia sicula*	*Proboscia barboi*	*Proboscia praebarboi*	*Synedra jouseana*	*Pseudotriceratium radiosoreticulatum*	*Pyxilla fragments*	*Rhizosolenia bergonii*	*Rhizosolenia* spp.	*Rocella gelida*	*Stellarima microtrias*	*Stephanopyxis turris*	*Rocella gelida* var. *schraderi*	*Rocella vigilans*	*Rossiella symmetrica*	*Sceptroneis* spp.	*Thalassionema nitzschioides*	*Thalassionema nitzschioides* var. *parva*	*Thalassiosira complicata*	*Thalassiosira eccentrica*	*Thalassiosira fasciculata*	*Thalassiosira gracilis*	*Thalassiosira insigna*	*Thalassiosira inura*	*Thalassiosira lentiginosa*	*Thalassiosira leptopus*	*Thalassiosira oestrupii*	*Thalassiosira oliverana*	*Thalassiosira* spp.	*Thalassiosira striata*	*Thalassiosira tetraoestrupii* var. *reimeri*	*Thalassiosira torokina*	*Thalassiosira trifulta*	*Thalassiothrix antarctica*	Silicoflagellate tests	Sponge spicules
189-1170A-																																						
1H-CC, 18-22	1.64	MG	C	R															F			R					C	R	R	R				R	F	F	F
2H-CC, 11-15	11.67	M	C								R								R	R							C		R					R	F	R	F
3H-CC, 12-16	20.75	MG	A							R			R									R					C		R						C	R	A
4H-CC, 18-23	29.07	MG	C																	R							C		R	R					R	R	F
5H-CC, 8-13	39.4	G	A		F														A								R		R	R					R	C	A
6H-CC, 8-13	49.03	MG	A		D						R											R		R			R	R		F			F		D	C	A
7H-CC, 10-15	58.25	G	A								R								R					R			R		R	F					D	C	A
8H-CC, 16-21	68.07	G	A											R					R		C	F	R			F		F		F	C		C			C	C	C
9H-CC, 15-20	77.86	G	C		C									R					R	R								C		F	C		C			C	C	C
10H-CC, 12-17	87.48	G	A		F														R				R		R	R	R			C					C	C	A
11H-CC, 12-17	96.88	MG	A																		C	R	C		R	F				C		R			D	F	A
12H-CC, 10-15	106.45	P	F																											F					R	F	R
13H-CC, 12-17	115.24	MP	F																																		F
14H-CC, 11-16	123.73	M	F																																		R
15H-CC, 12-17	133.94	P	T																																		T
16H-CC, 12-17	143.75	P	T																																T		
17H-CC, 21-25	153.57	P	F																																F		T
18H-CC, 23-28	163.7	MP	T		F															C															R		T
19X-CC, 3-9	167.13	MG	A		R																														C		A
20X-CC, 21-26	174.54	MG	C		C																														C	F	C
21X-CC, 11-16	180.91	P	R																																		R
22X-CC, 12-17	192.05	M	C																																F		
23X-CC, 12-17	201.09	P	R																																		T
24X-CC, 16-21	210.31	M	C																																C		T
25X-CC, 20-25	220.34	MP	R		R																														R		T
26X-CC, 10-15	227.55	M	R																																		T
27X-CC, 12-17	239.38	P	R																																		T
28X-CC, 20-25	250.7	P	R						R																										C		T
29X-CC, 10-15	259.44	M	F												T																				F		F
30X-CC, 9-14	270.22	P	T																																T		T
31X-CC, 12-17	281.74	P	T																																		
32X-CC, 15-20	290.89	G	F																	C																F	
33X-CC, 11-16	299.6	P	T				F																												R		T
34X-CC, 21-26	310.39	G	A				C								T																						C
35X-CC, 19-24	318.43	P	R				R								T																					R	R
36X-CC, 16-21	327.52	P	T																																		T

Table T8 (continued).

Core, section, interval (cm)	Depth (mbsf)	Preservation	Group abundance	*Actinocyclus actinochilus*	*Actinocyclus curvatulus*	*Actinocyclus dimorphus*	*Actinocyclus ingens*	*Actinocyclus ingens* var. *nodus*	*Actinocyclus ingens* var. *ovalis*	*Actinocyclus karstenii*	*Actinocyclus* cf. *karstenii*	*Actinocyclus* spp.	*Actinoptychus* spp.	*Asteromphalus parvulus*	*Asteromphalus* spp.	*Azpeitia gombosi*	*Azpeitia neocrenulata*	*Azpeitia nodulifer*	*Azpeitia* cf. *nodulifer*	*Azpeitia oligocenica*	*Azpeitia praenodulifera*	*Azpeitia tabularis* group	*Cestodiscus antarcticus*	*Cestodiscus pulchellus*	*Chaetoceros* resting spores	*Corethron criophilum*	*Coscinodiscus lewisianus* var. *levis*	*Coscinodiscus marginatus*	*Coscinodiscus rhombicus*	*Coscinodiscus* spp.	*Denticulopsis dimorpha*	*Denticulopsis hustedtii*	*Denticulopsis maccollumii*	*Diploneis bombus*	*Ethmodiscus rex*	*Eucampia antarctica*	*Fragilariopsis aurica*	*Fragilariopsis barronii*	*Fragilariopsis fossilis*	*Fragilariopsis kerguelensis*	*Fragilariopsis lacrima*	*Fragilariopsis reinholdii*	*Fragilariopsis* spp.	*Fragilariopsis weaveri*	*Hemiaulus* spp.	*Hemidiscus cuneiformis*	*Hemidiscus karstenii*	*Nitzschia evenscens*
37X-CC, 16-21	338.80	P	T																											T																
38X-CC, 13-18	347.18	P	T																											T																
39X-CC, 19-24	356.53		B																																											
40X-CC, 25-30	367.03	P	T																									R		T																
41X-CC, 29-34	376.53	P	R																																											
42X-CC, 29-34	387.17	MG	A													C				F				R				C	F																	
43X-CC, 14-19	396.63	G	A																	F	C						C	F																	
44X-CC, 31-36	405.83	G	A																	F	C																									
45X-CC, 30-35	410.05	G	A																																											
46X-CC, 20-25	421.82	MG	A													C				C					F																				
47X-CC, 10-15	430.95	G	A										F																															R		
48X-CC, 26-31	435.26	M	A										F		F								F																						
49X-CC, 10-15	450.25	G	A												F								C																						
50X-CC, 22-27	456.82		F																																										
51X-CC, 33-38	459.33		B																																										
52X-CC, 47-52	464.27		B																																										

Notes: Preservation: G = good, M = moderate, MG = moderate–good, P = poor. Abundance: D = dominant, A = abundant, C = common, F = few, R = rare, T = trace, B = barren.

Table T8 (continued).

Core, section, interval (cm)	Depth (mbsf)	Preservation	Group abundance	*Nitzschia sicula*	*Proboscia barboi*	*Proboscia praebarboi*	*Synedra jouseana*	*Pseudotriceratium radiosoreticulatum*	*Pyxilla fragments*	*Rhizosolenia bergonii*	*Rhizosolenia* spp.	*Rocella gelida*	*Stellarima microtrias*	*Stephanopyxis turris*	*Rocella gelida* var. *schraderi*	*Rocella vigilans*	*Rossiella symmetrica*	*Sceptroneis* spp.	*Thalassionema nitzschioides*	*Thalassionema nitzschioides* var. *parva*	*Thalassiosira complicata*	*Thalassiosira eccentrica*	*Thalassiosira fasciculata*	*Thalassiosira gracilis*	*Thalassiosira insigna*	*Thalassiosira inura*	*Thalassiosira lentiginosa*	*Thalassiosira leptopus*	*Thalassiosira oestrupii*	*Thalassiosira oliverana*	*Thalassiosira* spp.	*Thalassiosira striata*	*Thalassiosira tetraoestrupii* var. *reimeri*	*Thalassiosira torokina*	*Thalassiosira trifulta*	*Thalassiothrix antarctica*	Silicoflagellate tests	Sponge spicules
37X-CC, 16-21	338.8	P	T																																			T
38X-CC, 13-18	347.18	P	T																																			T
39X-CC, 19-24	356.53		B																																			T
40X-CC, 25-30	367.03	P	T																																			T
41X-CC, 29-34	376.53	P	R						R						R															R								T
42X-CC, 29-34	387.17	MG	A			F	C	R	C			C		F	C		F																					C
43X-CC, 14-19	396.63	G	A						F			R			A	C																						
44X-CC, 31-36	405.83	G	A				C		F							C																						A
45X-CC, 30-35	410.05	G	A				C		F							C																						C
46X-CC, 20-25	421.82	MG	A				C		C							C																						C
47X-CC, 10-15	430.95	G	A				C	R	C					F		C																				F	C
48X-CC, 26-31	435.26	M	A				C							C		C																				F	A
49X-CC, 10-15	450.25	G	A															T																				A
50X-CC, 22-27	456.82		F																																			
51X-CC, 33-38	459.33		B																																			F
52X-CC, 47-52	464.27		B																																			F

Table T9. Diatom bioevents identified, Holes 1170A and 1170D.

Bioevent	Age (Ma)	Interval (cm)		Depth (mbsf)		Mean (mbsf)	Error bar (m)
		Top	Bottom	Top	Bottom		
LO *Actinocyclus ingens*	0.64	2H-CC	3H-CC	11.67	20.75	16.21	4.54
LO *Fragilariopsis barronii*	1.44	4H-CC	5H-CC	29.07	39.40	34.24	5.17
LO *Proboscia baboi*	1.80	4H-CC	5H-CC	29.07	39.40	34.24	5.17
LO *Thalassiosira complicata*	2.50	7H-CC	8H-CC	58.25	68.97	63.61	5.36
LO *Thalassiosira inura*	2.50	7H-CC	8H-CC	58.25	68.97	63.61	5.36
LO *Fragilariopsis weaveri*	2.65	7H-CC	8H-CC	58.25	68.97	63.61	5.36
FO *Thalassiosira complicata*	4.44	11H-CC	12H-CC	96.88	106.45	101.67	4.79
FO *Thalassiosira inura*	4.92	11H-CC	12H-CC	96.88	106.45	101.67	4.79
LO *Actinocyclus ingens* var. *ovalis*	6.27	16H-CC	17H-CC	143.75	153.57	148.66	4.91
LO *Denticulopsis dimorpha*	10.70	22X-CC	23X-CC	192.05	201.09	196.57	4.52
FO *Denticulopsis dimorpha*	12.20	27X-CC	28X-CC	239.38	250.70	245.04	5.66
LO *Actinocyclus ingens* var. *nodus*	12.71	27X-CC	28X-CC	239.38	250.70	245.04	5.66
FO *Actinocyclus ingens* var. *nodus*	14.38	32X-CC	33X-CC	290.89	299.60	295.25	4.36
LO *Cavitatus (Synedra) jouseanus*	14.61	32X-CC	33X-CC	290.89	299.60	295.25	4.36
LO *Denticulopsis maccollumii*	14.70	33X-CC	34X-CC	299.60	310.39	305.00	5.39
LO *Azpeitia gombosi*	21.10	41X -CC	42X-CC	376.53	387.17	381.85	5.32
LO *Coscinodiscus lewisianus* var. *levis*	28.20	42X-CC	43X-CC	387.17	396.63	391.90	4.73
FO *Coscinodiscus lewisianus* var. *levis*	28.50	43X-CC	44X-CC	396.63	405.83	401.23	4.60
LO *Rocella vigilans* (small)	28.80	43X-CC	44X-CC	396.63	405.83	401.23	4.60
FO *Coscinodiscus lewisianus* var. *levis*	28.50	1R-CC	2R-CC	427.27	437.50	432.39	5.12
FO *Rocella vigilans* (small)	30.24	48X-CC	49X-CC	435.26	450.25	442.76	7.50
FO *Cavitatus (Synedra) jouseanus*	30.62	4R-1, 120	4R-CC	453.90	454.95	454.43	0.53

Note: LO = last occurrence, FO = first occurrence.

Table T10. Distribution of organic walled dinoflagellate cysts (dinocysts; specimens counted) and sporomorph and foraminifer linings percentages in selected samples, Hole 1170A.

Core, section, interval (cm)	Depth (mbsf)	Preservation	Group abundance	Dinocyst (%)	Sporomorph (%)	Foraminifer linings (%)	*Brigantedinium* spp.	*Corrudinium harlandii*	*Dalella chathamense*	*Impagidinium pallidum*	*Impagidinium aculeatum*	*Impagidinium paradoxum*	*Impagidinium patulum*	*Impagidinium sphaericum*	*Invertocysta tabulata*	*Nematosphaeropsis labyrinthea*	*Operculodinium centrocarpum*	*Spiniferites mirabilis*	*Spiniferites ramosus*
189-1170A-																			
1H-CC, 18–22	1.64	M	C	93.5	5.6	0.9	1		3	1		1	4	5		110	3	3	1
4H-CC, 18–23	29.07	M	F	83.7	14.3	2.0					11	5	4	1	1	11	6		2
8H-CC, 16–21	68.07	G	F	100.0	0	0		1			11	25	1						
12H-CC, 10–15	106.45		B																
16H-CC, 12–17	143.75		B																
20X-CC, 21–26	174.54		B																
24X-CC, 16–21	210.31		B																
28X-CC, 20–25	250.70		B																
32X-CC, 15–20	290.89		B																
36X-CC, 16–21	327.52		B																
40X-CC, 25–30	367.03		B																
44X-CC, 31–36	405.83		B																
48X-CC, 26–31	435.26		B																
52X-CC, 47–52	464.27		B																

Notes: Preservation: G = good, M = moderate. Abundance refers to abundance of dinocysts: C = common, F = few, B = barren.

Table T11. Useful stratigraphic dinocyst events, Holes 1170A and 1170D.

Bioevent	Age (Ma)	Interval Top	Interval Bottom	Depth (mbsf) Top	Depth (mbsf) Bottom	Mean (mbsf)	Error bar (m)	Source
LO *Invertocysta tabulata*	2.65	1170A-1H-CC	1170A-4H-CC	1.64	29.07	15.355	13.715	Williams et al., 1998a
FCO *Alterbidinium distinctum*	37.00	1170D-8H-CC	1170D-9R-CC	488.35	497.66	493.005	4.655	Raine et al., 1997
LO *Cerebrocysta bartonensis*	38.60	1170D-11R-CC	1170D-12R-CC	518.31	524.29	521.300	2.990	Williams et al., 1998a
LAO *Enneadocysta partridgei*	39.50	1170D-16R-CC	1170D-17R-CC	567.29	577.77	572.530	5.240	Raine et al., 1997
FAO *Enneadocysta partridgei*	43.00	1170D-36R-CC	1170D-38R-CC	760.56	779.69	770.125	9.565	Raine et al., 1997

Note: LO = last occurrence, FCO = first consistent occurrence, LAO = last abundant occurrence, FAO = first abundant occurrence.

Table T12. Distribution of organic walled dinoflagellate cysts (dinocysts; specimen counts) and percentages of other palynomorph groups in selected samples, Hole 1170D. (Continued on next page.)

Core, section, interval (cm)	Depth (mbsf)	Preservation	Group abundance	*N* (palynomorphs)	Sporomorphs (%)	Foraminifer linings (%)	Acritarchs (%)	*N* (dinocysts)	Reworked Cretaceous	*Achilleodinium biformoides*	*Alterbidinium distinctum*	*Alterbidinium* spp. (pars.)	*Arachnodinium antarcticum*	*Areosphaeridium diktyoplokum*	*Batiacasphaera compta*	*Cerebrocysta bartonensis*	*Cerebrocysta*? sp.	*Cordosphaeridium fibrospinosum*	*Cordosphaeridium minimum*	*Corrudinium* sp. (G&F '83)	*Dapsilidinium pseudocolligerum*	*Deflandrea phosphoritica group*	*Elytrocysta* spp.	*Enneadocysta harrisii*	*Enneadocysta partridgei*	*Enneadocysta pectiniforme*	*Fibrocysta axialis*	*Glaphyrocysta exuberans*	*Hemiplacophora semilunifera*
189-1170D-																													
1R-CC, 11-16	427.27		B																										
2R-CC, 14-21	437.50		B																										
3R-CC, 15-20	444.95		B																										
6R-CC, 21-27	472.72	G	C	100	5.0	10.0	1.0	103	1		1	1		1						1		33	5		3	1			
7R-CC, 17-22	479.85	G	A	195	7.7	3.1	1.0	238			7	5		1						1		47	15		6	1			
8R-CC, 0-7	488.35	G	A	195	6.7	2.6	0.5	220	2		7	14								1		30	10		3				
9R-CC, 10-15	497.66	G	C	156	4.5	3.2	0.6	170			1	15										12	5		4				
10R-CC, 10-15	506.41	G	A	218	1.4	0.5	0.5	215				1										200	1		2				
11R-CC, 16-21	518.31	G	C	90	2.2	5.6	1.1	83				3					1	1		1	1	16			32				
12R-CC, 16-22	524.59	G	A	183	7.1	1.1	0.5	259	1		2	3	3	1	2	3		1		1		62	1	5	120	1	1	2	1
13R-CC, 16-21	534.83	G	A	182	2.2	1.6	0.5	225				15	1		2	1				2		51			18				
14R-CC, 0-5	548.46	G	A	161	3.1	0.6	0.0	247				1	1									180			19				
15R-CC, 6-11	558.49	G	A	211	1.4	0.9	0.0	212				10	1			3			1			85			21				
16R-CC, 20-25	567.29	G	A	191	2.1	3.1	0.5	223					2	1		1			1			82			39				
17R-CC, 17-22	577.77	G	A	180	2.8	3.9	1.1	209				1		1								82		3	102				
18R-CC, 0-4	585.10	G	A	243	0.4	0.8	0.0	199				1		1								8		5	175				
19R-CC, 15-19	596.97	G	A	265	1.5	0.8	0.8	263				4	2	1								60	1	4	165				
20R-CC, 12-17	606.55	G	A	216	0.5	2.3	0.0	210						1								42	1	3	150				
21R-CC, 0-7	615.17	G	A	232	0.9	0.9	0.9	233				4	1									160	2		30				
22R-CC, 18-23	625.92	G	A	206	1.5	0.5	1.0	202				1	1									120		1	55				
23R-CC, 10-15	635.30	G	A	218	3.2	0.5	0.5	211				4	2	1				1				61	1	4	120				
24R-CC, 11-16	645.02	G	A	284	1.8	0.4	1.1	275				3	12									135	2		65				
25R-CC, 15-20	654.76	G	A	239	0.8	0.4	0.4	249				1	2	1					1			55	6	5	150				
26R-CC, 8-13	664.32	G	A	296	0.7	0.3	0.3	302					2	1	1	1						90	1	5	175				
27R-CC, 11-16	671.46	G	A	211	0.5	0.5	0.5	219				1	1	1								10		5	190				
28R-CC, 9-14	681.96	G	A	232	0.4	0.4	0.4	242				1	1	1								50	1	6	170				
30R-CC, 17-22	701.41	M	C	159	5.0	6.3	1.3	207	1			7	2					3				100	1	1	34				
32R-CC, 18-23	722.15	M	C	157	3.8	7.6	3.2	149	1			15						2				45			10				
34R-CC, 21-26	741.48	G	A	254	1.6	2.0	1.2	253		1		3	1	1				2				90		3	117				
36R-CC, 19-24	760.56	G	A	227	2.2	2.6	0.9	214				3	1	1				1				70		3	110				
38R-CC, 25-30	779.69	G	A	233	3.4	3.4	2.6	204				5	5	1				3				95		1	62				

Notes: G&F '83 = Goodman and Ford, 1983; B&B '93 = Brinkhuis and Biffi, 1993; C&H '96 = Crouch and Hollis, 1996. Group abundance refers to abundance of dinocysts: A = abundant, C = common, B = barren. Preservation: G = good, M = moderate.

Table T12 (continued).

Core, section, interval (cm)	Depth (mbsf)	Preservation	Group abundance	*Hystrichosphaeridium tubiferum*	*Hystrichostrogylon* spp.	*Impagidinium dispertitum*	*Impagidinium* sp. (B&B '93)	*Impagidinium* sp. a (C&H '96)	*Impagidinium victorianum*	*Lejeunecysta* spp.	*Octodinium askiniae*	*Operculodinium centrocarpum*	*Operculodinium* sp. A	*Operculodinium* sp. B	*Pentadinium goniferum*	*Phthanoperidinium* spp.	*Pyxidinopsis* sp.	*Pyxidinopsis waipawaensis*	*Samlandia chlamydophora*	*Selenopemphix nephroides*	*Spinidinium macmurdoense*	*Spiniferites membranaceus*	*Spiniferites ramosus*	*Stoveracysta kakanuiensis*	*Systematophora placacantha*	*Tectatodinium* spp.	*Thalassiphora pelagica*	*Turbiosphaera filosa*	*Vozzhennikovia* spp.	*Wetzeliella* spp.	*Wilsonidinium ornatum*
1R-CC, 11-16	427.27		B																											
2R-CC, 14-21	437.50		B																											
3R-CC, 15-20	444.95		B																											
6R-CC, 21-27	472.72	G	C				3	3	1	10	3	1	2	4			1		1	1	4		4	3	1	2	1	7	5		
7R-CC, 17-22	479.85	G	A			1	3	3	1	15	4	1	4	5					1	4	53		1		2	2	2	13	40		
8R-CC, 0-7	488.35	G	A	1				2		10	7	1	9			8				3	37				1	1	1	2	72		
9R-CC, 10-15	497.66	G	C					2		6	1		6			5				3	17		2						91		
10R-CC, 10-15	506.41	G	A								7		1								1								2		
11R-CC, 16-21	518.31	G	C							2	1		3			1				1		1			3	8		8		
12R-CC, 16-22	524.59	G	A				2			1	2	2	11	6		4				1		2	10				1		8		
13R-CC, 16-21	534.83	G	A	2	1	1	1	1	1	5	1	1	10		1		2	1		1	9	2	18				1		76		
14R-CC, 0-5	548.46	G	A		1				2				5							2	2		3			1	12		18		
15R-CC, 6-11	558.49	G	A	1		1		1	2		4	7	3	1			4	5			10		12				3		37		
16R-CC, 20-25	567.29	G	A					1		3	1	1	6	1		5		1		1	1		11				25		40		
17R-CC, 17-22	577.77	G	A	1						2			4	1		2		1		1	2		2				1		3		
18R-CC, 0-4	585.10	G	A				1	1						1				1		2			1				1		1		
19R-CC, 15-19	596.97	G	A	1						1	2		7								1		2				3		9		
20R-CC, 12-17	606.55	G	A	1				1					1	1									1				1		7		
21R-CC, 0-7	615.17	G	A					1			1	2	5		1			1			1		15				1		8		
22R-CC, 18-23	625.92	G	A				1	1			2	1	1	1									15				1		1		
23R-CC, 10-15	635.30	G	A	1							1	1	1		1						2		2				2		6		
24R-CC, 11-16	645.02	G	A					1		1	1	1		1				1					6				40		6		
25R-CC, 15-20	654.76	G	A					4			1	1	2	10									1				1		8		
26R-CC, 8-13	664.32	G	A								3	2	2	10			1	1					1				5		1		
27R-CC, 11-16	671.46	G	A							1	1			2				1		1							1		4		
28R-CC, 9-14	681.96	G	A							1	1	1		1						1			3			1	1		1	1	
30R-CC, 17-22	701.41	M	C				1	4		6	2		1	2				10		4	1		8				15		5		
32R-CC, 18-23	722.15	M	C							3				2				4		1	2		9				9		45		2
34R-CC, 21-26	741.48	G	A					1		1		1		1		1		5		1			1			1	10		12		
36R-CC, 19-24	760.56	G	A					2		1	1	1		3		1		1					6				2		7		
38R-CC, 25-30	779.69	G	A							3	1	1	1	3		11		1					1				2		8		

Table T13. Biostratigraphic events, Site 1170. (See table notes. Continued on next page.)

Group	Hole	Bioevent	Age (Ma)	Interval (cm) Top	Interval (cm) Bottom	Mean depth (mbsf)	Error bar (m)
N	1170A	FO *Emiliania huxleyi*	0.26	Top of core	1H-CC	0.82	0.82
R	1170A	LO *Stylatractus universus*	0.45	1H-CC	2H-CC	6.66	10.03
N	1170A	LO *Pseudoemiliania lacunosa*	0.46	1H-CC	2H-CC	6.66	5.02
D	1170A	LO *Actinocyclus ingens*	0.64	2H-CC	3H -CC	16.21	9.08
D	1170A	LO *Fragilariopsis barronii*	1.44	4H-CC	5H -CC	34.24	10.33
N	1170A	LO *Calcidiscus macintyrei*	1.67	4H-CC	5H-CC	34.24	5.17
D	1170A	LO *Proboscia baboi*	1.80	4H-CC	5H-CC	34.24	10.33
P	1170A	FO *Globorotalia truncatulinoides*	1.96	3H-CC	4H-CC	24.91	8.32
R	1170A	LO *Pseudocubus vema*	2.40	5H-CC	6H-CC	44.22	9.63
D	1170A	LO *Thalassiosira complicata*	2.50	7H-CC	8H-CC	63.61	10.72
D	1170A	LO *Thalassiosira inura*	2.50	7H-CC	8H-CC	63.61	10.72
D	1170A	LO *Fragilariopsis weaveri*	2.65	7H-CC	8H-CC	63.61	10.72
C	1170A	LO *Invertocysta tabulata*	2.65	1H-CC	4H-CC	15.36	13.72
P	1170A	FO *Globorotalia inflata*	3.20	7H-CC	8H-CC	63.16	9.25
N	1170A	LO *Reticulofenestra pseudoumbilica*	3.75	6H-CC	7H-CC	53.64	4.61
D	1170A	FO *Thalassiosira complicata*	4.44	11H-CC	12H-CC	101.67	9.57
R	1170A	FO *Pseudocubus vema*	4.50	6H-CC	7H-CC	53.64	9.22
P	1170A	LO *Globorotalia pliozea*	4.60	14H-CC	15H-CC	128.84	10.21
D	1170A	FO *Thalassiosira inura*	4.92	11H-CC	12H-CC	101.67	9.57
R	1170A	LO *Lychnocanoma grande*	5.00	9H-CC	10H-CC	82.67	9.62
N	1170A	LO *Ceratolithus acutus*	5.05	12H-CC	13H-CC	110.85	4.40
P	1170A	FO *Globorotalia puncticulata*	5.30	16H-CC	17H-CC	148.61	9.72
N	1170A	FO *Ceratolithus acutus*	5.37	12H-CC	13H-CC	110.85	4.40
R	1170A	LCO *Stichocorys delmontensis*	6.04	13H-CC	14H-CC	119.49	8.49
R	1170A	LO *Amphymenium challengerae*	6.10	17H-CC	18H-CC	158.64	10.13
D	1170A	LO *Actinocyclus ingens* var. *ovalis*	6.27	16H-CC	17H-CC	148.66	9.82
R	1170A	FO *Amphymenium challengerae*	6.60	18H-CC	19H-CC	165.42	3.43
P	1170A	FO *Globorotalia conomiozea*	6.90	18H-CC	19X-CC	165.42	3.43
P	1170A	LO *Paragloborotalia continuosa*	8.00	18H-CC	19X-CC	165.42	3.43
P	1170A	LO *Paragloborotalia nympha*	10.10	19X-CC	20X-CC	170.84	7.41
D	1170A	LO *Denticulopsis dimorpha*	10.70	22X-CC	23X-CC	196.57	9.04
P	1170A	LO *Paragloborotalia mayeri*	11.40	21X-CC	22X-CC	186.48	11.14
R	1170A	FO *Dictyophimus splendeus*	11.80	19X-CC	20X-CC	170.84	7.41
N	1170A	LO *Cyclicargolithus floridanus*	11.90	27X-CC	28X-CC	245.04	5.66
P	1170A	FO *Paragloborotalia mayeri*	12.10	29X-CC	30X-CC	264.83	10.78
D	1170A	FO *Denticulopsis dimorpha*	12.20	27X-CC	28X-CC	245.04	11.32
R	1170A	LAO *Cyrtocapsella tetrapera*	12.50	27X-CC	28X-CC	245.04	11.32
D	1170A	LO *Actinocyclus ingens* var. *nodus*	12.71	27X-CC	28X-CC	245.04	11.32
D	1170A	FO *Actinocyclus ingens* var. *nodus*	14.38	32X-CC	33X-CC	295.25	8.71
D	1170A	LO *Cavitatus (Synedra) jouseanus*	14.61	32X-CC	33X-CC	295.25	8.71
D	1170A	LO *Denticulopsis maccollumii*	14.70	33X-CC	34X-CC	305.00	10.79
N	1170A	LO *Helicosphaera ampliaperta*	15.60	29X-CC	30X-CC	264.83	5.39
R	1170A	LO *Lychnocanoma nipponica nipponica*	15.70	32X-CC	33X-CC	295.25	8.71
P	1170A	FO *Praeorbulina curva*	16.30	30X-CC	31X-CC	276.12	11.24
R	1170A	LO *Cenosphaera coronata*	16.70	35X-CC	36X-CC	322.98	9.09
N	1170A	FO *Calcidiscus premacintyrei*	17.40	34X-CC	35X-CC	314.41	4.02
P	1170A	FO *Globigerinoides trilobus*	18.80	36X-CC	37X-CC	333.01	11.58
P	1170A	FO *Globoturborotalita connecta*	20.90	37X-CC	38X-CC	342.99	8.38
D	1170A	LO *Azpeitia gombosii*	21.10	41X-CC	42X-CC	381.85	10.64
P	1170A	FO *Globoturborotalita woodi*	22.60	38X-CC	39X-CC	351.86	9.35
P	1170A	FO *Globoquadrina dehiscens*	23.20	41X-CC	42X-CC	381.85	10.64
R	1170A	FO *Cyrtocapsella tetrapera*	23.60	41X-CC	42X-CC	381.85	10.64
N	1170A	LO *Reticulofenestra bisecta*	23.90	41X-CC	42X-CC	381.85	5.32
N	1170A	LO *Chiasmolithus altus*	26.10	43X-CC	44X-CC	401.23	4.60
D	1170A	LO *Coscinodiscus lewisianus* var. *levis*	28.20	42X-CC	43X-CC	391.90	9.46
P	1170A	FO *Chiloguembelina cubensis*	28.50	42X-CC	43X-CC	391.90	9.46
D	1170A	FO *Coscinodiscus lewisianus* var. *levis*	28.50	43X-CC	44X-CC	401.23	9.20
D	1170D	FO *Coscinodiscus lewisianus* var. *levis*	28.50	1R - CC	2R - CC	432.39	5.12
D	1170A	LO *Rocella vigilans* (small)	28.80	43X-CC	44X-CC	401.23	9.20
P	1170A	LO *Subbotina angiporoides*	30.00	44X-CC	45X-CC	407.94	4.22
D	1170A	FO *Rocella vigilans* (small)	30.24	48X-CC	49X-CC	442.76	14.99
D	1170D	FO *Cavitatus* (*Synedra*) *jouseanus*	30.62	4R-1, 120	4R - CC	454.43	0.53
N	1170D	FO *Cyclicargolithus abisectus*	31.20	4R-CC	5R-CC	459.60	4.61
N	1170D	LO *Reticulofenestra reticulata*	35.00	6R-CC	8R-5, 50	479.54	6.82
C	1170D	FCO *Alterbidinium distinctum*	37.00	8R-CC	9R-CC	493.01	9.03
C	1170D	LO *Cerebryocysta bartonensis*	38.60	11R-CC	12R-CC	521.30	2.99
C	1170D	LAO *Enneadocysta partridgei*	39.50	16R-CC	17R-CC	581.44	3.67

Table T13 (continued).

Group	Hole	Bioevent	Age (Ma)	Interval (cm) Top	Interval (cm) Bottom	Mean depth (mbsf)	Error bar (m)
N	1170D	LO *Chiasmolithus solitus*	40.40	12R-CC	13R-CC	529.71	5.12
N	1170D	LAO *Reticulofenestra reticulata*	42.00	12R-CC	13R-CC	529.71	5.12
C	1170D	FAO *Enneadocysta partridgei*	43.00	36R-CC	38R-CC	770.13	9.57
N	1170D	FO *Reticulofenestra umbilica*	43.70	37R-CC	38R-CC	774.21	5.48

Notes: See individual microfossil sections in this chapter for top and bottom samples of event intervals. Mean depth is the midpoint between the top and bottom sample of the event interval. Group: N = nannofossil, R = radiolarian, D = diatom, P = planktonic foraminifer, C = dinocyst. FO = first occurrence, LO = last occurrence. LAO = last abundant occurrence, FAO = first abundant occurrence. This table is also available in **ASCII format.**

Table T14. Magnetostratigraphic results, Site 1170.

Chron	Age (Ma)	Depth (mbsf)
Hole 1170A, 0-100 mbsf:		
Onset C1n	0.78	28.20
Termination C1r1n	0.99	35.00
Onset C1r1n	1.07	39.90
Termination C2n	1.77	60.40
Onset C2n	1.95	68.00
Termination C2An.1n	2.58	83.70
Onset C2An.2n	3.22	96.20
Hole 1170B, 125-140 mbsf:		
Onset C3n.1n	4.29	126.00
Termination C3n.2n	4.48	128.50
Onset C3n.2n	4.62	130.50
Termination C3n.3n	4.8	133.50
Onset C3n.3n	4.89	135.20
Termination C3n.4n	4.98	135.80
Onset C3n.4n	5.23	138.00
Termination C3An.1n	5.89	144.20
Onset C3An.1n	6.14	150.30
Termination C3An.2n	6.27	152.90
Onset C3An.2n	6.57	157.25
Hole 1170A, 264-350 mbsf:		
Termination C5AAn	13	264.00
Onset C5AAn	13.15	268.50
Termination C5ABn	13.31	273.00
Onset C5ABn	13.51	277.00
Termination C5ACn	13.7	278.00
Onset C5ACn	14.05	283.50
Termination C5ADn	14.15	286.00
Onset C5ADn	14.61	292.00
Termination C5Bn.1n	14.8	294.00
Onset C5Bn.1n	14.88	296.00
Termination C5Bn.2n	15.03	297.50
Termination C5Cn.1n	16.01	308.00
Onset C5Cn.1n	16.29	310.50
Termination C5Cn.2n	16.33	311.00
Onset C5Cn.2n	16.49	312.00
Onset C5Dn	17.61	323.00
Onset C5En	18.78	338.00
Termination C6n	19.05	341.00
Hole 1170A, 390-410 mbsf:		
Termination C7n.1n	24.73	393.40
Onset C7n.1n	24.78	394.00
Termination C7n.2n	24.84	395.00
Onset C7n.2n	24.18	399.00
Termination C7An	25.45	402.00
Onset C7An	25.65	403.00
Termination C8n.1n	25.82	404.50

Table T15. Composite depth section for the APC interval, Site 1170.

Hole, core	Depth (mbsf)	Offset (m)	Depth (mcd)
189-1170A-			
1H	0.0	0.06	0.06
2H	1.7	3.06	4.76
3H	11.2	3.24	14.44
4H	20.7	5.35	26.05
5H	30.2	4.12	34.32
6H	39.7	3.54	43.24
7H	49.2	1.72	50.92
8H	58.7	2.96	61.66
9H	68.2	2.96	71.16
10H	77.7	2.96	80.66
11H	87.2	2.96	90.16
12H	96.7	2.96	99.66
13H	106.2	2.96	109.16
14H	115.7	2.96	118.66
15H	125.2	2.96	128.16
16H	134.7	2.96	137.66
17H	144.2	2.96	147.16
18H	153.7	2.96	156.66
189-1170B-			
1H	0.0	0.00	0.00
2H	4.8	0.06	4.86
3H	14.3	0.18	14.48
4H	23.8	0.06	23.86
5H	33.3	0.06	33.36
6H	42.8	0.06	42.86
7H	52.3	0.22	52.52
8H	61.8	0.74	62.54
9H	71.3	0.74	72.04
10H	80.8	0.74	81.54
11H	90.3	0.74	91.04
12H	99.8	0.74	100.54
13H	109.3	0.74	110.04
14H	118.8	0.74	119.54
15H	128.3	0.74	129.04
16H	137.8	0.74	138.54
17H	147.3	0.74	148.04
18H	156.8	0.74	157.54
19H	166.3	0.74	167.04
189-1170C-			
1H	0.0	0.56	0.56
2H	9.1	-0.52	8.58
3H	18.6	-10.96	7.64
4H	28.1	-3.56	24.54
5H	37.6	-4.04	33.56
6H	47.1	-4.10	43.00
7H	56.6	-0.92	55.68
8H	66.1	-4.82	61.28
9H	75.6	-4.82	70.78
10H	85.1	-4.82	80.28
11H	94.6	-4.82	89.78
12H	104.1	-4.82	99.28
13H	113.6	-4.82	108.78
14H	123.1	-4.82	118.28
15H	132.6	-4.82	127.78
16H	142.1	-4.82	137.28
17H	151.6	-4.82	146.78
18H	161.1	-4.82	156.28
19H	170.6	-4.82	165.78

Table T16. Splice tie points, Site 1170.

Hole, core, section, interval (cm)	Depth (mbsf)	Depth (mcd)		Hole, core, section, interval (cm)	Depth (mbsf)	Depth (mcd)
189-				189-		
1170B-1H-1, 132	1.32	1.32	Tie to	1170C-1H-1, 76	0.76	1.32
1170C-1H-5, 62	6.62	7.18	Tie to	1170B-2H-2, 82	7.12	7.18
1170B-2H-5, 146	12.26	12.32	Tie to	1170C-2H-3, 134	12.84	12.32
1170C-2H-6, 90	16.90	16.38	Tie to	1170A-3H-2, 44	13.14	16.38
1170A-3H-7, 70	20.62	23.86	Append to	1170B-4H-1, 0	23.80	23.86
1170B-4H-7, 66	33.46	33.52	Tie to	1170A-4H-6, 72	28.17	33.52
1170A-4H-6, 132	28.77	34.12	Tie to	1170B-5H-1, 76	34.06	34.12
1170B-5H-7, 52	42.52	42.58	Append to	1170A-6H-1, 0	39.70	43.24
1170A-6H-7, 20	48.63	52.17	Tie to	1170A-7H-1, 124.5	50.45	52.17
1170A-7H-6, 116	57.86	59.58	Tie to	1170B-7H-5, 106	59.36	59.58
1170B-7H-7, 54	61.84	62.06	Tie to	1170A-8H-1, 40	59.10	62.06
1170A-8H-CC, 14	68.05	71.01				

Table T17. Values for inorganic carbon, calcium carbonate, total carbon, total organic carbon, total nitrogen, total sulfur, and hydrogen in sediments, Hole 1170A. (See table notes. Continued on next three pages.)

Hole, core, section	Depth (mbsf)	IC (wt%)	$CaCO_3$ (wt%)	TC (wt%)	TOC (wt%)	N (wt%)	S (wt%)	H (mg H/g)
189-1170A-								
1H-1	0.71	10.42	86.85	11.30	0.86	0.00	0.00	0.17
2H-1	2.42	10.14	84.49	NA	NA	NA	NA	NA
2H-3	5.42	10.36	86.30	10.90	0.53	0.00	0.02	0.10
2H-5	8.43	10.65	88.72	NA	NA	NA	NA	NA
3H-1	11.92	11.18	93.12	NA	NA	NA	NA	NA
3H-3	14.92	10.30	85.80	10.60	0.34	0.00	0.03	0.16
3H-5	17.64	10.90	90.86	NA	NA	NA	NA	NA
4H-1	21.42	9.35	77.94	NA	NA	NA	NA	NA
4H-2	22.43	10.96	91.37	NA	NA	NA	NA	NA
4H-3	23.75	9.24	76.96	9.69	0.45	0.02	0.05	0.19
4H-4	25.21	8.71	72.61	NA	NA	NA	NA	NA
4H-5	26.67	9.19	76.57	NA	NA	NA	NA	NA
5H-1	30.91	10.01	83.45	NA	NA	NA	NA	NA
5H-3	33.92	9.44	78.68	9.69	0.24	0.00	0.00	0.20
5H-5	36.92	8.76	73.03	NA	NA	NA	NA	NA
6H-1	40.42	9.68	80.70	NA	NA	NA	NA	NA
6H-3	43.42	9.62	80.18	9.86	0.24	0.00	0.01	0.21
6H-5	46.42	10.01	83.39	NA	NA	NA	NA	NA
7H-1	49.92	9.51	79.24	NA	NA	NA	NA	NA
7H-3	52.92	9.87	82.24	10.20	0.28	0.00	0.01	0.16
7H-5	55.92	9.47	78.92	NA	NA	NA	NA	NA
8H-1	59.42	8.37	69.75	NA	NA	NA	NA	NA
8H-3	62.42	10.31	85.93	10.50	0.20	0.00	0.00	0.12
8H-5	65.32	10.37	86.43	NA	NA	NA	NA	NA
9H-1	68.92	10.42	86.80	NA	NA	NA	NA	NA
9H-3	71.92	9.02	75.14	10.20	1.15	0.00	0.00	0.18
9H-5	74.92	8.32	69.35	NA	NA	NA	NA	NA
10H-1	78.42	10.24	85.37	NA	NA	NA	NA	NA
10H-3	81.42	6.80	56.70	7.33	0.52	0.02	0.00	0.45
10H-5	84.42	9.72	80.97	NA	NA	NA	NA	NA
11H-3	90.92	9.76	81.37	9.91	0.14	0.02	0.00	0.22
11H-5	93.92	11.08	92.30	NA	NA	NA	NA	NA
12H-5	103.42	10.83	90.25	10.90	0.09	0.00	0.00	0.11
13H-3	109.93	11.36	94.65	11.60	0.20	0.01	0.00	0.06
13H-5	112.92	11.11	92.59	NA	NA	NA	NA	NA
14H-1	116.53	11.14	92.83	NA	NA	NA	NA	NA
14H-3	119.42	11.30	94.19	11.50	0.17	0.00	0.01	0.00
14H-5	122.52	10.87	90.61	NA	NA	NA	NA	NA
15H-1	125.92	11.31	94.24	NA	NA	NA	NA	NA
15H-3	128.94	11.04	92.02	11.30	0.26	0.00	0.00	0.08
15H-5	131.94	11.01	91.78	NA	NA	NA	NA	NA
16H-1	135.84	11.47	95.62	NA	NA	NA	NA	NA
16H-3	138.48	11.22	93.48	11.30	0.06	0.00	0.00	0.06
16H-5	141.42	11.23	93.61	NA	NA	NA	NA	NA
17H-1	144.92	11.42	95.19	NA	NA	NA	NA	NA
17H-4	149.23	11.14	92.81	11.20	0.05	0.00	0.00	0.05
17H-6	152.23	11.06	92.19	NA	NA	NA	NA	NA
18H-1	154.42	11.23	93.60	NA	NA	NA	NA	NA
18H-3	157.42	11.06	92.16	11.30	0.21	0.00	0.00	0.08
18H-6	161.89	11.11	92.56	NA	NA	NA	NA	NA
19X-1	163.92	11.27	93.91	NA	NA	NA	NA	NA
19X-3	166.92	10.82	90.19	10.90	0.05	0.00	0.00	0.10
20X-1	167.42	10.95	91.28	NA	NA	NA	NA	NA
20X-3	170.42	11.28	93.95	11.50	0.23	0.00	0.00	0.08
20X-5	173.42	11.29	94.06	NA	NA	NA	NA	NA
21X-1	177.02	11.04	92.04	NA	NA	NA	NA	NA
21X-3	180.02	10.90	90.81	11.00	0.13	0.00	0.00	0.11
22X-1	186.62	11.43	95.27	NA	NA	NA	NA	NA
22X-3	189.62	11.48	95.69	11.70	0.26	0.01	0.00	0.06
23X-1	196.22	11.30	94.14	NA	NA	NA	NA	NA
23X-3	199.22	11.50	95.80	11.70	0.18	0.00	0.01	0.05
24X-1	205.82	11.49	95.76	NA	NA	NA	NA	NA
24X-3	208.80	11.57	96.39	11.70	0.14	0.00	0.00	0.05
25X-1	215.42	11.33	94.45	NA	NA	NA	NA	NA

Table T17 (continued).

Hole, core, section	Depth (mbsf)	IC (wt%)	$CaCO_3$ (wt%)	TC (wt%)	TOC (wt%)	N (wt%)	S (wt%)	H (mg H/g)
25X-3	218.42	11.56	96.29	11.60	0.02	0.00	0.00	0.06
26X-1	225.02	11.21	93.43	11.80	0.57	0.00	0.00	0.03
27X-1	234.62	11.32	94.34	NA	NA	NA	NA	NA
27X-3	237.62	11.56	96.36	11.80	0.18	0.00	0.00	0.03
28X-1	244.22	11.19	93.29	NA	NA	NA	NA	NA
28X-3	247.22	11.32	94.30	11.60	0.32	0.01	0.06	0.04
28X-5	250.22	11.20	93.31	NA	NA	NA	NA	NA
29X-1	253.82	11.35	94.59	NA	NA	NA	NA	NA
29X-3	256.82	11.13	92.72	11.60	0.47	0.00	0.00	0.06
30X-1	263.42	11.45	95.41	NA	NA	NA	NA	NA
30X-3	266.42	11.43	95.28	11.70	0.31	0.00	0.00	0.04
30X-5	269.42	11.48	95.68	NA	NA	NA	NA	NA
31X-1	273.02	11.43	95.25	NA	NA	NA	NA	NA
31X-3	276.02	11.52	95.96	11.60	0.05	0.00	0.00	0.07
31X-5	279.02	11.38	94.83	NA	NA	NA	NA	NA
32X-1	282.62	11.40	95.03	NA	NA	NA	NA	NA
32X-3	285.62	11.29	94.08	11.80	0.49	0.01	0.00	0.04
32X-5	288.62	11.41	95.10	NA	NA	NA	NA	NA
33X-1	292.22	11.03	91.88	NA	NA	NA	NA	NA
33X-3	295.22	11.12	92.64	11.50	0.34	0.00	0.00	0.04
33X-5	298.22	11.21	93.44	NA	NA	NA	NA	NA
34X-1	301.52	10.94	91.14	NA	NA	NA	NA	NA
34X-3	304.52	11.07	92.22	11.50	0.38	0.01	0.00	0.10
34X-5	307.52	11.19	93.21	NA	NA	NA	NA	NA
35X-1	310.82	10.91	90.89	NA	NA	NA	NA	NA
35X-3	313.82	11.10	92.51	11.40	0.29	0.01	0.00	0.08
35X-5	316.82	11.17	93.10	NA	NA	NA	NA	NA
36X-1	320.42	11.12	92.66	NA	NA	NA	NA	NA
36X-3	323.42	11.01	91.73	11.01	0.00	0.02	0.00	0.11
36X-5	326.42	11.33	94.37	NA	NA	NA	NA	NA
37X-1	330.02	10.97	91.42	NA	NA	NA	NA	NA
37X-3	333.02	11.21	93.43	11.06	0.00	0.02	0.00	0.09
37X-5	336.02	10.99	91.60	NA	NA	NA	NA	NA
38X-1	339.69	11.41	95.10	NA	NA	NA	NA	NA
38X-3	342.50	11.24	93.65	11.08	0.00	0.01	0.00	0.09
38X-3	342.62	11.37	94.77	NA	NA	NA	NA	NA
39X-1	349.07	11.09	92.44	NA	NA	NA	NA	NA
39X-3	352.32	11.36	94.63	11.29	0.00	0.01	0.00	0.07
39X-5	355.18	11.28	94.01	NA	NA	NA	NA	NA
40X-1	358.87	11.16	93.00	NA	NA	NA	NA	NA
40X-3	361.92	11.07	92.28	11.07	0.00	0.02	0.02	0.11
40X-5	364.92	11.14	92.84	NA	NA	NA	NA	NA
41X-1	368.52	11.41	95.08	NA	NA	NA	NA	NA
41X-3	371.52	11.13	92.78	10.96	0.00	0.01	0.00	0.09
41X-5	374.50	10.39	86.58	NA	NA	NA	NA	NA
42X-1	378.12	10.15	84.55	NA	NA	NA	NA	NA
42X-3	381.12	10.42	86.83	10.30	0.00	0.02	0.00	0.16
42X-5	384.12	9.32	77.64	NA	NA	NA	NA	NA
43X-1	387.68	10.23	85.23	NA	NA	NA	NA	NA
43X-3	390.70	10.37	86.40	10.26	0.00	0.02	0.00	0.17
43X-5	393.70	9.92	82.69	NA	NA	NA	NA	NA
44X-1	397.32	10.05	83.73	NA	NA	NA	NA	NA
44X-3	400.32	9.66	80.47	9.60	0.00	0.02	0.00	0.23
44X-5	403.32	9.70	80.82	NA	NA	NA	NA	NA
45X-1	406.92	10.71	89.22	10.68	0.00	0.01	0.00	0.12
46X-1	416.52	11.10	92.51	NA	NA	NA	NA	NA
46X-3	419.52	11.11	92.59	10.44	0.00	0.02	0.00	0.14
47X-3	429.24	10.82	90.17	10.46	0.00	0.02	0.00	0.13
49X-1	445.32	9.23	76.91	NA	NA	NA	NA	NA
49X-3	448.67	9.61	80.10	9.51	0.00	0.01	0.00	0.19
50X-1	454.92	10.06	83.81	9.87	0.00	0.02	0.00	0.18
189-1170D-								
1R-1	425.36	9.90	82.50	9.93	0.02	0.00	0.00	0.20
2R-1	434.22	10.74	89.50	NA	NA	NA	NA	NA
2R-3	437.04	10.53	87.70	10.62	0.09	0.00	0.00	0.14
3R-1	443.82	9.80	81.70	9.90	0.09	0.00	0.00	0.20
4R-1	453.42	9.47	78.90	9.73	0.25	0.00	0.01	0.19
5R-1	463.02	10.97	91.40	11.54	0.57	0.00	0.00	0.06
6R-CC	472.54	0.05	0.43	0.26	0.21	0.04	0.00	0.65

Table T17 (continued).

Hole, core, section	Depth (mbsf)	IC (wt%)	$CaCO_3$ (wt%)	TC (wt%)	TOC (wt%)	N (wt%)	S (wt%)	H (mg H/g)
7R-1	477.33	0.63	5.32	1.00	0.36	0.04	0.25	0.79
8R-1	482.22	0.04	0.33	NA	NA	NA	NA	NA
8R-3	485.22	0.02	0.24	0.85	0.82	0.01	0.44	1.00
8R-5	488.22	0.20	1.67	NA	NA	NA	NA	NA
9R-1	491.82	0.34	2.86	NA	NA	NA	NA	NA
9R-3	494.82	0.40	3.37	0.80	0.40	0.01	0.53	0.87
10R-2	502.77	0.47	3.93	NA	NA	NA	NA	NA
10R-4	505.92	0.28	2.35	0.91	0.63	0.06	1.50	0.92
11R-1	511.02	0.24	2.01	NA	NA	NA	NA	NA
11R-3	514.01	0.41	3.47	0.83	0.41	0.06	0.33	0.84
11R-5	517.02	1.14	9.52	NA	NA	NA	NA	NA
12R-1	520.52	1.32	11.10	NA	NA	NA	NA	NA
12R-3	523.52	0.81	6.77	1.46	0.65	0.05	0.79	0.71
13R-1	530.09	0.31	2.65	NA	NA	NA	NA	NA
13R-3	533.08	0.06	0.54	0.57	0.50	0.06	0.51	0.83
14R-1	539.82	0.14	1.23	NA	NA	NA	NA	NA
14R-3	542.82	0.09	0.76	0.74	0.65	0.08	2.58	0.77
14R-5	545.82	0.40	3.37	NA	NA	NA	NA	NA
15R-1	549.42	0.38	3.16	NA	NA	NA	NA	NA
15R-3	552.42	0.43	3.63	1.02	0.58	0.02	2.25	0.67
15R-5	555.42	0.27	2.27	NA	NA	NA	NA	NA
16R-1	559.02	0.29	2.43	NA	NA	NA	NA	NA
16R-3	562.51	0.11	0.95	0.68	0.57	0.06	2.88	0.69
17R-1	568.55	0.30	2.50	NA	NA	NA	NA	NA
17R-3	571.62	0.39	3.29	0.78	0.38	0.05	2.39	0.68
17R-5	574.62	0.26	2.22	NA	NA	NA	NA	NA
18R-1	578.22	0.24	2.02	NA	NA	NA	NA	NA
18R-3	581.22	0.21	1.82	0.86	0.64	0.06	2.61	0.66
18R-5	584.18	0.07	0.61	NA	NA	NA	NA	NA
19R-1	587.48	10.76	89.70	NA	NA	NA	NA	NA
19R-3	589.74	0.18	1.51	0.85	0.67	0.07	1.53	0.77
19R-5	592.74	0.15	1.25	NA	NA	NA	NA	NA
20R-1	597.58	0.16	1.33	NA	NA	NA	NA	NA
20R-3	600.43	0.01	0.09	1.19	1.18	0.08	1.18	0.55
20R-5	603.39	0.03	0.27	NA	NA	NA	NA	NA
21R-1	607.02	0.08	0.70	NA	NA	NA	NA	NA
21R-3	610.02	0.06	0.52	1.06	1.00	0.08	1.67	0.72
21R-5	613.02	0.04	0.35	NA	NA	NA	NA	NA
22R-3	618.47	0.03	0.30	1.93	1.89	0.12	1.64	0.76
22R-5	621.47	0.01	0.14	NA	NA	NA	NA	NA
23R-1	626.27	0.03	0.29	NA	NA	NA	NA	NA
23R-3	629.36	0.03	0.28	1.21	1.18	0.08	1.75	0.70
23R-5	632.34	0.03	0.32	NA	NA	NA	NA	NA
24R-1	636.07	0.02	0.17	NA	NA	NA	NA	NA
24R-3	639.08	0.06	0.53	1.06	1.00	0.07	1.53	0.67
24R-5	641.96	0.05	0.41	NA	NA	NA	NA	NA
25R-1	645.62	0.03	0.31	NA	NA	NA	NA	NA
25R-3	648.62	0.51	4.25	2.14	1.63	0.07	1.36	0.72
25R-5	651.62	0.02	0.17	NA	NA	NA	NA	NA
26R-1	655.32	0.26	2.18	NA	NA	NA	NA	NA
26R-3	658.32	0.03	0.32	1.44	1.40	0.12	1.12	0.69
26R-5	661.32	0.03	0.25	NA	NA	NA	NA	NA
27R-1	664.92	0.19	1.62	NA	NA	NA	NA	NA
27R-3	667.92	0.47	3.93	1.57	1.10	0.08	1.12	0.63
27R-5	670.92	0.34	2.86	NA	NA	NA	NA	NA
28R-1	674.52	0.31	2.62	NA	NA	NA	NA	NA
28R-3	677.34	0.22	1.85	1.49	1.27	0.11	1.45	0.68
28R-5	679.86	0.20	1.71	NA	NA	NA	NA	NA
29R-1	684.22	0.72	6.02	NA	NA	NA	NA	NA
29R-3	687.08	0.33	2.82	1.82	1.48	0.09	1.70	0.75
29R-5	690.02	0.10	0.85	NA	NA	NA	NA	NA
30R-1	693.92	0.15	1.26	NA	NA	NA	NA	NA
30R-3	696.77	0.05	0.47	2.61	2.56	0.14	1.80	0.85
30R-5	699.77	0.14	1.17	NA	NA	NA	NA	NA
31R-1	703.52	0.04	0.40	NA	NA	NA	NA	NA
31R-3	706.52	0.07	0.65	1.90	1.83	0.12	2.00	0.85
31R-5	709.52	0.21	1.82	NA	NA	NA	NA	NA
32R-1	713.12	0.09	0.79	NA	NA	NA	NA	NA
32R-3	716.12	0.10	0.86	1.47	1.36	0.11	1.77	0.79

Table T17 (continued).

Hole, core, section	Depth (mbsf)	IC (wt%)	$CaCO_3$ (wt%)	TC (wt%)	TOC (wt%)	N (wt%)	S (wt%)	H (mg H/g)
32R-5	719.12	0.09	0.76	NA	NA	NA	NA	NA
33R-1	722.72	0.07	0.60	NA	NA	NA	NA	NA
33R-3	725.72	0.11	0.95	2.96	2.85	0.17	2.52	0.92
33R-5	728.72	0.13	1.13	NA	NA	NA	NA	NA
34R-1	732.32	0.11	0.98	NA	NA	NA	NA	NA
34R-3	735.32	0.98	8.19	2.16	1.18	0.07	1.74	0.70
34R-5	738.32	0.53	4.48	NA	NA	NA	NA	NA
35R-1	741.92	0.07	0.58	NA	NA	NA	NA	NA
35R-3	744.92	0.10	0.87	1.32	1.21	0.11	1.62	0.72
35R-5	747.92	0.45	3.78	NA	NA	NA	NA	NA
36R-1	751.52	1.15	9.65	NA	NA	NA	NA	NA
36R-3	754.52	0.06	0.52	1.57	1.50	0.11	1.53	0.77
36R-5	757.52	0.15	1.30	NA	NA	NA	NA	NA
37R-1	761.22	0.10	0.89	NA	NA	NA	NA	NA
37R-3	764.22	0.25	2.10	NA	NA	NA	NA	NA
37R-5	767.22	0.14	1.23	NA	NA	NA	NA	NA
38R-1	770.82	0.34	2.85	NA	NA	NA	NA	NA
38R-3	773.80	0.28	2.33	NA	NA	NA	NA	NA
38R-5	776.80	1.17	9.76	NA	NA	NA	NA	NA

Notes: IC = inorganic carbon, $CaCO_3$ = calcium carbonate, TC = total carbon, TOC = total organic carbon, N = total nitrogen, S = total sulfur, H = hydrogen. NA = not analyzed.

Table T18. Results of Rock-Eval analyses on sediments, Hole 1170A. (See table notes. Continued on next page.)

Hole, core, section	Depth (mbsf)	T_{max} (°C)	S_1	S_2	S_3	TOC (%)	HI	OI
189-1170A-								
1H-1	1.41	456	0.05	0.04	1.24	0.01	400	12,400
2H-4	6.20	344	0.09	0.16	1.31	0.04	400	3,262
3H-4	15.70	339	0.08	0.08	1.14	0.02	400	5,700
4H-4	24.49	378	0.07	0.11	1.33	0.02	550	6,650
5H-4	34.70	375	0.08	0.12	1.19	0.05	213	2,483
6H-4	44.20	408	0.06	0.24	1.19	0.03	800	3,966
7H-4	53.70	300	0.05	0.04	1.02	1.06	4	164
8H-4	63.20	357	0.13	0.21	1.22	0.05	420	2,440
9H-4	72.70		0.08	0.16	0.92	0.03	533	3,066
10H-4	82.20	300	0.20	0.11	0.91	0.03	366	3,033
11H-4	91.70	320	0.15	0.06	1.17	0.04	123	3,137
12H-4	101.20	323	0.12	0.12	0.96	0.03	400	3,200
13H-4	110.70		0.09	0.05	0.77	0.02	250	3,850
14H-4	120.20	300	0.09	0.01	0.82	0.01	100	8,250
15H-4	129.72	343	0.17	0.04	0.84	0.06	66	1,400
16H-4	139.20		0.02	0.00	0.92	0.02	0	4,600
17H-6	151.51		0.00	0.00	0.85	0.02	0	4,250
18H-4	158.20		0.42	0.00	0.83	0.05	0	1,660
19X-2	164.70		0.31	0.00	0.83	0.03	0	2,766
20X-4	171.20	300	0.12	0.01	0.75	0.05	6	3,850
21X-2	177.80		0.10	0.00	0.75	0.02	0	5,700
22X-4	190.40		0.19	0.00	0.82	0.02	0	4,100
23X-3	198.50	393	0.20	0.04	0.70	0.03	133	2,333
24X-3	208.10	375	0.06	0.04	0.66	0.02	175	3,300
25X-3	217.70	424	0.20	0.10	0.75	0.03	333	2,500
26X-2	225.80	465	0.29	0.10	0.70	0.04	250	1,750
27X-3	236.90	482	0.13	0.13	0.75	0.04	325	1,875
28X-4	248.00	450	0.13	0.11	0.73	0.03	366	2,433
29X-4	257.60	418	0.14	0.03	0.71	0.02	150	3,550
30X-4	267.20	432	0.08	0.03	0.69	0.02	150	3,450
31X-4	276.80	402	0.11	0.01	0.75	0.01	100	7,500
32X-4	286.40	347	0.02	0.02	0.30	0.00		
33X-4	296.00		0.08	0.00	0.76	0.01	0	1,700
34X-4	305.30	370	0.06	0.02	0.75	0.01	150	3,450
35X-4	314.60		0.03	0.00	0.32	0.00		
36X-4	324.20	395	0.08	0.02	0.70	0.01	200	7,000
37X-4	333.80	355	0.12	0.02	0.62	0.01	200	6,200
38X-4	343.40	435	0.04	0.08	0.60	0.02	700	3,400
39X-4	353.10	403	0.00	0.01	0.29	0.00		
40X-4	362.70	347	0.01	0.01	0.49	0.01	100	4,300
41X-4	372.30		0.03	0.00	0.56	0.01	0	5,500
42X-4	381.90	407	0.02	0.03	0.63	0.01	300	6,300
43X-4	391.50	344	0.04	0.06	0.95	0.02	275	4,725
44X-4	401.10	462	0.04	0.06	0.84	0.02	300	4,200
45X-3	409.20	402	0.01	0.02	0.75	0.01	200	7,500
46X-4	420.30		0.03	0.00	0.71	0.01	0	7,100
47X-3	428.40	340	0.01	0.02	0.79	0.00		
48X-CC	435.00	453	0.08	0.12	0.77	0.02	600	5,350
49X-3	447.60		0.00	0.00	0.78	0.01	0	7,800
50X-2	455.70		0.01	0.00	0.79	0.01	0	7,900
189-1170D-								
1R-2	426.50	422	0.01	0.04	0.85	0.01	400	8500
2R-2	435.00	422	0.00	0.04	0.81	0.01	400	8100
3R-2	444.30	467	0.01	0.11	0.81	0.02	550	4050
4R-2	454.20	385	0.00	0.01	0.72	0.01	100	7200
5R-2	463.50		0.00	0.00	0.90	0.06	0	1500
6CC	472.61	462	0.00	0.79	0.60	0.24	329	250
7R-2	478.10		0.04	1.07	1.22	0.41	260	297
8R-4	486.00		0.07	1.35	0.67	0.34	397	197
9R-4	495.60		0.05	0.59	1.08	0.28	210	385
10R-2	502.20	424	0.01	0.26	0.90	0.42	61	214
11R-3	513.30	417	0.05	0.31	1.18	0.36	86	327
12R-2	521.30	423	0.02	0.24	1.32	0.36	66	366
13R-3	532.40	590	0.04	0.90	0.98	0.46	195	213
14R-4	543.60	425	0.07	1.10	0.75	0.41	268	182
15R-4	553.20	425	0.07	1.08	0.92	0.41	263	224

Table T18 (continued).

Hole, core, section	Depth (mbsf)	T_{max} (°C)	S_1	S_2	S_3	TOC (%)	HI	OI
16R-2	559.79		0.08	1.21	0.56	0.32	378	175
17R-4	572.40	422	0.10	0.96	0.96	0.32	300	300
18R-4	582.00	425	0.09	1.53	1.08	0.49	312	220
19R-5	592.02	426	0.11	1.01	1.24	0.55	183	225
20R-4	601.23	430	0.09	1.93	0.73	0.99	194	73
21R-4	610.81	540	0.08	2.10	0.79	0.99	212	79
22R-4	619.35	413	0.17	3.11	0.55	1.24	250	44
23R-4	630.20	424	0.05	1.36	0.49	0.64	212	76
24R-4	639.80	428	0.08	1.48	0.57	0.50	296	114
25R-4	649.40	431	0.10	2.23	0.47	0.79	282	59
26R-4	659.10	550	0.12	1.47	0.59	0.64	229	92
27R-4	668.70	433	0.04	1.37	0.72	0.68	201	105
28R-4	677.79	429	0.07	1.20	0.85	0.70	171	121
29R-4	687.86	433	0.05	1.81	1.09	1.05	172	103
30R-4	697.55	430	0.06	3.40	0.89	1.83	185	48
31R-4	707.30	431	0.08	4.08	1.03	2.13	191	48
32R-4	716.90	431	0.02	1.36	0.73	0.74	183	98
33R-4	726.50	434	0.04	1.55	1.46	1.21	128	120
34R-4	736.10	432	0.05	2.47	1.06	1.15	214	92
35R-4	745.70	434	0.05	3.67	0.80	2.06	178	38
36R-4	755.30	434	0.05	0.98	0.71	0.77	127	92
37R-4	765.00	435	0.04	0.90	0.63	0.61	147	103
38R-4	774.58	435	0.05	0.68	0.60	0.39	174	153

Notes: T_{max} = temperature (°C) of maximum hydrocarbon generation from kerogen. S_1 = volatile hydrocarbons; S_2 = kerogen-derived hydrocarbons; S_3 = organic CO_2 from kerogen. TOC = total organic carbon obtained by Rock-Eval pyrolysis analysis. HI = hydrogen index, OI = oxygen index. Blanks = no data.

Table T19. Headspace gas composition, Site 1170. (See table notes. Continued on next page.)

Hole, core, section	Depth (mbsf)	C_1/C_2 (ppmv)	C_1 (ppmv)	C_2 (ppmv)	C_3 (ppmv)	*n*-C_4 (ppmv)	*i*-C_4 (ppmv)	*n*-C_5 (ppmv)	*i*-C_5 (ppmv)	*n*-C_6 (ppmv)	*i*-C_6 (ppmv)
189-1170A-											
1H-1	1.41	3									
2H-4	6.20	3									
3H-4	15.70	4									
4H-4	24.49	7									
5H-4	34.70	10									
6H-4	44.20	5									
7H-4	53.70	12									
8H-4	63.20	11									
9H-4	72.70	11									
10H-4	82.20	10									
11H-4	91.70	15									
12H-4	101.20	11									
13H-4	110.70	17									
14H-4	120.20	14									
15H-4	129.72	13									
16H-4	139.20	14									
17H-6	151.51	14									
18H-4	158.20	11									
19X-2	164.70	10									
20X-4	171.20	12									
21X-2	177.80	9									
22X-4	190.40	13									
23X-3	198.50	15									
24X-3	208.10	17									
25X-3	217.70	12									
26X-2	225.80	14									
27X-3	236.90	14									
28X-4	248.00	25									
29X-4	257.60	12									
30X-4	267.20	9									
31X-4	276.80	10									
32X-4	286.40	11									
33X-4	296.00	11									
34X-4	305.30	5									
35X-4	314.60	4									
36X-4	324.20	6									
37X-4	333.80	4									
38X-4	343.40	3									
39X-4	353.10	6									
40X-4	362.70	4									
41X-4	372.30	4									
42X-4	381.90	7									
43X-4	391.50	13									
44X-4	401.10	40									
45X-3	409.20	56									
46X-4	420.30	110									
47X-3	428.40	78									
48X-CC	435.00	141									
49X-3	447.60	199									
50X-2	455.70	236									
189-1170D-											
1R-2	426.50		100	0	0						
2R-2	435.00		104	0	0						
3R-2	444.30		64	0	0						
4R-2	454.20		18	0	0						
5R-2	463.50		162	0	0						
7R-2	478.10		1,027	0	0						
8R-4	486.00	10,949	15,329	1	0						
9R-4	495.60	11,556	15,023	1	0						
10R-2	502.20	8,796	6,157	1	0						
11R-3	513.30	6,121	20,198	3	0						
12R-2	521.30	3,508	15,434	4	0						
13R-3	532.40	1,470	13,369	9	0						
14R-4	543.60	577	32,213	56	10						
15R-4	553.20	480	863	2	0						
16R-2	559.79	417	792	2	0						

Table T19 (continued).

Hole, core, section	Depth (mbsf)	C_1/C_2 (ppmv)	C_1 (ppmv)	C_2 (ppmv)	C_3 (ppmv)	*n*-C_4 (ppmv)	*i*-C_4 (ppmv)	*n*-C_5 (ppmv)	*i*-C_5 (ppmv)	*n*-C_6 (ppmv)	*i*-C_6 (ppmv)
17R-4	572.40	335	536	2	0						
18R-4	582.00	281	1,545	6	0						
19R-5	592.02	269	835	3	0						
20R-4	601.23	198	1,327	7	0						
24R-4	639.80	160	5,636	35	9						
24R-4	639.80	230	1,652	7	0	0	0	0	0	0	0
25R-4	649.30	123	11,433	93	27						
26R-4	659.10	143	2,155	15	6						
27R-4	668.70	110	41,109	375	168						
27R-4	668.70	103	34,148	333	198	43	73	20	79	0	0
28R-4	677.79	109	45,959	423	184						
28R-4	677.79	103	41,473	403	228	54	93	27	101	0	3
29R-4	687.86	108	36,052	335	122						
29R-4	687.86	103	30,181	293	162	28	45	15	39	4	4
30R-4	697.55	94	66,449	704	245						
30R-4	697.55	100	56,395	563	289	41	77	7	49	0	0
31R-4	707.30	57	21,843	385	229						
31R-4	707.30	62	24,866	401	363	95	128	42	123	0	5
32R-4	716.90	77	20,509	266	192	33	57	8	45	0	0
32R-4	716.90	76	26,260	345	174						
33R-4	726.50	46	27,464	602	426						
33R-4	726.50	51	18,196	357	377	91	125	33	112	0	2
34R-4	736.10	57	21,044	371	328	66	102	21	85	0	0
34R-4	736.10	51	32,839	648	388						
35R-4	745.70	76	70,303	925	527	68	111	11	64	0	0
36R-4	755.30	80	34,585	431	167						
36R-4	755.30	80	20,719	260	135	9	21	0	9	0	0
37R-4	765.00	75	39,082	520	208						
38R-4	774.58	89	46,402	525	194						

Notes: C_1 = methane, C_2 = ethane, C_3 = propane, C_4 = butane, C_5 = pentane, C_6 = hexane, *i* = iso, *n* = nona. ppmv = parts per million by volume. Blanks = no data.

Table T20. Interstitial water data, Site 1170.

Core, section, interval (cm)	Depth (mbsf)	pH	Alkalinity (mM)	Salinity	Cl^- (mM)	SO_4^{2-} (mM)	Na^+ (mM)	Mg^{2+} (mM)	Ca^{2+} (mM)	K^+ (mM)	$H_4SiO_4^0$ (µM)	NH_4^+ (µM)	Sr^{2+} (µM)	Li^+ (µM)
189-1170A-														
2H-3, 145-150	6.15	7.54	4.26	35.5	554	26.7	473	51.1	10.4	10.9	561	109	131	21
3H-3, 145-150	15.65	7.49	4.61	35.0	557	26.0	474	52.2	10.6	10.7	635	115	166	18
4H-4, 141-146	25.90	7.54	5.39	35.0	561	26.1	473	49.8	10.3	11.3	747	202	239	15
5H-3, 145-150	34.65	7.47	5.22	35.0	562	25.1	474	51.5	10.5	11.1	751	233	269	12
6H-3, 145-150	44.15	7.38	5.26	35.0	562	24.7	475	50.5	10.4	11.4	795	317	316	10
7H-3, 145-150	53.65	7.38	5.36	35.0	561	24.3	476	49.8	10.4	11.2	795	298	351	9
8H-3, 145-150	63.15	7.35	5.26	35.0	560	25.0	476	50.9	10.5	11.2	846	313	387	8
9H-3, 145-150	72.65	7.42	5.59	35.0	560	23.4	468	50.2	10.6	10.7	844	318	409	6
10H-3, 140-150	82.10	7.34	5.47	35.0	557	23.4	476	50.0	11.0	10.5	861	365	459	5
11H-3, 140-150	91.60	7.37	5.40	35.0	559	23.7	478	48.3	11.2	10.7	875	328	476	5
14H-3, 140-150	120.10	7.42	5.63	35.0	557	22.2	481	48.1	11.7	10.5	743	371	621	4
17X-5, 140-150	151.41	7.44	5.49	35.0	557	21.4	470	46.4	12.8	10.3	838	400	726	4
20X-3, 140-150	171.10	7.46	5.34	35.0	558	21.5	474	46.1	12.8	10.0	863	403	787	5
23X-2, 140-150	198.40	7.42	5.62	34.5	559	21.4	476	44.7	13.5	10.0	820	450	857	5
27X-2, 140-150	236.80	7.36	5.46	34.5	558	21.0	469	44.2	14.0	9.4	938	499	912	9
30X-3, 140-150	267.10	7.33	5.44	35.0	561	20.5	473	43.5	13.8	9.4	960	518	902	14
33X-3, 140-150	295.90	7.38	4.97	35.0	559	20.7	478	42.5	14.0	9.3	1146	581	918	20
36X-3, 140-150	324.10	7.22	5.40	34.5	561	19.6	473	41.3	15.0	9.0	1146	648	969	26
39X-3, 140-150	353.00	7.37	5.71	34.0	558	18.0	475	38.6	15.5	8.6	1235	733	943	36
42X-3, 140-150	381.80	7.34	5.06	34.0	556	17.5	473	37.8	15.3	8.3	1197	770	NM	NM
45X-2, 140-150	409.10	7.45	4.96	34.0	557	18.1	480	38.4	15.2	8.7	1128	745	NM	57
49X-2, 140-150	447.50	7.57	3.92	34.0	557	17.4	476	36.5	13.8	8.8	1134	826	NM	63
189-1170D-														
7R-1, 140-150	478.00	7.83	4.83	35.0	542	0.0	447	22.35	14.6	5.0	216	1391	398	390
10R-1, 140-150	502.10	7.93	2.21	28.0	503	0.0	415	20.17	13.2	4.4	85	1062	NM	379
13R-2, 140-150	532.30	7.84	4.23	28.0	497	0.0	413	19.48	13.8	3.8	113	1109	358	404
16R-1, 140-150	559.69	7.47	5.66	30.0	535	0.0	450	20.16	14.4	4.5	157	1042	NM	417
19R-4, 135-150	591.87	7.60	4.04	30.0	523	0.0	437	18.39	14.5	4.0	118	1385	341	449
22R-5, 135-150	622.10	7.78	5.66	29.0	501	0.0	421	17.02	14.2	3.4	105	1216	NM	433
25R-3, 140-150	649.30	NM	NM	29.0	519	0.0	441	16.04	14.3	3.5	116	1327	324	427
28R-3, 105-117	677.67	7.58	4.82	30.0	517	0.0	442	15.62	14.4	3.2	128	1409	NM	406
31R-3, 135-150	707.15	8.04	3.84	26.0	461	0.0	392	14.80	13.0	2.8	40	1211	284	379
34R-3, 135-150	735.95	NM	NM	NM	467	0.0	390	14.66	13.3	2.4	25	1379	295	390
37R-3, 135-150	764.85	NM	NM	NM	502	0.0	425	13.90	14.4	2.8	23	1599	NM	411

Note: NM = not measured.

Table T21. *P*-wave velocities measured at discrete intervals, Hole 1170A. (See table notes. Continued on next page.)

Core, section, interval (cm)	Depth (mbsf)	PWS1 (km/s)	PWS2 (km/s)	PWS3 (km/s)
189-1170A-				
1H-1, 49.90	0.50			1.644
2H-1, 50.00	2.20			1.617
2H-2, 84.30	4.04			1.631
2H-3, 50.00	5.20			1.589
2H-4, 50.00	6.70			1.563
2H-5, 86.80	8.57			1.574
2H-6, 50.00	9.70			1.578
3H-1, 50.00	11.70			1.623
3H-2, 80.10	13.50			1.547
3H-3, 50.00	14.70			1.621
3H-4, 55.80	16.26			1.640
4H-2, 55.20	22.15			1.610
4H-4, 63.40	25.12			1.558
4H-5, 83.10	26.78			1.628
4H-6, 50.00	27.95			1.528
5H-3, 54.90	33.75			1.604
5H-4, 114.80	35.85			1.580
5H-5, 119.90	37.40			1.601
6H-1, 50.10	40.20			1.649
6H-2, 53.40	41.73			1.643
6H-3, 50.10	43.20			1.552
6H-4, 50.00	44.70			1.699
6H-5, 50.00	46.20			1.657
6H-6, 50.30	47.70			1.584
7H-2, 50.00	51.20			1.581
7H-3, 50.10	52.70			1.640
7H-4, 80.40	54.50			1.577
7H-5, 50.00	55.70			1.583
7H-6, 50.10	57.20			1.590
8H-2, 50.00	6.70			1.601
8H-3, 50.00	62.20			1.583
8H-4, 50.40	63.70			1.597
8H-5, 50.10	65.10			1.635
8H-6, 50.00	66.60			1.592
9H-2, 54.60	70.25			1.618
9H-3, 50.10	71.70			1.626
9H-4, 25.20	72.95			1.702
9H-5, 48.40	74.68			1.596
9H-6, 49.90	76.20			1.611
10H-1, 48.90	78.19	1.562	1.550	1.646
10H-3, 49.20	81.19	1.522	1.541	1.571
10H-4, 48.40	82.68	1.540		1.609
10H-5, 48.70	84.19	1.568	1.559	1.647
10H-6, 63.70	85.84	1.562	1.573	1.646
11H-2, 35.90	89.06			1.657
11H-2, 48.40	89.18	1.570		
11H-3, 48.80	90.69	1.545		1.567
11H-4, 48.90	92.10	1.533		1.541
11H-5, 47.70	93.68	1.581		1.590
11H-6, 48.60	95.19	1.551		1.561
12H-1, 94.30	97.64	1.566		1.562
12H-2, 52.60	98.73			1.573
12H-3, 31.50	100.01	1.561		1.574
12H-4, 48.10	101.68	1.560		1.572
12H-5, 41.70	103.12	1.573		1.569
12H-6, 49.20	104.69	1.565		1.567
13H-1, 56.40	106.76	1.585	1.605	1.593
13H-2, 48.60	108.19	1.604		1.623
13H-3, 49.30	109.69	1.672		1.683
13H-4, 56.40	111.26			1.689
13H-5, 52.70	112.73	1.644		1.638
13H-6, 49.20	114.19			1.668
14H-1, 91.80	116.62			1.680
14H-2, 37.30	117.57	1.618		1.639
14H-2, 47.30	117.67	1.631		1.641
14H-4, 79.90	121.00	1.642		1.666
14H-5, 48.60	122.19	1.621		1.626
15H-1, 34.60	125.55	1.588		1.584
15H-2, 51.90	127.24	1.593		1.584
15H-3, 48.80	128.71	1.571		1.578
15H-4, 48.20	130.20	1.553		1.543
15H-5, 39.10	131.61	1.546		1.540
15H-6, 48.20	133.20	1.591		1.585
16H-2, 49.30	136.69	1.561		1.567
16H-3, 49.80	138.20	1.554		1.560
16H-4, 30.30	139.50	1.549		1.551
16H-5, 50.10	141.20	1.546		1.529
16H-6, 52.00	142.72	1.614		1.605
17H-4, 50.00	149.01	1.550		1.530
17H-5, 50.00	150.51	1.547		1.526
17H-6, 49.50	152.01	1.523		1.552
18H-5, 50.00	160.20	1.549		1.522
18H-6, 50.10	161.70	1.547		1.544
19X-1, 50.40	163.70	1.535		1.563
19X-2, 70.10	165.40	1.545		1.535
19X-3, 15.20	166.35	1.578		1.603
20X-1, 50.20	167.20	1.605		1.611
20X-2, 50.40	168.70			1.627
20X-3, 49.30	170.19			1.558
20X-3, 49.70	170.20	1.551		
20X-4, 49.90	171.70	1.567		1.564
20X-5, 49.10	173.19			1.571
20X-5, 49.80	173.20	1.569		
21X-1, 50.50	176.80	1.564		1.555
21X-2, 50.00	178.30	1.555		1.546
21X-3, 50.20	179.80	1.565		1.554
22X-1, 50.40	186.40	1.552		
22X-1, 51.10	186.41			1.570
22X-2, 50.90	187.91	1.582		1.579
22X-3, 50.10	189.40	1.570		
22X-3, 51.10	189.41			1.559
23X-1, 50.60	196.01	1.571		1.594
23X-3, 50.00	199.00	1.546		1.554
24X-1, 49.70	205.60	1.543		1.560
24X-2, 49.50	207.10	1.562		1.568
24X-3, 49.80	208.60	1.567		1.576
25X-1, 50.40	215.20	1.531		1.589
25X-3, 39.80	218.10			1.550
25X-3, 48.20	218.18	1.528		
26X-1, 50.30	224.80	1.548		1.573
27X-1, 50.10	234.40	1.542		1.561
27X-2, 50.00	235.90	1.534		
27X-2, 50.70	235.91			1.523
27X-3, 50.10	237.40	1.520		1.522
28X-2, 48.90	245.49	1.541		1.567
28X-3, 48.60	246.99	1.558		1.570
28X-4, 50.50	248.51	1.557		1.573
28X-5, 40.00	249.90	1.571		1.594
29X-1, 46.60	253.57	1.545		1.566
29X-2, 49.50	255.10	1.528		1.547
29X-3, 49.50	256.60	1.551		1.566
29X-4, 48.20	258.08	1.567		1.587
30X-1, 48.30	263.18	1.549		1.581
30X-2, 48.10	264.68	1.546		1.559
30X-3, 48.20	266.18	1.540		1.543
30X-4, 46.20	267.66	1.551		1.582
30X-5, 47.30	269.17	1.562		1.588
31X-1, 52.40	272.82	1.564		1.579
31X-2, 49.00	274.29	1.586		1.614
31X-3, 60.30	275.90			1.607
31X-4, 48.00	277.28	1.604		1.611
31X-5, 31.60	278.62	1.552		1.586
31X-6, 58.10	280.38			1.633
32X-1, 49.40	282.39			1.638
32X-3, 44.80	285.35			1.581

Table T21 (continued).

Core, section, interval (cm)	Depth (mbsf)	PWS1 (km/s)	PWS2 (km/s)	PWS3 (km/s)
32X-4, 73.70	287.14			1.616
32X-5, 51.80	288.42			1.560
32X-6, 72.60	289.97			1.582
33X-1, 58.00	292.08			1.598
33X-2, 63.60	293.64			1.598
33X-3, 83.40	295.33			1.586
33X-4, 79.70	296.80			1.573
33X-5, 88.20	298.38			1.588
34X-1, 88.30	301.68			1.632
34X-2, 57.80	302.88			1.826
34X-3, 63.30	304.43			1.710
34X-3, 88.00	304.68			1.646
34X-5, 119.5	307.99			1.789
34X-6, 94.10	309.24			1.666
35X-1, 48.40	310.58			1.694
35X-2, 62.20	312.22			1.641
35X-5, 106.00	317.16			1.609
36X-1, 63.20	320.33			1.623
36X-2, 70.60	321.91			1.615
36X-3, 95.10	323.65			1.657
36X-4, 90.4	325.10			1.657
36X-5, 60.80	326.31			1.614
36X-6, 45.60	327.16			1.569
37X-1, 49.90	329.80			1.571
37X-2, 50.60	331.31			1.588
37X-3, 50.10	332.80			1.606
37X-4, 56.50	334.36			1.582
37X-5, 89.30	336.19			1.639
37X-6, 28.00	337.08			1.632
38X-1, 65.10	339.55			1.710
38X-2, 98.60	341.39			1.603
38X-3, 101.80	342.92			1.597
38X-4, 13.50	343.54			1.600
38X-5, 43.20	345.33			1.587
39X-1, 70.50	349.30			1.585
39X-2 126.10	351.36			1.650
39X-3, 28.50	351.89			1.583
39X-4, 69.50	353.80			1.571
39X-5, 32.90	354.93			1.612
40X-1, 81.90	359.02			1.587
40X-2, 96.20	360.66			1.562
40X-3, 36.10	361.56			1.618
40X-4, 52.20	363.22			1.633
40X-5, 100.80	365.21			1.684
40X-6, 76.60	366.47			1.667
41X-1, 64.80	368.45			1.686
41X-2, 94.60	370.25			1.709
41X-3, 100.80	371.81			1.669
41X-4, 115.20	373.45			1.604
41X-5, 91.40	374.71			1.636
41X-6, 55.60	375.86			1.646
42X-1, 80.60	378.21			1.757
42X-2, 78.00	379.68			1.712
42X-3, 57.20	380.97			1.711
42X-4, 20.90	382.11			1.693
42X-5, 53.60	383.94			1.748
42X-6, 24.20	385.14			1.660
43X-1, 75.30	387.75			1.602
43X-2, 84.70	389.35			1.723
43X-3, 102.90	391.03			1.678
43X-4, 52.00	392.02			1.675
43X-5, 62.20	393.62			1.695
43X-6, 75.50	395.26			1.665
44X-1, 86.30	397.46			1.746
44X-2, 61.70	398.72			1.791
44X-3, 51.70	400.12			1.663
44X-4, 67.40	401.77			1.672
44X-5, 33.50	402.93			1.679
44X-6, 43.80	404.54			1.648
45X-1, 116.60	407.37			1.575
45X-2, 40.30	408.10			1.637
46X-1, 82.40	416.62			1.686
46X-2, 65.30	417.95			1.563
46X-3, 116.50	419.96			1.687
46X-4, 67.40	420.97			1.605
47X-1, 90.70	426.31			1.694
47X-2, 95.60	427.86			1.687
47X-3, 97.80	429.38			1.722
47X-4, 40.60	430.31			1.667
49X-1, 102.40	445.62			1.682
49X-2, 69.60	446.80			1.637
49X-3, 129.80	448.90			1.703
49X-4, 83.50	449.93			1.711
50X-2, 56.10	456.26			1.660
50X-1, 103.00	455.23			1.738

Notes: All *P*-wave velocities measured at discrete intervals. PSW1 = measured along the core, PSW2 = measured perpendicular to the core, PSW3 = measured across the core (Hamilton frame).

Table T22. *P*-wave velocities measured at discrete intervals across the core (modified Hamilton frame, PWS3), Hole 1170D.

Core, section, interval (cm)	Depth (mbsf)	PWS3 velocity (km/s)		
		X-direction	Y-direction	Z-direction
189-1170D-				
1R-1, 54.00	425.54	1.774		
1R-2, 9.10	426.59	1.771		
2R-1, 78.00	434.28	1.821		
2R-2, 62.00	435.62	1.799		
2R-3, 48.00	436.98	1.792		
3R-1, 43.00	443.53	1.719		
4R-1, 101.20	453.71	1.812		
4R-2, 27.10	454.47	1.781		
5R-1, 40.00	462.70	2.140		
5R-1, 79.00	463.09	2.162		
5R-2, 28.00	463.78	2.056		
6R-1, 42.00	472.32	3.792		
7R-1, 73.00	477.33	2.663	2.706	2.707
8R-1, 70.00	482.20	1.719	1.743	1.676
8R-2, 70.00	483.70	1.677	1.695	1.611
8R-3, 68.00	485.18	1.674	1.719	1.657
8R-4, 67.00	486.67		1.809	1.709
8R-4, 68.00	486.68	1.769		
9R-1, 71.00	491.81	1.622	1.647	1.592
9R-2, 71.00	493.31	1.660	1.653	1.582
9R-3, 71.00	494.81	1.634	1.626	1.600
9R-4, 71.00	496.31	1.606	1.625	1.598
10R-2, 51.00	502.71	1.728		
10R-3, 116.00	504.86	1.631		
11R-1, 99.00	511.29	1.753		
11R-2, 57.00	512.37	2.355		
11R-3, 145.00	514.75	1.739		
11R-4, 69.00	515.49	1.905		
11R-5, 114.00	517.44	2.305		
12R-1, 20.00	520.00	2.589	2.741	2.617
12R-1, 77.00	520.57	1.853		
12R-1, 81.00	520.61	2.407	2.508	2.376
13R-1, 51.00	529.91	1.830		
14R-3, 47.40	542.57	1.922		
14R-3, 97.00	543.07	1.936		
14R-6, 33.30	546.93	1.879		
15R-1, 30.50	549.01	1.917		
15R-2, 60.40	550.80	1.893		
15R-3, 31.00	552.01	1.986		
15R-4, 47.00	553.67	1.865		
15R-6, 123.00	557.43	1.906		
16R-6, 101.00	566.82	1.965		
17R-1, 92.20	568.82	1.761		
17R-2, 36.00	569.76	1.737		
17R-5, 28.00	574.18	1.830		
17R-7, 40.40	577.30	1.667		
18R-1, 56.00	578.06	1.825		
18R-2, 34.80	579.35	1.785		
18R-3, 37.60	580.88	1.818		
18R-4, 58.30	582.58	1.767		
18R-4, 59.10	582.59	1.775		
19R-1, 39.00	587.49	4.815		
19R-3, 94.00	589.96	1.833		
19R-4, 59.00	591.11	1.846		
19R-5, 24.00	592.26	1.908		
19R-7, 89.00	595.91	1.905		
20R-1, 109.00	597.79	1.852		
20R-1, 148.00	598.18	2.184		
20R-2, 109.00	599.32	1.883		
20R-3, 82.00	600.55	1.827		
20R-4, 19.00	601.42	1.890		
20R-5, 110.00	603.83	1.868		
20R-6, 135.00	605.58	1.847		
21R-1, 120.00	607.50	1.837		
21R-2, 40.00	608.20	1.873		
21R-3, 50.00	609.80	1.878		
21R-5, 95.00	613.25	1.877		
22R-2, 95.00	617.20	1.826		
22R-3, 110.00	618.85	1.870		
22R-4, 57.00	619.82	1.868		
22R-5, 93.00	621.68	1.871		
22R-6, 84.00	623.09	1.869		
22R-7, 81.00	624.56	1.865		
23R-2, 15.00	627.25	1.875		
23R-3, 115.00	629.75	1.913		
23R-4, 120.00	631.30	1.892		
23R-5, 56.00	632.16	1.918		
24R-1, 44.00	635.74	1.879		
24R-2, 17.00	636.97	1.901		
24R-3, 48.50	638.78	1.896		
24R-4, 94.00	640.74	1.891		
24R-5, 105.00	642.35	1.909		
25R-1, 135.00	646.25	1.932		
25R-3, 115.00	649.05	1.922		
25R-4, 117.00	650.57	1.906		
25R-5, 81.00	651.71	2.260		
25R-6, 91.00	653.31	1.868		
26R-1, 61.00	655.21	1.870		
26R-2, 61.00	656.71	1.899		
26R-4, 35.00	659.45	1.906		
26R-5, 24.00	660.84	1.884		
27R-2, 26.00	665.96	1.908		
27R-3, 31.00	667.51	1.907		
27R-4, 84.00	669.54	1.968		
27R-5, 83.00	671.03	1.900		
28R-1, 19.00	673.99	1.881		
28R-2, 79.00	676.01	1.893		
28R-3, 52.00	677.14	1.888		
28R-4, 84.00	678.63	1.893		
28R-5, 38.00	679.52	1.917		
29R-1, 72.00	684.22	1.909		
29R-3, 53.00	686.89	1.980		
29R-4, 72.00	688.58	1.965		
29R-5, 44.00	689.74	1.938		
29R-5, 44.00	689.74	1.961		
30R-1, 71.00	693.91	1.919		
30R-2, 96.00	695.51	1.943		
30R-3, 98.00	697.03	1.953		
30R-4, 21.00	697.76	1.974		
30R-5, 55.00	699.60	1.924		
31R-1, 87.00	703.67	1.945		
31R-2, 106.00	705.36	2.041		
31R-3, 51.00	706.31	1.990		
31R-4, 60.00	707.90	2.015		
31R-5, 50.00	709.30	2.066		
31R-6, 58.00	710.88	2.003		
32R-1, 86.00	713.26	2.029		
32R-2, 69.00	714.59	2.044		
32R-3, 65.00	716.05	1.983		
32R-4, 65.00	717.55	1.860		
32R-5, 123.00	719.63	2.012		
32R-6, 47.00	720.37	1.965		
33R-3, 47.00	725.47	1.863		
33R-4, 84.00	727.34	1.985		
33R-5, 84.00	728.84	1.996		
33R-6, 84.00	730.34	3.896		
34R-6, 103.00	740.13	2.000		
35R-5, 103.00	748.23	2.102		
36R-2, 129.00	753.59	3.299		

Note: All *P*-wave velocities measured at discrete intervals.

Table T23. Thermal conductivity measured on whole core sections, Hole 1170A.

Core, section, interval (cm)	Depth (mbsf)	Average thermal conductivity (W/[m·K])
189-1170A-		
2H-3, 75	5.45	0.989
3H-3, 75	14.95	1.077
5H-3, 75	33.95	1.092
6H-3, 75	43.45	1.079
7H-3, 75	52.95	1.040
8H-3, 75	62.45	1.025
9H-3, 75	71.95	1.048
10H-3, 75	81.45	0.863
11H-3, 75	90.95	1.041
12H-3, 75	100.45	1.098
13H-3, 75	109.95	1.129
14H-3, 75	119.45	1.244
15H-3, 75	128.97	0.988
16H-3, 75	138.45	0.917
17H-3, 75	147.95	1.322
18H-3, 75	157.45	1.188
19X-2, 75	165.45	1.174
20X-3, 75	170.45	1.174

Table T24. Undrained shear strength from miniature vane-shear measurements, Hole 1170A.

Core, section, Interval (cm)	Depth (mbsf)	Undrained shear strength (kPa)
189-1170A-		
2H-1, 99.1	2.69	23.840
2H-2, 133.4	4.53	21.290
2H-3, 99.1	5.69	5.101
2H-5, 135.9	9.06	22.732
2H-6, 59.7	9.80	42.026
3H-2, 83.0	13.53	21.955
3H-3, 99.1	15.19	7.540
3H-4, 61.4	16.31	30.272
4H-2, 104.3	22.64	28.941
4H-4, 112.5	25.61	37.590
4H-5, 132.2	27.27	44.576
4H-6, 99.1	28.44	34.596
5H-3, 104.0	34.24	21.401
5H-4, 114.3	35.84	31.935
5H-5, 118.9	37.39	30.937
6H-1, 99.2	40.69	21.290
6H-2, 102.5	42.22	27.500
6H-3, 99.2	43.69	28.498
6H-4, 99.1	45.19	14.193
6H-5, 99.1	46.69	44.687
6H-6, 99.4	48.19	22.066
7H-2, 99.1	51.69	25.171
7H-3, 99.2	53.19	25.725
7H-4, 129.5	54.99	15.746
7H-5, 99.1	56.19	27.500
7H-6, 99.2	57.69	24.617
8H-2, 99.1	61.19	15.635
8H-3, 99.0	62.69	27.943
8H-4, 99.5	64.19	53.558
8H-5, 99.2	65.59	21.733
8H-6, 99.1	67.09	28.276
9H-2, 95.9	70.66	34.707
9H-3, 90.9	72.11	19.738
9H-4, 95.6	73.66	19.738
9H-5, 99.3	75.19	17.963
9H-6, 105.8	76.76	19.848
10H-1, 94.9	78.65	12.197
10H-3, 90.6	81.61	25.836
10H-4, 85.8	83.06	9.093
10H-5, 90.6	84.61	17.409
10H-6, 95.7	86.16	25.836
11H-2, 111.4	89.81	7.762
11H-4, 95.0	92.65	27.167
11H-5, 96.8	94.17	18.740
11H-6, 96.2	95.66	15.746
12H-1, 112.3	97.82	12.087
12H-3, 117.8	100.88	5.212
12H-4, 95.0	102.15	20.625
12H-5, 92.7	103.63	9.314
12H-6, 95.6	105.16	10.534
13H-1, 80.7	107.01	26.058
13H-2, 95.8	108.66	11.754
13H-3, 91.0	110.11	16.855
13H-4, 80.2	111.50	20.181
13H-5, 89.6	113.10	30.493
13H-6, 101.1	114.71	28.054
14H-1, 110.6	116.81	24.617
14H-2, 89.3	118.09	24.949
14H-4, 109.7	121.30	19.072
14H-5, 104.3	122.74	19.627
15H-1, 110.1	126.30	24.062
15H-2, 102.5	127.75	19.848
15H-3, 89.6	129.12	21.623
15H-4, 103.3	130.75	16.078
15H-5, 95.1	132.17	23.619
15H-6, 56.7	133.29	20.957
16H-2, 106.1	137.26	19.072
16H-3, 104.8	138.75	36.038
16H-4, 88.9	140.09	16.633
16H-5, 99.1	141.69	24.284
16H-6, 101.5	143.21	21.068
17H-4, 99.4	149.50	26.391
17H-5, 99.0	151.00	25.171
17H-6, 98.7	152.50	21.068
18H-5, 98.7	160.69	25.171
18H-6, 81.1	162.01	25.171
19X-1, 99.7	164.20	44.909
19X-2, 119.4	165.89	13.085
19X-3, 64.7	166.85	23.064
20X-1, 99.5	167.70	22.177
20X-3, 98.4	170.68	12.087
20X-4, 99.0	172.19	9.536
20X-5, 98.2	173.68	11.865
21X-1, 99.6	177.30	11.532
21X-3, 99.3	180.29	11.865
22X-1, 100.2	186.90	12.419
22X-2, 100.0	188.40	10.091
22X-3, 100.2	189.90	14.748
23X-1, 99.8	196.50	5.323
23X-3, 99.3	199.49	14.083
24X-1, 99.0	206.09	12.641
24X-2, 99.0	207.59	14.415
24X-3, 99.0	209.09	22.953
25X-1, 99.3	215.69	9.758
25X-3, 88.9	218.59	10.978
26X-1, 99.4	225.29	23.397
27X-1, 99.7	234.90	4.990
27X-2, 99.8	236.40	22.953
27X-3, 99.3	237.89	6.542
28X-2, 94.9	245.95	25.836
28X-3, 95.1	247.45	11.532
28X-4, 95.2	248.95	13.417
28X-5, 89.2	250.39	21.512
29X-1, 102.3	254.12	4.657
29X-2, 94.8	255.55	23.175
29X-3, 94.3	257.04	7.984
29X-4, 94.9	258.55	11.865
30X-1, 94.8	263.65	21.955
30X-2, 97.4	265.17	8.427
30X-3, 92.0	266.62	10.978
30X-4, 105.8	268.26	26.612
30X-5, 96.4	269.66	12.641
31X-1, 103.5	273.33	19.959
31X-2, 99.6	274.80	27.278
31X-3, 96.8	276.27	12.974
31X-4, 106.3	277.86	10.756
31X-6, 94.1	280.74	27.721
32X-1, 94.7	282.85	27.278
32X-2, 94.9	284.35	23.729
32X-3, 113.6	286.04	14.083
32X-4, 122.8	287.63	21.623
32X-5, 100.9	288.91	24.728
32X-6, 97.2	290.21	26.280
33X-1, 107.6	292.58	22.510
33X-2, 99.1	293.99	25.282
33X-3, 87.4	295.37	16.078
33X-4, 79.6	296.80	10.091
33X-5, 118.4	298.68	31.270
34X-1, 116.2	301.96	39.586
34X-2, 96.3	303.26	28.498

Table T25. Index properties measured at discrete intervals, Site 1170. (Continued on next three pages.)

Core, section, interval (cm)	Depth (mbsf)	Water content (wt%)		Density (g/cm^3)			Porosity (%)	Void ratio
		Bulk	Dry	Wet bulk	Dry bulk	Grain		
189-1170A-								
1H-1, 70.0-72.0	0.70	41.4	70.5	1.610	0.944	2.698	65.0	1.858
2H-1, 70.0-72.0	2.40	42.9	75.1	1.586	0.906	2.698	66.4	1.979
2H-2, 70.0-72.0	3.90	42.0	72.3	1.606	0.932	2.729	65.8	1.927
2H-3, 70.0-72.0	5.40	39.7	65.9	1.633	0.984	2.686	63.4	1.729
2H-4, 70.0-72.0	6.90	41.0	69.4	1.628	0.961	2.757	65.1	1.867
2H-5, 70.0-72.0	8.40	39.7	65.8	1.639	0.988	2.709	63.5	1.741
3H-1, 70.0-72.0	11.90	36.8	58.3	1.693	1.069	2.735	60.9	1.558
3H-2, 70.0-72.0	13.40	36.7	57.9	1.681	1.064	2.674	60.2	1.513
3H-3, 70.0-72.0	14.90	45.1	82.2	1.571	0.862	2.800	69.2	2.248
3H-4, 70.0-72.0	16.40	42.5	74.0	1.602	0.921	2.752	66.5	1.988
4H-2, 80.0-82.0	22.40	35.5	54.9	1.709	1.103	2.704	59.2	1.451
4H-3, 80.0-82.0	23.83	38.6	62.9	1.624	0.997	2.572	61.3	1.581
4H-4, 70.0-72.0	25.19	39.1	64.2	1.634	0.995	2.644	62.4	1.658
4H-5, 70.0-72.0	26.65	39.6	65.7	1.632	0.985	2.677	63.2	1.717
5H-4, 90.0-92.0	35.60	34.6	52.8	1.724	1.128	2.699	58.2	1.393
5H-5, 130.0-132.0	37.50	37.3	59.4	1.677	1.052	2.699	61.0	1.565
5H-6, 70.0-72.0	38.40	36.2	56.8	1.684	1.074	2.658	59.6	1.475
6H-2, 70.0-72.0	41.90	35.8	55.7	1.704	1.095	2.706	59.5	1.472
6H-3, 70.0-72.0	43.40	39.7	65.7	1.627	0.982	2.652	63.0	1.702
6H-4, 70.0-72.0	44.90	40.3	67.5	1.619	0.966	2.663	63.7	1.756
6H-5, 70.0-72.0	46.40	39.1	64.2	1.641	0.999	2.673	62.6	1.675
6H-6, 70.0-72.0	47.90	43.6	77.2	1.563	0.882	2.635	66.5	1.988
7H-1, 100.0-102.0	50.20	48.9	95.8	1.478	0.755	2.571	70.6	2.406
7H-2, 70.0-72.0	51.40	39.3	64.6	1.633	0.992	2.654	62.6	1.675
7H-3, 70.0-72.0	52.90	38.4	62.2	1.648	1.016	2.655	61.7	1.613
7H-4, 70.0-72.0	54.40	39.1	64.2	1.642	0.999	2.680	62.7	1.681
7H-5, 70.0-72.0	55.90	41.6	71.2	1.605	0.938	2.691	65.2	1.870
7H-6, 70.0-72.0	57.40	44.9	81.3	1.542	0.850	2.621	67.6	2.082
8H-1, 120.0-122.0	59.90	41.1	69.8	1.601	0.943	2.641	64.3	1.801
8H-2, 70.0-72.0	60.90	40.3	67.6	1.616	0.964	2.651	63.6	1.751
8H-3, 70.0-72.0	62.40	37.3	59.4	1.670	1.047	2.670	60.8	1.550
8H-4, 70.0-72.0	63.90	39.3	64.9	1.625	0.985	2.623	62.4	1.662
8H-5, 70.0-72.0	65.30	35.3	54.6	1.708	1.105	2.688	58.9	1.433
8H-6, 70.0-72.0	66.80	35.9	56.0	1.699	1.089	2.695	59.6	1.474
9H-1, 70.0-72.0	68.90	34.7	53.1	1.720	1.123	2.689	58.2	1.394
9H-2, 70.0-72.0	70.40	43.3	76.5	1.560	0.884	2.602	66.0	1.943
9H-3, 70.0-72.0	71.90	42.3	73.4	1.585	0.914	2.652	65.5	1.900
9H-4, 70.0-72.0	73.40	37.9	61.0	1.809	1.124	3.402	67.0	2.028
9H-5, 95.0-97.0	75.15	37.2	59.1	1.647	1.035	2.573	59.8	1.485
9H-6, 70.0-72.0	76.40	37.2	59.4	1.670	1.048	2.668	60.7	1.546
10H-1, 70.0-72.0	78.40	39.0	63.9	1.632	0.995	2.629	62.1	1.641
10H-2, 91.0-93.0	80.11	42.9	75.2	1.578	0.900	2.659	66.1	1.953
10H-3, 63.0-65.0	81.33	50.3	101.0	1.457	0.725	2.546	71.5	2.511
10H-4, 70.0-72.0	82.90	39.3	64.7	1.634	0.992	2.660	62.7	1.681
10H-5, 70.0-72.0	84.40	39.5	65.2	1.628	0.986	2.646	62.7	1.683
10H-6, 77.0-79.0	85.97	40.2	67.1	1.626	0.973	2.686	63.8	1.761
11H-1, 129.0-131.0	88.49	36.2	56.8	1.688	1.076	2.674	59.7	1.484
11H-2, 69.0-71.0	89.39	35.8	55.8	1.700	1.091	2.691	59.4	1.465
11H-3, 70.0-72.0	90.90	42.3	73.3	1.593	0.919	2.689	65.8	1.925
11H-4, 71.0-73.0	92.41	42.2	72.9	1.585	0.917	2.640	65.3	1.879
11H-5, 70.0-72.0	93.90	33.9	51.2	1.742	1.152	2.721	57.7	1.362
11H-6, 70.0-72.0	95.40	37.6	60.3	1.667	1.040	2.683	61.3	1.581
12H-1, 84.0-86.0	97.54	34.0	51.4	1.723	1.138	2.656	57.2	1.334
12H-2, 70.0-72.0	98.90	35.9	55.9	1.693	1.086	2.665	59.3	1.455
12H-3, 106.0-108.0	100.76	34.8	53.3	1.719	1.121	2.695	58.4	1.404
12H-4, 70.0-72.0	101.90	34.2	52.1	1.731	1.138	2.701	57.9	1.373
12H-5, 70.0-72.0	103.40	34.8	53.4	1.730	1.128	2.737	58.8	1.427
12H-6, 75.0-77.0	104.95	34.0	51.4	1.726	1.140	2.667	57.2	1.339
13H-1, 70.0-72.0	106.90	32.9	49.0	1.762	1.183	2.725	56.6	1.303
13H-2, 70.0-72.0	108.40	32.8	48.9	1.752	1.177	2.685	56.2	1.281
13H-3, 70.0-72.0	109.90	30.4	43.8	1.800	1.252	2.694	53.5	1.152
13H-4, 71.0-73.0	111.41	29.2	41.2	1.829	1.295	2.705	52.1	1.089
13H-5, 70.0-72.0	112.90	29.2	41.2	1.822	1.291	2.685	51.9	1.080
13H-6, 70.0-72.0	114.40	33.1	49.4	1.763	1.180	2.740	56.9	1.322
14H-1, 80.0-82.0	116.50	31.4	45.7	1.782	1.224	2.693	54.6	1.201
14H-2, 78.0-80.0	117.98	33.6	50.6	1.740	1.155	2.692	57.1	1.330

Table T25 (continued).

Core, section, interval (cm)	Depth (mbsf)	Water content (wt%)		Density (g/cm^3)			Porosity (%)	Void ratio
		Bulk	Dry	Wet bulk	Dry bulk	Grain		
14H-3, 70.0-72.0	119.40	32.1	47.3	1.767	1.200	2.689	55.4	1.241
14H-4, 70.0-72.0	120.90	31.6	46.3	1.780	1.217	2.705	55.0	1.222
14H-5, 79.0-81.0	122.49	35.3	54.6	1.715	1.109	2.717	59.2	1.449
15H-1, 70.0-72.0	125.90	31.7	46.5	1.782	1.216	2.717	55.2	1.234
15H-2, 70.0-72.0	127.42	33.1	49.6	1.750	1.170	2.700	56.7	1.307
15H-3, 70.0-72.0	128.92	33.9	51.2	1.746	1.155	2.732	57.7	1.366
15H-4, 76.0-78.0	130.48	33.1	49.6	1.746	1.167	2.683	56.5	1.299
15H-5, 70.0-72.0	131.92	32.1	47.3	1.767	1.200	2.689	55.4	1.241
15H-6, 65.0-67.0	133.37	29.6	42.1	1.821	1.281	2.706	52.7	1.112
16H-1, 113.0-114.0	135.83	32.4	48.0	1.758	1.188	2.679	55.7	1.256
16H-3, 77.0-79.0	138.47	34.0	51.5	1.736	1.146	2.704	57.6	1.359
16H-5, 70.0-72.0	141.40	34.4	52.4	1.729	1.135	2.703	58.0	1.382
17H-1, 70.0-72.0	144.90	32.3	47.7	1.767	1.196	2.701	55.7	1.258
17H-4, 70.0-72.0	149.21	31.4	45.9	1.779	1.220	2.689	54.6	1.204
17H-6, 70.0-72.0	152.21	31.7	46.5	1.778	1.214	2.702	55.1	1.226
18H-1, 70.0-72.0	154.40	32.0	47.0	1.767	1.202	2.681	55.2	1.231
18H-6, 70.0-72.0	161.90	32.9	48.9	1.763	1.184	2.726	56.6	1.303
19X- 1, 70.0-72.0	163.90	34.1	51.7	1.742	1.148	2.732	58.0	1.379
19X- 3, 70.0-72.0	166.90	35.3	54.6	1.705	1.103	2.677	58.8	1.426
20X- 1, 70.0-72.0	167.40	34.9	53.6	1.713	1.115	2.680	58.4	1.403
20X- 3, 70.0-72.0	170.40	35.5	55.1	1.764	1.138	2.933	61.2	1.578
20X- 5, 70.0-72.0	173.40	38.3	62.0	1.670	1.031	2.742	62.4	1.660
21X- 1, 70.0-72.0	177.00	34.8	53.5	1.725	1.124	2.721	58.7	1.421
21X- 3, 70.0-72.0	180.00	38.7	63.1	1.675	1.027	2.797	63.3	1.725
22X- 1, 70.0-72.0	186.60	35.9	56.0	1.703	1.092	2.709	59.7	1.481
22X- 3, 70.0-72.0	189.60	34.4	52.4	1.650	1.082	2.426	55.4	1.242
23X- 1, 70.0-72.0	196.20	33.3	50.0	1.759	1.173	2.744	57.3	1.340
23X- 3, 70.0-72.0	199.20	35.6	55.3	1.717	1.106	2.743	59.7	1.480
24X- 1, 70.0-72.0	205.80	36.0	56.3	1.706	1.092	2.731	60.0	1.502
24X- 3, 70.0-72.0	208.80	34.2	51.9	1.740	1.146	2.732	58.1	1.385
25X- 1, 70.0-72.0	215.40	34.7	53.2	1.726	1.126	2.716	58.5	1.412
25X- 3, 70.0-72.0	218.40	35.4	54.7	1.711	1.106	2.705	59.1	1.446
26X- 1, 70.0-72.0	225.00	34.7	53.1	1.723	1.125	2.703	58.4	1.403
27X- 1, 70.0-72.0	234.60	35.0	53.8	1.754	1.141	2.844	59.9	1.493
27X- 3, 70.0-72.0	237.60	34.1	51.7	1.734	1.143	2.702	57.7	1.364
28X- 2, 70.0-72.0	245.70	37.0	58.8	1.692	1.065	2.744	61.2	1.576
28X- 3, 70.0-72.0	247.20	36.3	57.1	1.707	1.087	2.756	60.6	1.536
28X- 5, 74.0-76.0	250.24	31.2	45.3	1.787	1.230	2.698	54.4	1.194
29X- 1, 70.0-72.0	253.80	36.6	57.7	1.691	1.072	2.711	60.4	1.528
29X- 3, 70.0-72.0	256.80	37.5	60.0	1.679	1.050	2.726	61.5	1.597
30X- 1, 70.0-72.0	263.40	35.7	55.5	1.712	1.101	2.729	59.6	1.478
30X- 3, 70.0-72.0	266.40	36.4	57.2	1.692	1.076	2.698	60.1	1.507
30X- 5, 70.0-72.0	269.40	37.3	59.4	1.699	1.066	2.794	61.8	1.621
31X- 1, 70.0-72.0	273.00	36.1	56.5	1.697	1.085	2.701	59.8	1.489
31X- 3, 70.0-72.0	276.00	36.6	57.7	1.699	1.077	2.742	60.7	1.546
31X- 5, 70.0-72.0	279.00	35.6	55.2	1.710	1.101	2.713	59.4	1.464
32X- 1, 68.0-70.0	282.58	34.0	51.5	1.734	1.145	2.696	57.5	1.355
32X- 3, 50.0-52.0	285.40	33.6	50.5	1.749	1.162	2.725	57.4	1.345
32X- 5, 70.0-72.0	288.60	33.7	50.8	1.734	1.150	2.676	57.0	1.327
33X- 1, 65.0-67.0	292.15	34.7	53.2	1.734	1.132	2.747	58.8	1.426
33X- 3, 71.0-73.0	295.21	33.9	51.2	1.731	1.145	2.678	57.3	1.340
33X- 5, 70.0-72.0	298.20	34.7	53.2	1.729	1.129	2.728	58.6	1.416
34X- 1, 70.0-72.0	301.50	36.8	58.2	1.601	1.012	2.384	57.5	1.355
34X- 3, 54.0-56.0	304.34	33.9	51.3	1.743	1.151	2.724	57.7	1.366
34X- 5, 74.0-76.0	307.54	36.4	57.3	1.709	1.086	2.772	60.8	1.553
35X- 1, 70.0-72.0	310.80	35.4	54.7	1.705	1.102	2.680	58.9	1.432
35X- 3, 83.0-85.0	313.93	36.0	56.3	1.701	1.088	2.708	59.8	1.489
35X- 5, 94.0-96.0	317.04	35.6	55.3	1.709	1.101	2.713	59.4	1.465
36X- 1, 70.0-72.0	320.40	35.0	53.9	1.716	1.115	2.698	58.7	1.419
36X- 3, 70.0-72.0	323.40	35.4	54.8	1.704	1.100	2.678	58.9	1.434
36X- 5, 70.0-72.0	326.40	36.5	57.4	1.702	1.081	2.748	60.7	1.541
37X- 1, 70.0-72.0	330.00	34.7	53.2	1.727	1.127	2.721	58.6	1.414
37X- 3, 70.0-72.0	333.00	33.9	51.4	1.742	1.151	2.722	57.7	1.365
37X- 5, 70.0-72.0	336.00	36.1	56.4	1.702	1.088	2.718	59.9	1.497
38X- 1, 80.0-82.0	339.70	31.7	46.4	1.784	1.218	2.722	55.2	1.234
38X- 3, 62.0-64.0	342.52	33.1	49.4	1.758	1.177	2.724	56.8	1.315
38X- 5, 43.0-45.0	345.33	33.7	50.9	1.739	1.152	2.697	57.3	1.341
39X- 1, 49.0-51.0	349.09	33.2	49.8	1.762	1.177	2.748	57.2	1.335

Table T25 (continued).

Core, section, interval (cm)	Depth (mbsf)	Water content (wt%)		Density (g/cm^3)			Porosity (%)	Void ratio
		Bulk	Dry	Wet bulk	Dry bulk	Grain		
39X- 3, 105.0-107.0	352.65	32.2	47.5	1.784	1.210	2.752	56.1	1.276
39X- 5, 55.0-57.0	355.15	29.3	41.4	1.839	1.301	2.745	52.6	1.111
40X- 1, 64.0-66.0	358.84	30.9	44.6	1.811	1.252	2.757	54.6	1.202
40X- 3, 67.0-69.0	361.87	30.7	44.4	1.805	1.250	2.728	54.2	1.183
40X- 5, 70.0-72.0	364.90	32.4	47.8	1.767	1.195	2.707	55.9	1.265
41X- 1, 70.0-72.0	368.50	30.2	43.3	1.824	1.273	2.755	53.8	1.164
41X- 3, 80.0-82.0	371.60	30.0	42.8	1.830	1.281	2.763	53.6	1.156
41X- 5, 68.0-70.0	374.48	34.8	53.3	1.723	1.123	2.709	58.5	1.411
42X- 1, 70.0-72.0	378.10	35.2	54.3	1.713	1.110	2.697	58.8	1.429
42X- 3, 69.0-71.0	381.09	35.1	54.2	1.700	1.103	2.645	58.3	1.399
42X- 5, 70.0-72.0	384.10	35.1	54.0	1.710	1.111	2.679	58.5	1.412
43X- 1, 68.0-70.0	387.68	37.7	60.5	1.673	1.042	2.714	61.6	1.604
43X- 3, 69.0-71.0	390.69	36.1	56.5	1.695	1.083	2.692	59.8	1.486
43X- 5, 70.0-72.0	393.70	38.3	62.0	1.650	1.019	2.657	61.7	1.608
44X- 1, 70.0-72.0	397.30	32.8	48.9	1.743	1.171	2.655	55.9	1.268
44X- 3, 70.0-72.0	400.30	32.7	48.5	1.750	1.178	2.667	55.8	1.263
44X- 5, 70.0-72.0	403.30	34.3	52.3	1.717	1.127	2.656	57.5	1.355
45X- 1, 77.0-79.0	406.97	36.5	57.5	1.686	1.070	2.683	60.1	1.508
46X- 1, 71.0-73.0	416.51	31.6	46.1	1.769	1.210	2.662	54.5	1.199
46X- 3, 100.0-102.0	419.80	36.3	56.9	1.688	1.076	2.675	59.8	1.485
47X- 1, 81.0-83.0	426.21	31.9	46.9	1.787	1.216	2.744	55.7	1.256
47X- 3, 82.0-84.0	429.22	26.5	36.1	1.881	1.382	2.693	48.7	0.948
49X- 1, 72.0-74.0	445.32	32.2	47.5	1.756	1.190	2.658	55.2	1.233
49X- 3, 106.0-108.0	448.66	37.4	59.8	1.680	1.051	2.723	61.4	1.590
50X- 1, 82.0-84.0	455.02	29.2	41.3	1.826	1.293	2.700	52.1	1.088
189-1170D-								
1R-1, 35.0-37.0	425.35	31.1	45.1	1.789	1.233	2.701	54.3	1.190
2R-1, 70.0-72.0	434.20	32.5	48.2	1.772	1.196	2.734	56.3	1.286
2R-2, 52.0-54.0	435.52	30.4	43.6	1.814	1.263	2.732	53.8	1.163
3R-1, 48.0-50.0	443.58	32.5	48.1	1.768	1.194	2.717	56.1	1.277
4R-1, 109.0-111.0	453.79	34.5	52.8	1.711	1.120	2.648	57.7	1.364
5R-1, 73.0-75.0	463.03	21.8	27.8	2.046	1.601	2.834	43.5	0.770
6R-1, 36.0-38.0	472.26	14.0	16.3	1.916	1.647	2.234	26.3	0.357
7R-3, 30.0-32.0	479.40	31.5	46.0	1.810	1.240	2.796	55.7	1.255
8R-1, 69.0-71.0	482.19	37.9	60.9	1.653	1.027	2.641	61.1	1.571
8R-2, 70.0-72.0	483.70	36.8	58.2	1.677	1.060	2.669	60.3	1.518
8R-3, 67.0-69.0	485.17	35.8	55.7	1.822	1.170	3.219	63.7	1.752
9R-1, 70.0-72.0	491.80	44.5	80.0	1.535	0.853	2.557	66.6	1.998
9R-2, 70.0-72.0	493.30	42.7	74.5	1.574	0.902	2.624	65.6	1.910
9R-3, 71.0-73.0	494.81	41.0	69.4	1.604	0.947	2.643	64.2	1.791
9R-4, 71.0-73.0	496.31	41.7	71.6	1.002	0.584	0.986	40.8	0.689
10R-1, 128.0-130.0	501.98	32.1	47.2	1.812	1.230	2.845	56.7	1.312
10R-2, 56.0-58.0	502.76	26.4	35.8	1.861	1.370	2.632	47.9	0.921
11R-1, 71.0-73.0	511.01	30.0	42.9	1.828	1.279	2.757	53.6	1.156
11R-3, 70.0-72.0	514.00	27.3	37.6	1.870	1.359	2.714	49.9	0.997
11R-5, 70.0-72.0	517.00	26.6	36.2	1.893	1.389	2.733	49.2	0.967
12R-1, 22.0-24.0	520.02	18.1	22.2	1.911	1.565	2.365	33.8	0.512
12R-1, 80.0-82.0	520.60	20.5	25.7	2.200	1.749	3.123	44.0	0.785
12R-2, 71.0-73.0	522.01	28.4	39.7	1.925	1.378	2.956	53.4	1.145
12R-3, 70.0-72.0	523.50	29.3	41.4	1.851	1.309	2.783	53.0	1.126
13R-1, 68.0-70.0	530.08	27.9	38.8	1.848	1.331	2.685	50.4	1.017
13R-3, 66.0-68.0	533.06	27.2	37.3	1.874	1.365	2.715	49.7	0.989
13R-4, 48.0-50.0	534.38	27.3	37.6	1.784	1.297	2.476	47.6	0.909
14R-1, 70.0-72.0	539.80	32.4	47.8	1.720	1.163	2.548	54.3	1.190
14R-3, 70.0-72.0	542.80	25.9	35.0	1.850	1.370	2.579	46.9	0.882
14R-5, 75.0-77.0	545.85	31.3	45.5	1.756	1.207	2.603	53.6	1.156
15R-1, 69.0-71.0	549.39	28.9	40.7	1.782	1.266	2.550	50.4	1.015
15R-3, 70.0-72.0	552.40	29.7	42.3	1.765	1.240	2.545	51.3	1.052
15R-5, 69.0-71.0	555.39	28.4	39.7	1.811	1.297	2.606	50.3	1.010
16R-1, 69.0-71.0	558.99	35.4	54.9	1.674	1.081	2.570	58.0	1.379
16R-3, 120.0-122.0	562.49	29.8	42.4	1.757	1.234	2.525	51.1	1.046
16R-5, 80.0-82.0	565.09	28.8	40.5	1.756	1.250	2.471	49.4	0.976
17R-1, 64.0-66.0	568.54	28.7	40.2	1.803	1.286	2.597	50.5	1.020
17R-3, 70.0-72.0	571.60	30.9	44.7	1.759	1.215	2.589	53.1	1.131
17R-5, 70.0-72.0	574.60	30.9	44.6	1.743	1.205	2.538	52.5	1.106
18R-1, 70.0-72.0	578.20	31.2	45.3	1.762	1.213	2.614	53.6	1.155
18R-3, 71.0-73.0	581.21	29.6	42.0	1.768	1.245	2.543	51.0	1.042
18R-5, 67.0-69.0	584.17	29.5	41.8	1.800	1.269	2.634	51.8	1.075

Table T25 (continued).

Core, section, interval (cm)	Depth (mbsf)	Water content (wt%)		Density (g/cm^3)			Porosity (%)	Void ratio
		Bulk	Dry	Wet bulk	Dry bulk	Grain		
19R-1, 38.0-40.0	587.48	3.3	3.4	2.493	2.412	2.620	8.0	0.086
19R-2, 14.0-16.0	587.66	5.1	5.4	2.512	2.382	2.726	12.6	0.144
19R-3, 70.0-72.0	589.72	33.8	51.0	1.717	1.137	2.623	56.7	1.307
19R-5, 70.0-72.0	592.72	29.7	42.2	1.789	1.258	2.614	51.9	1.077
20R-1, 87.0-89.0	597.57	33.6	50.7	1.730	1.148	2.658	56.8	1.317
20R-3, 70.0-72.0	600.43	27.6	38.1	1.832	1.327	2.619	49.3	0.974
20R-5, 66.0-68.0	603.39	29.7	42.3	1.788	1.257	2.612	51.9	1.078
20R-7, 54.0-56.0	606.27	28.2	39.4	1.823	1.308	2.630	50.3	1.011
21R-1, 72.0-74.0	607.02	30.3	43.5	1.795	1.251	2.670	53.1	1.134
21R-3, 70.0-72.0	610.00	30.1	43.0	1.782	1.246	2.616	52.4	1.100
21R-5, 70.0-72.0	613.00	31.6	46.3	1.756	1.200	2.625	54.3	1.187
22R-1, 19.0-21.0	616.09	31.5	46.1	1.723	1.180	2.515	53.1	1.131
22R-3, 70.0-72.0	618.45	28.5	39.9	1.820	1.301	2.637	50.7	1.027
22R-5, 70.0-72.0	621.45	30.8	44.5	1.734	1.200	2.509	52.2	1.091
22R-7, 70.0-72.0	624.45	30.4	43.6	1.765	1.229	2.580	52.3	1.098
23R-1, 64.0-66.0	626.24	30.4	43.6	1.746	1.216	2.522	51.8	1.074
23R-3, 74.0-76.0	629.34	29.7	42.2	1.777	1.249	2.577	51.5	1.063
23R-5, 72.0-74.0	632.32	32.4	47.8	1.704	1.153	2.498	53.9	1.167
24R-1, 75.0-77.0	636.05	32.9	49.0	1.712	1.149	2.554	55.0	1.223
24R-3, 76.0-78.0	639.06	31.8	46.5	1.687	1.151	2.415	52.3	1.097
24R-5, 64.0-66.0	641.94	29.9	42.7	1.748	1.225	2.506	51.1	1.046
25R-1, 70.0-72.0	645.60	29.4	41.6	1.749	1.235	2.481	50.2	1.008
25R-3, 69.0-71.0	648.59	29.7	42.3	1.785	1.255	2.603	51.8	1.074
25R-5, 72.0-74.0	651.62	32.3	47.6	1.720	1.165	2.543	54.2	1.182
26R-1, 73.0-75.0	655.33	30.7	44.4	1.741	1.206	2.525	52.3	1.095
26R-3, 70.0-72.0	658.30	33.7	50.9	1.674	1.109	2.473	55.1	1.230
26R-5, 69.0-71.0	661.29	28.4	39.7	1.782	1.276	2.522	49.4	0.977
27R-1, 73.0-75.0	664.93	31.8	46.7	1.738	1.185	2.578	54.1	1.177
27R-3, 70.0-72.0	667.90	36.1	56.5	1.648	1.053	2.513	58.1	1.386
27R-5, 70.0-72.0	670.90	30.6	44.1	1.743	1.210	2.525	52.1	1.086
28R-1, 70.0-72.0	674.50	33.9	51.4	1.693	1.118	2.547	56.1	1.278
28R-2, 70.0-72.0	675.92	32.2	47.6	1.724	1.169	2.556	54.3	1.187
28R-3, 70.0-72.0	677.32	34.4	52.5	1.671	1.096	2.501	56.2	1.281
28R-5, 70.0-72.0	679.84	30.1	43.1	1.782	1.246	2.618	52.4	1.102
29R-1, 70.0-72.0	684.20	28.5	39.9	1.791	1.281	2.555	49.9	0.995
29R-3, 70.0-72.0	687.06	26.9	36.8	1.833	1.339	2.584	48.2	0.930
29R-5, 70.0-72.0	690.00	26.6	36.3	1.857	1.363	2.637	48.3	0.935
30R-1, 73.0-75.0	693.93	27.2	37.3	1.830	1.333	2.591	48.6	0.944
30R-3, 70.0-72.0	696.75	28.1	39.1	1.803	1.296	2.566	49.5	0.980
30R-5, 70.0-72.0	699.75	26.2	35.5	1.878	1.385	2.668	48.1	0.926
31R-1, 73.0-75.0	703.53	27.2	37.3	1.846	1.344	2.635	49.0	0.960
31R-3, 70.0-72.0	706.50	29.6	42.1	1.801	1.267	2.645	52.1	1.087
31R-5, 70.0-72.0	709.50	24.2	31.9	1.933	1.465	2.698	45.7	0.842
32R-1, 71.0-73.0	713.11	24.3	32.2	1.937	1.466	2.717	46.1	0.854
32R-3, 70.0-72.0	716.10	28.5	39.8	1.855	1.327	2.740	51.6	1.065
32R-5, 70.0-72.0	719.10	26.4	36.0	1.904	1.400	2.756	49.2	0.968
33R-1, 70.0-72.0	722.70	26.7	36.5	1.882	1.379	2.712	49.2	0.967
33R-3, 70.0-72.0	725.70	25.3	33.9	1.898	1.417	2.671	46.9	0.885
33R-5, 70.0-72.0	728.70	25.7	34.5	1.888	1.403	2.663	47.3	0.898
34R-1, 70.0-72.0	732.30	24.2	31.9	1.931	1.464	2.693	45.6	0.840
34R-3, 70.0-72.0	735.30	24.1	31.8	1.463	1.110	1.694	34.5	0.527
34R-5, 70.0-72.0	738.30	25.7	34.6	1.906	1.416	2.714	47.8	0.916
35R-1, 71.0-73.0	741.91	22.6	29.2	1.941	1.502	2.629	42.9	0.751
35R-3, 69.0-71.0	744.89	29.3	41.4	1.829	1.294	2.711	52.3	1.096
35R-5, 70.0-72.0	747.90	23.4	30.6	1.948	1.492	2.690	44.5	0.803
36R-1, 71.0-73.0	751.51	21.9	28.0	2.004	1.566	2.740	42.9	0.750
36R-3, 71.0-73.0	754.51	22.1	28.3	1.965	1.531	2.657	42.4	0.735
36R-5, 71.0-73.0	757.51	22.1	28.3	1.980	1.543	2.692	42.7	0.745
37R-1, 67.0-69.0	761.17	26.5	36.1	1.867	1.371	2.657	48.4	0.937
37R-3, 71.0-73.0	764.21	25.0	33.3	1.918	1.439	2.703	46.8	0.878
37R-5, 70.0-72.0	767.20	23.2	30.2	1.953	1.501	2.689	44.2	0.792
38R-3, 69.0-71.0	773.77	26.0	35.1	1.888	1.397	2.682	47.9	0.919
38R-5, 49.0-51.0	776.57	22.1	28.4	1.984	1.545	2.705	42.9	0.751